Downloaded from orbit.dtu.dk on: May 05, 2023

DTU Library

Hydrogen from Metal Ammines

Klerke, Asbjørn

Publication date:
2009

Document Version
Publisher's PDF, also known as Version of record

Link back to DTU Orbit

Citation (APA):
Klerke, A. (2009). *Hydrogen from Metal Ammines*. Technical University of Denmark.

General rights
Copyright and moral rights for the publications made accessible in the public portal are retained by the authors and/or other copyright owners and it is a condition of accessing publications that users recognise and abide by the legal requirements associated with these rights.

- Users may download and print one copy of any publication from the public portal for the purpose of private study or research.
- You may not further distribute the material or use it for any profit-making activity or commercial gain
- You may freely distribute the URL identifying the publication in the public portal

If you believe that this document breaches copyright please contact us providing details, and we will remove access to the work immediately and investigate your claim.

Hydrogen from Metal Ammines

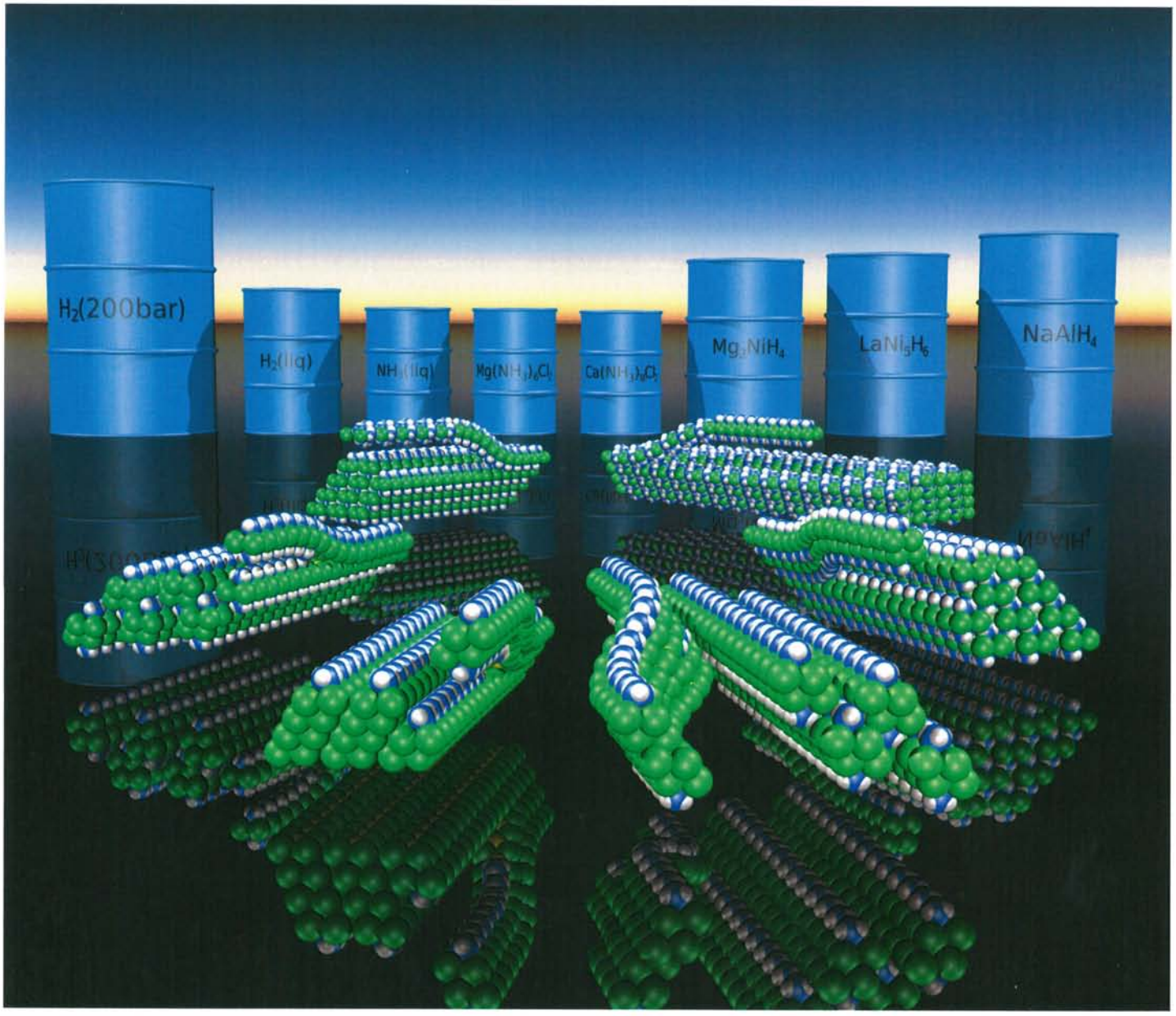

Asbjørn Klerke
PhD Thesis
DTU Chemistry
June 2009

Centre for Catalysis and Sustainable Chemistry

Danish National Research Foundation's
Center for Sustainable and Green Chemistry

DTU

Hydrogen from Metal Ammines

Asbjørn Klerke

PhD. Thesis

Center for Catalysis and Sustainable Chemistry

Department of Chemistry

Technical University of Denmark

June 2009

Preface

This thesis is submitted in candidacy of the PhD degree from the Technical University of Denmark (DTU). The work was done in Center for Catalysis and Sustainable Chemistry (CS) formerly Center for Sustainable and Green Chemistry (CSG), Department of Chemistry, Technical University of Denmark. The work was supervised by Professor Claus Hviid Christensen, which after 2 years sought new carrier opportunities. I would like to thank Claus for always being available for a discussion of the progress of the PhD study and scientific work and always following up on ideas and opportunities.

The final year the supervision was done by Docent Rasmus Fehrmann. I would thank Rasmus for standing in and taking over the project helping with all the formalities of the thesis and finalization of the PhD work.

During the three years a lot of people have helped with advice and input. Thanks to the people I convinced that they have to proofread the thesis. A few people need special mentioning those are, Rasmus Z. Sørensen, Jakob Engbæk, Jens S. Hummelshøj, Tejs Vegge, and Søren K. Klitgaard. I would also thank all my present and former colleagues at CSG for making it three good years. Further the people in Amminex A/S and Danish Technological Institute also deserve thanks for their input to the project. The collaboration has showed that the science can be use for commercial application in the near future.

The PhD work has been financed with grants from the "Danish National Research Foundation" and "The Danish Council for Strategic Research" under the program committee for "Sustainable Energy and Environment".

The object of this thesis is to give an overview of the possibilities of using ammonia for indirect hydrogen storage. The thesis starts with a short introduction to hydrogen as an energy carrier and what the possibilities of producing hydrogen are, but also the challenges of storing and transporting hydrogen. These challenges are hard to overcome by direct hydrogen storage techniques so this thesis focus on using ammonia as an indirect hydrogen carrier.

In the thesis the experimental work on ammonia synthesis, solid ammonia storage in metal ammines, and ammonia decomposition are the main focal point. Further the work done on developing an ammonia cracker, done at the Danish Technological

Institute, is described. The work with the ammonia cracker has been a good opportunity to use some of the catalytic and engineering knowledge in practice. The development show possibilities and the hope is that the project will end up in a finished prototype combining, both solid ammonia storage in metal ammines and a PEM fuel cell stack.

Asbjørn Klerke

DTU Chemistry, June 16th 2009.

Abstract

This project shows the possibilities of using ammonia as an energy carrier and indirect hydrogen storage medium. This is done by going through the known infrastructure of ammonia synthesis, storage and transportation.

The investigation of the ammonia infrastructure includes experiments on ammonia synthesis on iron cobalt and nickel promoted with barium supported on high surface area graphite.

The possibilities of solid storage of ammonia in metal ammine complexes is explained and demonstrated by experiments with $Ca(NH_3)_8Cl_2$, $Mg(NH_3)_6Cl_2$, $Mn(NH_3)_6Cl_2$, and $Ni(NH_3)_6Cl_2$. The metal ammines are investigated by temperature programmed desorption. This demonstrates that all show feasible ammonia desorption only limited by heat transfer. The volumetric and gravimetric hydrogen densities are calculated from solid tablets of the metal ammines. This shows that all have densities of above 95% of the crystal densities.

The catalytic decomposition of ammonia is studied. There has been focus on the existing literature and experimental testing of decomposition catalysts.

The promoter effects of caesium and barium on iron, cobalt and nickel, supported on high surface area graphite is studied. This shows that the promoters work very differently on the three metals. It is shown that caesium is the best promoter for iron particles and barium is the best promoter for cobalt and nickel.

The effect of novel synthesis nanotitanates with incorporated alkali metal promoters is investigated as support materials for ruthenium particles. The results show large effect of making sodium titanates $Na_2Ti_3O_7$ nanotubes, potassium titanates $K_2Ti_6O_{13}$ nanowires and cesium titanates $Cs_2Ti_6O_{13}$ nanowires compared to the TiO_2 nanoparticles. The materials are characterized to verify that they are nanomaterials. The result shows that $Cs_2Ti_6O_{13}$ nanowires are the titanate support for ruthenium particles that gives the highst catalytic activity.

The final part of the project is a description of the work done developing an ammonia cracker. The goal is to develop an ammonia cracker that can work with a proton exchange membranefuel cell. The work was done at the Danish Technological Institute. The prototype of the ammonia cracker was shown to work. The heat for the endothermic ammonia decomposition is supplied by oxidizing a part of the

ammonia stream over a platinum on alumina catalyst. The decomposition catalyst is ruthenium promoted with caesium supported on high surface area graphite.

Dansk Résume

Projektet er en demonstration af mulighederne for anvendelse af ammoniak som en energibærer og som indirekte hydrogenlager. Det starter med en gennemgang af ammoniakinfrastrukturen det vil sige, ammoniaksyntese, opbevaring og transport. Som en del af undersøgelsen af der foretaget forsøg med ammoniaksyntese med barium promoteret jern, kobolt, og nikkel på grafit som katalysatorer.

Fast ammoniaklagring i metalamminkomplekser er forklaret og demonstreret ved forsøg med $Ca(NH_3)_8Cl_2$, $Mg(NH_3)_6Cl_2$, $Mn(NH_3)_6Cl_2$, og $Ni(NH_3)_6Cl_2$. Metalamminernes desorptionen er undersøgt under en kontrolleret temperaturrampe. Det er demonstreret at alle de undersøgte metalamminer viser hurtig ammoniak desorption, kun hindret af varmetransport i metalamminerne. Den volumetriske og gravimetriske indirekte hydrogendensitet er målt for piller af metalamminkomplekserne. Det viser at de alle opnår hydrogendensiteter på >95% af krystaldensiteten der er den teoretisk maksimale.

Katalytis kammoniakdekomponering er gennemgået, med fokus på den eksisterende litteratur og eksperimentelle undersøgelser af ammoniakdekomponerings-katalysatorer.

Den eksperimentelle undersøgelse har drejet sig om promotoreffekter af cæsium og barium på jern, kobolt og nikkel deponeret på grafit. Her viser eksperimenterne at promotorene virker forskelligt på de tre metaller. Cæsium er den bedste promotor for jern og barium er den bedste promoter for kobolt og nikkel.

Effekten ved brug af de tre nano titanater, $Na_2Ti_3O_7$, $K_2Ti_6O_{13}$, og $Cs_2Ti_6O_{13}$ som support materiale for ruthenium er undersøgt og sammenlignet med TiO_2. Resultaterne visser at ruthenium deponeret på de tre nanotitanater har højere katalytisk aktivitet end ruthenium deponeret på titania. Aktiviteten er også højere end hvad der kunne forventes for den rene promotor effekt af alkalimetalerne.

Afslutningsvis er en beskrives den ammoniakkraker der er blevet udviklet på Tekenologisk Institut som en del af projektet. Ammoniakkrakeren er designet til at kunne dekomponere ammoniak der skal bruges i en PEM brændselscelle. Varmen til dekomponeringen fås ved samtidig katalytisk oxidation af en delstrøm af ammoniakken. Ammoniakkrakeren udført i rør af syrefaststål med oxidationskatalysatoren i det inderste rør og dekomponerigskatalysatoren i et rør uden om. Den første prototype er testet og kan effektivt dekomponere ammoniak.

Publications

Publications with relevance to this thesis include as appendix:

1 A. Klerke, S. K. Klitgaard, R. Fehrmann, **Catalytic ammonia decomposition over ruthenium nanoparticles supported on nano-titanates**, *Catal. Lett.* 2009, accepted.

2 R. Z. Sørensen, J. S. Hummelshøj, A. Klerke, J. B. Reves, T. Vegge, J. K. Nørskov, C. H. Christensen, **Indirect, reversible high-density hydrogen storage in compact metal ammine salts**, *J. Am. Chem. Soc.*, 2008, 130, 8660-8668.

3 A. Klerke, C. H. Christensen, J. K. Nørskov, T. Vegge, **Ammonia for Hydrogen Storage: Challenges and Opportunities**, *J. Mater. Chem.*, 2008, 18, 2304-2310.

4 R. Z. Sørensen, A. Klerke, U. Quaade, S. Jensen, O. Hansen, C. H. Christensen, **Promoted Ru on high-surface area graphite for efficient miniaturized production of hydrogen from ammonia**, *Catal. Lett.*, 2006, 112, 77-81.

5 T. Vegge, R. Z. Sørensen, A. Klerke, J. S. Hummelshøj, T. Johannessen, J. K. Nørskov, C. H. Christensen, **Indirect Hydrogen Storage in Metal Ammines**, *Solid-state hydrogen storage: Materials and chemistry,* Woodhead Publishing LTD., England, 2008.

6 A. Klerke, J. Engbæk, R. Z. Sørensen, R. Fehrmann, **Ammonia and Metal Ammines for High Density Hydrogen Storage**, 2009 AIChE Spring National Meeting, conference proceeding paper.

7 A. Klerke, R. Z. Sørensen, C. H. Christensen, U. Quaade, J. K. Nørskov, **Compact Hydrogen Production from Ammonia Stored in Solid Metal Ammines**, World Hydrogen Technologies Convention 2007, conference proceeding paper.

Other publications:

8 A. Klerke, S. Saadi, M. B. Toftegaard, A. T. Madsen, J. H. Nielsen, S. Jensen, O. Hansen, C. H. Christensen, U. Quaade, **PtRu colloid nanoparticles for CO oxidation in microfabricated reactors**, *Catal. Lett.*, 2006, 109, 7-12.

9 A. M. Frey, A. Klerke, J. Due-Hansen, C. H. Christensen, **Biobrændsel-et varmt alternativ**, *Nye Kemiske Horisonter*, DTU, Denmark, 2007.

10 R. Z. Sørensen, A. Klerke, C. H. Christensen, **Bivirkninger ved brintpiller**, *LMFK-bladet*, 2008, 2, 39-41.

Table of Content

Energy Storage

The Hydrogen Economy

The hydrogen economy has been considered as the idea of replacing fossil fuels as energy carriers with hydrogen[1,2,3]. This technology will solve a lot of pollution problems as conversion of hydrogen into energy in a fuel cell or combustion engine only results in water. Furthermore, hydrogen can be produced from renewable resources; this could be from wind and water power via electrolysis of water, from biomass gasification, or by direct solar conversion in a photo catalytic water splitting reaction. The incorporation of hydrogen production in the power grid could also help integrating larger amounts of renewable energy sources.

The challenges of many sources of renewable energy not can be regulated to demand this could be wind, solar and wave. This put high demands on the power grid that need to adjust for fluctuations in power production. Ideally the power grid is large and flexible enough for all the renewable energy to be used, but this is not always the case. This overproduction of electricity from renewable sources can make it commercially viable to store the energy even with a considerable loss. So conversion of cheap electricity into a more valuable fuel like hydrogen has promoted the hydrogen economy. The need for energy storage will increase with increasing production of renewable energy.

The limited nature of the fossil resources and the increased focus on climate changes due to pollution with CO_2 and other green house gases has further increased the focus on alternatives that are clean and renewable. As oil is the first fossil resource that will become sparse[4,5], ways to substitute oil based transportation with an alternative has gained industrial interest and several companies have produced experimental hydrogen fuelled cars[6,7].

This focus on hydrogen as a chemical energy carrier and an energy storage medium, formulated as the hydrogen economy, includes a number of challenges. These challenges can be divided into three areas: clean and efficient hydrogen production; high density storage and transportation of hydrogen; efficient use of hydrogen for energy production. In the following a short summary is given of how far the research has progressed in meeting these challenges.

Hydrogen Production

The production of hydrogen is today mainly done by steam reforming of natural gas. This process is energy intensive requiring a reforming temperature of 800-900°C[8] and uses large amount of process steam. The process is not sustainable due to the limited fossil resources and the pollution by CO_2 that contributes to global warming. CO_2 could be sequestrated out and deposited underground but this process is only currently working in small scale experimental plants. The sequestration of CO_2 is energy intensive[9], but necessary to lower the amount of CO_2 in the atmosphere in the near future. CO_2 sequestration could make steam reforming and other fossil processes greener.

Today there are three major consumers of hydrogen, these are: ammonia synthesis, petroleum refining and methanol synthesis. Together they consume ~95% of the world's hydrogen production[10]. The steam reforming of methane and the water gas shift reaction will for the foreseeable future remain the main way of obtaining hydrogen.

Production of renewable energy is a large challenge, this is mainly due to the large amount of hydrogen needed at a low cost of $2-3 pr. kg of hydrogen delivered at the pump[11]. Below a short work through of how renewable hydrogen is produced by electrolysis of water is given. Water electrolysis is a green process, where water is split into hydrogen and oxygen by electricity. To produce CO_2 free hydrogen the electricity needs to be renewable, e.g. from water, wind, solar *etc.*

The ideal reversible potential under standard condition is 1.228V corresponding to the Gibbs free energy of the process, but the reaction is in nature not reversible and therefore additional energy is needed corresponding to $T\Delta S$ at standard temperature and pressure(STP) this value is 0.252V, giving a minimum potential for water splitting of 1.48V at standard conditions.

The traditional water electrolysis is done in an alkaline solution, typically ~25% KOH heated to 80-90°C with a cell voltage of 1.7-2.1V. The power consumption is around 4 to 5 kWh/m^3 hydrogen (STP).This corresponds to an overall thermal efficiency of 50-60% based on higher heating values (HHV)[9]. So far all large water electrolysis plants use variations of the alkaline electrolysis[12]. A lot of research has gone into developing alternatives like the use of proton exchange membrane (PEM) or high temperature ceramics membranes. As of yet no plants have been commercialized on

a large scale, mainly due to high price and problems with long term stability of the membranes.

Hydrogen Storage and Transportation

Hydrogen storage can be divided into two main categories: I) direct hydrogen storage as gas or liquid or II) chemical bound hydrogen. Depending on how strong the chemical binding is, chemically bound hydrogen can either be labeled direct or indirect chemical storage.

Storage of hydrogen as a compressed gas is straight forward but expensive. This is due to low gas density and the large storage volumes needed. A way to obtain large storage volumes is by underground storage in naturally occurring geologic formations[11]. This is the cheapest way to store hydrogen, but the number and placement of suited underground storage areas are unknown. Furthermore, more knowledge of long-time diffusion and safety for locals in the area are a concern[8]. For automotive use, compressed hydrogen has been the preferred method for demonstration. This could be seen in Reykjavik, Iceland where several busses for some years ran on high pressure (300 bar) hydrogen[13]. The biggest drawback of high pressure hydrogen is the low volumetric density that is 14 g/L at 20 MPa rising to 36 g/L at 80 MPa[14].

Condensing hydrogen into a liquid is another commercial available option for storage of hydrogen. The liquefaction of hydrogen is energy intensive and has a cost of 1/3 of the lower heating value. At the same time the evaporation cost to keep hydrogen as a liquid is 1-3% pr. day for small tanks. For large scale storage of liquid hydrogen, this can be brought down to an evaporation of less than 0.1% pr. day[8]. The volumetric density of liquid hydrogen is 70.8 g/L[14].

The difficulties with liquid and pressurized hydrogen storage have led to research in alternative hydrogen storage materials. The search for high capacity materials has led to the synthesis and characterization of more and more exotic and reactive compounds for hydrogen storage: Complex metal hydrides like $NaAlH_4$[15], $LiAlH_4$[16], and AlH_3[17]; metal organic frameworks (MOFs)[18]; borohydrides like $LiBH_4$[19,20] and $Mg(BH_4)_2$[21]; destabilized borohydrides[22]; ammonia borane[23]; and amide/imide systems[24]. All these systems display high potential storage capacities, but fall short on other parameters necessary for hydrogen storage. Currently, complex metal hydrides do not reach the target for reversible hydrogen storage capacity, MOFs

require operational temperatures around liquid nitrogen (-196°C). Systems based on borohydrides are practically irreversible and suffer from relatively slow kinetics[25], production and regeneration of ammonia borane is very costly[26], and the amide/imide systems have low reversible capacity.

This lack of a good candidate for direct hydrogen storage in a solid medium, gives indirect hydrogen storage with strong chemical binding renewed focus. The main indirect hydrogen storage mediums are hydrocarbons and ammonia. Both can be stored and transported with well-known and proven technologies.

The use of hydrocarbons is more or less an extension of the fossil economy we have today, with the option of applying green alternatives as bio-ethanol and biomass. Use of biomass is a step in the right direction as biomass can replace fossil alternatives, but the problem is that biomass is a limited resource also needed for food and chemicals in the future. This limits the amount of energy we can get from biomass.

The conversion of hydrocarbons into hydrogen also produces CO_2, even if they are from biomass. A lowering of the total CO_2 in the atmosphere requires complete CO_2 free alternatives in the future. For now, hydrocarbons of different types provide a range of possibilities, such as methanol combined directly with a methanol fuel cell, for small scale application in computers or other portable devices or for the generation of heat and electricity in combined heat and power plants (CHP).

Ammonia as an indirect hydrogen carrier is not a new idea, Norsk Hydro build a car prototype running on ammonia in 1933[27]. Since then ammonia as energy carrier has been proposed at various intervals but it is only in recent years that it has gained a broader acceptance in the scientific community as a viable solution to the storage and transportation of hydrogen. This has come from the new use of metal ammines as solid storage materials for ammonia[28].

Hydrogen Conversion to Energy

The conversion of hydrogen back into energy is mainly done in fuel cells, but can also be done in a combustion engine. Fuel cells are chosen for their high energy efficiency and direct electricity production. A disadvantage of many fuel cells is the high production cost and problems with long time stability due to either catalyst deactivation or membrane failure.

A range of different fuel cell types exist, some of these are proton electrolyte membrane fuel cells (PEMFC) which is the most widely used, phosphoric acid fuel cells (PAFC), alkaline fuel cells (AFC), molten carbonate fuel cells (MCFC) and solid oxide fuel cell (SOFC). The technology required for a range of fuel cell systems to work is described by J. Larmine in several publications[29,30].

Summary

This section has described some of the main challenges of the hydrogen economy. It has shown that a lot of problems still need to be solved and hydrogen placed as a winning technology is not guaranteed. A number of challenges on the road to the hydrogen economy would have to be overcome before this would be the case.

Therefore, other alternatives to hydrogen that can more easily be adopted by known technology are becoming more interesting, for example SOFC running on reformed hydrocarbons. This is a battery technology for cars instead of hydrogen (gas?). It could also be used with ammonia as an indirect carbon free energy carrier. The properties of ammonia as an energy carrier and storage medium are described below.

Ammonia as Energy Storage Medium

The chemistry of ammonia makes it interesting as an energy carrier in the hydrogen economy[31]. This is due to a hydrogen gravimetric density in ammonia of 17.7 wt% and a volumetric density as a liquid at room temperature and 8 bars pressure of 108 g/L[32]. The fact that ammonia can be stored and transported as a liquid at room temperature and moderate pressure makes it interesting compared to other indirect storage mediums[33] such as methane that has a higher gravimetric hydrogen density of 25.1%, but only a volumetric density of 25 g/L at 200 bar and room temperature. The advantage of methane of course is the well established infrastructure for distribution along with the low level of processing required before distribution. The problems associated with methane, aside from the low volumetric density, are the high temperatures required for bond breaking, and the presence of CO_X in the hydrogen stream. This is very damaging for most types of low temperature fuel cells.

Ammonia can solve several of the problems associated with methane, besides the high volumetric density. Ammonia bonds can be broken without generating any CO_X in the final hydrogen stream. Ammonia is also easier to dissociate, requiring much reduced temperatures. In Figure 1 a schematic is shown of the ammonia lifecycle for indirect hydrogen storage, with the option of solid ammonia storage in the form of a metal ammine salt.

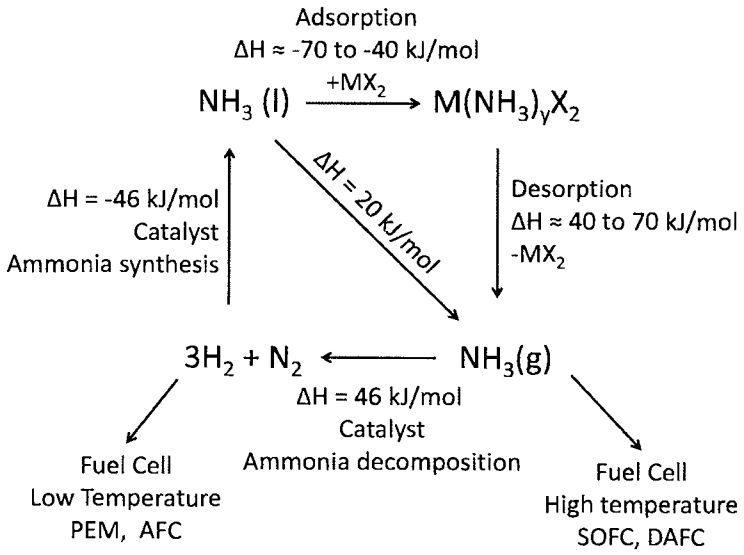

Figure 1: The life-cycle of hydrogen stored as ammonia in metal ammines, $M(NH_3)_yX_2$[34].

The hydrogen for ammonia synthesis is produced from natural gas via the steam reforming and water gas shift reaction. The end product in the ammonia synthesis is liquid ammonia. The liquid ammonia is stored below its boiling point (-33°C) and at 1 bar.

Ammonia Synthesis

Process

The synthesis of ammonia in the Haber-Bosch process is among the largest and best studied chemical processes in the world[35]. The annual production of ammonia exceeds 125 million tons[36], of which about 85% is used for fertilizer. In Figure 2 a process scheme for an ammonia synthesis plant is shown.

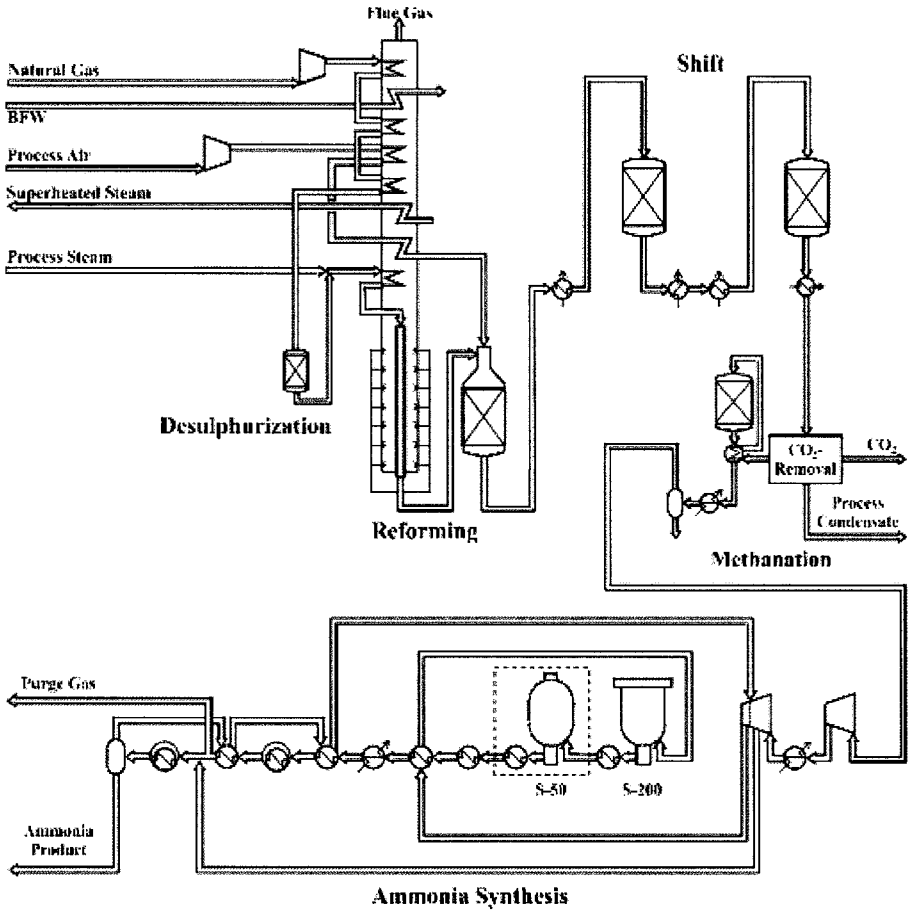

Figure 2: Process scheme for ammonia plant from Haldor Topsøe A/S[37].

The ammonia plant process scheme shown in Figure 2 has five main process steps. The first is desulphurization of natural gas. The desulphurization is typically done in two steps, first a hydrogenation to ensure that all sulphur is in the form of inorganic hydrogen sulphide. The hydrogen sulphide is then absorbed on zinc oxide, this will bring the sulphur concentration down to around 5 ppb[38]. The next step is steam reforming, here the clean natural gas is reacted with water to form carbon monoxide and hydrogen. The reaction is done over a nickel catalyst at high temperatures of 800-900°C[32]. The third step is water gas shift, where CO from the reformation step is reacted with water to give hydrogen and carbon dioxide. This is done in two steps, a high temperature step with an iron and chromium oxide catalyst at 320-350°C, followed by a low temperature conversion at 200-210°C on a copper, zinc catalyst supported on alumina. The fourth process is clean up of the process gas, this will remove CO_2 by pressure swing absorption and by a methanation reaction, remove CO and the rest of the CO_2. Finally, the water from this process is removed by

absorption in a molecular sieve. The final process step is the ammonia synthesis, first the pressure is increase to 150-250 bars in a series of compressors were it is mixed with recycled synthesis gas at the same time. The mixture is reacted in two ammonia conversion reactors with a total of three catalyst beds (2+1). The catalyst is a promoted iron/iron(II)oxide catalyst, where the typical promoters are alumina, potassium, calcium, and silicium. The temperature in the catalyst beds vary from 350°C at the inlet to around 530°C at the outlet. This heat is recovered and used for the production of superheated steam. The outlet ammonia concentration is 15-25 mol% which is then recovered by condensation at -5°C.

The interesting thing here is that the four first process steps are the same as used for conventional hydrogen production. The largest difference between the processes is the need to remove nitrogen during the hydrogen production. This is normally done before the steam reformer, so the feed is composed of only oxygen, steam and natural gas.

Economy of Ammonia Synthesis

The economy of the ammonia synthesis is mainly focused on methane consumption as this is the largest contributor to the overall running cost of a modern ammonia plant.

The energy cost for ammonia production is also interesting to look at. The net energy input in the form of methane for fuel and reformer feed is 29 GJ/t NH_3 and the energy in 1 t NH_3 is 17 GJ giving an efficiency based on low heating values (LHV) of 58%[39]. But this efficiency based on LHV is not the most interesting parameter; it is more interesting to look at the thermodynamic limit for ammonia production, here you need to feed in methane corresponding to 21 GJ/t NH_3, which gives a minimum energy loss in the conversion of 4GJ/t NH_3. The last 8 GJ/t NH_3 is needed for running the process and is lost via the turbines and compressors due to their use of superheated steam for propulsion. This steam is produced by heat recovery in the reformer[39,40].

The cost of ammonia on the world marked is closely correlated to the natural gas cost. In the production of ammonia, natural gas constitutes 75% of the running cost. This has lead to huge rises in ammonia prices in the summer and autumn of 2008, going from a normal of $250-300 pr. ton to over $900 pr. ton. More recently the price has fallen back to more normal level as oil and gas prices have fallen[41].

If ammonia is used as an energy storage and transportation medium, it is also important to calculate what the price pr. kg hydrogen is. For the normal interval of ammonia prices this gives \$1.40 to \$1.70 pr. kg H_2. This price is lower than the U.S. Department of Energy (DOE) targets for the hydrogen economy[42], which is \$2-3 pr. kg of hydrogen delivered to the end user[11].

Environmental Challenges

The challenge with the production of ammonia is to find a way of making the process cleaner and more sustainable. In the short term it would be to reduce CO_2 emissions, in the longer term to find a sustainable way to supply hydrogen.

Ammonia production is a candidate for CO_2 sequestration, because CO_2 is being removed from the synthesis gas feed by pressure swing absorption, this is done to avoid deactivation of the ammonia synthesis catalyst[39]. Furthermore, ammonia plants are typically located close to natural gas reservoirs, where the captured CO_2 could then be pumped into[43].

The hydrogen for ammonia synthesis can also be produced from coal by gasification. Coal is interesting for hydrogen production for several reasons: first of all, coal is cheap compared to other hydrocarbon energy sources[5]; secondly, the coal reserves are large enough to last for at least 200 years[5]; and finally, coal can be converted into hydrogen by gasification with a high efficiency[44,45,46]. This is not a permanent solution to the energy problem, but it can turn out to be the scenario we are facing.

The price of sustainable hydrogen is still high compared to fossil hydrogen such that large scale application of sustainable hydrogen is simply not yet competitive. A few places where renewable energy is abundant, like Iceland[47], production of sustainable hydrogen can be feasible, if the price of fossil resources continues rising to high levels.

Ammonia Safety

The safety of any future energy transportation medium is important to address. The properties and hazards of different alternatives must be evaluated. Some of the main concerns for energy storage mediums are flammability, explosion limits and toxicity.

The risk of explosion and fire is an essential safety concern in the handling of liquid and gaseous fuels, which can block the potential use of any energy carrier. The traditional hydrocarbon energy carrier is highly flammable and explosive in air. This is also true for some of the proposed alternatives, but there are significant differences in the flammability and explosion limits, see table 1. Here the apparent toxicity is shown as another important factor for public acceptance.

Table 1: Vapour pressures of different energy carriers, their relative toxicities, flammability and explosion limits in air[32,46,48,49]

	Vapour pressure @ 293K (bar)	IDLH* ppm	Apparent toxicity p/IDLH	Flammability limits (in air)	Explosion limits (in air)
Gasoline	0.047	750	63	1.4-7.6%	1.1-3.3%
Methanol	0.13	6000	21.6	6-36%	5.5–44%
Hydrogen	-	-	-	4-74%	18.3-59%
Natural gas	-	-	-	5.3-15%	5.7-14%
Liquid ammonia	8	300	$\sim 2.7 \times 10^4$	-	16-25%
$Mg(NH_3)_6Cl_2$	0.0014	300	4.65	-	-

*NIOSH Immediately Dangerous To Life or Health Concentration

The first important observation from Table 1, is that all hydrocarbon based energy carriers and hydrogen are highly flammable in air. Ammonia is non-flammable in air as gas, liquid or stored in at solid medium. With respect to explosion limits, both hydrogen and ammonia show significantly higher limits when compared to gasoline vapour, methanol vapour and natural gas.

The toxicity of energy carriers is clearly also an important issue. This is specially a problem for ammonia. Comparing the toxicity of liquid ammonia to that of gasoline and methanol, liquid ammonia is approximately three orders of magnitude higher in "apparent toxicity", *i.e.* the vapour pressure relative to the toxicity, at room temperature[50]. The apparent toxicity takes both the IDLH concentration and the vapour pressure into account, since substances with a low vapour pressure can have a low IDLH concentration and still rate safer than a substance with higher IDLH concentration but higher vapour pressure. For the case of ammonia both the low IDLH of 300 ppm and the high vapour pressure of 8 bar give it the high apparent toxicity. This makes it interesting to look at ways to decrease the vapour pressure of

ammonia at room temperature. This can be done with solid storage in metal ammines. For ammonia stored in metal ammines, *e.g.* $Mg(NH_3)_6Cl_2$, the apparent toxicity falls below that of both gasoline and methanol.

Safety issues remain the main challenge for using ammonia as an energy carrier for distributed use. The considerations outlined above are in line with a recent EU-funded report looking at ammonia for transportation fuel, which concluded that "the use of ammonia as a transport fuel wouldn't cause more risks than currently used fuels"[51].

Bulk Ammonia Storage and Transportation

The infrastructure for storage and transportation of liquid ammonia is well known technology, which is already used on a large scale for the fertilizer industry.

Storing and transporting liquid ammonia is mainly done in two ways: The first method is in pressurised vessels at 16-25 bars, obtained by applying an over-pressure of inert gas, at ambient temperature. Spherical pressure vessels can contain up to 1500 ton of ammonia (spherical diameter of 20-22 m). The second way is in isolated tanks at the boiling point of ammonia (-33°C) and ambient pressure, these tanks contain up to 50 000 t of ammonia[32]. Examples of the two different type of ammonia storage are showed in Figure 3.

Figure 3: Spherical ammonia storage tank (left) and two 30,000 ton insulated ammonia storage tanks (right).

The pressure vessels are normally used for localized storage of small ammonia quantities, here is the ammonia usually delivered under pressure by rail or truck. Pressurised storage would also be the only way of using liquid ammonia as a transportation fuel in cars. The insulated storage tanks are used for ammonia production sites, where the ammonia is condensed to a liquid and the tanks are kept cooled by the evaporating ammonia. The evaporated ammonia is condensed and pumped back. The insulated tanks would be the backbone of ammonia transportation and storage due to their lower cost and greater capacity.

For transportation of large amounts of ammonia over land, pipelines are the best alternative as they are cheap reliable and robust. In Figure 4 the current grid of pipelines for ammonia in the U.S. is shown.

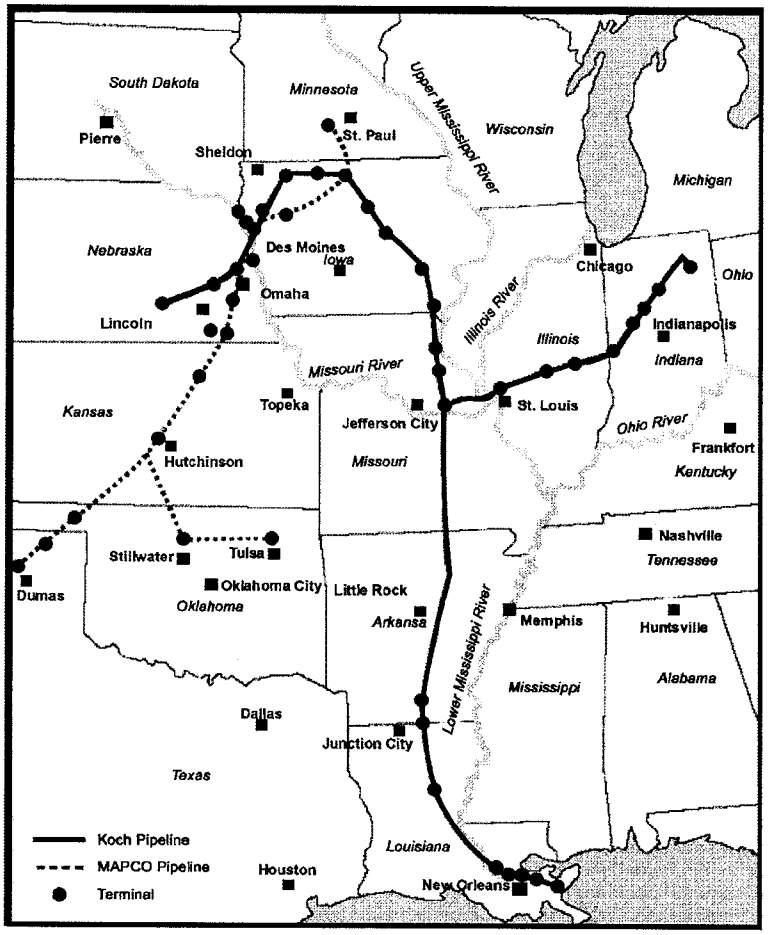

Figure 4: Ammonia Pipelines in the U.S.[52]

Liquid ammonia can also be transported by ship and barge, as this is a cheap alternative to pipelines and road or rail transportation. The safety concerns listed above makes it hard for liquid ammonia to gain market acceptance, therefore the possibility of storing ammonia in a solid metal ammine wold make it much easier for the end user to handle.

Experimental Data on Ammonia Synthesis

In the following is a short description of the experimental work done in ammonia synthesis, this has not been published and is done mainly to gain further understanding of the promoting effects of barium on iron, cobalt and nickel supported on high surface area graphite (HSAG). The result gained from synthesis will be compared to data obtained from decomposition.

Barium as a promoter for the ammonia synthesis process is well established in several different studies[53,54].

Experimental

The starting catalyst of 5% Fe, Co, or Ni supported on HSAG is prepared by incipient wetness impregnation with nitrate solutions of the metals, for a detailed procedure see the experimental section page 53. The samples are first dried and then calcined. The barium promoted samples are made by several incipient wetness impregnations of the prepared 5% metal samples. Between each impregnation the sample is dried and after the final impregnation the sample is calcined.

For testing of the prepared catalyst, 0.25g of catalyst is placed in a stainless steel reactor with an inner diameter of 4.6 mm. The catalysts are reduced in-situ in a 100 mL/min. flow of hydrogen at 500 °C. The catalyst testing was performed in a flow of 20 mL/min. of nitrogen and 60 mL/min. of hydrogen. The temperature was decreased from 500°C in steps of 15°C down to 300 °C. The reduction and testing was done under a pressure of 10 bars. The ammonia concentration in the stream was determined using a Fischer-Rosemount NGA 2000 equipped with a MLT analyzer calibrated to NH_3 concentrations from 0.03-30%.

Results

The data shows that promotion of iron, cobalt, and nickel with barium has very different effects on the activity. This indicates that the three catalysts have different rate limiting steps. The results of rate measurements can be seen in Figure 5.

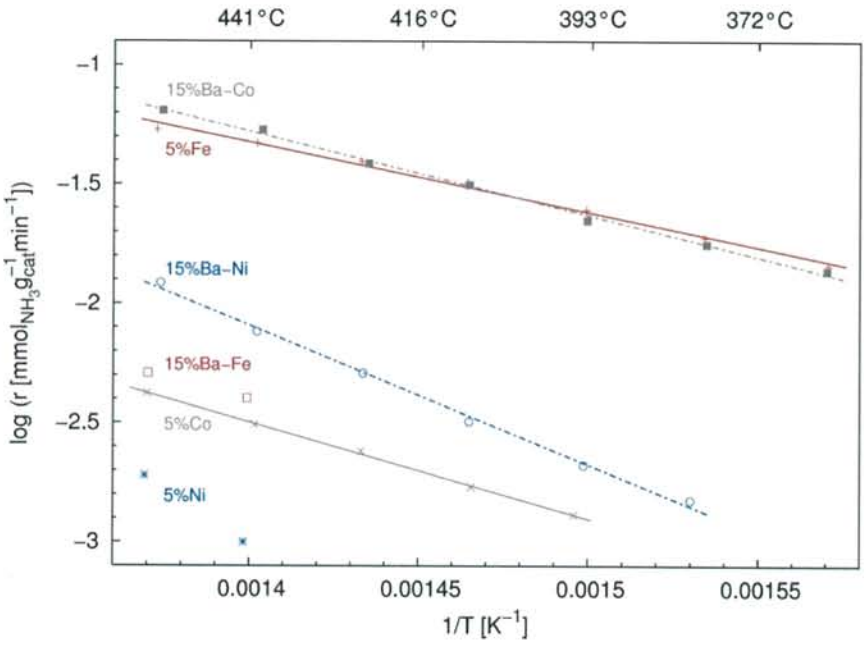

Figure 5: Arrhenius type plot for ammonia synthesis on 5% Fe, Co, and Ni supported on HSAG (solid), and 15% Ba promoted Fe, Co, and Ni supported on HSAG (dashed).

From the plot in Figure 5, it is clear to see that promoting has a significant effect. For cobalt and nickel the effect is an increase in the rate, for cobalt by a factor of ~15, which is in the range that would be expected[55]. For nickel the rate is increased by a factor of ~8, nickel has only gained a little attention as ammonia synthesis catalyst. This is probably due to the low activity in the ammonia synthesis reaction. For iron, on the other hand, addition of barium gives a decrease in the rate to ~1/12. This deactivation effect of barium promotion on iron has earlier been described for high barium loadings (Ba/Fe>1)[56], in this experiment the Ba/Fe ratio is ~1.5.

The big difference in how barium influences the catalysts with similar loadings could indicate that the limiting step in the reaction is different for iron, cobalt, and nickel. This can also be seen in the data from Hagen *et al*[56]. Here they apply simple power-

law kinetics (see equation 1), to a range of different catalysts with iron, cobalt, iron and cobalt combinations, or ruthenium as active metal.

$$r_{NH_3} = kp_{NH_3}^{\alpha} p_{N_2}^{\beta} p_{H_2}^{\gamma} \qquad (1)$$

Experimental determination of the three reaction orders gives varying results for the reaction order of ammonia and hydrogen, depending on catalyst and reaction conditions. The reaction order of nitrogen is given in all literature data as one. At the same time nitrogen dissociation is considered the rate determining step in ammonia synthesis[57]

The reaction order of ammonia varies from -0.1 to -1.6 depending on the active metal. This indicates that ammonia is blocking sites on the catalyst, which could make ammonia desorption slower. The optimal catalyst has low ammonia inhibition, as a higher ammonia concentration in the product stream can then be obtained. The low ammonia inhibition is found on a caesium promoted ruthenium catalyst.

The reaction order of hydrogen varies from -1.2 to 2.3. This is a large difference, from inhibition in some catalysts like ruthenium and unprompted cobalt, to iron and promoted cobalt having a positive effect of hydrogen.

To summarise, several things need to be achieved to have the optimal synthesis catalyst. The catalyst should not be inhibited by ammonia in the product stream, this can be obtained by a ruthenium catalyst. At the same time the catalyst should be able to activate both nitrogen and hydrogen, for this iron is the best catalyst. The cost of iron makes it the favourite industrial synthesis catalyst, but some plants have been build with a final catalyst bed of ruthenium on graphitized carbon by KBR (formerly Kellogg Brown & Root)[58].

Here the data is studied in relation to our experiments and the focus is on barium. The indication is that barium aids in the handling of hydrogen and therefore has an effect on cobalt and nickel which are hydrogen inhibited. With iron there is a large deactivation when promoted with barium, this could be explained by barium increasing the ammonia inhibition.

Summary

The use of ammonia as a backbone in a new energy system is a good possibility. All the technology is already well known. The chemistry of ammonia synthesis is well understood and plants can be ordered "off-the–shelf" from several manufacturers.

The main concern by use of ammonia as an energy storage medium is safety for the end user. This can be solved by using solid ammonia storage as the distribution medium, then the user never comes in direct contact with liquid ammonia.

The chemistry and use of metal ammines as solid ammonia storage medium is discussed in the following sections.

Solid Ammonia Storage in Metal Ammines

The recent idea of using ammonia as a hydrogen carrier has been promoted by the development of safe storage in solid form by binding ammonia in metal ammine complexes[28]. A large number of metals salts are known to form stable metal ammines, and these are generally well described in the classical chemistry literature[59,60,61].

The solid storage of ammonia solves the safety issues of handling ammonia in liquid form under pressure. At the same time, the volumetric hydrogen density is high for the metal ammines compared to that of liquid ammonia and metal hydrides as shown in Figure 6. The figure also compares the mass of the different hydrogen storage materials, when the weight of the storage tank is not taken into consideration. This shows that the metal ammines stand out by being lighter than the metal hydrides, but heavier than the liquids and gasses. The volume of the metal ammines is the smallest of the compared materials.

The current development in high pressure hydrogen storage is a move towards lighter cylinders of composite materials. The composite materials will still have a high weight compared to the stored amount of gas. Further there are the safety issues of using and refilling to pressures between 35-70 MPa. Liquid hydrogen is difficult to handle on a small scale, mainly because of the very low temperature of -252°C and the evaporation loss of 2-3 % per day. The amount of insulation also adds to the mass and volume of the overall storage system[14]. Liquid ammonia needs to be transported in pressurized tanks, and for the safety issues mentioned previous, it appears unlikely to obtain the required public acceptance. This leaves the solid storage of hydrogen and ammonia as the best alternatives for mobile use.

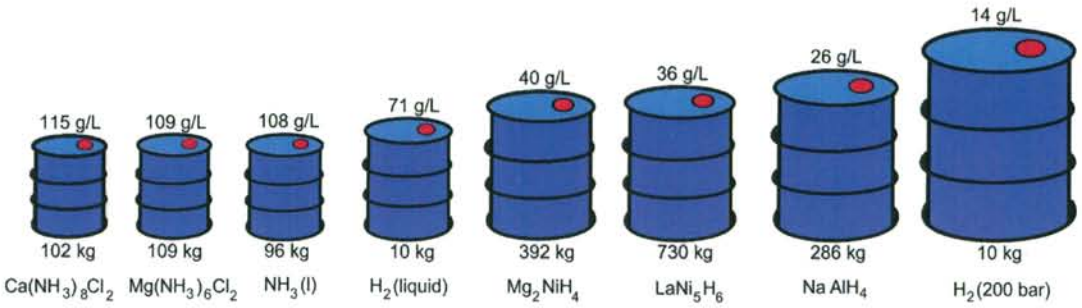

Figure 6: Mass and volumetric densities of 10 kg hydrogen stored reversibly by 8 different methods. Based on the best obtained reversible densities reported in the literature without considering the space or weight of the container [28,62,63,64,65,66,67].

From literature data a van't Hoff plot, showing the logarithm to the equilibrium pressure as function of the inverse temperature can be made for a range of different stable metal ammine salts. The correlation of temperature and pressure in the van't Hoff plot makes it possible to compare the desorption properties of different metal ammine salts. In Figure 7 metal ammines of 10 different metal chlorides are plotted. Chloride as an anion is interesting due to its molecular weight compared to the other halides. Fluoride would be even lower in weight but only a small number of metal ammine fluorides are reported in the literature[68]. The van't Hoff plot, is made from the thermodynamic data using equation 2. The slope is determined by the enthalpy and the intersection with the y axis is defined by the entropy. For the metal ammines all entropies are in the same range from 225 to 240 $Jmol^{-1}K^{-1}$.

$$\ln(P) = \frac{\Delta H_{des}}{RT} + \frac{\Delta S_{des}}{R} \quad \textbf{(2)}$$

There is no reliable entropy data available for all metal ammine chlorides so estimation of the entropy has been necessary for some. In all these cases the entropy is estimated at 230 $Jmol^{-1}K^{-1}$. The error from this estimate is small and does not disturb the general trends seen in Figure 7.

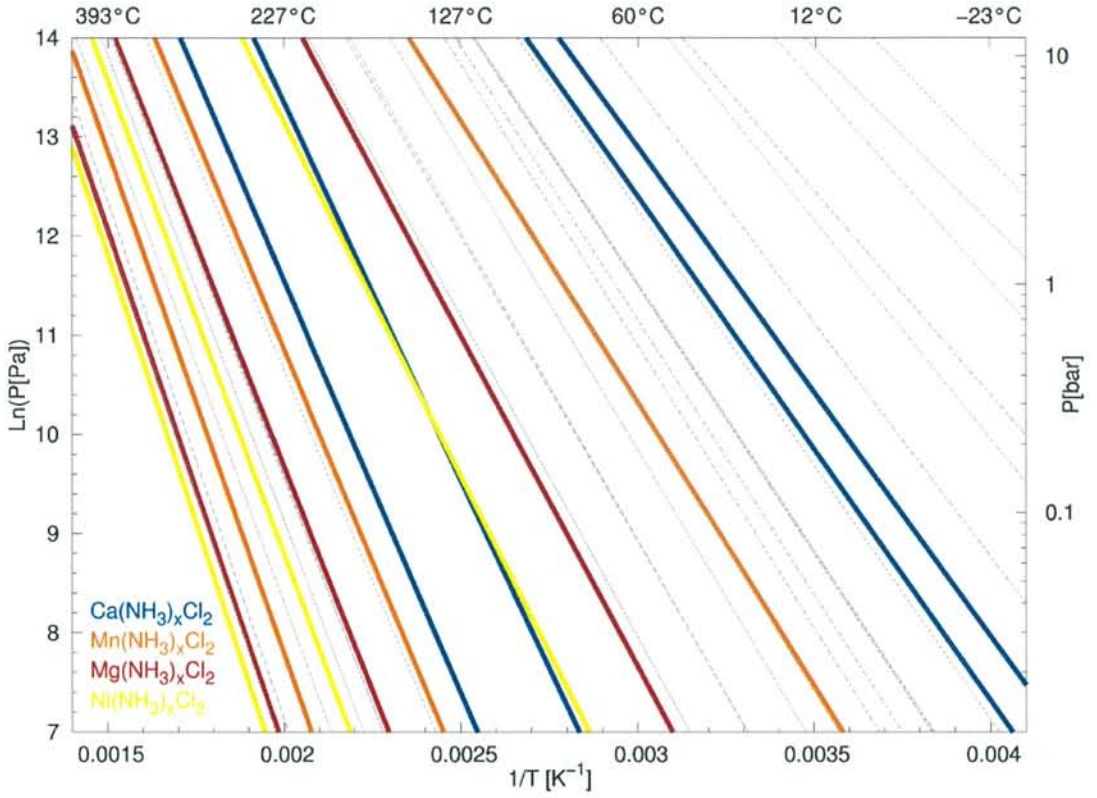

Figure 7: Van't Hoff plot for the metal ammines of 10 different metal chlorides, see Table 2. In the figure the metal ammines of four different salts are highlighted, these salts are chosen for further investigation. Data from[61,69].

The data used for Figure 7 is presented in Table 2, here the enthalpy data and calculated temperature for one bar ammonia pressure is shown for all the different metal ammine chlorides.

The data is used to compare the desorption properties for the metal ammine chlorides and evaluate which is suitable for further investigation. The parameters for investigation are as follows: That desorption should be above room temperature as otherwise handling is complicated further, this corresponds to an enthalpy above 40 kJ/mol for the first useful desorption step. Desorption of all ammonia should be from a solid medium. The base salts should be available in anhydrous form. Further the metal ammine chlorides should have medium to high hydrogen storage capabilities, so low molecular weight of the base salt is preferable. Finally the selected salt should represent a broad group of these elements to show the general trends of the materials of interest. These parameters made us chose $MgCl_2$ due to its high hydrogen storage capability, and being the original salt of interest for making metal ammines[28]. The second salt is $CaCl_2$ that has the highest hydrogen density at room

temperature. Third salt is $MnCl_2$ representing the transition metals medium hydrogen storage capability and midrange desorption temperatures. The final salt $NiCl_2$ is highly stable and forms coloured ammine complexes. It demonstrates the broad range in desorption properties.

Table 2: Desorption data for the metal ammine chlorides of the 10 different metal chloride salts used in Figure 7, with enthalpy of formation and calculated temperature for an ammonia pressure of 1 bar[61,69].

$Li(NH_3)_5Cl$	5->4	4->3	3->2	2->1	1->0
ΔH_{des} (kJ/mol)	33.5	36.8	44.8	48.1	51.9
$T_{1\ bar}$	-24°C	1°C	61°C	85°C	113°C
$Mg(NH_3)_6Cl_2$	6->2	2-1	1-0		
ΔH_{des} (kJ/mol)	55.7	74.9	87.0		
$T_{1\ bar}$	140°C	284°C	371°C		
$Ca(NH_3)_8Cl_2$	8->4	4->2	2->1	1->0	
ΔH_{des} (kJ/mol)	41.0	42.3	63.2	69.1	
$T_{1\ bar}$	32°C	43°C	173°C	226°C	
$Mn(NH_3)_6Cl_2$	6->2	2->1	1->0		
ΔH_{des} (kJ/mol)	47.4	71.0	84.2		
$T_{1\ bar}$	85°C	247°C	340°C		
$Fe(NH_3)_6Cl_2$	6->2	2->1	1->0		
ΔH_{des} (kJ/mol)	51.3	76.2	86.9		
$T_{1\ bar}$	115°C	286°C	360°C		
$Co(NH_3)_6Cl_2$	6->2	2->1	1->0		
ΔH_{des} (kJ/mol)	54.0	78.1	88.3		
$T_{1\ bar}$	135°C	300°C	371°C		
$Ni(NH_3)_6Cl_2$	6->2	2->1	1->0		
ΔH_{des} (kJ/mol)	59.2	79.5	89.8		
$T_{1\ bar}$	176°C	310°C	381°C		
$Zn(NH_3)_6Cl_2$	10->6	6->4	4->2	2->1	1->0
ΔH_{des} (kJ/mol)	29.6	44.8	49.5	80.4	104.3
$T_{1\ bar}$	-33°C	59°C	95°C	327°C	504°C
$Cd(NH_3)_{10}Cl_2$	10->6	6->4	4->2	2->1	1->0
ΔH_{des} (kJ/mol)	31.0	42.7	44.8	70.7	75.3
$T_{1\ bar}$	-42°C	45°C	60°C	184°C	288°C
$Pb(NH_3)_8Cl_2$	8->3¼	3¼->2	2->1½	1½->1	1->0
ΔH_{des} (kJ/mol)	34.3	39.3	46.0	47.3	55.7
$T_{1\ bar}$	-5°C	19°C	68°C	73°C	138°C

From literature data some general trends for the stability of different metal ammines can be found. For the halides the stability increase down through the group in the order (F<)Cl<Br<I[61], the stability of fluorides is not well understood and only limited data is available. The main problem with metal fluorides is that they do not react with ammonia directly in an absorption process.

For the cations the trend is different, here the stability decreases down through the groups. This can be seen for the alkali metals which have decreasing stability in the order Li>Na(>K>Rb)[61]. For potassium and rubidium there are no metal ammine halides, that are stable at room temperature. The metal ammines of potassium and rubidium are made in liquid ammonia cooled by dry ice[61].

The alkali earth metals show similar trend with a decreasing stability in the order Be>Mg>Ca>Sr>Ba[61,70]. The divalent earth alkali metals are generally more stable than the univalent alkali metals. This could be due to the different crystal structures of the salts that make earth alkali metals more stable.

For the transition state metals the stability increases from manganese to nickel in the order Mn<Fe<Co<Ni[61]. At the same time the stability seems to go down when going down through the groups Cu>Ag>Au[61,71] and Zn>Cd>Hg[61,72]. This is the same trend as for alkali and earth alkali metals.

To summarize the stability investigation it can be observed that small cations make more stable ammines and that large halides make more stable metal ammines. This is seen by decreasing stability down through the groups for the cations and increasing stability for halides down through the group.

Experimental

Preparation

The four metal ammines are prepared from the anhydrous base salts, $CaCl_2$, $MnCl_2$, $MgCl_2$, and $NiCl_2$. The anhydrous salts are transferred to a specially designed reactor in a dry atmosphere. The reactor is designed for temperatures of up to 600 °C, with gas inlet and outlet valves. The reactor is electrically heated and can be cooled by water. Temperature measurements are made in the middle of the reactor. The anhydrous salt is heated to 400-500°C under a flow of argon. This is done to remove any water either by desorption, which is preferred, or by decomposing to form the oxide and hydrochloric acid. The dried metal chlorides are cooled and the reactor flushed with gaseous ammonia for several minutes. Then the reactor outlet is sealed and an ammonia pressure of 4 bar is applied. The metal chlorides absorb ammonia and form the metal ammine chlorides. The pressure is applied to increase the absorption rate and ensure full saturation of the metal ammines. Each metal ammine

halide was pressed into tablets to determine the maximal bulk density of the storage material.

Temperature Programmed Desorption

Desorption characteristics were determined by temperature programmed desorption (TPD). Samples of approximately 0.5g were transferred to a closed test tube under NH_3 atmosphere and heated following a desired temperature ramp. NH_3 was released into a carrier stream of Ar through a T-joint with a thin connection tube to maintain the NH_3 atmosphere over the sample. This procedure gave an NH_3 pressure slightly above atmospheric pressure over the ammine sample. The ammonia content in the carrier stream was determined using a Fischer-Rosemount NGA 2000 equipped with an MLT analyzer calibrated to NH_3 concentrations from 0.03-30%. Desorption rates were calculated from the ammonia content in the carrier stream and the flow of Ar, which was kept constant at 213 NmL/min using a calibrated Brooks 5850 TR mass flow controller. For all four ammines, TPDs were obtained with heating rates of both 1 and 5 K/min.

Results and Discussion

The indirect hydrogen storage capabilities of the metal ammine salt were tested by pressing the prepared metal ammines into solid tablets and measuring their weight and volume. The result of this are compared to the crystal densities that can be calculated from the lattice constants, the result is shown in Table 3.

Table 3: Tablet densities, volumetric, and gravimetric hydrogen densities[73].

	ρ_{tablet} g/cm^3	% of $\rho_{crystal}$	Volumetric H kgH/L	Gravimetric H wt%H
$Ca(NH_3)_8Cl_2$	1.18	99	0.12	9.78
$Mg(NH_3)_6Cl_2$	1.19	95	0.11	9.19
$Mn(NH_3)_6Cl_2$	1.34	95	0.11	7.96
$Ni(NH_3)_6Cl_2$	1.41	95	0.11	7.83

The data in Table 3 show that it is possible to obtain hydrogen densities in solid metal ammine tablets close to the theoretic limit of the crystal density. Desorption of ammonia from solid tablets of metal ammines is fast and only limited by heat transfer through the salt[76].

Under the formation of metal ammine the lattice expands resulting in a volumetric growth of the starting salt with a factor of 4-6. This expansion need to be taken into account under the absorption process. At the same time the absorption of ammonia is exothermic resulting in shift of the solid gas equilibrium towards higher ammonia pressure over the sample. To optimize the absorption process three parameters are important: the ammonia pressure over the sample; heat removal as the absorption is exothermic; and finally mixing to minimize the diffusion path way. The pressure difference between the equilibrium pressure and the applied ammonia pressure is the driving force of the process. This favours high ammonium pressures. Heat removal is important as an increase in temperature gives a higher ammonia equilibrium pressure slowing the reaction. Finally good mixing shortens the diffusion pathway and helps with a uniform saturation, minimizing the chance of blocking due to increasing volume. For optimal energy efficiency the heat from the exothermic absorption should be recovered.

Desorption characteristics for the four metal ammine chlorides during TPD are shown in Figure 8. As expected from literature data, the trend in temperature for the first desorption peak is Ca<Mn<Mg<Ni.

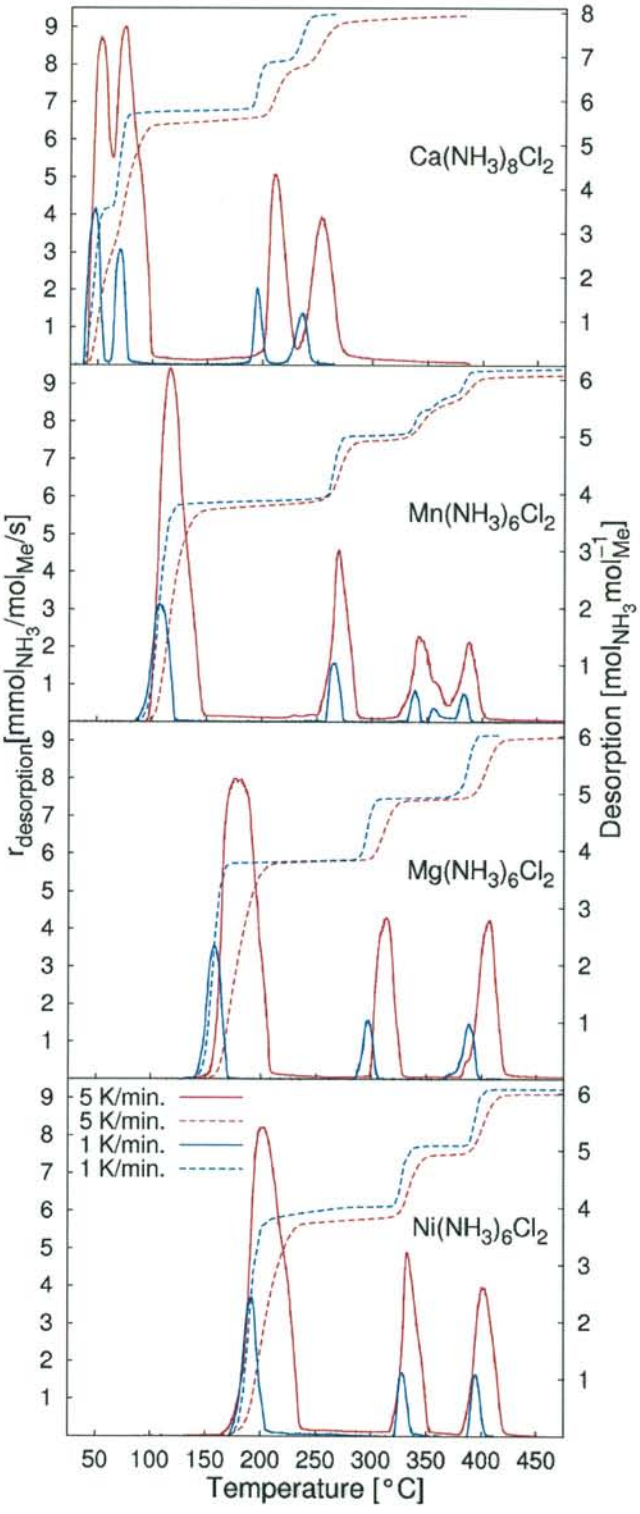

Figure 8: TPDs of $Ca(NH_3)_8Cl_2$, $Mn(NH_3)_6Cl_2$, $Mg(NH_3)_6Cl_2$, and $Ni(NH_3)_6Cl_2$, with a temperature ramp of 5 K/min (red) and 1 K/min (blue). The solid lines show the desorption rate and the dashed lines show the amount of ammonia desorbed pr. metal[73].

During TPD, $Ca(NH_3)_nCl_2$ has stable compositions with n = 8, 4, 2, 1 and essentially all ammonia desorbs in the temperature range 20-280°C. $Mn(NH_3)_nCl_2$ has stable compositions with n = 6, 2, 1 and two compositions with n<1. Stable structures with less than 1 ammonia molecule pr. metal atom are well known for a range of transition metal complexes, and are not unlikely even though they have not previously been reported for $MnCl_2$. Essentially all ammonia desorbs in the temperature range 80-400°C. TPDs of $Mg(NH_3)_nCl_2$ were also reported previously and have stable compositions with n = 6, 2, 1. Essentially all ammonia desorbs in the temperature range 130-430°C. During TPD, $Ni(NH_3)_nCl_2$ has stable compositions with n = 6, 2, 1 and all ammonia desorbs in the temperature range 169-430°C. Independently of the temperature ramp, all the TPD peaks start within few degrees of the temperature for 1 bar equilibrium pressure calculated from literature data[69].

This and the near exponential rise in desorption rate with temperature indicates that desorption is equilibrium limited even at high desorption rates.

If we compare the calculated temperatures of one bar ammonia pressure in Table 2 to the onset temperature of ammonia desorption in Figure 8. It is clear that the calculated and measured values of desorption temperatures is almost identical for all but one measurement. For the fast ramping of $Mg(NH_3)_6Cl_2$ the measured temperature is above the calculated. This is properly due to bad placement of the thermocouple in the experiment. The placement of the thermocouple on the outside of the reactor can give this kind of problems, it needed to be place directly outside the reactor were the sample are. In the setup it s not possible to put the thermocouple inside the reactor, as this will make it even more difficult to keep the sample in an ammonia atmosphere under the entire preparation and testing. Otherwise it measures the temperature of the oven instead of the sample temperature. The heat gradient is also larger with fast ramping as desorption rate increases and require faster energy transfer to the sample.

To demonstrate that ammonia also can be desorped from solid tablets of metal ammine salts, a solid tablet of $Ni(NH_3)_6Cl_2$ was heated, see Figure 9. The first picture shows the fully saturated $Ni(NH_3)_6Cl_2$ with clear purple colour. When this is heated ammonia desorped seen as the green colour of $Ni(NH_3)_2Cl_2$. When the green of $Ni(NH_3)_2Cl_2$ is broken the desorption front is clearly visible as the tablet have a purple centre. When all ammonia is desorped the yellow $NiCl_2$ is left.

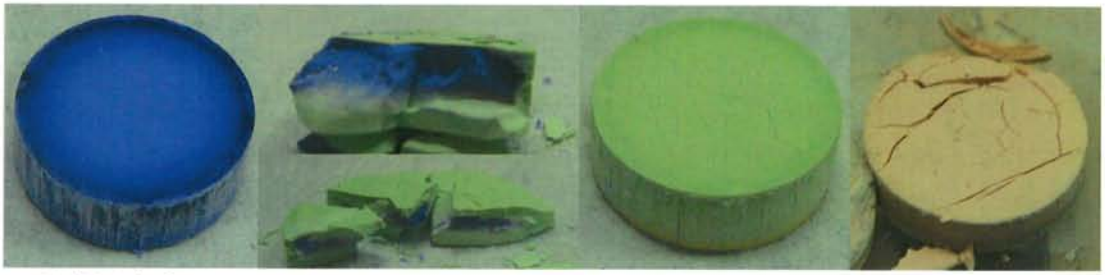

Figure 9: Desorption of ammonia from solid tablet of $Ni(NH_3)_6Cl_2$.

The desorption of ammonia from $Ni(NH_3)_6Cl_6$ is shown as pictures in Figure 9, this demonstrates how the desorption is going in steps, like the TPDs in Figure 8. At the same time the intermediate desorption shows that the desorption moves through the tablet with the heat front. Another reason for the fast desorption is the intrinsic formation of a nanoporous, sponge-like skeletal structure from the compact metal ammines during ammonia desorption, which has recently been documented in a detailed *in situ* small-angle X-ray scattering (SAXS) study[74]. This is an important aspect, since compact tablets of metal ammines maintain their physical shape, as seen in Figure 9, even after desorption of all the ammonia, corresponding to a loss of approximately half the mass and three quarters of the occupied volume. The formation of nanopores has also been investigated by density functional theory (DFT) calculations, which show that metal ammine crystals can release ammonia by a change of the lattice constant and a slight internal rearrangement; this can be interpreted as the individual crystallites gradually shrinking to form pores[75]. The formation of nanopores makes the diffusion of ammonia through the salt fast. This also shows that the limiting step for desorption of ammonia from metal ammine salts is heat transfer. Heat transfer is limited, because the metal ammines are poor heat conductors, this result in ammonia gas being the main conductor of heat through the metal ammines [76] and as gases have limited heat capacity this slows desorption.

The slow heat transfer can be seen in the TPDs in Figure 8 as a shoulder in the TPD experiments with fast heating. This is most clearly seen for the metal ammines of calcium and nickel, ramp of 5K/min. Here a clear shoulder is visible in the end of the first desorption peak indicating that a heat gradient through the sample results in uneven desorption of ammonia. Further the broadening of the desorption peaks at faster ramping also indicates heat transfer being the limiting factor of the experiment. This becomes even more pronounced with desorption from solid tablets,

as seen in Figure 9, where there are clearly different phases in the tablet going from hexa-ammine to di-ammine.

For practical purposes a temperature and desorption gradient through the sample is not only a bad thing. The broader desorption intervals makes it easy to get uniform ammonia desorption and a suitable ammonia gas pressure. The use of metal ammines as solid ammonia storage has also been demonstrated to work in large scale by Amminex A/S[77], who is selling their storage material under the trade name AdAmmine.

Summary

The possibilities of using metal ammines as an indirect hydrogen storage medium have been investigated. The experiments demonstrate that all the metal ammine salts have facile ammonia desorption kinetics that is limited by heat transportation in the materials.

The known thermodynamic data can be used as a valuable tool for predicting the desorption temperatures of the metal ammines and thereby choose the best metal ammine for the application.

Catalytic Ammonia Decomposition

The development of solid ammonia storage in metal ammine salts makes it interesting to look further into efficient use of ammonia as an energy carrier. For ammonia as an energy carrier to work better knowledge and understanding of the conversion of ammonia back to hydrogen is needed.

Ammonia can be converted into energy by catalytic decomposition or oxidation. The catalytic oxidation is done in a range of fuel cells running directly on ammonia. The catalytic decomposition is studied as a way of converting ammonia into hydrogen and nitrogen, and this decomposition could be used in fuel cell applications.

The ammonia decomposition reaction has a long history[78], mainly as a way to gain further information on the catalytic ammonia synthesis[79,80]. The focus on optimizing and understanding the synthesis catalyst has in the last decade start shifting towards using ammonia as an alternative hydrogen carrier. This has developed into specialized research in producing CO_X free hydrogen from ammonia by catalytic decomposition.

The development of a solid ammonia storage medium has further promoted the interest for ammonia as an indirect hydrogen carrier[81].

In the following, different uses of ammonia as an energy storage medium will be described. The main focus will be on research in ammonia decomposition and understanding the catalytic process.

Ammonia and fuel cells

Solid Oxide Fuel Cells

The direct use of ammonia in high temperature Solid Oxide Fuel Cells (SOFC) has been shown to work with a performance similar to pure hydrogen[82,83]. The SOFC can also run on other fuels such as methanol or methane, but these fuels need to be reformed and this leads to the possibility of carbon poisoning of the anode[84,85]. The CO_X free ammonia can be fed directly into a high temperature SOFC and the endothermic ammonia decomposition reaction will help cool the SOFC which, combined with an entropy gain, means that ammonia as a direct fuel increases the fuel cell performance at high temperatures[86].

In the SOFC, ammonia is decomposed directly on the nickel anode. The high operating temperatures (>750°C) and constant removal of hydrogen makes it possible to achieve full conversion if desired. Normally SOFC stacks run with a fuel conversion of 80-90% in the fuel cell and a burner for conversion of leftover fuels.

The high temperatures needed in a SOFC system gives the possibility of using a large range of metal ammines as ammonia storage materials. The heat from the SOFC stack can easily be used for ammonia desorption and thereby increasing system efficiency.

The main problem with SOFC is that they cannot handle thermal cycling. Therefore they are mainly designed for stationary or large scale application where they are not turned off and on. In stationary and large applications the need for solid ammonia storage is small as handling of liquid ammonia is easy, safe and a well known technology[29,30].

Direct Ammonia Fuel Cells

Direct ammonia fuel cells (DAFC) are a broad range of intermediate temperature fuel cells that all operate on ammonia. A range of different types has been suggested and tested, these include molten alkaline hydroxides[87], in this setup the electrolyte is a molten eutectic mixture of NaOH and KOH. This mixture has a low melting point of 170°C. The setup uses nickel both as anode and cathode, the oxidant is air and the fuel ammonia gas. The test is performed at intermediate temperatures from 200-450°C and the results show this to be a possible way of lowering the operating temperature and still use ammonia as fuel. Another idea for a DAFC is a $BaCe_{0.8}Gd_{0.15}Pr_{0.05}O_3$ (BCGP) electrolyte with a NiO on $BaCe_{0.85}Eu_{0.15}O_3$ (Ni-BCE) anode and platinum cathode[88]. This FC runs at temperatures of 400-600°C. This setup is using a proton conducting ceramic as electrolyte which helps the ionic conductivity compared to oxide conducting ceramics in SOFCs[29,30].

Low temperature Fuel Cells

In low temperature fuel cell systems, such as polymer electrolyte membrane (PEMFC), Phosphoric acid (PAFC) and Alkaline Fuel Cells (AFC), ammonia needs to be decomposed to hydrogen and nitrogen before it is fed to the fuel cell. Furthermore the ammonia tolerance on PEMFC and PAFC are very low, therefore cleaning of the

reformed ammonia is necessary to get ammonia content down to below 1 ppm[89]. Removal of ammonia from the feed can be done by absorption in an acidic medium for instant an acidic solution or a solid acid. The benefits of using low temperature FC is that they can tolerate the thermal cycling of turning the stack on and off. They are more compact and also easier to produce. The low temperature also makes it easier to find suited materials. The problem is that the active catalyst is platinum. Platinum is expensive and quite large amount is needed to operate a fuel cell stack. Furthermore most commercially available fuel cell stacks are PEMFC this makes it interesting to design a system that uses available technology[29,30].

Ammonia Decomposition

From the literature it is easy to find investigations of different ammonia decomposition catalysts for delivering hydrogen to a fuel cell stack[90,91,92,93,94,95]. The ammonia decomposition reaction has traditionally been studied to gain more information about the ammonia synthesis catalyst[80,96,97,98].

The studies of catalytic decomposition of ammonia are done under a range of different conditions. The old literature focused on understanding the synthesis process by studying decomposition, this is done in low ammonia pressure[79,80,96,97,98]. For hydrogen production an ammonia pressure of around 1 bar is preferred. For hydrogen production catalyst performance close to full conversion is interesting, to maximize the hydrogen production and minimizing the amount of unconverted ammonia left in the gas.

The equilibrium pressure of ammonia is reached differently in decomposition and synthesis, this is important for understanding why it can be difficult to compare them. For ammonia decomposition, the equilibrium is approached from high ammonia concentration and ends with less than one percent ammonia concentration in the outlet at ambient pressure and temperatures of 400-600°C[99]. In synthesis the equilibrium is reached from no ammonia to around 5-10% at high pressure (200-250bar) and temperatures from 350-500°C. The high temperature for the ammonia decomposition reaction is needed to force the equilibrium towards full conversion. At present, the commercially used catalyst for ammonia decomposition is nickel supported on alumina[100]. The catalyst is mechanically strong and heat resistant, but further development and optimization is needed. To understand the role of the

catalysts for ammonia decomposition a more detailed understanding of the reaction kinetics is necessary.

Kinetic of Catalytic Ammonia Decomposition

The basic kinetics of ammonia decomposition can be illustrated in a micro kinetic model. Here the reaction is split up into small steps that can be handled individually on a theoretic level.

$2NH_3(g) \rightarrow N_2(g) + 3H_2(g)$ (a)

$NH_3(g) + {}^* \rightarrow NH_3{}^*$ (b)

$NH_3{}^* + 3^* \rightarrow N^* + 3H^*$ (c)

$2\,N^* \rightarrow N_2(g) + 2^*$ (d)

$2H^* \rightarrow H_2(g) + 2^*$ (e)

Where * is a free surface site.

The overall reaction (a) is split up into four elementary reactions (b-e), the first is adsorption of ammonia on the surface (b), the ammonia adsorption kinetic is fast and exothermic. The next process is N-H bond cleavage (c), this is considered rate determined step (RDS) in combination with the recombinative ammonia desorption (d). The final reaction is hydrogen desorption (e), this reaction is fast, but at high hydrogen pressures it results in hydrogen inhibition due to adsorbed hydrogen blocking the active surface[91,101,102]. The literature on the kinetics of ammonia decomposition generally agrees on expressing the rate in a simple power-law model, see equation 3.

$$-r_{NH_3} = kP_{NH_3}^{a}P_{H_2}^{b} \text{ where } k = k_0 e^{-\frac{E_{app}}{RT}} \qquad (3)$$

Depending on the specific catalyst the values of *a* and *b* change. The reaction order of nitrogen is zero in all available literature[96,97]. This is different from ammonia synthesis were the reaction order of nitrogen is one. Typical values of *a* is 0 to 1 and the values of *b* -2 to 0[92,101,103]. These values are derived from a range of experiments using different reaction conditions. The reaction pressure over the catalysts is changed from vacuum to atmospheric pressure so a large variation is to be expected. At vacuum to low pressure the reaction order for ammonia is often zero and steadily increases. At pressures close to ambient pressure, the reaction order of ammonia is normally 0.5-1, depending on the catalyst. The reaction order of hydrogen is often zero at pressure of around 1 bar[92].

The apparent activation energy is also dependant on the catalyst and the reaction conditions. For experiments at vacuum to low pressures the apparent activation energy is lower than it is at ambient pressure, this indicates a change in the rate determining step. There are basically three things that can be changed in the catalyst: the active metal, the support material and the promoter.

Active Metals for Catalytic Ammonia Decomposition

The main focus on active metals for the ammonia decomposition is the transition metal series. All the transition metals have been investigated for their activity in the decomposition of ammonia[96,97]. The most investigated active metals are: iron[96,97,104,105,106,107], cobalt[96,97,106,108], nickel[96,97,107,109,110,111], and ruthenium[96,97,107,112,113,114,115]. A range of other metals have also been investigated for their activity as ammonia decomposition catalysts. Some of these include: vanadium[116,117], molybdenum[118], tungsten[119,120,121], rhodium[96,97,107,122], paladium[107], iridium[123,124,125], and platinum[92,96,97,107]. Of these metals only molybdenum and iridium shows some significant activity, all the others have very low activities or were investigated only under very low pressures. .

A useful way of comparing the activity of ammonia decomposition catalysts is by construction of a volcano plot. In a volcano plot the rate of ammonia decomposition is plotted against a descriptor. An example of such a volcano curve can be seen in Figure 10. In the figure the calculated and measured rate is plotted against the dissociative nitrogen adsorption energy.

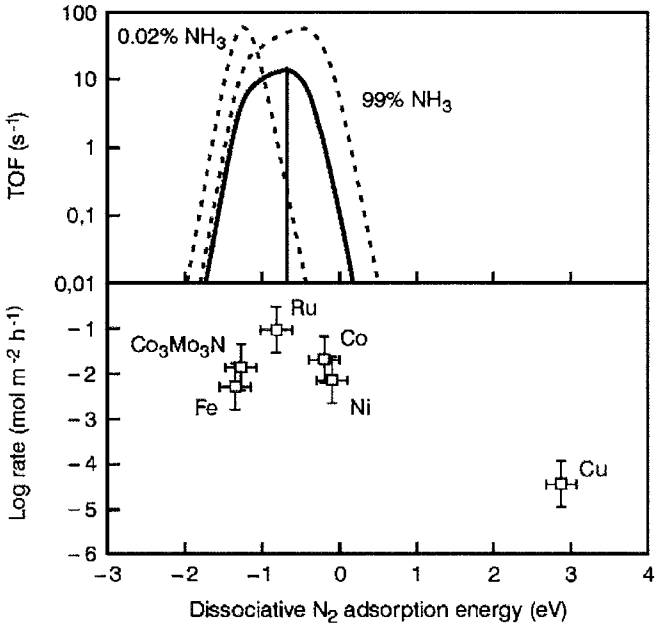

Figure 10: Calculated turnover frequencies of ammonia synthesis/decomposition at 773 K, 1 bar, 3:1 H_2/N_2, and 0.02%, 20% (solid line), and 99% NH_3 as a function of the reaction energy of dissociative N_2 adsorption (Top). Experimental rates of ammonia decomposition over various catalysts at 773 K, 1bar,3:1 H_2/N_2, and 20% NH_3 (bottom)[99].

The data in Figure 10 can be used to predict which catalyst would be optimal at the given reaction conditions. In this example, ruthenium stands out as the best catalyst under decomposition conditions with high ammonia concentration, but also cobalt can be seen as a good alternative.

In the rest of this report the focus will be on ruthenium, iron, cobalt, and nickel. They are all investigated under a range of different conditions and with the use of different support materials and promoters. The effect of support and promoters on the catalytic activity is described in the following with the focus of how the support and promoters interact with the catalyst and their role in the process.

Support Materials in Ammonia Decomposition Catalysts

The second parameter that can be changed is the support material, a range of different support materials has been tested in the literature and it can be difficult to make a direct comparison of different studies. Materials studied as support in ammonia decomposition catalyst are many, in the following some of the more promising are described. Alumina is the traditionally support for nickel oxide

particles and several studies report on this catalyst[92,126], however alumina is generally a rather poor support for ammonia decomposition[127,128]. Another oxide used is potassium hydroxide treated ZrO_2[129]. This support reveals some interesting features as a digestion process with a strong alkaline solution gives higher activity compared to the untreated oxide. This indicates that making a support more alkaline is good for reactivity, which in part also explains why Al_2O_3 is a poor support due to high acidity. Different silicon oxides have also been used as support materials for both nickel and ruthenium catalyst. The catalytic activity of ruthenium and nickel supported on SiO_2, SBA-15, and MCM-41 show that the change in support material only changes the activity slightly[124,130,131]. Generally, MCM-41 is slightly better than the others, but this is probably due to the higher surface area of the support and not directly related to the structure. Different magnesium compounds are also used as support materials in the ammonia decomposition reaction, materials like $MgAl_2O_4$-spinel[132] and MgO[115,133]. $MgAl_2O_4$-spinel as a support material for ruthenium based catalyst is relative active compared to some of the other oxide supports. $MgAl_2O_4$-spinel is not studied as much as alumina and silica. The alkaline MgO is the best oxide support in the ammonia decomposition reaction, almost as active as graphitized carbon. Carbon in different forms is probably the most tested support material for ammonia decomposition catalyst and it is generally agreed upon that graphitized carbon and cabon nano-tubes (CNT) are the support materials with highest activity for ammonia decomposition[94,134,135,136]. Several studies has looked specially of the role on different carbon supports[137,138].

The study by Li *et al.*[137] investigates the influence of the carbon support on the catalytic activity. This is done by investigation of six different carbon supports for the ammonia decomposition with ruthenium particles. The six different carbons are: activated carbon (AC), 2 versions carbon black (CB), a synthesised and a commercial version; a commercial mesoporous CMK-3, CNTs, and graphitized carbon (GC). For all materials the porosity, surface area, x-ray diffraction (XRD) and dispersion of ruthenium is measured. The results show that the most important parameter for the activity is the degree of graphitization as determined from XRD. For the porosity, surface area and ruthenium dispersion there is no correlation to the activity, this can be seen by the fact that CNTs have higher dispersion, surface area and porosity than GC and still have a significant lower activity. The same can be seen by comparing the two different CBs where the dispersion of the two materials is close to same value but the commercial has a 10 to 12 time higher surface area but is still lower in activity due to lower degree of graphitization. The very high correlation between

graphitization and activity is explained by the graphite being able to easily conduct electrons from the support to the active site. This is supposed to help the nitrogen recombinative desorption normally considered as one the rate limiting steps in combination with N-H bond cleavage.

Another interesting study by Li *et al.*[138] investigated the influence of different treatments of a CMK-3 carbon support. The CMK-3 in itself is a rather poor support for ruthenium in ammonia decomposition. The treatment comprises a range of acid and alkaline solutions. The results show that the treatment has a significant influence on the catalytic properties. The problem is that the change observed, is not only due to the acidic or alkaline treatment, but more as a consequence of the chosen counter ion, as it is well known that alkali and earth alkali metals can act as promoters for the decomposition reaction. At the same time, halogens like chloride will often deactivate the catalyst for a long period of time until it is removed. In the following, a more detailed study of the promoter effects known for ammonia decomposition is discussed.

Promoters for Ammonia Decomposition Catalysts

Promoters are an important factor for ammonia decomposition and many different studies have been made on promoter effects[103,105,110,111,133,135]. The most studied promoters for ammonia decomposition are the alkali and earth alkali metals, but lanthanum and cerium have also been studied. The promoter can typically increase the reaction rate or stabilize the catalyst, but is in itself not catalytically active. Promoters can increase the reaction rate in a range of ways: they can help lowering the activation energy barrier; can stabilize smaller more active catalyst particles; or prevent deactivation of some of the active sites.

Several studies of the promoter effects of the alkali metals have found that the promoter order of the alkali metals is Cs>K>Na>Li[136,138,139] for supported ruthenium catalysts. For the earth alkali metals the promotion effect is Ba>Ca[136,138] again for supported ruthenium catalysts. Lanthanum and cerium has mostly been investigated as promoters for nickel catalysts[103,110,111]. The most studied promoters are caesium and barium for ruthenium catalysts, this is mainly due to ruthenium having the highest activity for ammonia decomposition[94,127,132,134]. The barium and cesium promoted ruthenium catalysts have been investigated even more in depth for the

ammonia synthesis reaction[140,141,142,143,144,145,146]. The synthesis data for these promoters is useful in understanding how these promoters work.

The studies of decomposition and synthesis are done under different reaction conditions, but a lot of information can still be gained from the data. The first observation is that different promoter to ruthenium contents are optimal for barium and caesium. Several studies show that a barium to ruthenium ratio of 0.7-1 and a caesium to ruthenium ratio of around three are optimal for ammonia synthesis[141,142]. The same ratios have been applied in the study of decomposition catalyst[94,132,134]. For the ammonia synthesis it has also been shown that the promoter effect of caesium and barium is additive[142,145]. The additive effect shows that the two promoters work differently, furthermore barium is the best single promoter in synthesis and caesium is the best single promoter in decomposition. The surface species for a synthesis catalyst is dominated by hydrogen and ammonia. In ammonia decomposition the surface is dominated by adsorbed nitrogen, but also hydrogen. The rate determining step in ammonia synthesis is dissociation of nitrogen, so barium can help increase the rate of adsorption and dissociation of nitrogen by adding active sites for this process. This could also explain why barium is a better promoter for synthesis than for decomposition of ammonia. Caesium is the best promoter for ammonia decomposition[132,133,134], the literature suggest that caesium helps in desorption of hydrogen. The high amount of caesium needed to gain the optimal promoter effect is not well understood. Some have suggested that a large part of the caesium interacts with the support rather than the ruthenium particles[146]. Therefore the support needs to be saturated before the optimal effect of the promoter is seen. Some of our results show that for iron, cobalt, and nickel this is not the case.

Summary

The data shows that using ammonia as an indirect hydrogen storage medium is a viable solution to the problem of transporting hydrogen. The literature gives at lot of useful information of catalysts for ammonia decomposition. The activity of a large range of metals is described in the literature and there is a common agreement that caesium promoted ruthenium, supported on GC is the most active catalyst.

The effects of the promoters for ammonia decomposition catalyst are well known, but the working mechanism is mostly speculated. Furthermore only ruthenium has

been tested for promoter effects of barium and caesium in any details. Therefore; it was decided to investigate the effect of barium and caesium on iron, cobalt, and nickel. This is done to gain information on how the promoters work in relation to the catalytic properties of the three different metals.

Testing of Ammonia Decomposition Catalysts

The experimental section is focused on two different projects. The first project is a investigation of the promoter effect of barium and caesium on iron, cobalt, and nickel, supported on high surface area graphite (HSAG). This part will discuss and analyze the effect of the promoters. The aim is to get a more detailed understanding of the promoter mechanism. The second project reports the use of nanostructured titanates with incorporated alkali metal promoters as support materials for ruthenium in the ammonia decomposition, the aim being to show that by designing novel materials, the activity of ruthenium can be enhanced. The support material and final catalyst is tested for catalytic activity and characterized in an attempt to try and understand the support effect.

The use of iron, cobalt, and nickel as ammonia decomposition catalysts is done to get a more detailed understanding of how the promoters caesium and barium work. There has been several studies of both promoters on ruthenium, these have come up with a range of theories of how the promoters work[94,127,132,134]. The problem is that on ruthenium both barium and caesium have a promoting effect and this effect is additive[142,145]. This makes it difficult to separate the effect of the individual promoter, but it can with high probability be said that caesium and barium promote different parts of the process. To get more information on the promoter effect active metals that are further from the top in the volcano plot (see Figure 10), should have different rate determining steps depending on which side of the peak they are located on. The HSAG support is known to be highly active for ruthenium and doesn't react with the active metals at high temperatures as can be seen with some oxide supports.

The second project concerns with synthesis and use of nanotitanates as support material for ruthenium, started as a way of using the nanotitanates, $Na_2Ti_3O_7$, $K_2Ti_6O_{13}$, and $Cs_2Ti_6O_{13}$, as support materials in a catalytic process. The ammonia decomposition is ideal as it is well known that alkali metals have a promoting effect. The synthesized nanotitanates show remarkable activity compared with pure titania as a support for the ruthenium catalyst. This effect was larger than expected from just simply the promoter effect, and therefore a more detailed study of the support was undertaken.

Experimental for Iron, Cobalt, and Nickel Catalysts

Catalyst Preparation

The catalysts were prepared in two steps: first a starting batch of catalyst (~5g) was prepared, and then samples from this were used for promotion tests.

The starting catalyst was prepared from a solution of the metal nitrate using incipient wetness impregnation on Timrex HSAG300 to a final metal concentration of 5 wt%. The prepared sample was dried and calcined at 250°C in air for 3h. The calcined catalyst was then pre-reduced in a flow of hydrogen overnight at a temperature of 400°C.

For promotion 0.5g of the starting catalyst was impregnated with a nitrate solution of barium and caesium to the desired concentration (5 or 15 wt%). The promoted sample was then calcined in air at 250°C for 3 h.

Catalyst Testing

The catalyst testing was performed in a specialized setup for ammonia decomposition, see Figure 11. 0.1g of catalyst was transferred to the stainless steel reactor with an inner diameter of 4.6 mm, where it was reduced for 5 hours at 500°C in a 100 ml/min flow of hydrogen. The testing was done from 600°C and decreasing in steps of 15°C whilst maintaining a flow of 20 ml/min ammonia and 50 ml/min argon. The ammonia concentration in the carrier stream was determined using a Fischer-Rosemount NGA 2000 equipped with a MLT analyzer calibrated to NH_3 concentrations of 0.03-30%.

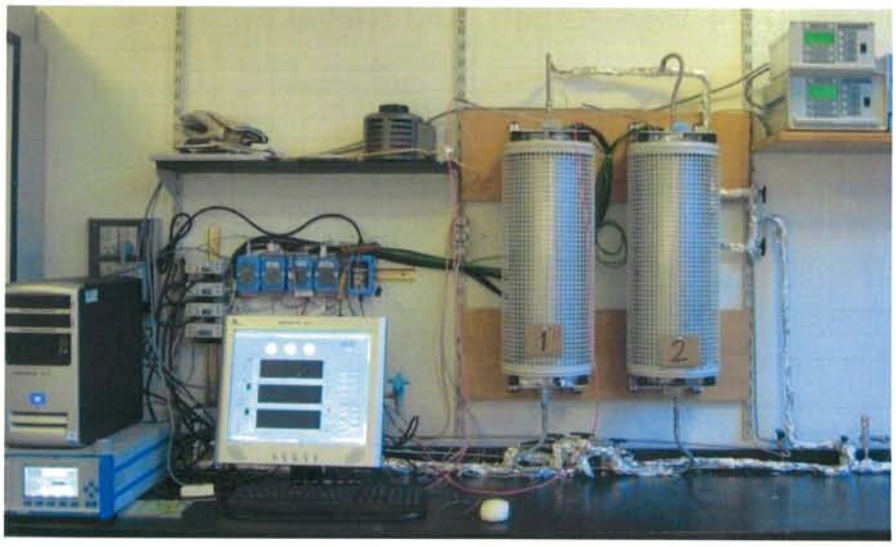

Figure 11: Experimental setup for testing ammonia decomposition and synthesis catalysts.

Catalyst Characterization

The interesting catalysts were also investigated using transmission electron microscopy (TEM) and energy dispersive x-ray spectroscopy (EDX), with the help of Wiebke Frandsen at Fritz Haber Institut der Max Planck Gesellschaft in Berlin, using Philips CM200 microscopes.

Experimental for Nanotitanates

Catalyst Preparation

Synthesis of Alkaline Titanate Nanomaterial Supports

Alkaline nanostructured titanates were prepared by hydrothermal treatment of TiO_2 (Sigma-Aldrich anatase nanopowder) with different alkaline bases. The hydrothermal treatment of TiO_2 was done with NaOH (Sigma-Aldrich 98%), KOH (Sigma-Aldrich 90%), and $CsOH{\cdot}H_2O$ (Sigma-Aldrich, cabot high-purity grade) giving the corresponding alkaline titanate nanostructures: sodium titanates $Na_2Ti_3O_7$ nanotubes, potassium titanates $K_2Ti_6O_{13}$ nanowires and cesium titanates $Cs_2Ti_6O_{13}$ nanowires[147,148,149]. The synthesised materials were then used as supports for ruthenium nanoparticles.

In a typical synthesis of the alkaline titanate nanomaterials, 1.92 g of the commercial TiO_2 anatase nanoparticles were suspended in 160 ml of aqueous 10 M alkaline solution, followed by hydrothermal treatment at 150°C in a stainless Teflon-lined autoclave for 72 h. The resulting powders were washed with large amounts of distilled water until neutral pH was achieved and then dried at room temperature.

Preparation of Ruthenium Nanoparticles

The catalysts were prepared from 0.5 g of the titanate nanostructured material by incipient wetness impregnation using a ruthenium nitrosyl nitrate solution with a ruthenium content of 8.1 wt%. After impregnation, the sample was calcined in air at 250°C.

Physicochemical characterization

Transmission Electron Microscopy

Transmission electron microscopy (TEM) was performed on a JEM 2000 FX with an accelerating voltage of 300 kV. A few mg of the powdered samples were suspended in 2 ml ethanol, and the suspension was sonicated for 30 min. The suspension was allowed to settle for 15 min, before a drop was taken and dispersed on a 300 mesh copper grid coated with Holey carbon film.

X-ray Powder Diffraction

X-ray powder diffraction patterns (XRPD) were recorded using Cu-K_α radiation in the 2θ interval of 5 to 100° by a Philips PW 1820/3711 powder diffractometer.

Nitrogen Adsorption and Desorption

Nitrogen adsorption and desorption measurements were performed at liquid nitrogen temperature (-196°C) on a Micromeretics ASAP 2020. The samples were degassed in vacuum at 200°C prior to measurement. Total surface areas were calculated according to the BET method.

CO-pulse Chemisorption

CO-pulse chemisorption was performed on the same catalyst batch as used for activity testing. The CO-pulse chemisorbtion was carried out on a Micromeretics Auto Chem II chemisorption analyzer. A sample of 0.1g catalyst was reduced in hydrogen for 2h at 400°C, then the gas was then switched to helium for 1h before the sample was then cooled in a flow of helium to 50°C and pulsed with a 5% CO in helium mixture. From the amount of adsorbed CO the apparent particle size was calculated.

Catalyst Testing

The catalyst testing was performed in a specialized setup for ammonia decomposition. 0.1g of catalyst was transferred to the stainless steel reactor with an inner diameter of 4.6 mm, where it was reduced for 5 hours at 400°C in a 100 ml/min flow of hydrogen. The temperature of 400°C for reduction in all experiments is selected to avoid decomposition of the alkali nanotitanate supports. The decomposition of the supports was observed in catalytic testing at a temperature of 490°C as a rapid deactivation of the catalysts. This is likely due to ammonia or hydrogen destabilizing the nanostructure at these high temperatures. The temperature can also influence the degree of reduction; if the reduction is not complete the measured apparent particle size will increase. The testing was done from 400°C and down using steps of 15°C in a flow of 20 ml/min ammonia and 50 ml/min argon. The ammonia concentration in the carrier stream was determined using a Fischer-Rosemount NGA 2000 equipped with a MLT analyzer calibrated to NH_3 concentrations from 0.03-30%.

Results and Discussion

Promoted Iron, Cobalt and Nickel Supported on HSAG

The activity testing of promoted iron, cobalt, and nickel reveal some interesting results, especially regarding the effect of the different promoters. The activity of the un-promoted catalyst was as expected from the literature and shown in Figure 10. The un-promoted iron and nickel have comparable activities, with the cobalt having the slightly higher catalytic activity. The results of all the experiments are shown in Figure 12. Here the logarithm to the ammonia decomposition rate is plotted as a function of the inverted temperature in an Arrhenius style plot. The direct plot of the rate has some disadvantages however, mainly it does not take into account the reactor type and the volume expansion as ammonia is being decomposed. The advantage of plotting the rate directly is that no assumptions about the kinetics are necessary and that new errors from modelling the reactor are not introduced. This makes it easier to explain the derivations seen in the data. The main derivations seen in Figure 12 are a smaller than expected slope and flattening of the logarithm to the rate ratio at high temperatures and conversions. Both come from the lack of

the plug flow reactor model taking into account the concentration profile throughout the reactor.

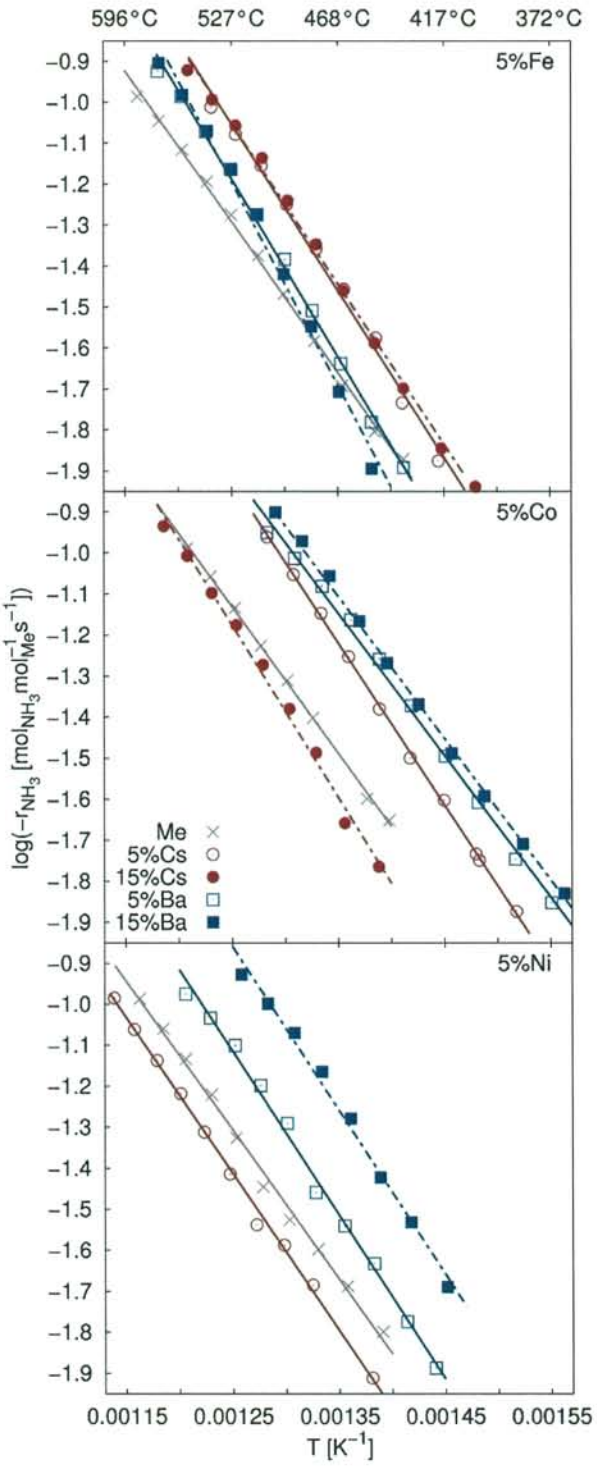

Figure 12: Arrhenius style plot of catalytic activities of iron (top), cobalt (middle), and nickel (bottom) supported on HSAG. Promotion by caesium (red) and barium (blue) in different loadings of 5 wt%(solid) and 15 wt% (dashed).

Figure 12 is split up in three parts, one for each of the three base metals iron, cobalt, and nickel. In the top part, showing the activity of iron, the first observation is that there is a promotion effect with both caesium and barium. The effect of the promoter is almost independent of mass of promoter used. This can be seen as overlapping data points for 5 and 15 wt% plots. The best promoter for iron is caesium, whilst the effect with barium is small.

The middle part of Figure 12 shows activities of cobalt catalysts. The first observation is that cobalt is a better catalyst than iron at ammonia decomposition. Barium is the best promoter for cobalt and again there is no effect in changing the amount of barium. Caesium loading of cobalt shows an effect of promoter loading, the low loading of 5 wt% gives a higher activity but increasing the caesium loading to 15 wt% makes the catalyst less active than the initial cobalt catalyst. This indicates that caesium blocks active sites on the cobalt particles as the slope of the two caesium promotions is similar.

In the bottom of Figure 12 the activities of nickel are shown. The pure nickel catalyst has a similar activity to the pure iron, but the effect of promotion is much larger. Promotion with even low loadings of caesium results in deactivation of the catalyst without change to the apparent activation energy, indicating blocking of active sites. The effect seen with barium promotion of cobalt is an increase in activity with both 5 and 15 wt% loading. From the slope of the Arrhenius style plot the apparent activation energies were calculated and shown in Table 4, the apparent activation energy is an expression of the overall energy barrier in the system.

Table 4: Apparent activation energies as calculated from Figure 12

Active metal Promoter	Fe/HSAG $E_{app.}$ (kJ/mol)	Co/HSAG $E_{app.}$ (kJ/mol)	Ni/HSAG $E_{app.}$ (kJ/mol)
5 wt% Metal	70.5	68.5	69.7
5 wt% Cs	74.8	75.4	73.2
15 wt% Cs	77.8	80.3	-
5 wt% Ba	83.1	66.2	76.4
15 wt% Ba	94.8	66.1	76.3

From the data in Table 4 it is seen that we get lower than expected values of the apparent activation energy even with the high linearity of the data. The reason for the low activation energy is that no correction of the concentration gradient is made. The concentration gradient causes an uneven utilization of the catalyst as the first

part of the catalyst has higher specific rate than the last part simply because the first part is in contact with much more ammonia than parts further down the reactor length. Interesting observations are that the apparent activation energy of the pure metals is almost the same, another trend is that promotion with caesium increases the apparent activation energy in all cases. Promotion with barium increases the apparent activation energy for iron and nickel but lowers it for cobalt, this is strange as it works well as a promoter for both cobalt and nickel. To get a better overview of the activity a plot of catalyst activity at 500°C is shown in Figure 13.

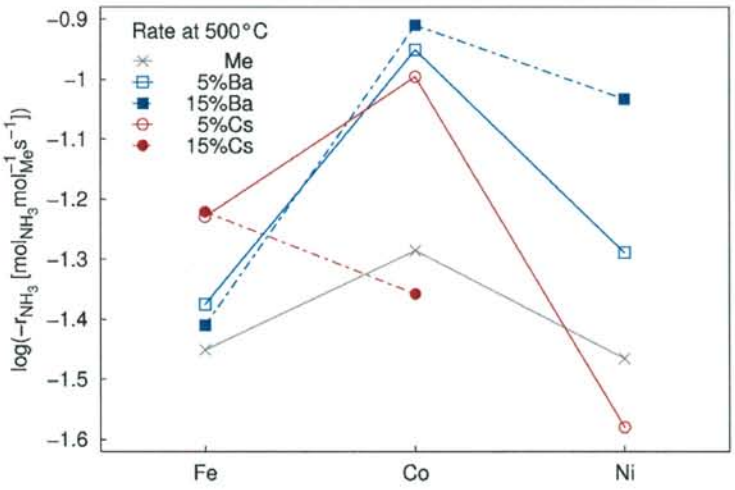

Figure 13: Plot of the catalytic rate at 500°C. Showing un-promoted metals (grey) barium promoted catalysts (blue) and caesium promoted catalysts (red).

When the apparent activation energies and catalytic activity are compared, it can be seen that iron promoted with barium has a significant increase in apparent activation energy, but the activity is slightly higher than for the pure metal. The effect of barium promotion on iron seems to be an increase in the number of active sites, but the new active sites have a higher apparent activation barrier than before. When the amount of barium is increased, the number of active sites also increases further, but the apparent activation barrier becomes high. As a result, with 15 wt% barium a slightly lower activity is seen when compared with 5 wt% barium on iron.

For caesium on iron the increase in apparent activation energy is small and the effect of promotion with caesium is an increase in the catalyst activity. An increased amount of caesium has very little influence on both the apparent activation energy and activity.

Promotion of cobalt with barium results in a large increase in activity and a slightly lower apparent activation barrier. The barium increases the number of active sites without changing the activation barrier. There is no effect observed by increasing the barium loading, the apparent activation energy and activity remain the same. Caesium promotion of cobalt is an example of the significant influence that promoter loading can have. As caesium loading is increased, the result is a lower activity than that of pure cobalt. This indicates that caesium is blocking the active cobalt sites and decreasing the catalyst activity.

Promotion of nickel with barium results in an increase in both activity and apparent activation energy. With an increase in promoter loading, the activity increases further but the apparent activation energy remains unchanged, pointing to an increase in the number of active sites. The only attempt of caesium promotion of nickel resulted in a lower activity than that of the pure nickel catalyst. The increase in activation energy is small so it looks as if caesium is blocking active sites at the nickel surface.

The caesium promotion on iron and nickel is investigated with TEM and EDX, the pictures can be seen in Figure 14 and Figure 15. This is done to see if there are any interactions between the active metal and the caesium promoter, and how the caesium is distributed on the support. This could reveal more information about why caesium works as a promoter for iron but as an inhibitor for nickel.

For the caesium promoted iron catalyst in Figure 14, there are clear caesium peaks on the EDX spectra of both the overview and the single particle. This shows that caesium is interacting with the iron particles and promoting the catalytic ammonia decomposition. For nickel on the other hand, there are only weak signs of caesium in the EDX spectra in Figure 15. This could indicate that caesium is not interacting with the nickel or that it is completely incorporated into the nickel particle. The nickel particle also appears to have grown very large, this could explain the deactivation as large particles decrease the active surface area and number of active sites. For iron the particles looks nice and small, which increases the active surface area and number of active sites.

The particle size is usually important for the catalytic activity as the sites responsible for catalytic conversion are the defect edge and corner sites on the nano-particles. The number of defects increases as the particle size decreases[57].

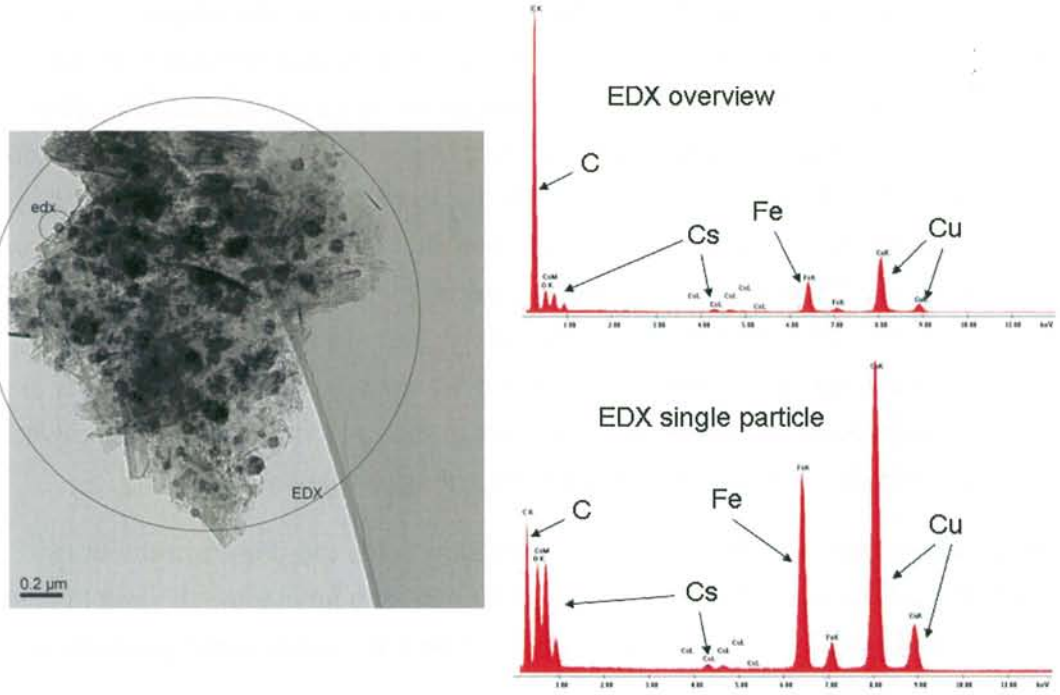

Figure 14: TEM image and EDX spectrums of 5 wt% Cs on Fe/HSAG

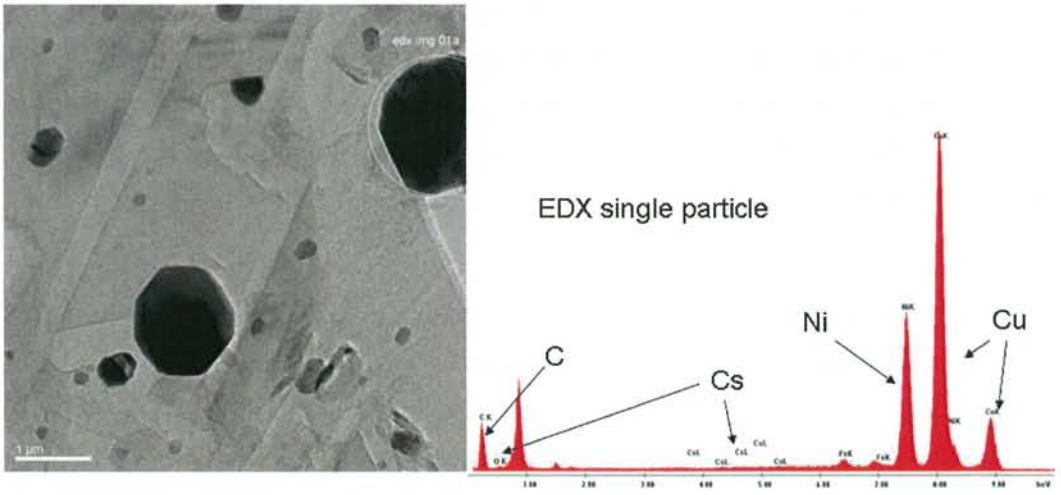

Figure 15: TEM image and EDX spectra of 5 wt% Cs on Ni/HSAG.

The copper peak seen in all the EDX spectrums in Figure 14 and Figure 15 originates from the grid used to suspend the catalysts on.

The comparison of promoter effect of barium in synthesis and decomposition reveals that for nickel and cobalt the promoter effect is strong in both ammonia synthesis and decomposition. This is as would be expected and is well in line with the general idea that barium helps handling nitrogen dissociation in some way[80,144]. The barium promotion of iron displays a completely different trend as barium deactivates the iron in ammonia synthesis but acts as a promoter for the decomposition of ammonia. An explanation of this could be that barium lowers the binding energy of hydrogen on the surface[144]. This would increase the coverage of adsorbed nitrogen on the surface of all the catalysts. This could give a deactivation of iron as a synthesis catalyst if no hydrogen is available at the surface, but as a decomposition catalyst the lower hydrogen coverage would not affect the reaction rate negatively.

Further investigation of the influence of different species could be carried out by varying the inlet gas mixture of hydrogen, nitrogen, and ammonia. This would give a more detailed mapping of the influence of the different reactants and products on the observed activity.

Nanotitanates

The use of a combined synthesis for a high surface area support material with incorporated promoters for the ammonia decomposition makes it possible to achieve a uniform distribution of promoter throughout the crystals and at the same time stops the agglomeration of the promoter particles. At the same time, the incorporation in the crystal lattice ensures uniform oxidation and reduction of the promoter.

The prepared titanate nanostructured support materials were analyzed with high-resolution TEM. Representative TEM images of the titanate nanomaterials can be seen in Figure 16. The use of TEM makes it possible to see the different structure of TiO_2 nanoparticles, $Na_2Ti_3O_7$ nanotubes, $K_2Ti_6O_{13}$ nanowires, and $Cs_2Ti_6O_{13}$ nanowires.

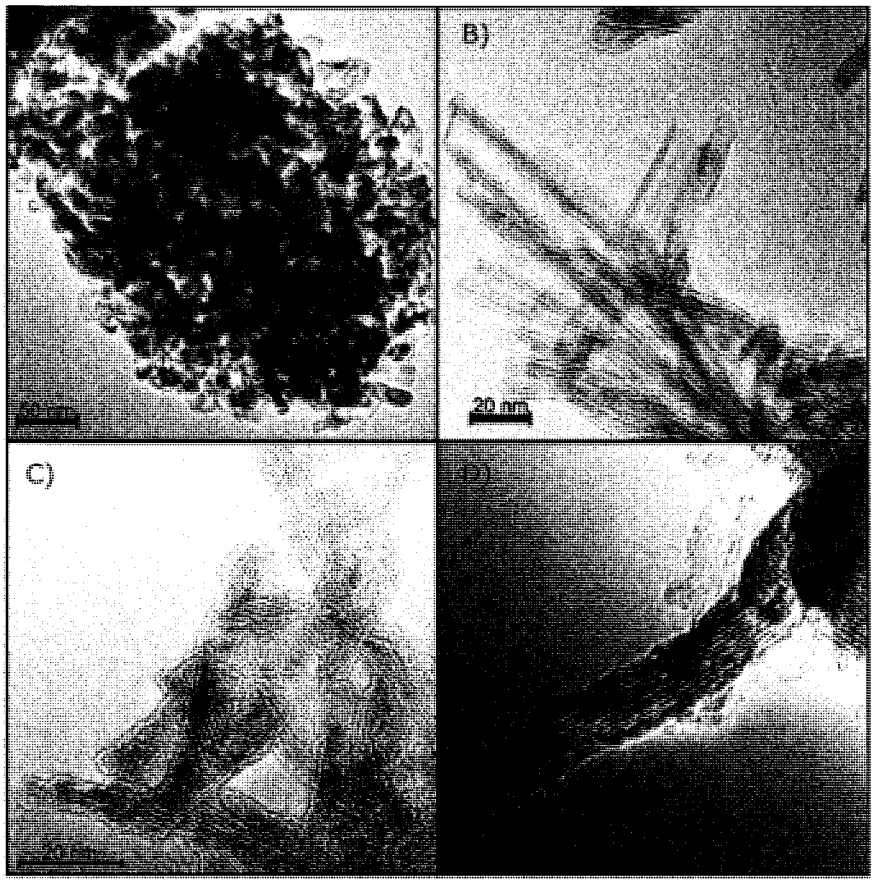

Figure 16: TEM images of (A) TiO_2 nanoparticles, (B) $Na_2Ti_3O_7$ nanotubes, (C) $K_2Ti_6O_{13}$ nanowires and (D) $Cs_2Ti_6O_{13}$ nanowires[139].

In Figure 16A, the TiO_2 anatase nanoparticles used as starting material for the synthesis of the alkaline titanate nanomaterials are shown. The results of the hydrothermal treatments of TiO_2 anatase nanoparticles with different alkaline bases, NaOH, KOH, and CsOH, are shown in Figure 16B, C and D, respectively. From the TEM images, it can be seen that the hydrothermal treatment gives nanotubes in the case of NaOH, whereas the use of KOH or CsOH gives small flakes/nanowires. To determine the change in the surface, BET surface areas of the samples were obtained after hydrothermal treatment with the different alkaline bases.

The result of the BET measurements are shown in Table 5, it is seen that the surface areas of the nanostructured titanates increase significantly after the hydrothermal treatments with the different alkaline bases in comparison with the starting anatase TiO_2. The increased surface area should help ruthenium dispersion on the final catalyst, improving the catalytic activity.

Table 5: BET surface areas of anatase TiO_2 before and after hydrothermal treatment with different alkaline bases[139].

Main product	BET surface area(m^2/g)	Base (M)	Time (h)	Temperature (°C)
TiO_2	139	-	0	-
$Na_2Ti_3O_7$	224	NaOH	72	150
$K_2Ti_6O_{13}$	309	KOH	72	150
$Cs_2Ti_6O_{13}$	208	$CsOH{\cdot}H_2O$	72	150

The support materials were also investigated using XRPD. The obtained XRPD-patterns for all the nanomaterial samples are shown in Figure 2. This is done to show that the nano-structured materials are crystalline and have the expected structures.

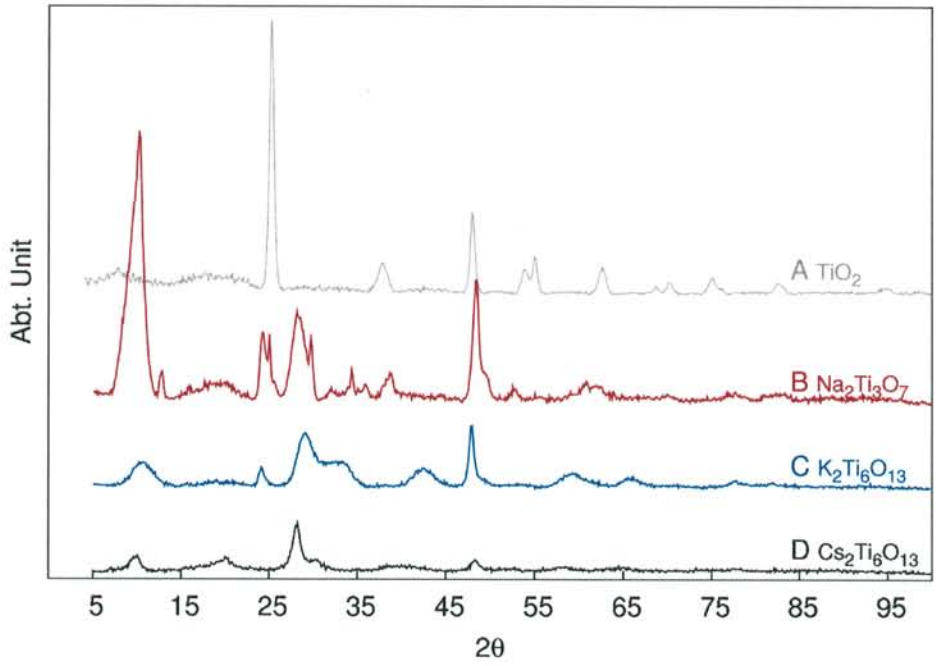

Figure 17: XRPD patterns of (A) TiO_2 nanoparticles, (B) $Na_2Ti_3O_7$ nanotubes, (C) $K_2Ti_6O_{13}$ nanowires and (D) $Cs_2Ti_6O_{13}$ nanowires[139].

The XRPD patterns were obtained in the interval between 5 to 100 (2θ) degrees. XRPD patterns for nanostructured titanates were obtained after hydrothermal treatment. Figure 17A shows crystalline TiO_2 anatase. The other nanomaterials appear less crystalline but this is only because the nanotubes and nanowires are too thin to yield good diffraction. Thus, it is concluded that all the titanium in the

samples is present as nanostructured titanate materials and that no TiO_2 nanoparticles are present.

The obtained XRPD patterns are good agreement with those previously published for $Na_2Ti_3O_7$ nanotubes[150], $K_2Ti_6O_{13}$ nanowires[151], and $Cs_2Ti_6O_{13}$ nanowires [152,153].

All catalysts were tested under the same conditions in a constant flow of ammonia diluted with argon as described in the experimental section. In Figure 18, an Arrhenius type plot is shown showing the catalytic rate based on active metal concentration of 3% ruthenium on TiO_2 nanoparticles, $Na_2Ti_3O_7$ nanotubes, $K_2Ti_6O_{13}$ and $Cs_2Ti_6O_{13}$ nanowires. This confirms the general trend for promotion of ruthenium catalysts with different alkali metals in the ammonia decomposition reaction [133,135,136,154].

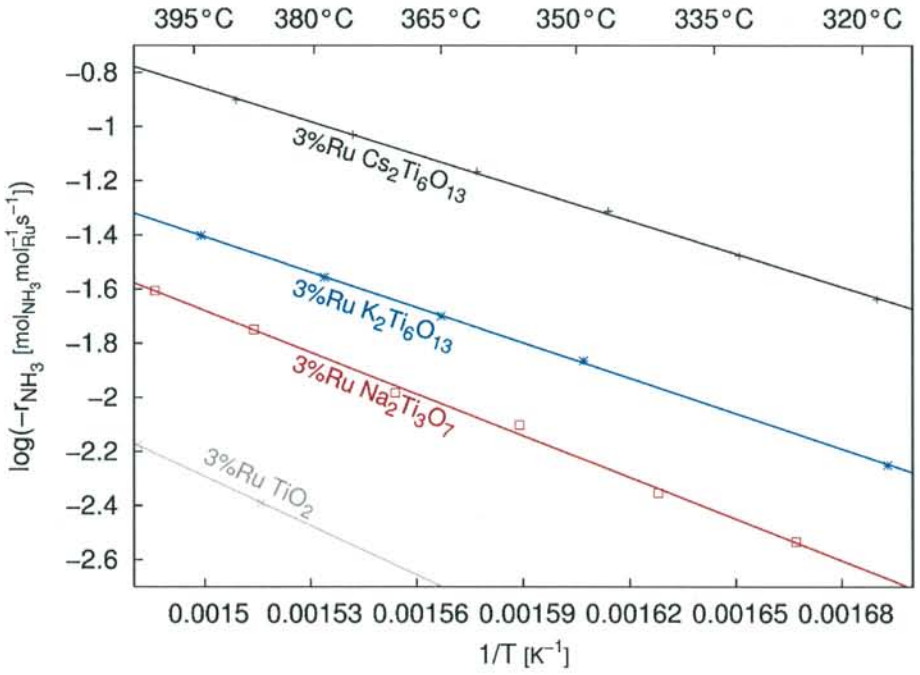

Figure 18: Arrhenius type plot for catalytic ammonia decomposition with 3 wt% ruthenium respectively on TiO_2 nanoparticles, $Na_2Ti_3O_7$ nanotubes, $K_2Ti_6O_{13}$ and $Cs_2Ti_6O_{13}$ nanowires as support materials[139].

From Figure 18, it is seen that the promoting effect of alkali metals increases in the order: Cs>K>Na. To verify that the higher catalytic activity of $Cs_2Ti_6O_{13}$ nanowires was due to structural changes, the ruthenium on TiO_2 support was promoted with a

similar caesium loading(~30 wt%) using a $CsNO_3$ solution. The promoter was deposited on the already prepared 3% Ru/TiO_2 with incipient wetness impregnation. The catalyst was calcined and tested (not shown), but it showed lower activity than the pure ruthenium on TiO_2. This shows that incorporaton of alkali metal promoters into the crystal lattice of the nano-titanates, gives a stronger promoting effect than surface deposition of the promoter on top of the ruthenium. The lower activity after promotion has not been seen in other studies where high caesium loadings had been impregnated on a ruthenium catalyst[94,134,135].

The relatively high catalytic activity of ruthenium on the nano-titanates can thus be explained by the promoting effect of the alkali metals in the crystal lattice. Furthermore, the higher surface area of the alkali titanates will increase the dispersion of the Ru-nanoparticles on the surface.

To further investigate the effect of the $Cs_2Ti_6O_{13}$ support material, samples with different ruthenium loadings were prepared in order to find the optimum ruthenium content. The effect of varying the ruthenium loading is shown in Figure 19, the rates are plotted at 377°C.

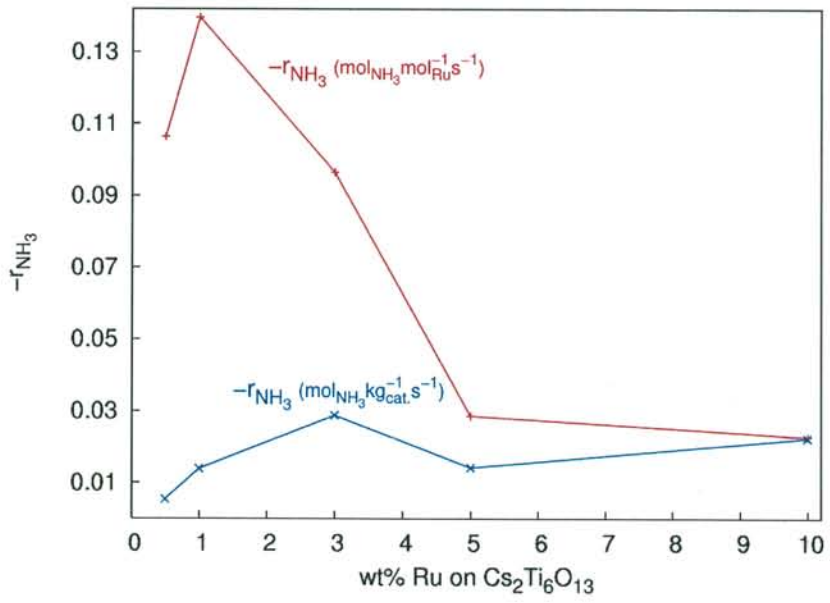

Figure 19: Reaction rate at 377°C plotted as a function of the ruthenium loading in wt%. The rates are normalised to molar ruthenium loading (red) and catalyst weight (blue)[139].

The two plots in Figure 19 illustrate that different normalizing factors is important for understanding the data. For the weight based normalization the normalization factor is constant as all tests are done with same amount of catalyst (0.1g). For normalization to molar ruthenium content the normalization factor changes with a factor of 20 from 0.05 mmol/g to 0.99 mmol/g. This favours low loading, best seen by a comparison between 1 and 5 wt% ruthenium. The two catalysts have similar rates on weight basis, but on a molar basis the five times higher Ru-loading of 5 wt% gives a rate that is one fifth of the 1 wt% sample.

From Figure 19, it is seen that the best utilization of the available ruthenium on a molar basis is achieved with a loading of 1 wt%. The reaction rate also shows that the activity per mole ruthenium decreases until a loading of 5 wt% is reached, hereafter the activity stabilizes. However, the change in specific activity as a function of ruthenium loading is almost invariant, the main features being a lower spread in activity and a shift of the maximum activity to a loading of 3 wt% ruthenium. This is interesting regarding catalyst mass optimization.

The change in activity can be partly explained by different particle sizes, which were measured by CO-chemisorption, see Table 6.

Table 6: CO-pulse chemisorption measurements of particle sizes and molar ratios between caesium and ruthenium in the different catalysts for the same catalyst batches as used for activity measurements in Figure 4[139].

Wt% Ru $Cs_2Ti_6O_{13}$	Apparent particle size nm	Molar ratio Cs/Ru
0.5%	26.0	52.6
1%	7.8	26.2
3%	23.6	8.5
5%	-	5.0
10%	28.6	2.4

By comparison of the particle size and activity normalized to the ruthenium amount in moles, it is seen that there is a good correlation between the measured particle size and the relative activity. The loading of 1% ruthenium has the highest activity and the lowest particle size. We have no experimental explanation of the observed lower particle size of this catalyst compared to the others displayed in Table 6. The 0.5% and 3% ruthenium loadings have particle sizes and activities in the same ranges. The 10% ruthenium loading has the highest measured particle size and lowest activity. This is however, not the full picture as the particle size for the 10%

ruthenium is only slightly larger than that for the 3% ruthenium. This indicates that the ratio between caesium and ruthenium also has an influence on the measured activity.

Thus, if we look at the particle size and activity for 0.5%, 3%, and 10% ruthenium, the particle size is in the same range. If particle size this should not result in large differences in activity, if particle size was limiting for the catalytic activity. This shows that the caesium loading is also important for the activity. Looking at the ratios of caesium to ruthenium in Table 6, it is clear that a ratio greater than 5 is preferable, if it is assumed that the 5% loading of ruthenium has a similar particle size to the other loadings.

To determine the optimal ratio of caesium to ruthenium, the particle size must be better controlled, otherwise it is difficult to determine which effect is the most important. This also means that the optimal loading of 1% ruthenium may be a combination of small better dispersed particles and more frequent contact between caesium and ruthenium. This is due to the limited surface exposure of the caesium ions, defined by the distribution of caesium in the crystal lattice of the caesium titanate. This scenario is also supported by the non-promoting effect observed by loading non-titanate caesium on the surface of the Ru-TiO_2 catalyst.

Summary

The catalytic ammonia decomposition on iron, cobalt, and nickel has been investigated and it is shown that the promotion with barium and caesium work in different ways. The precise effect of the two promoters is not understood fully, but the data suggest that they mainly alter the number of active sites. This is based on the fact that the changes in apparent activation energies are small compared to the changes in rate. Some significant differences between ammonia decomposition and synthesis, has also been pointed out mainly looking at iron compared to barium promoted iron for both synthesis and decomposition. The barium has a slightly positive effect on iron as a decomposition catalyst, but for ammonia synthesis barium is making iron less active. This can be due to different dominating surface species in synthesis and decomposition, particularly the amount of adsorbed nitrogen on the surface.

Synthesized nanostructured support materials of $Na_2Ti_3O_7$, $K_2Ti_6O_{13}$, and $Cs_2Ti_6O_{13}$, have been used as support materials for ruthenium in the ammonia decomposition

reaction. The promoting effect of alkaline metals increases in the sequence: Cs>K>Na. Furthermore, a significant effect of the incorporation of the promoters in the support crystal lattice instead of classic surface promoting procedures was obtained. Finally, the optimal apparent ruthenium loading on $Cs_2Ti_6O_{13}$ was found to be 1%, however further studies on the influence of particle size and metal loading are required to confirm this conclusion.

Ammonia Cracker

Part of the project has been to develop an ammonia cracker in corporation between the Danish Technological Institute, Amminex, Grundfoss and DTU. The unit should operate on ammonia stored in a metal ammine salt and work with a PEM fuel cell stack. The unit should be of a size were it could compete with traditional battery operation. This could be in small electric vehicles, wheelchairs, pallet trucks, *etc.* The unit could also work as an alternative power supply for computers or for field applications in combination with solar panels or small windmills. The electric output calculated for this type of application is 500-1000W. This also gives at suitable size of reactor for laboratory testing.

Design of the Ammonia Cracker

The ammonia cracker is designed to decompose up to 8 NL/min. ammonia, this will give enough hydrogen to produce 1.2 kW of energy with complete decomposition and a efficiency of the fuel cell stack of 60%. For PEMFC operation an ammonia free feed is needed, this make removing of unconverted ammonia from the decomposition reactor important. In the prototype a sulfated carbon filter is used that is capable of removing ammonia down to <<1 ppm. The filter is simple and efficient but other alternatives could be used. Ammonia is easily absorbed in solid acids filters and the filter can easily be regenerated by heating.

The reactor needs a supply of heat for the endothermic decomposition of ammonia. The most efficient way to gain this heat is by catalytic ammonia oxidation. Other alternatives were discussed such as electric heating. Electric heating is easy to control, but is not efficient as power is required to run it and the fuel cell is only operating with a 60% efficiency. Another possibility is hydrogen oxidation. This is easy and very efficient but requires that the ammonia first be decomposed. This led to the easiest solution of using ammonia directly as fuel for the heating.

The normal testing is done with ammonia decomposition of 4 NL/min. This gives hydrogen corresponding to 600W electricity. Some of this will go to operate the system, for example air pumps for the fuel cell and oxidation catalyst, control power for the lambda sensor and other system controls. The heat for decomposition is supplied by catalytic ammonia oxidation. The ammonia oxidation is exothermic see the reaction scheme f.

$2NH_3 + 1.5O_2 \rightarrow N_2 + 3H_2O$ $\Delta H=-633$ kJ/mol (f)

From the enthalpies it can be calculated that catalytic oxidation of one mole ammonia generates enough energy for decomposition of 6.8 mole ammonia. With this limit of the system a minimum of 0.73 NL/min. ammonia would need to be oxidized to decompose 5 NL/min ammonia. This ratio is not possible to achieve in practice due to heat loss and the need for high temperatures (~600°C) for the decomposition reaction to reach an equilibrium conversion of over 99.8%. To minimize the heat loss in the system a tube in tube design has been chosen. This design can be constructed from commercial available materials, the schematic design can be seen in Figure 20

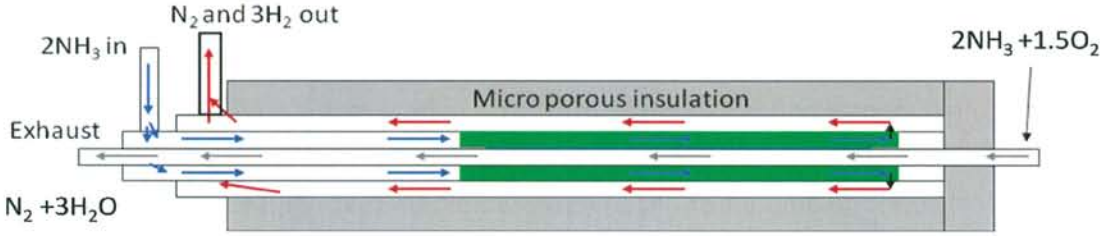

Figure 20: Schematic of ammonia decomposition unit, middle (gray arrows)catalyst bed is Pt on Al_2O_3 for catalytic combustion of ammonia, green bed is Ru on high surface area graphite (HSAG) promoted with Cs for catalytic ammonia decomposition

The design shown in Figure 20 is selected to minimize energy loss. This is done by placing the ammonia oxidation catalyst inside the double pipe, so as much heat as possible can be transferred to the decomposition unit. With this design it is possible to decompose 4.5-5 NL/min. ammonia by the oxidation of 1 NL/min. ammonia. This is an efficiency of ~70% of the theoretic limit. The plan is to integrate the decomposition unit with a metal ammine storage unit. The hot exhaust from ammonia oxidation and decomposition should then be used to desorb the stored ammonia, this would increase the overall system efficiency. The prototype of the ammonia cracker unit can be seen in Figure 21.

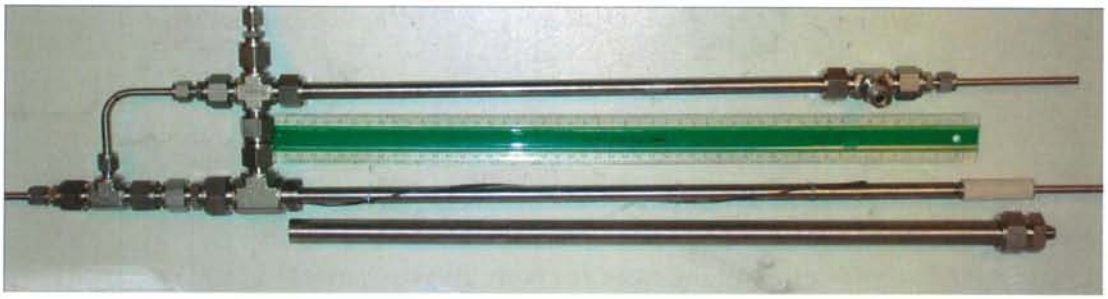

Figure 21: Prototype of the ammonia cracker unit.

The reactor shown in Figure 21 use a 1% platinum on alumina catalyst for the ammonia oxidation and caesium promoted ruthenium on HSAG for ammonia decomposition. The platinum catalyst is commercially available and is delivered in pellets that can be used directly in the inner tube. The platinum catalyst can also be preheated easily by applying a flow of hydrogen and air. The caesium promoted ruthenium supported on HSAG is the most active catalyst for ammonia decomposition. This makes it possible to obtain high conversion at a wide range of flow minimizing the amount of unconverted ammonia that need to be removed in the ammonia absorber. The ammonia absorber applied so far is activated carbon treated with sulphuric acid and dried.

The integration of metal ammine storage and a functioning fuel cell stack has not yet been demonstrated. The main reason for this was that integration of control of the ammonia desorption with the ammonia cracker proved difficult. The separate control system could not just be put together as expected, further the heat integration of the two system required design of a new metal ammine storage unit. This was realized too late to change the project goal.

Ammonia Cracker Testing

The ammonia cracker prototype has been tested to optimize the operation. The first simple setup applied a conductivity measurement to see if it was possible to achieve the expected high conversion of ammonia. The exit gas from the ammonia decomposition was bubbled through ion exchanged water and the conductivity is measured. This in combination with the ammonia flow and temperature on the outside of the decomposition catalyst is used to evaluate the ammonia conversion.

The ammonia oxidizing catalyst is more difficult to monitor continuously. The inlet mixture of ammonia and air is controlled by a lambda sensor measuring oxygen content. This can be used to determine the amount of available oxygen. The exhaust is controlled by taking gas samples at different lambda values and investigate them with Fourier transformed infrared spectroscopy (FTIR). The flow control of both ammonia and air, to the combustion catalyst is important to avoid harmful emission of NO_X and N_2O. The reaction to NO_X and N_2O is primarily a problem if the air content is too high, but if the amount of air is low there will be a ammonia slip. In Figure 22 FTIR spectra at different lambda values around one is showed. Lambda one correspond to a measurement of 0.45V which is close to stociometric amount of oxygen.

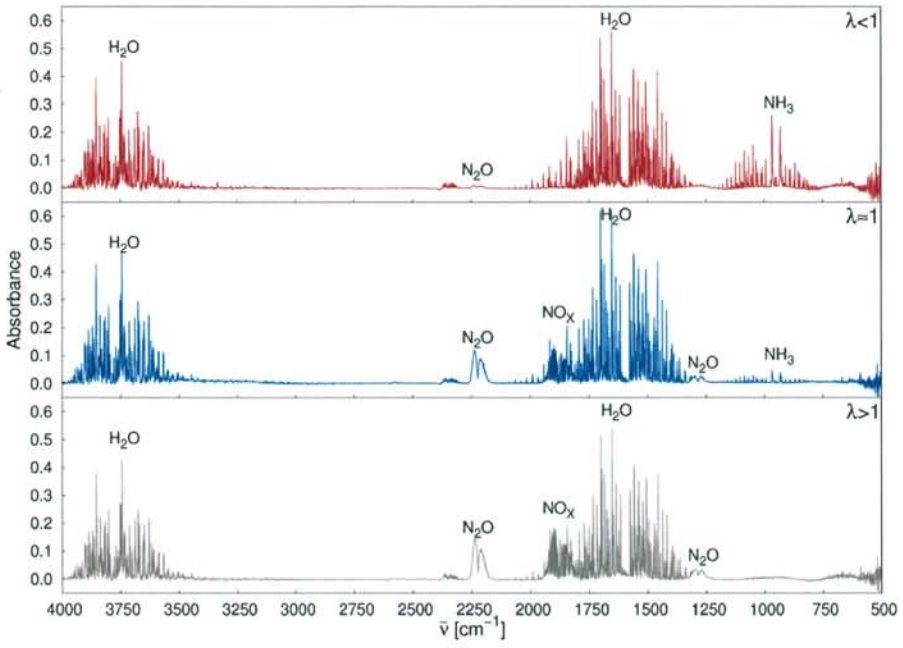

Figure 22: FTIR spectra for ammonia combustion for lambda close to one.

From the FTIR spectra in Figure 22, the gas composition is shown at different lambda values from stociometric oxygen content for $\lambda<1$ to oxygen rich for $\lambda>1$. This is used to analyze the ammonia oxidation catalyst operation.

The first spectra show under a stociometric amount of oxygen in the ammonia oxidation. This results in some ammonia and only traces amounts of N_2O. The NO_X formation is suppressed as long as there is available ammonia and oxygen for the

reduction of NO_X. The middle spectra show a stociometric amount of oxygen to ammonia. This eliminates all but trace ammonia, but increases the formation of N_2O and NO_X significantly. This is even clearer in the bottom spectra of an oxygen rich mix. Here there are no ammonia traces, but rather large amounts of both N_2O and NO_X.

The production of NO_X and N_2O can be reduced by changing the oxidation catalyst, this could be a copper, silver or gold catalyst[155,156]. These are known to have high selectivity for nitrogen. This will hopefully lower the nitrous oxide problem especially in the next generation of the prototype. Another observation is that the ammonia oxidizing makes the catalyst very hot in a small zone. This makes heat distribution to the decomposition catalyst difficult. Different designs of the decomposition catalyst bed with better heat distribution by building in a heat exchange is being designed and tested.

The trade off between not combusting all the ammonia and formation of harmful emissions of N_2O and NO_X will probably favour not burning all the ammonia. The main reason for this is that N_2O is a green house gas with a long life time in the atmosphere and NO_X causes smog in urban environments. Ammonia on the other hand is relatively harmless and reacts with the soil as fertilizer. Ammonia can also easily be captured in a solid acid filter, such as sulphated carbon.

The catalyst for ammonia decomposition is ruthenium promoted with caesium and supported on HSAG. This is a very active catalyst and can push the conversion close to the theoretic equilibrium conversion, given by the thermodynamic Gibbs free energy. As a prototype the catalyst works as expected and gives high conversion, but there are two issues that need to be dealt with, mainly coming from the HSAG support. The first problem is the fine structure of HSAG, this gives a rather large pressure drop over the catalyst. The support is difficult to make in larger fractions and thereby reducing the pressure drop. The second problem is methanation of the graphite, this is because ruthenium is a methanation catalyst and the inside of the catalyst gets very hot (~900°C). These two problems can both be solved by changing the support material to $MgAl_2O_4$ spinel. This would be easier to make into larger particles, it is stable at very high temperatures and no metanation is possible.

The exit gas from the decomposition of ammonia was also investigated with FTIR, both before and after passing through a sulphated carbon filter. This is done to demonstrate that unconverted ammonia from the decomposition can be removed.

Efficiently down to ppb levels. The final part of Figure 23 is a FTIR spectrum of the exit gas from a single fuel cell fed with the cleaned ammonia reformate and air.

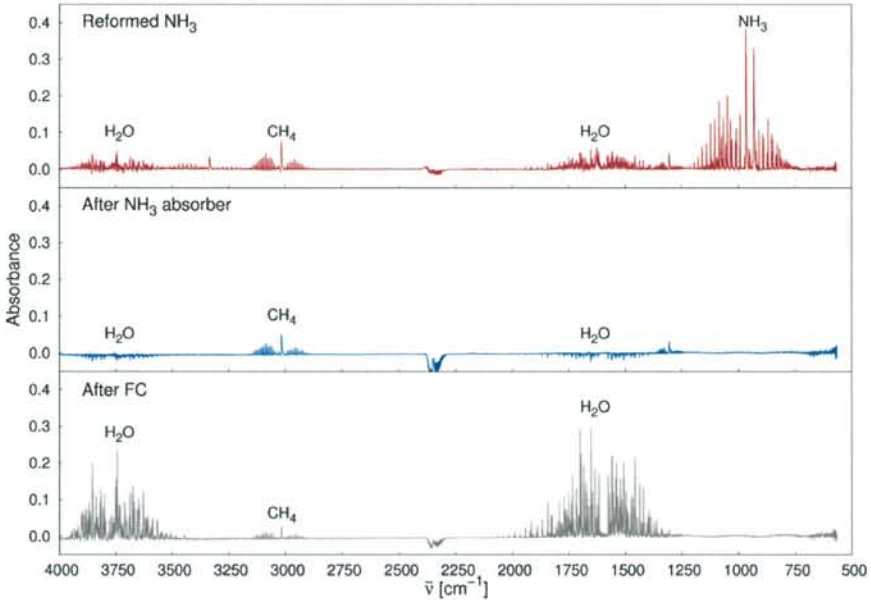

Figure 23: FTIR spectra of reformed ammonia, reformed ammonia after ammonia slip filter, and finally after the fuel cell[139].

The top spectra in Figure 23 show the exit gas from the decomposition catalyst before any cleaning. The gas contains ammonia, methane, and trace amount of water. The ammonia is expected as it is well known and described earlier that the reaction is limited by the equilibrium. The methane is undesired and arises from the HSAG support reacting with hydrogen. To determine if it is a serious problem long time test and monitoring of the unit is necessary, those test has not yet been performed. Another solution is a change of support material as discussed earlier. The middle spectra in Figure 23 show the reformed ammonia after passing through the sulphated carbon filter. It is clear that all ammonia and the traces of water are absorbed in the filter, at the same time the methane is still present in the reformed ammonia gas. The bottom spectra in Figure 23 show the exit gas from the fuel cell fed with the reformed ammonia, this shows water and methane as expected.

The PEM fuel cell used for the experiment was supplied by IRD Fuel Cell[157]. In the experiment the fuel cell was run in constant current mode. The PEM fuel cell is operated on different feeds to give a comparison of hydrogen verses the decomposed ammonia. The data from the experiment of running a fuel cell on the feed of reformed ammonia cleaned in a sulphated carbon filter can be seen in Figure

24. Here a fuel cell is run first on hydrogen and then reformed ammonia. The change in voltage over time on different feeds is most likely the drying of the membrane, but this is pure speculation. The data is first attempts at making power directly from the cleaned ammonia reformat.

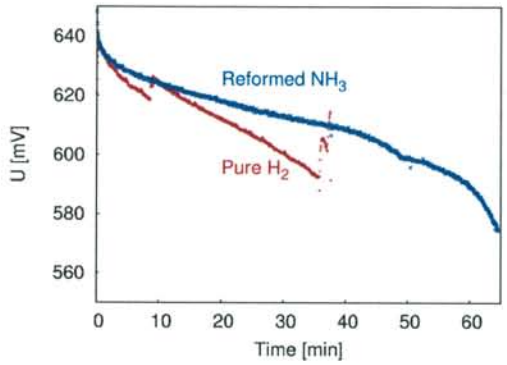

Figure 24: Constant current experiments, with a fuel cell fed with hydrogen and reformed ammonia[139].

The experiment is done to demonstrate that an ordinary fuel cell can run on the reformed ammonia out of the box. The combination of fuel cell and ammonia cracker looks promising from this initial experiment.

Future Developments on the Ammonia Cracker

The development of the next prototype of the ammonia cracker includes a lot of the previously suggested changes. The reactor will have integrated heat fans to give better heat distribution in the decomposition catalyst, several designs are being tested both for ease of manufacture and efficiency during operation. The catalyst for ammonia oxidation will be changed and hopefully that will give a better temperature profile in the ammonia oxidizer. The platinum catalyst is almost too active and all ammonia is more or less oxidized in the start of the catalyst bed, this results in very high temperatures in a short reaction zone. The change of oxidation catalyst should also minimize the production of NO_X and N_2O. Finally, the support material for the ammonia decomposition catalyst is being changes to avoid the pressure drop and methantion of the support material.

After optimization of the ammonia cracker, the hope is to build an integrated unit containing ammonia storage in the form of a metal ammine, the ammonia cracker for decomposition of ammonia, and a fuel cell stack for power production.

Summary

In corporation with Danish Technological Institute an ammonia cracker prototype has been build and tested. This has showed promising results with a high efficiency and a simple design using easily available materials. The different catalysts have been tested and several ideas for improvements of stability and operation have been discussed and are going to be tested. The main problems of the current prototype are, pressure drop and methanation of the decomposition catalyst, and production of NO_X and N_2O from the ammonia oxidizing catalyst. Further work with heat integration and reactor size is also important to increase the overall system efficiency.

Conclusion

This thesis has shown the possibilities of using ammonia as an energy carrier and indirect hydrogen storage medium. The ammonia synthesis, storage and transportation are well known and proven technologies on large scales. At the same time ammonia has the advantage over carbon based indirect hydrogen storage medium that it is carbon free. Which means no CO_2 is produced at the end user.

The use of metal ammine complexes for solid indirect hydrogen storage is described and a range of metal ammines are tested. The results show that the ammonia desorption for $Ca(NH_3)_8Cl_2$, $Mg(NH_3)_6Cl_2$, $Mn(NH_3)_6Cl_2$, and $Ni(NH_3)_6Cl_2$, are fast and only limited by heat transfer. The desorption rate of all four metals is similar and the main change is the onset temperature of the desorption. The tested metal ammines have gravimetric hydrogen densities of 7.8 – 9.8 wt% H compressed to tablets and volumetric hydrogen densities of 0.11 -0.12 kg H/L.

It is demonstrated that ammonia can be desorbed efficiently from solid tablets of metal ammine complexes. The fast desorption is due to formation of nanopores in the crystal structure. These findings have been confirmed by a range of measurements and calculations.

The desorbed ammonia can be efficiently decomposed into hydrogen and nitrogen. Different catalyst for the ammonia decomposition are discussed and tested. The tests were done to investigate the effect of barium and caesium as promoters for iron, cobalt, and nickel catalyst in the catalytic ammonia decomposition.

The tests show that the two promoters work differently and that the promoter effect seems to correlate with placement in the volcano curve based on nitrogen dissociation. This is most prominent when iron and nickel are compared. Barium on iron gives little improvement of the activity, whilst barium on nickel gives a large improvement of activity increasing with the barium loading. For caesium the trend is the opposite, iron is promoted by caesium but there is no effect of increased loading. Nickel, on the other hand, is inhibited and the activity goes down when compared to the pure nickel catalyst. The effect on cobalt is that the low loading of both barium and caesium have promoting effects. The effect of increased promoter loading for caesium results in a drop in activity to below that of the pure cobalt catalyst, for barium there is only a small increase in activity.

The ammonia decomposition with ruthenium was investigated with TiO_2 nanoparticles, $Na_2Ti_3O_7$ nanotubes, $K_2Ti_6O_{13}$, and $Cs_2Ti_6O_{13}$ nanowires as support materials. These showed that the synthesized nanotitanates increase the activity. This is due to promotion of the active catalyst, but also due to the structure of the new support. The incorporation of the promoter in the crystal lattice gives high promoter dispersion and increases the contact between promoter and ruthenium. The incorporation also prevents the promoter from blocking active surface sites, as can be the case with incipient wetness impregnation. The activity measurements show that caesium titanates are the best support material for ruthenium. The optimal ruthenium loading on $Cs_2Ti_6O_{13}$ nanowires is found to be 1 wt%, when the rate is based on molar concentration and 3 wt% based on catalyst mass.

The knowledge about ammonia decomposition has been used in the construction of an ammonia cracking unit at Danish Technological institute. The unit was designed to decompose ammonia corresponding to a power output of 500W from a fuel cell. The heat for ammonia decomposition comes from ammonia oxidation with air over a platinum on alumina catalyst. The decomposition catalyst is caesium promoted ruthenium on HSAG. The unit is a tube in tube design to minimize heat loss. The ammonia cracker is demonstrated to work and the flow of ammonia and air to the oxidation catalyst can be controlled by a lambda sensor. The reformed ammonia is cleaned of ammonia trace residues in a sulphate carbon filter and operation with a single fuel cell is shown to work. Alterations to the setup are proposed for the next generation of the ammonia cracker, that include better heat exchange between the two catalysts, new support material for the decomposition catalyst, and change of oxidation catalyst. Further work on a complete system incorporating both a metal ammine storage unit and an operating fuel cell stack is also necessary.

References

[1] L. Bareto, A. Makihira, K. Riahi, *Int. J. Hydrogen Energy,* 2003, 28, 267-284.

[2] D. Kennedy, *Science,* 2004, 305, 917.

[3] R. F. Service, *Science,*2004, 305,958-961

[4] http://www.eia.doe.gov/emeu/international/reserves.html

[5] International Energy Agency, *Key World Energy Statistics 2008*, Paris, www.iea.org, 2008.

[6] http://www.chevrolet.com/fuelcell/

[7] http://automobiles.honda.com/fcx-clarity/

[8] P. Häusinger, R. Löhmüller. A. M. Watson, *Ullmann's Encyclopedia of Industrial Chemistry: Hydrogen*, Weinheim, Wiley-VCH Verlag GmbH & Co. KGaA, 2000.

[9] J. D. Holladay, J. Hu, D.L. King, Y. Wang, *Catal. Today*, 2009, 139, 244-260.

[10] W. F. Baade, U. N. Parekh, V. S. Raman, *Kirk-Othmer Encyclopedia of Chemical Technology: Hydrogen*, John Wiley & Sons, Inc. 2001.

[11] M. Gardiner, J. Holladay, R. Garland, R. Farmer, *The USDOE Hydrogen Program: Status and Performance of Hydrogen Production and Delivery Technologies,* AIChE Spring Meeting 2009, Tampa, Florida.

[12]H. Wendt, H. Vogt, G. Kreysa, D. M. Kolb, G. E. Engelmann, J. C. Ziegler, H. Goldacker, K. Jüttner, U. Galla, H. Schmieder, E. Steckhan, *Ullmann's Encyclopedia of Industrial Chemistry: Electrochemistry*, Weinheim, Wiley-VCH Verlag GmbH & Co. KGaA, 2008.

[13] T. I. Sigfusson, *Mitig. Adapt. Strat. Glob. Change.* 2007, 12, 407-418.

[14] A. Züttel, *Materials Today,* 2003 September, 24-33.

[15] D. Sun, S. S. Srinivasan, G. Chen, C. M. Jensen, Rehydrogenation, *J. Alloy. Compd.,* 2004, 373, 1-2, 265-269.

[16] G. Sandrock, J. Reilly, J. Greatz, W.-M. Zhou, J. Johnson, J. Wegrzyn, *J. Alloy. Compd.,* 2006, 421, 185-189.

[17] G. Sandrock, J. Reilly, J. Greatz, W.-M. Zhou, J. Johnson, J. Wegrzyn, *Appl. Phys. A.,* 2005, A80, 687-690.

[18] H. Furukawa, M. A. Miller, O. M. Yaghi, *J. Mater. Chem.*, 2007, 17, 3197-3204.

[19] A. Züttel, P. Wenger, S. Rentsch, P. Sudan, P. Mauron, C. Ernmenegger, *J. Power Sources*, 2003, 118, 1-7

[20] Z. Łodziana, T. Vegge, *Phys. Rev. Lett.*, 2004, 93, 145501

[21] K. Chłopek, C. Frommen, A. Leon, O. Zabara, M. Fichtner, *J. Mater. Chem.*, 2007, 17, 3496-3503.

[22] J. J. Vajo, S. L. Skeith, F. Mertens, *J. Phys. Chem. B*, 2005, 109, 3719-3722.

[23] A. Feaver, S. Sepehri, P. Shamberger, A. Stowe, T. Autrey, G. Cao, *J. Phys. Chem. B Letters,* 2007, 111, 7469-7472.

[24] W. Lohstroh, M. Fichtner, *J. Alloys Compounds,* 2007, 332, 446-447.

[25] S. Orimo, Y. Nakamori, G. Kitahara, K. Miwa, N. Ohba, S. Towata, A, Zuttel, *J. Alloys Compounds,* 2005, 447, 404-406.

[26] P. V. Ramachandran, P. D. Gagare, *Inorg. chem.,* 2007, *46,* 7810-7817.

[27] Norsk Hydro, *Worth a try - Research and Development in Norsk Hydro through 90 years*, Oslo, 1997.

[28] C. H. Christensen, R. Z. Sørensen, T. Johannessen, U. Quaade, K. Honkala, T. D. Elmøe, R. Køhler, J. K. Nørskov, *J. Mater. Chem.*, 2005, 15, 4106–4108.

[29] J. Larmine, *Fuel Cells, Kirk-Othmer Encyclopedia of Chemical Technology,* John Wiley & Sons, Inc. 2002.

[30] J. larmine, A. Dicks, *Fuel Cell Systems Explained 2nd Edition,* John Wiley & Son s Ltd., Chichester, 2003.

[31] P. J. Feibelman, *Physics Today*, 2005, 58, 13-14.

[32] M. Appl, *Ullmann's Encyclopedia of Industrial Chemistry: Ammonia*, Weinheim, Wiley-VCH Verlag GmbH & Co. KGaA, 2007.

[33] L. Green, *Int. J. Hydrogen Energy,* 1982, 7, 355-359.

[34] A. Klerke, C. H. Christensen, J. K. Nørskov, T. Vegge, *J. Mater. Chem.* 2008, 18, 2304-2310.

[35] R. Schlögl, *Angew. Chem. Int. Ed.,* 2003, 42, 2004-2008.

[36] International Fertilizer Industry Association, *World Ammonia (NH_3) Statistics by Region,* 2007, http://www.fertilizer.org/ifa/statistics.asp.

[37] P. V. Christensen, *Design and Operation of Large Capacity Ammonia Plants*, 4th Conference for Development and Integration of Petrochemical Industries in the Arab States, May 2001, Bahrain.

[38] *Feed Purification Catalyst*, Haldor Topsøe A/S, Denmark.

[39] I. Dybkjaer, *Ammonia, Catalysis and Manufacture* (Ed.: A. Nielsen), Springer, Heidelberg, 1995, 199–308.

[40] T. Eggmann, *Kirk-Othmer Encyclopedia of Chemical Technology: Ammonia*, John Wiley & Sons, Inc. 2001.

[41] ICIS pricing Chemical Pricing Reports, *Ammonia,* http://www.icis.com/v2/chemicals/9075153/ammonia/pricing.html

[42] *Roadmap on Manufacturing R&D for the Hydrogen Economy*, 2005, Washington, Department of Energy.

[43] U.S. Department of Energy, *Carbon Sequestration Technology Roadmap and Program Plan 2007*, 2007.

[44] J. Wu, Y. Fang, H. Peng, Y. Wang, *Fuel Process. Technol.*, 204, 86, 261-266.

[45] W. de Jong, Ö. Ünal, J. Andries, K. R. G. Hein, H. Spliethoff, *Biomass Bioenerg.*, 2003, 25, 59-83.

[46] P. Häussinger, R. Löhmuller, A. M. Watson, *Ullmann's Encyclopedia of Industrial Chemistry: Hydrogen*, Weinheim, Wiley-VCH Verlag GmbH & Co. KGaA, 2000.

[47] Gross energy consumption by source 2007, Statistics Iceland, www.statice.is/?PageID=2043&highlight=energy.

[48] A. English, J. Rovner, J. Brown, S. Davies, *Kirk-Othmer Encyclopedia of Chemical Technology: Methanol*, John Wiley & Sons, Inc. 2005.

[49] E. Fiedler, G. Grossmann, D. B. Kersebohm, G. Weiss, C. Witte, *Ullmann's Encyclopedia of Industrial Chemistry: Methanol*, Weinheim, Wiley-VCH Verlag GmbH & Co. KGaA, 2000.

[50] http://www.cdc.gov/niosh/idlh/intridl4.html

[51] N. J. Duijm, F. Markert, J. L. Paulsen, *Safety assessment of ammonia as a transport fuel*, Risø-R-1504(EN), 2005. http://www.risoe.dk/rispubl/SYS/syspdf/ris-r-1504.pdf

[52] T. Vegge, R. Z. Sørensen, A. Klerke, J. S. Hummelshøj, T. Johannessen, J. K. Nørskov, C. H. Christensen, *Solid-state hydrogen storage: Materials and chemistry, Indirect Hydrogen Storage in Metal Ammines,* Woodhead Publishing LTD., England, 2008.

[53] K. Aika, K. Tamaru, *Ammonia Synthesis over Non-Iron Catalysts and Related Phenomena, Catalysis and Manufacture* (Ed.: A. Nielsen), Springer, Heidelberg, 1995, 103-148.

[54] W. Raróg-Pilecka, A. Jedynak-Koczuk, J. Petryk, E. Miśkiewicz, S. Jodzis, Z. Kaszkur, Z. Kowalczyk, *Appl. Catal. A*, 2006, 300, 181-185.

[55] S. Hagen, R. Barfod, R. Fehrmann, C. J. H. Jacobsen, H. T. Teunissen, K. Ståhl, I. Chorkendorff, *Chem. Commun*. 2002, 1206-1207.

[56] S. Hagen, R. Barfod, R. Fehrmann, C. J. H. Jacobsen, H. T. Teunissen, I. Chorkendorff, *J. Catal.* 2003, 214, 327-335.

[57] I. Chorkendorff, J. W. Niemantsverdriet, *Concepts of Modern Catalysis And Kinetics*, Weinheim, Wiley-VCH Verlag GmbH & Co. KGaA, 2003.

[58] http://www.kbr.com/technology/Ammonia-and-Fertilizer/KBR-Advanced-Ammonia-Process-KAAP.aspx

[59] F. Ephraim, *Ber. D. D. Chem. Gesell.,* 1912, 45, 1322-1331

[60] F. Ephraim, *Z. Phys. Chem.,* 1913, 81, 513-542.

[61] W. Biltz, *Z. Anorg. Allgem. Chem.,* 1923, 130, 93-139.

[62] D. Mosher, X. Tang, S. Arsenault, *High Density Hydrogen Storage System Demonstration Using $NaAlH_4$ Based Complex Hydrides*, FY 2006 Annual Progress Report, DoE Hydrogen Program, 2006, 281-284.

[63] X. Liu, Y. Zhu, L. Li, *Int. J. Hydrogen Energy*, 2007, 32, 2450-2454.

[64] K. Nomura, S. Fujiwara, H. Hayakawa, E. Akiba, Y. Ishido, S. Ono, *Journal of the Less-Common Metals*, 1991, 169, 9-17.

[65] E. Suissa, I. Jacob, Z. Hadari, *Journal of the Less-Common Metals*, 1984, 104, 287-295

[66] M. A. El-Osairy, I. A. El-Osery, A. M. Metwally, M. A. Hassan, *Int. J. Hydrogen Energy*, 1993, 18 (6), 517-524.

[67] Laidler, K. J.; Meiser, J. H. Physical Chemistry, third edition, New York, Houghton Mifflin Company, 1999.

[68] W. Biltz, E. Rahlfs, *Z. Anorg. Allgem. Chem.,* 1927, 166, 351-376.

[69] E. Lepinasse, B. Spinner, *Rev. Int. Froid.,* 1994, 17, 309-321.

[70] W. Biltz, C. Messerknecht, *Z. Anorg. Allgem. Chem.,* 1925, 148, 157-189.

[71] W. Biltz, *Z. Anorg. Allgem. Chem.,* 1925, 148, 192-206.

[72] W. Biltz, C. Mau, *Z. Anorg. Allgem. Chem.,* 1925, 148, 170-191.

[73] R. Z. Sørensen, J. S. Hummelshøj, A. Klerke, J. B. Reves, T. Vegge, J. K. Nørskov, C. H. Christensen, *J. Am. Chem. Soc.,* 2008, 130, 8660-8668.

[74] H. S. Jacobsen, H. A. Hansen, J. W. Andreasen, Q. Shi, A. Andreasen, R. Feidenhans'l, M. M. Nielsen, K. Ståhl, T. Vegge, *Chem. Phys. Lett.*, 2007, 441, 255-260.

[75] J. S. Hummelshøj, R. Z. Sørensen, M. Y. Kustova, T. Johannesen, J. K. Nørskov, C. H. Christensen, *J. Am. Chem. Soc.*, 2006, 128, 16-17.

[76] T. D. Elmøe, R. Z. Sørensen, U. Quaade, C. H. Christensen, J. K. Nørskov, T. Johannessen, *Chem. Eng. Sci,.* 2006, 61, 2618–2625.

[77] http://www.amminex.net/

[78] A. H. White, Wm. Melville, *J. Am. Chem. Soc.,* 1905, 27, 373-386.

[79] G. Ertl, M. Huber, *J. Catal.,* 1980, 61, 537-539.

[80] J. B. Hansen, *Ammonia, Catalysis and Manufacture* (Ed.: A. Nielsen), Springer, Heidelberg, 1995, 149-198.

[81] C. H. Christensen, T. Johannessen, R. Z. Sørensen, J. K. Nørskov, *Catal. Today*, 2006, 111, 140-144.

[82] G. G. M. Fournier, I. W. Cumming, K. Hellgardt, *J. Power Sources*, 2006, 162, 198-206.

[83] G. Meng, C. Jiang, J. Ma, Q. Ma, X. Liu, *J. Power Sources*, 2007, 173, 189.

[84] C. M: Finnerty, N. J. Coe, R. H. Cunningham, R. M. Ormerod, *Catal. Today,* 1998, 46, 137-145.

[85] M. Itome, A. E. Nelson, Catal. Lett., 2006, 106, 21-27.

[86] C. H. Christensen, International Symposium on Materials Issues in a Hydrogen Economy, Richmond, Virginia, 2007.

[87] J. C. Ganley, *J. Power Sources*, 2008, 178, 44-47.

[88] N. Maffei, L. Pelletier, A. McFarlan, *J. Power Sources,* 2008, 175, 221-225.

[89] R. Halseid, P. J. S. Vie, R. Tunold, *J. Power Sources*, 2006, 154, 343-350.

[90] T. V. Choudhary, C. Sivadinarayana, D. W. Goodman, *Chem. Eng. J.,* 2003, 93, 69-80.

[91] J. C. Ganley, F. S. Thomas, E. G. Seebauer, R. I. Masel, *Catal. Lett.,* 2004, 96, 117-122.

[92] A. S. Chellappa, C. M. Fisher, W. J. Thomson, *Appl. Catal. A: Gen ,* 2002, 227, 231-240.

[93] J. C. Ganley, E. G. Seebauer, R. I. Masel, *J. Power Sources,* 2004, 137, 53-61.

[94] R. Z. Sørensen, A. Klerke, U. Quaade, S. Jensen, O. Hansen, C. H. Christensen, *Catal. Lett.* 2006, 112, 77-81.

[95] T. V. Choudhary, D. W. Goodman, *Catal. Today,* 2002, 77, 65-78.

[96] S. R. Logan, R. L. Moss, C. Kemball, *T. Faraday Soc.,* 1958, 54, 922-930.

[97] S. R. logan, C. Kemball, *T. Faraday Soc.,* 1960, 56, 144-153.

[98] J. H. Sinfelt, *AIChE J.*, 1973, 19, 673-683.

[99] A. Boisen, S. Dahl, J. K. Nørskov, C. H. Christensen, *J. Catal.*, 2005, 230, 309-312.

[100] http://www.nikki-chem.co.jp/eng/products/pro3_2.html

[101] M. C. J. Bradford, P. E. Fanning, M. A. Vannice, *J. Catal.*, 1997, 172, 479-484.

[102] S. R. Deshmukh, A. B. Mhadeshwar, D. G. Vlachos, *Ind. Eng. Chem. Res.*, 2004, 43, 2986-2999.

[103] J. Zhang, H. Xu, W. Li, *Appl. Catal. A: Gen.*, 2005, 296, 257-267.

[104] W. Arabczyk, J. Zamłynny, *Catal. Lett.*, 1999, 60, 167-171.

[105] A. Jedynak, Z. Kowalczyk, D. Szmigiel, W. Raróg, J, Zieliński, *Appl. Catal. A: Gen.*, 2002, 237, 223-226.

[106] J. Zhang, M. Comotti, F. Schüth, R. Schlögl, D. S. Su, *Chem. Commun.*, 2007, 19, 1916-1918.

[107] S.-F. Yin, Q.-H. Zhang, B.-Q. Xu, W.-X. Zhu, C.-F. Ng, C.-T. Au, *J. Catal.*, 2004, 224, 384-396.

[108] Z. Lendzion-Bieluń, R. Pelka, W. Arabczyk, *Catal. Lett.*, 2009, 119-123.

[109] Y. Liu, H. Wang, J. Li, Y. Lu, H. Wu, Q. Xue, L. Chen, *Appl. Catal. A: Gen.*, 2007, 328, 77-82.

[110] W. Zheng, J. Zhang, Q. Ge, H. Xu, W. Li, *Appl. Catal. B: Environ.*, 2008, 80, 98-105.

[111] H. Liu, H. Wang, J. Shen, Y. Sun, Z. Liu, *Catal. Today*, 2008, 131, 444-449.

[112] W. Raróg, Z. Kowalczyk, J. Sentek, D. Składanowski, D. Szmigiel, J. Zieliński, *Appl. Catal. A: Gen.*,2001, 208,213-216.

[113] W. Raróg-Pilecka, D. Szmigiel, A. Komornicki, J. Zieliński, Z. Kowalczyk, *Carbon*, 2003, 41, 589-591.

[114] S.-F. Yin, B.-Q. Xu, C.-F. Ng, C.-T. Au, *Appl. Catal. B: Environ.*, 2004, 48, 237-241.

[115] S.-F. Yin, B.-Q. Xu, W.-X. Zhu, C.-F. Ng, X.-P. Zhou, C.-T. Au, *Catal. Today*, 2004, 93-95, 27-38.

[116] S. T. Oyama, *J. Catal.*, 1992, 133, 358-369.

[117] J.-G. Choi, *J. Catal.*, 1999, 182, 104-116.

[118] H. Liu, H. Wang, J. Shen, Y. Sun, Z. Liu, *React. Kinet. Catal. Lett.*, 2008, 97, 11-17.

[119] M. Grosman, D. G. Löffler, *J. Catal.*, 1983, 80, 188-193.

[120] S. S. Pansare, J. G. Goodwin, Jr., *Ind. Eng. Chem. Res.*, 2008, 47, 4063-4070.

[121] S. S. Pansare, W. Torres, J. G. Goodwin, Jr., *Catal. Commun.* 2007, 8, 649-654.

[122] A. Vavere, R. S. Hansen, *J. Catal.*, 1981, 69, 158-171.

[123] A. K. Santra, B. K. Min, C. W. Yi, K. Luo, T. V. Choudhary, D. W. Goodman, *J. Phys. Chem. B,* 2002, 106, 340-344.

[124] T. V. Choudhary, C. Sivadinarayana, D. W. Goodman, *Catal. Lett.*, 2001, 72, 197-201.

[125] T. V. Choudhary, A. K. Santra, C. Sivadinarayana, B. K. Min, C.-W. Yi, K. Davies, D. W. Goodman, *Catal. Lett.*, 2001, 77, 1-5.

[126] J. Zhang, H. Xu, X. Jin, Q. Ge, W. Li, *Appl. Catal. A: Gen.* 2005, 290, 87-96.

[127] R. Z. Sørensen, L. J. E. Nielsen, S. Jensen, O. Hansen, T. Johannesen, U. Quaade, C. H. Christensen, *Catal. Commun.*, 2005, 6, 229-232.

[128] W. Zheng, J. Zhang, H. Xu, *Catal. Lett.*, 2007, 119, 311-318.

[129] S.-F. Yin, B.-Q. Xu, S.-J. Wang, C.-T. Au, *Appl. Catal. A: Gen.*, 2006, 301, 202-210.

[130] X.-K. Li, W.-J. Ji, J. Zhao, S.-J. Wang, C.-T. Au, *J. Catal.* 2005, 236, 181-189.

[131] H. Liu, H. Wang, J. Shen, Y. Sun, Z. Liu, *Appl. Catal. A: Gen.*, 2008, 337, 138-147.

[132] D. Szmigiel, W. Raróg-Pilecka, E. Miśkiewicz, Z. Kaszkur, Z. Kowalczyk, *Appl. Catal. A: Gen.*, 2004, 264, 59-63.

[133] J. Zhang, H. Xu, Q. Ge, W. Li, *Catal. Commun.*, 2006, 7, 148-152.

[134] W. Raróg-Pilecka, D. Szmigeel, Z. Kowalczyk, S. Jodis, J. Zielinski, *J. Catal.*, 2003, 218, 465-469.

[135] S.-F. Yin, B.Q. Xu, X.P. Zhou, C.T. Au, *Appl. Catal. A: Gen.*, 2004, 277, 1-9.

[136] S.-J. Wang, S.-F. Yin, L. Li, B.-Q. Xu, C.-F. Ng, C.-T. Au, *Appl. Catal. B: Environ.*, 2004, 52, 287-299.

[137] L. Li, Z. H. Zhu, Z. F. Yan, G. Q. Lu, L. Rintoul, *Appl. Catal. A: Gen.*, 2007, 320, 166-172.

[138] L. Li, Z. H. Zhu, G. Q. Lu, Z. F. Yan, S. Z. Qiao, *Carbon,* 2007, 45, 11-20.

[139] A. Klerke, S. K. Klitgaard, R. Fehrmann, *Catal. Lett.*, 2009, *in press.*

[140] L. Forni, D. Molinari, I. Rossetti, N. Pernicone, *Appl. Catal. A: Gen.,* 1999, 185, 269-275.

[141] W. Raróg, Z. Kowalczyk, J. Sentek, D. Składanowski, J. Zieliński, *Catal. Lett.,* 2000, 68, 163-168.

[142] Z. Kowalczyk, M. Krukowski, W. Raróg-Pilecka, D. Szmigiel, J. Zieliński, *Appl. Catal. A: Gen.,* 2003, 248, 67-73.

[143] S. E. Siporin, R. J. Davis, W. Raróg-Pilecka, D. Szmigiel, Z. Kowalczyk, *Catal. Lett.,* 2004, 93, 61-65.

[144] S. E. Siporin, R. J. Davis, *J. Catal.,* 2004, 225, 359-368.

[145] W. Raróg-Pilecka, E. Miśkiewicz, D. Szmigiel, Z. Kowalczyk, *J. Catal.,* 2005, 231, 11-19.

[146] W. Raróg-Pilecka, E. Miśkiewicz, S. Jodzis, J. Petryk, D. Łomot, Z. Kaszkur, Z. Karpiński, Z. Kowalczyk, *J. Catal.,* 2006, 239, 313-325.

[147] L. Miao, Y. Ina, S. Tanemura, T. Jiang, M. Tanemura, K. Kaneko, S. Toh, Y. Mori, *Surf. Science,* 2007, 601, 2792-2799.

[148] G. H. Du, Q. Chen, L.-M. Peng, *Appl. Phys. Lett.,* 2001, 79, 3702-3704.

[149] S. K. Klitgaard, A. T. DeLaRiva, S. Helveg, R. M. Werchmeister, C. H. Christensen, *Catal. Lett.,* 2008, 126, 213-217.

[150] Q. Chen, W. Zhou, G. Du, L.-M. Peng, *Adv. Mater.,* 2002, 14, 1208-1211.

[151] G. H. Du, Q. Chen, P. D. Han,1,3 Y. Yu, L. -M. Peng, *Phys. Rev. B,* 2003, 67, 35323-1-7.

[152] I. E. Grey, I. C. Madsen, J. A. Watts, L. A. Bursill, J. Kwiakowska, *J. Solid state chem.,* 1985, 58, 350-356.

[153] N. Masaki, S. Uchida, T. Sato, *J. Mater. Chem.,* 2002, 12, 305-308.

[154] M. Guraya, S. Sprenger, W. Rarog-Pilecka, D. Szmigiel,Z. Kowalczyk, M. Muhler, *Appl. Surf. Sci.,* 2004, 238, 77-81.

[155] M. J. Lippits, A. C. Gluhoi, B. E. Nieuwenhuys, *Catal. Today,* 2008, 137, 446-452.

[156] L. Gang, B. G. Anderson, J. van Grondelle, R. A. van Santen, W. J. H. van Gennip, J. W. Niemantsverdriet, P. J. Kooyman, A. Knoester, H. H. Brongersma, *J. Catal.,* 2002, 206, 60-70.

[157] http://www.ird.dk/

Appendix

Publications with relevance to this thesis include as appendix:

1 A. Klerke, S. K. Klitgaard, R. Fehrmann, **Catalytic ammonia decomposition over ruthenium nanoparticles supported on nano-titanates**, *Catal. Lett.* 2009, accepted.

2 R. Z. Sørensen, J. S. Hummelshøj, A. Klerke, J. B. Reves, T. Vegge, J. K. Nørskov, C. H. Christensen, **Indirect, reversible high-density hydrogen storage in compact metal ammine salts**, *J. Am. Chem. Soc.*, 2008, 130, 8660-8668.

3 A. Klerke, C. H. Christensen, J. K. Nørskov, T. Vegge, **Ammonia for Hydrogen Storage: Challenges and Opportunities**, *J. Mater. Chem.*, 2008, 18, 2304-2310.

4 R. Z. Sørensen, A. Klerke, U. Quaade, S. Jensen, O. Hansen, C. H. Christensen, **Promoted Ru on high-surface area graphite for efficient miniaturized production of hydrogen from ammonia**, *Catal. Lett.*, 2006, 112, 77-81.

5 T. Vegge, R. Z. Sørensen, A. Klerke, J. S. Hummelshøj, T. Johannessen, J. K. Nørskov, C. H. Christensen, **Indirect Hydrogen Storage in Metal Ammines**, *Solid-state hydrogen storage: Materials and chemistry,* Woodhead Publishing LTD., England, 2008.

6 A. Klerke, J. Engbæk, R. Z. Sørensen, R. Fehrmann, **Ammonia and Metal Ammines for High Density Hydrogen Storage**, 2009 AIChE Spring National Meeting, conference proceeding paper.

7 A. Klerke, R. Z. Sørensen, C. H. Christensen, U. Quaade, J. K. Nørskov, **Compact Hydrogen Production from Ammonia Stored in Solid Metal Ammines**, World Hydrogen Technologies Convention 2007, conference proceeding paper.

Springer

Catalytic ammonia decomposition over ruthenium nanoparticles supported on nano-titanates.

Journal:	*Catalysis Letters*
Manuscript ID:	CATLET-2009-0136.R1
Manuscript Type:	Original Manuscript
Date Submitted by the Author:	27-Mar-2009
Complete List of Authors:	Klerke, Asbjørn; Technical University of Denmark, DTU Chemistry Klitgaard, Søren; Technical University of Demark, Department of Chemistry Fehrmann, Rasmus; Technical University of Demark, Department of Chemistry
Keywords:	Ammonia decomposition, ruthenium nanoparticles, titanate nanowires, titanate nanotubes, hydrogen production

scholarONE™ Manuscript Central

For Review Only

Catalytic ammonia decomposition over ruthenium nanoparticles supported on nano-titanates.

Asbjørn Klerke, Søren Kegnæs Klitgaard, Rasmus Fehrmann*.

Centre for Catalysis and Sustainable Chemistry, Department of Chemistry, Building 206, Technical University of Denmark, DK-2800 Kgs. Lyngby, Denmark.

*E-mail: rf@kemi.dtu.dk Phone: +45 4525 2388

Abstract:

Nanosized $Na_2Ti_3O_7$, $K_2Ti_6O_{13}$ and $Cs_2Ti_6O_{13}$ materials were prepared and used as supports of ruthenium nanoparticles for catalytic ammonia decomposition. It is shown that these catalysts exhibit higher catalytic activity than ruthenium supported on TiO_2 nanoparticles promoted with cesium. The difference is attributed to the use of nanostructured materials with incorporated alkali metals in the crystal lattice, which apparently gives a higher effect of the promoter. All samples were characterized by X-ray powder diffraction (XRPD), transmission electron microscopy (TEM) and N_2 physisorption measurements. Furthermore, the effect of ruthenium loading on the catalytic decomposition of ammonia was investigated.

Short title: Catalytic ammonia decomposition.

Keywords: Ammonia decomposition, ruthenium nanoparticles, titanate nanowires, titanate nanotubes, hydrogen production.

1. Introduction

In the past decades, the increased CO_2-emission to the atmosphere from utilization of fossil fuels has led to intensive research in order to substitute the fossil resources, like oil and coal, with suitable alternatives. One of the more promising ideas is to use hydrogen as energy carrier [1,2,3].

For Peer Review

KOH (Sigma-Aldrich 90%), and $CsOH{\cdot}H_2O$ (Sigma-Aldrich, cabot high-purity grade) giving the corresponding alkaline titanate nanostructures: sodium titanates $Na_2Ti_3O_7$ nanotubes, potassium titanates $K_2Ti_6O_{13}$ nanowires and cesium titanates $Cs_2Ti_6O_{13}$ nanowires [35,36,37]. The produced materials were then used as supports for ruthenium nanoparticles.

In a typical synthesis of the alkaline titanate nanomaterials, 1.92 g of the commercial TiO_2 anatase nanoparticles were suspended in 160 ml of aqueous 10 M alkaline base, followed by hydrothermal treatment at 150°C in a stainless Teflon-lined autoclave for 72 h. The resulting powders were washed with large amounts of distilled water until neutral pH was achieved and dried at room temperature.

Preparation of ruthenium nanoparticles

The catalysts were prepared from 0.5 g of the titanate nanostructured material by incipient wetness impregnation using a ruthenium nitrosyl nitrate solution with a ruthenium content of 8.1 wt%. After impregnation, the sample was calcined in air at 250°C.

2.2. Physicochemical characterization

Transmission electron microscopy

Transmission electron microscopy (TEM) was performed on a JEM 2000 FX with an accelerating voltage of 300 kV. A few mg of the powdered samples were suspended in 2 ml ethanol, and the suspension was sonicated for 30 min. The suspension was allowed to settle for 15 min, before a drop was taken and dispersed on a 300 mesh copper grid coated with Holey carbon film.

X-ray powder diffraction

X-ray powder diffraction patterns (XRPD) were recorded using Cu-K_α radiation in the 2θ interval of 5 to 100° by a Philips PW 1820/3711 powder diffractometer.

Nitrogen adsorption and desorption

For Peer Review

Nitrogen adsorption and desorption measurements were performed at liquid nitrogen temperature on a Micromeretics ASAP 2020. The samples were outgassed in vacuum at 200°C prior to measurement. Total surface areas were calculated according to the BET method.

CO-pulse chemisorption

CO-pulse chemisorption was performed on the same catalyst batch used for activity testing. The CO-pulse chemisorbtion was done on a Micromeretics Auto Chem II chemisorption analyzer. A sample of 0.1g catalyst was reduced in hydrogen for 2h at 400°C, then the gas was switched to helium for 1h before the sample was cooled in a flow of helium to 50°C and pulsed with 5% CO in helium. From the amount of adsorbed CO the apparent particle size was calculated.

2.3 Catalyst testing

The catalyst testing was performed in a specialized setup for ammonia decomposition. 0.1g of catalyst was transferred to the stainless steel reactor with an inner diameter of 4.6 mm, where it was reduced for 5 hours at 400°C in a 100 ml/min flow of hydrogen. The temperature of 400°C for reduction in all experiments is selected to avoid decomposition of the alkali nano-titanate supports. The decomposition of the supports was observed in catalytic testing at 490°C as a rapid deactivation of the catalysts and can be due to ammonia or hydrogen destabilizing the nanostructure at high temperatures. The temperature can influence the degree of reduction; if the reduction is not complete the measured apparent particle size will increase. The testing was done from 400°C and down using steps of 15°C in a flow of 20 ml/min ammonia and 50 ml/min argon. The ammonia concentration in the carrier stream was determined using a Fischer-Rosemount NGA 2000 equipped with a MLT analyzer calibrated to NH_3 concentrations from 0.03-30%.

3. Results and discussion

For Peer Review

3.1 Characterisation

The prepared titanate nanostructured support materials were analysed with high-resolution TEM. Representative TEM images of the titanate nanomaterials can be seen in Figure 1.

In Figure 1A, the TiO_2 anatase nanoparticles used as starting material for the synthesis of the alkaline titanate nanomaterials are shown. The results of the hydrothermal treatments of TiO_2 anatase nanoparticles with different alkaline bases, NaOH, KOH, and CsOH, are shown in Figures 1B, 1C and 1D, respectively. From the TEM images, is it seen that the hydrothermal treatment gives nanotubes in the case of NaOH, whereas the use of KOH or CsOH gives small flakes/nanowires. Table 1 shows the BET surface areas of samples obtained after hydrothermal treatment with different alkaline bases. From Table 1, it is seen that the surface areas of the nanostructured titanates increase significantly after the hydrothermal treatments with the different alkaline bases in comparison with the starting anatase TiO_2.

The support materials were also investigated using XRPD. The obtained XRPD-patterns for all the nanomaterial samples are shown in Figure 2.

The XRPD patterns were obtained in the interval from 5 to 100 (2θ) degrees. XRPD patterns for nanostructured titanates were obtained after hydrothermal treatment. Figure 2A shows crystalline TiO_2 anatase. The other nanomaterials appear less crystalline but this is only because the nanotubes and nanowires are too thin to yield good diffraction. Thus, it is concluded that all the titanium in the samples is present as nanostructured titanate materials and that no TiO_2 nanoparticles are present. The obtained XRPD patterns are very similar to those previously published for $Na_2Ti_3O_7$ nanotubes [38], $K_2Ti_6O_{13}$ nanowires [39] and $Cs_2Ti_6O_{13}$ nanowires [40,41].

For Peer Review

3.2 Catalyst testing

All catalysts were tested under the same conditions in a constant flow of ammonia diluted with argon as described in the experimental section. In Figure 3, an Arrhenius type plot showing the catalytic rate based on active metal concentration of 3% ruthenium on TiO_2 nanoparticles, $Na_2Ti_3O_7$ nanotubes, $K_2Ti_6O_{13}$ and $Cs_2Ti_6O_{13}$ nanowires is given. This confirms the general trend for promotion of ruthenium catalysts with different alkali metals in the ammonia decomposition reaction [34,42,43,44].

From Figure 3, it is seen that the promoting effect of alkali metals increases in the order: Cs>K>Na. To verify that the higher catalytic activity of $Cs_2Ti_6O_{13}$ nanowires was due to structural changes, the ruthenium on TiO_2 support was promoted with a similar cesium loading(~30 wt%) using a $CsNO_3$ solution. The promoter was deposited on the already prepared 3% Ru TiO_2 with incipient wetness impregnation, calcined, and tested (not shown), but it showed lower activity than the pure ruthenium on TiO_2. This shows that incorporating alkali metal promoters into the crystal lattice of the nano-titanates, gives a stronger promoting effect than surface deposition of the promoter on top of the ruthenium. The lower activity after promotion has not been seen in other studies were high cesium loadings has been impregnated on a ruthenium catalyst [31,34,45].

The relatively high catalytic activity of ruthenium on the nano-titanates can thus be explained by the promoting effect of the alkali metals in the crystal lattice. Furthermore the higher surface area of the alkali titanates will increase the dispersion of the Ru-nanoparticles on the surface.

To further investigate the effect of the $Cs_2Ti_6O_{13}$ support material, samples with different ruthenium loadings were prepared, in order to find the optimum ruthenium content. The effect of varying the ruthenium loading is shown in Figure 4, the rates are plotted at 377°C.

For Peer Review

The two plots in Figure 4 illustrate that different normalizing factors is important for understanding the data. For the weight based normalization the normalization factor is constant as all test is done with same amount of catalyst (0.1g)For normalization to molar ruthenium content the normalization factor changes with a factor of 20 from 0.05 mmol/g to 0.99 mmol/g. This favours low loading best seen with a comparison between 1 and 5 wt% ruthenium. The two catalysts have similar rates on weight base but on mole base the five times higher Ru-loading of 5 wt% sample gives a rate on mole base that is one fifth of the 1 wt% sample.

From Figure 4, it is seen that the best utilization of the available ruthenium on a molar base is achieved with a loading of 1 wt%. The reaction rate also show that the activity per mole ruthenium decreases until a loading of 5 wt% is reached, here after the activity stabilizes. However, the change in specific activity as a function of ruthenium loading is almost invariant, the main features being a lower spread in activity and a shift of the maximum activity to a loading of 3 wt% ruthenium. This is interesting regarding catalyst mass optimization.

The change in activity can partly be explained by different particle sizes, which were measured by CO-chemisorption, see Table 2.

By comparison of the particle size and activity normalised to the ruthenium amount in mole, it is seen that there is a good correlation between the measured particle size and the relative activity. The loading of 1% ruthenium has the highest activity and the lowest particle size. We have no experimental explanation of the observed lower particle size of this catalyst compared to the others displayed in Table 2. The 0.5% and 3% ruthenium loadings have particle sizes and activities in the same ranges. The 10% ruthenium loading have the highest measured particle size and lowest activity. This is however, not the full picture, as the particle size for the 10% ruthenium is only

For Peer Review

slightly larger than for the 3% ruthenium. This indicates that the ratio between cesium and ruthenium also has influence on the measured activity.

Thus, if we look at the particle size and activity for 0.5%, 3%, and 10% ruthenium, the particle size is in the same range and should not result in large differences in activity due to changes in particle size. This tells us that the cesium loading is also important for the activity and from the ratios of cesium to ruthenium in Table 2, it is clear that a ratio higher than 5 is preferable, if it is assumed that the 5% loading of ruthenium has similar particle size.

To determine what ratio of cesium to ruthenium is optimal the particle size must be controlled better. Otherwise it is difficult to determine which effect is most important. This also means that the optimal loading of 1% ruthenium may be a combination of small better dispersed particles and more frequent contact between cesium and ruthenium. This is due to the limited surface exposure of the cesium ions, defined by the distribution of cesium in the crystal lattice of the cesium titanate. This scenario is also supported by the non-promoting effect observed by loading non-titanate cesium on the surface of the Ru-TiO_2 catalyst.

4. Conclusions

In conclusion, the synthesis of the nanostructured support materials $Na_2Ti_3O_7$, $K_2Ti_6O_{13}$, and $Cs_2Ti_6O_{13}$ from anatase TiO_2 nanoparticles has been performed. The produced nanostructured materials were loaded with ruthenium and tested in the ammonia decomposition reaction. The clear promoting effect of alkaline metals increasing in the sequence: Cs>K>Na was shown. Furthermore, a significant effect of the incorporation of the promoters in the support crystal lattice instead of classic surface promoting procedures was obtained. Further development of these Ru-titanate catalysts should also include long term stability measurement in the desired temperature interval.

For Peer Review

Finally, the optimal apparent ruthenium loading on $Cs_2Ti_6O_{13}$ was found to be 1%, but further studies on the influence of the ruthenium particle size and the metal loading on the catalytic activities are needed, for this conclusion.

Acknowledgements

The Danish National Research Foundation is sponsoring the Center for Sustainable and Green Chemistry. The project is also supported by The Danish Council for Strategic Research (Project no. 2104-05-0016).

References:

1 M. Dresselhaus, G. Crabtree and M. Buchanan, Basic Research Needs for a Hydrogen Economy (U.S. Department of Energy, 2003).

2 G. Crabtree, M. Dresselhaus and M. Buchanan, Physics Today 57, 12 (2004) 39.

3 J. A. Turner, Science 305 (2004) 972.

4 D. Sun, S. S. Srinivasan, G. Chen and C. M. Jensen, Rehydrogenation, J. Alloy. Compd. 373, 1-2 (2004) 265.

5 H. Furukawa, M. A. Miller and O. M. Yaghi, J. Mater. Chem. 17 (2007) 3197.

6 Z. Łodziana and T. Vegge, Phys. Rev. Lett. 93 (2004) 145501.

7 K. Chłopek, C. Frommen, A. Leon, O. Zabara and M. Fichtner, J. Mater. Chem. 17 (2007) 3496.

8 J. J. Vajo, S. L. Skeith and F. Mertens, J. Phys. Chem. B 109 (2005) 3719.

9 W. Lohstroh and M. Fichtner, J. Alloys Compounds 332 (2007) 446.

10 A. Zûttel, Mater. Today, September (2003) 24.

11 J. R. Rostrup-Nielsen and T. Rostrup-Nielsen, Cattech, 6 (2002) 150.

12 W. W. Clark II and J. Rifkin, Energy Policy 34 (2006) 2630.

13 M. Ni, D. Y. C. Leung, M. K. H. Leung and K. Sumathy, Fuel Process. Technol. 87 (2006) 461.

14 M. Saxe and P. Alvfors, Energy 32 (2007) 42.

15 M. Ni, M. K. H. Leung, D. Y. C. Leung and K. Sumathy, Renew. Sust. Energ. Rev. 11 (2007) 401.

16 http://www.ballard.com/

For Peer Review

17 http://www.dantherm-power.com/

18 V. Neburchilov, J. Martin, H. Wang and J. Zhang, J. Power Sources 169 (2007) 221.

19 E.R. Delsman, C.U. Uju, M.H.J.M. de Croon, J.C. Schouten and K.J. Ptasinski, Energy 31 (2006) 3300.

20 G. Thomas and G. Parks, Potential Roles of Ammonia in a Hydrogen Economy (U.S. Department of Energy, 2006).

21 C. Zamfirescu and I. Dincer, J. Power Sources 185 (2008) 459.

22 A. Klerke, C. H. Christensen, J. K. Nørskov and T. Vegge, J. Mater. Chem. 18 (2008) 2304.

23 R. Z. Sørensen, J. S. Hummelshøj, A. Klerke, J. B. Reeves, T. Vegge, J. K. Nørskov and C. H. Christensen, J. Am. Chem. Soc. 130 (2008) 8660.

24 T. Vegge, R. Z. Sørensen, A. Klerke, J. S. Hummelshøj, T. Johannessen, J. K. Nørskov and C. H. Christensen, Solid-state hydrogen storage: Materials and chemistry (Woodhead Publishing LTD., England, 2008).

25 C. H. Christensen, R. Z. Sørensen, T. Johannessen, U. Quaade, K. Honkala, T. D. Elmøe, R. Køhler and J. K. Nørskov, J. Mater. Chem. 15 (2005) 4106.

26 C. H. Christensen, T. Johannessen, R. Z. Sørensen and J. K. Nørskov, Catal. Today 111 (2006) 140.

27 J. B. Hansen, Ammonia, Catalysis and Manufacture, Ed.: A. Nielsen (Springer, Heidelberg, 1995).

28 A. S. Chellappa, C. M. Fisher, and W. J. Thomson, Appl. Catal. A 227 (2002) 231.

29 T.V. Choudhary, C. Sivadinarayan and D. W. Goodman, Catal. Lett. 72 (2001) 197.

30 J. C. Ganley, E. G. Seebauer, R. I. Masel, J. Power Sources, 2004, 137, 53-61.

31 W. Raróg-Pilecka, D. Szmigeel, Z. Kowalczyk, S. Jodis and J. Zielinski, J. Catal. 218 (2003) 465.

32 R.Z. Sørensen, L.J.E. Nielsen, S. Jensen, O. Hansen, T. Johannesen, U. Quaade and C.H. Christensen, Catal. Commun. 6 (2003) 229.

33 R.Z. Sørensen, A. Klerke, U. Quaade, S. Jensen, O. Hansen and C. H. Christensen, Catal. Lett. 112 (2006) 77.

34 S.F. Yin, B.Q. Xub, X.P. Zhou and C.T. Au, Appl. Catal. A. 277 (2004) 1.

35 L. Miao, Y. Ina, S. Tanemura, T. Jiang, M. Tanemura, K. Kaneko, S. Toh, Y. Mori, Surf. Science 601 (2007) 2792.

36 G. H. Du, Q. Chen, L.-M. Peng, Appl. Phys. Lett. 79 (2001) 3702.

For Peer Review

37 S. K. Klitgaard, A. T. DeLaRiva, S. Helveg, R. M. Werchmeister, C. H. Christensen, Catal. Lett., 126 (2008) 213.

38 Q. Chen, W. Zhou, G. Du and L.-M. Peng, Adv. Mater., 14 (2002) 1208.

39 G. H. Du, Q. Chen, P. D. Han,1,3 Y. Yu and L. -M. Peng, Phys. Rev. B 67 (2003) 035323.

40 I. E. Grey, I. C. Madsen, J. A. Watts, L. A. Bursill and J. Kwiakowska, J. Solid state chem., 58, (1985) 350.

41 N. Masaki, S. Uchida and T. Sato, J. Mater. Chem., 12 (2001) 305.

42 S. J. Wang, S. F. Yin, L. Li, B. Q. Xu, C. F. Ng, C. T. Au, Appl. Catal B-Environ., 52 (2004) 287.

43 M. Guraya, S. Sprenger, W. Rarog-Pilecka, D. Szmigiel,Z. Kowalczyk and M. Muhler, Appl. Surf. Sci. 238 (2004) 77.

44 J. Zhang, H. Xu, Q. Ge and W. Li, Catal Commun. 7 (2006) 152.

45 R. Z. Sørensen, A. Klerke, U. Quaade, S. Jensen, O. Hansen, and C. H. Christensen, Catal. Lett. 112 (206) 77.

For Peer Review

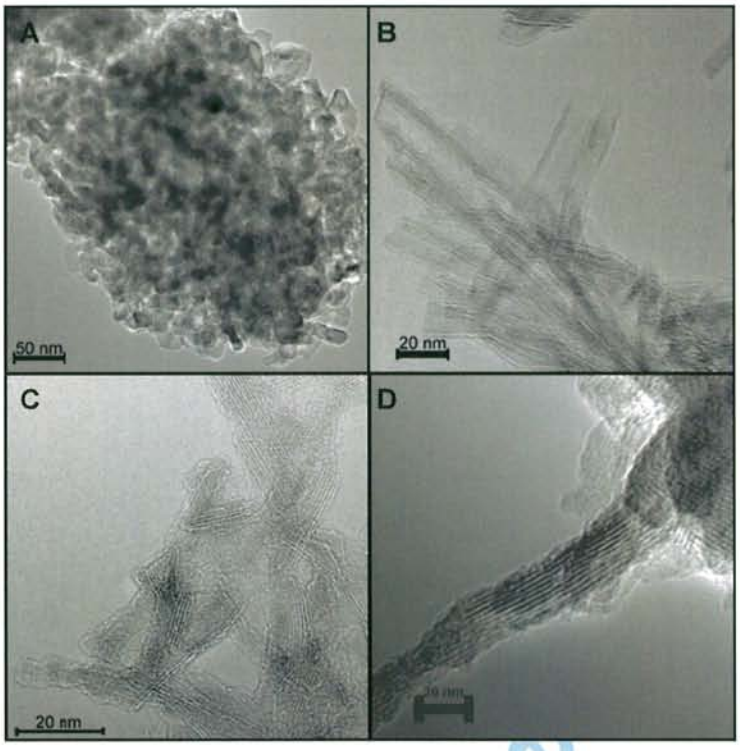

Figure 1. TEM images of (A) TiO_2 nanoparticles, (B) $Na_2Ti_3O_7$ nanotubes, (C) $K_2Ti_6O_{13}$ nanowires and (D) $Cs_2Ti_6O_{13}$ nanowires.

er Review

Table 1. BET surface areas of anatase TiO_2 before and after hydrothermal treatment with different alkaline bases.

Main product	BET surface area(m^2/g)	Base (M)	Time (h)	Temperature (°C)
TiO_2	139	-	0	-
$Na_2Ti_3O_7$	224	NaOH	72	150
$K_2Ti_6O_{13}$	309	KOH	72	150
$Cs_2Ti_6O_{13}$	208	$CsOH{\cdot}H_2O$	72	150

For Peer Review

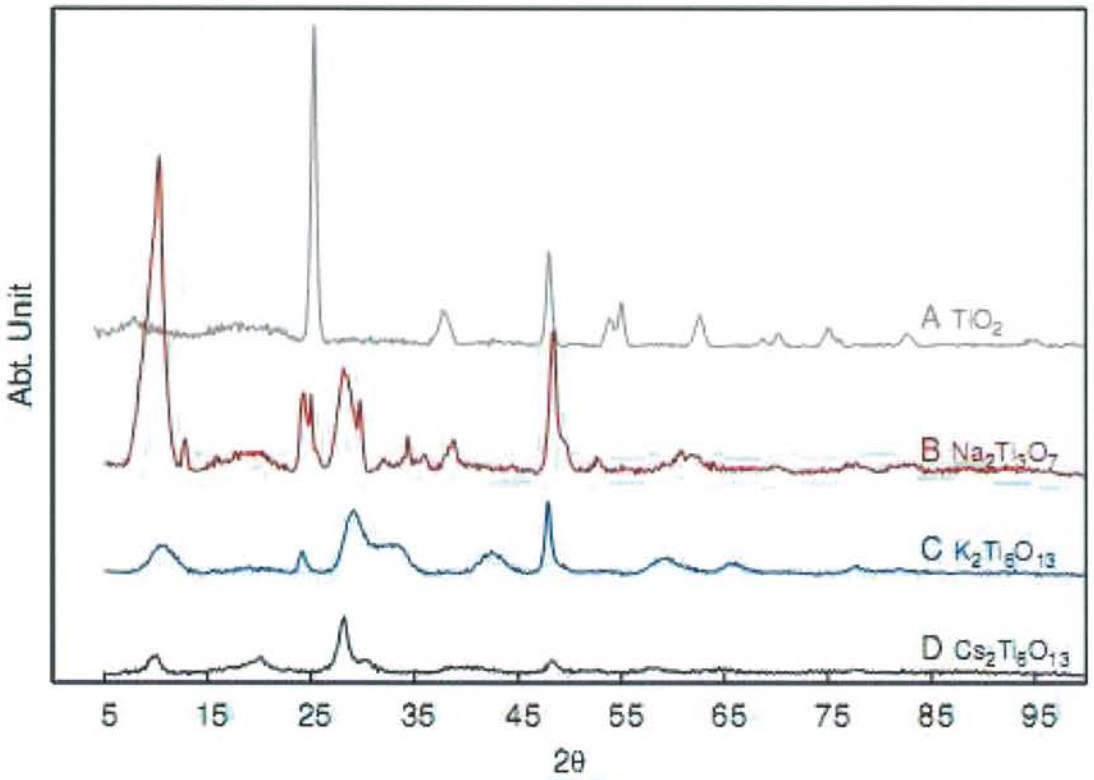

Figure 2. XRPD patterns of (A) TiO_2 nanoparticles, (B) $Na_2Ti_3O_7$ nanotubes, (C) $K_2Ti_6O_{13}$ nanowires and (D) $Cs_2Ti_6O_{13}$ nanowires.

For Review

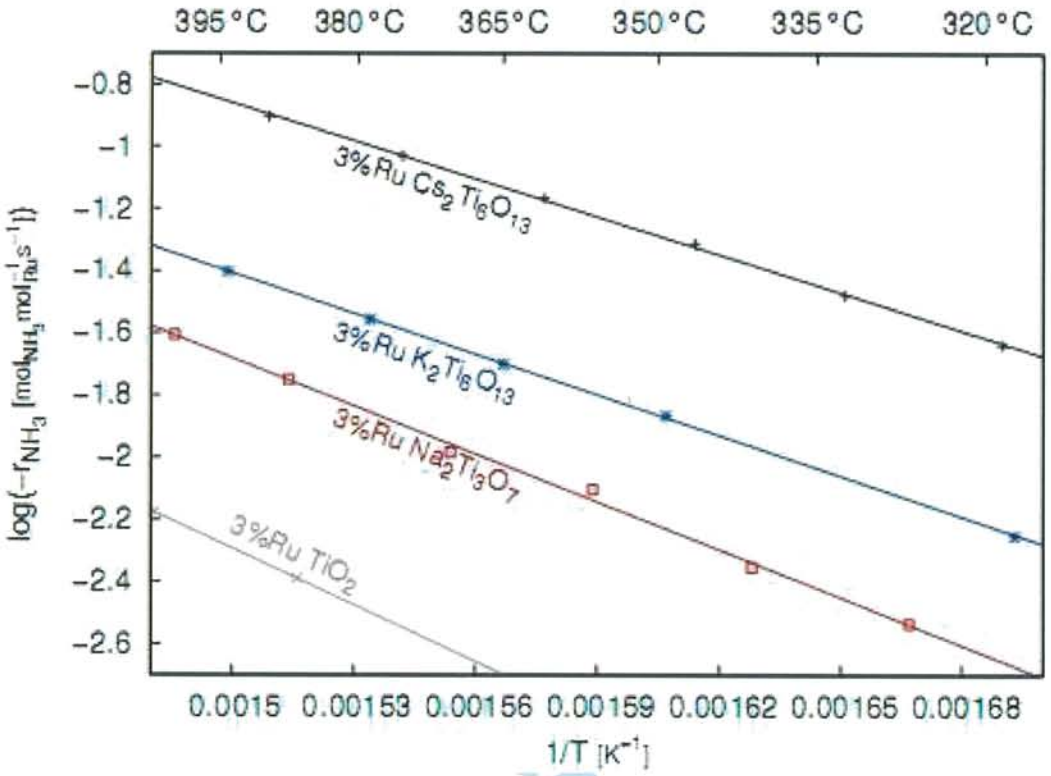

Figure 3. Arrhenius type plot for catalytic ammonia decomposition with 3 wt% ruthenium respectively on TiO_2 nanoparticles, $Na_2Ti_3O_7$ nanotubes, $K_2Ti_6O_{13}$ and $Cs_2Ti_6O_{13}$ nanowires as support materials

er Review

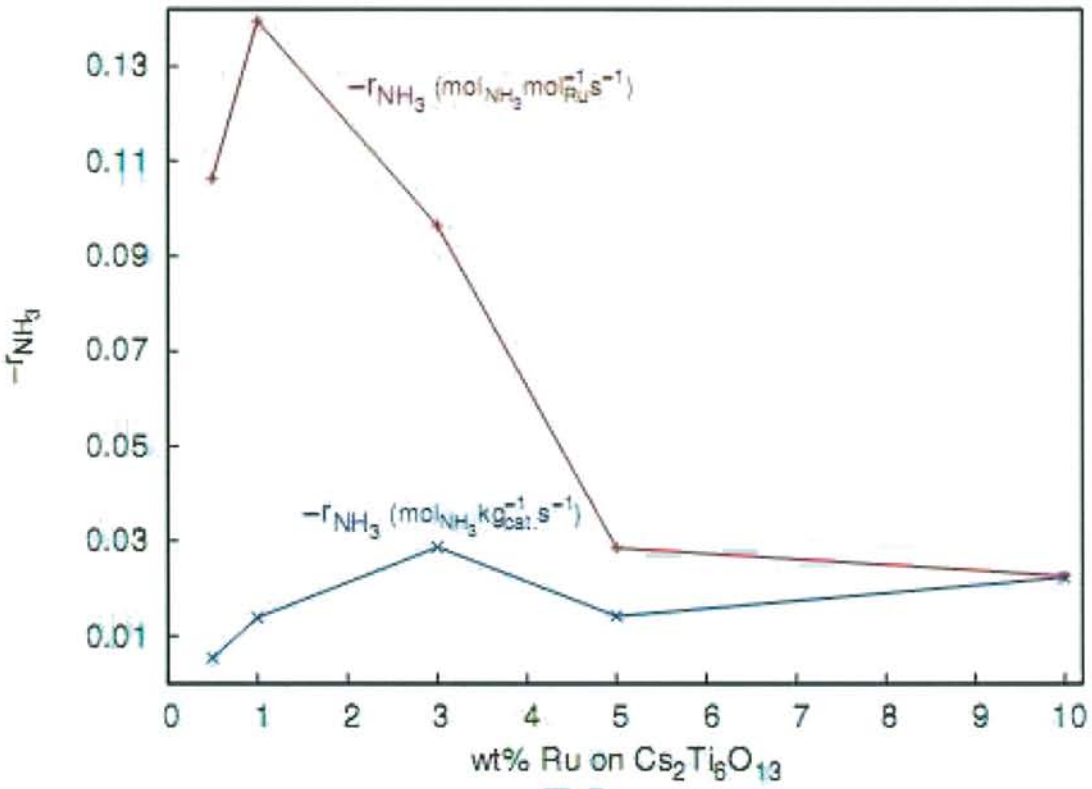

Figure 4. Reaction rate at 377°C plotted as a function of the ruthenium loading in wt%. The rates are normalised to molar ruthenium loading (red) and catalyst weight (blue).

For Review

Table 2: Measured particle sizes and molar ratios between cesium and ruthenium in the different catalysts for the same catalyst batches as used for activity measurements in Figure 4.

Wt% Ru $Cs_2Ti_6O_{13}$	Apparent particle size nm	Molar ratio Cs/Ru
0.5%	26.0	52.6
1%	7.8	26.2
3%	23.6	8.5
5%	-	5.0
10%	28.6	2.4

For Peer Review

Journal of the American Chemical Society

Subscriber access provided by Technical Knowledge Center | of Denmark

Article

Indirect, Reversible High-Density Hydrogen Storage in Compact Metal Ammine Salts

Rasmus Z. Sørensen, Jens S. Hummelshøj, Asbjørn Klerke, Jacob Birke Reves, Tejs Vegge, Jens K. Nørskov, and Claus H. Christensen

J. Am. Chem. Soc., **2008**, 130 (27), 8660-8668 • DOI: 10.1021/ja076762c • Publication Date (Web): 13 June 2008

Downloaded from http://pubs.acs.org on November 21, 2008

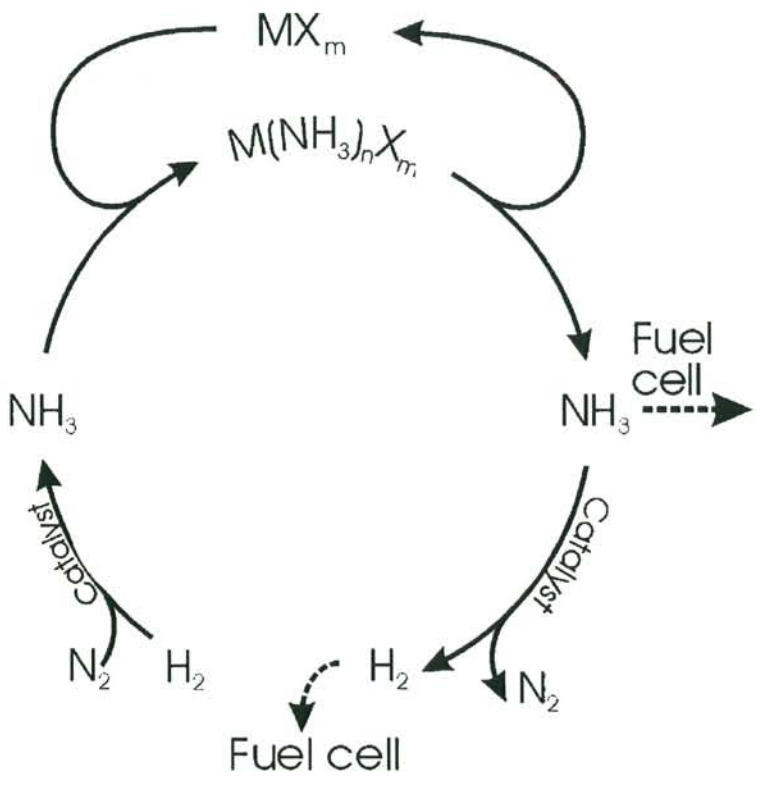

More About This Article

Additional resources and features associated with this article are available within the HTML version:

- Supporting Information
- Access to high resolution figures
- Links to articles and content related to this article

ACS Publications
High quality. High impact.

Journal of the American Chemical Society is published by the American Chemical Society. 1155 Sixteenth Street N.W., Washington, DC 20036

Journal of the American Chemical Society

Subscriber access provided by Technical Knowledge Center | of Denmark

- Copyright permission to reproduce figures and/or text from this article

View the Full Text HTML

ACS Publications
High quality. High impact.

Journal of the American Chemical Society is published by the American Chemical Society. 1155 Sixteenth Street N.W., Washington, DC 20036

J|A|C|S
ARTICLES

Published on Web 06/13/2008

Indirect, Reversible High-Density Hydrogen Storage in Compact Metal Ammine Salts

Rasmus Z. Sørensen,[†] Jens S. Hummelshøj,[‡,§] Asbjørn Klerke,[†] Jacob Birke Reves,[†] Tejs Vegge,[§] Jens K. Nørskov,[‡] and Claus H. Christensen*[,†]

Center for Sustainable and Green Chemistry, Department of Chemistry, Building 206, Technical University of Denmark, DK-2800 Kgs. Lyngby, Denmark, Center for Atomic-scale Materials Design, Department of Physics, Building 310, Technical University of Denmark, DK-2800 Kgs. Lyngby, Denmark, and Materials Research Department, Risø National Laboratory for Sustainable Energy, NanoDTU, Building 228, Technical University of Denmark, DK-4000 Roskilde, Denmark

Received September 14, 2007; E-mail: chc@kemi.dtu.dk

Ⓦ **This paper contains enhanced objects available on the Internet at http://pubs.acs.org/jacs.**

Abstract: The indirect hydrogen storage capabilities of $Mg(NH_3)_6Cl_2$, $Ca(NH_3)_8Cl_2$, $Mn(NH_3)_6Cl_2$, and $Ni(NH_3)_6Cl_2$ are investigated. All four metal ammine chlorides can be compacted to solid tablets with densities of at least 95% of the crystal density. This gives very high indirect hydrogen densities both gravimetrically and volumetrically. Upon heating, NH_3 is released from the salts, and by employing an appropriate catalyst, H_2 can be released corresponding to up to 9.78 wt % H and 0.116 kg H/L for the $Ca(NH_3)_8Cl_2$ salt. The NH_3 release from all four salts is investigated using temperature-programmed desorption employing different heating rates. The desorption is found mainly to be limited by heat transfer, indicating that the desorption kinetics are extremely fast for all steps. During desorption from solid tablets of $Mg(NH_3)_6Cl_2$, $Mn(NH_3)_6Cl_2$, and $Ni(NH_3)_6Cl_2$, nanoporous structures develop, which facilitates desorption from the interior of large, compact tablets. Density functional theory calculations reproduce trends in desorption enthalpies for the systems studied, and a mechanism in which individual chains of the ammines are released from the surface of the crystal is proposed to explain the fast absorption/desorption processes.

Introduction

The rising concern over dwindling resources and the environmental impact of burning fossil fuels has generated interest in using hydrogen as an alternative energy carrier. Significant challenges remain in the development of economically viable solutions for production, storage, and use of hydrogen as an energy carrier.[1–6]

Widespread use of hydrogen as a fuel is limited by the lack of safe and efficient systems for its storage.[7] The large deviation from ideality observed upon compression of hydrogen to high pressures, combined with the low condensing point and low density even in the liquid state, has limited the use of conventional storage systems, and a plethora of strategies for direct storage of hydrogen have been proposed.[8–14] Clearly, direct hydrogen storage methods will involve the lowest possible number of chemical transformations, and thereby minimize the inherent losses associated with multistep chemical reactions, but in practice there are still a large number of challenges to be dealt with before such large-scale direct hydrogen storage is technically and economically feasible. This has led to increased interest in indirect storage of hydrogen, e.g., in the form of methanol, ethanol, ammonia, urea, or guanidine.[15–18]

[†] Center for Sustainable and Green Chemistry, Department of Chemistry.
[‡] Center for Atomic-scale Materials Design, Department of Physics.
[§] Materials Research Department, Risø National Laboratory for Sustainable Energy.

(1) Dresselhaus, M.; Crabtree, G.; Buchanan, M. Basic Research Needs for the Hydrogen Economy; U.S. Department of Energy: Washington, DC, 2003. (available online at http://www.sc.doe.gov/bes/hydrogen.pdf).
(2) Crabtree, G.; Dresselhaus, M.; Buchanan, M. *Phys. Today* **2004**, *57*, *12*, 39–44.
(3) Kennedy, D. *Science* **2004**, *305*, 917.
(4) Turner, J. A. *Science* **2004**, *305*, 972–974.
(5) Wu, W.; Kawamoto, K.; Kuramochi, H. *J. Mater. Cycles Waste Manag.* **2006**, *8*, 70–77.
(6) Avci, A. K.; Önsan, Z. I.; Trimm, D. L. *Top. Catal.* **2003**, *22*, 359–367.
(7) Takimoto, M.; Hou, Z. *Nature* **2006**, *443*, 400–401.
(8) Zütel, A. *Naturwissenschaften* **2004**, *91*, 157–172.
(9) Cheng, P.; Xiong, Z.; Lou, J.; Lin, J.; Tan, K. L. *Nature* **2002**, *420*, 302–304.
(10) Bououdina, M.; Grant, D.; Walker, G. *Int. J. Hydrogen Energy* **2006**, *31*, 177–182.
(11) Stephens, F. H.; Baker, R. T.; Matus, M. H.; Grant, D. J.; Dixon, D. A. *Angew. Chem., Int. Ed.* **2006**, *46*, 746–749.
(12) Bogdanoviæ, B.; Felderhoff, M.; Pommerin, A.; Schüthe, F.; Spielkamp, N. *Adv. Mater.* **2006**, *18*, 1198–1201.
(13) Latroche, M.; Surblé, S.; Serre, C.; Mellot-Draznieks, C.; Llewellyn, P. L.; Lee, J.-H.; Chang, J.-S.; Jhung, S. H.; Férey, G. *Angew. Chem., Int. Ed.* **2006**, *45*, 8227–8231.
(14) Welch, G. C.; Juan, R. R. S.; Masuda, J. D.; Stephan, D. W. *Science* **2006**, *314*, 1124–1126.
(15) Metkemeijer, R.; Achard, P. *Int. J. Hydrogen Energy* **1994**, *19*, 535–542.
(16) Thomas, G.; Parks, G. Potential Roles of Ammonia in a Hydrogen Economy; U.S. Department of Energy: Washington, DC, 2006. (available online at http://hydrogen.energy.gov/pdfs/nh3_paper.pdf).
(17) Christensen, C. H.; Johannessen, T.; Sørensen, R. Z.; Nørskov, J. K. *Catal. Today* **2006**, *111*, 140–144.

10.1021/ja076762c CCC: $40.75 **© 2008 American Chemical Society**

Table 1. Mass and Volume of 10 kg of Hydrogen Stored Reversibly by Six Different Methods[a]

$Mg(NH_3)_6Cl_2$	H_2 (liquid)	Mg_2NiH_4	$LaNi_5H_6$	$NaAlH_4$	H_2 (g, 200 bar)
91.4 L	141.2 L	252.6 L	276.9 L	380.9 L	714.2 L
109 kg	10 kg	392 kg	730 kg	286 kg	10 kg

[a] All data are based on the best-obtained reversible densities reported in the literature without considering the space occupied by the container.[26–32]

Molecular ammonia contains 17.8 wt % hydrogen and can be used directly as a fuel in internal combustion engines[19] or in solid oxide fuel cells,[20] but it can also be catalytically converted to hydrogen and nitrogen at temperatures below 650 K[21–23] in high yields. The production of ammonia from hydrogen and nitrogen using natural gas as the feedstock has been optimized in the Haber–Bosch process,[24] which is among the largest catalytic processes currently in industrial operation.[25] Commercially, ammonia is transported as a liquid at a pressure around 16 bar, achieved by addition of nitrogen, but for distribution to consumers the safety of this solution is a concern.[26]

In Table 1, the practically obtainable hydrogen storage density of a selection of the more promising direct hydrogen storage approaches is compared to the results of a recently published method of hydrogen storage in the ammine complex $Mg(NH_3)_6Cl_2$. From Table 1, it is evident that reversible storage of 10 kg of H in a compact and convenient way is not a trivial task. Since the comparison indicates that the hexaammine magnesium salt is a promising candidate for hydrogen storage, it is interesting to explore the hydrogen storage potential for a broader range of metal ammine salts. Recently, metal ammines have also been proposed for ammonia storage in connection with vehicular $DeNO_x$ systems,[33] giving an extra incentive for studying these materials in more detail.

Here, $Ca(NH_3)_8Cl_2$, $Mn(NH_3)_6Cl_2$, and $Ni(NH_3)_6Cl_2$ are investigated and compared with $Mg(NH_3)_6Cl_2$ as hydrogen/ammonia storage materials to demonstrate that the family of metal ammine salts, in fact, represents a large number of compounds that can potentially be used for reversible, indirect hydrogen storage. Furthermore, the investigated metal ammine complexes are found to exhibit facile ammonia release kinetics.

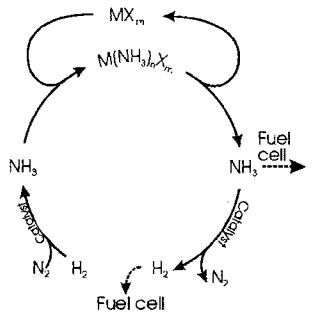

Figure 1. Principle of hydrogen storage in metal ammine salts of the general formula $M(NH_3)_nX_m$.

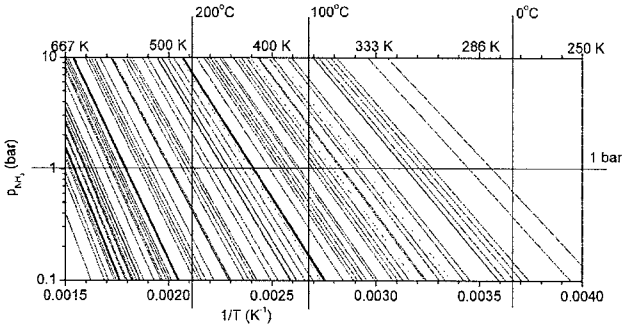

Figure 2. Van't Hoff plot showing the equilibrium pressure of ammonia over 90 metal ammine halides of the general formula $M(NH_3)_nX_2$.[34] The complete list of complexes is given as Supporting Information.

The general principle of storing hydrogen in metal ammine complexes is shown in Figure 1. The absorption of ammonia is exothermic (negative absorption enthalpy) for all salts. Thus, the release is necessarily endothermic and must require the same amount of energy as is released during the absorption. The equilibrium vapor pressures can be determined by the van't Hoff relationship given as eq 1, from which it is seen that the safer the storage material (low vapor pressure at ambient temperature), the more energy required for releasing NH_3 at a given pressure.

$$\ln(p) = -\frac{\Delta H_{des}}{RT} + \frac{\Delta S_{des}}{R} \quad (1)$$

The possibility for choosing a metal ammine salt with the desired thermodynamic properties is illustrated in Figure 2.

Compared to hydrides and alanates with comparable storage pressures, the pressure change with temperature is larger for metal ammines. This is because the ammine salts generally have higher entropies of desorption than those of metal hydrides. Thus, it is evident from the van't Hoff relationship that metal complexes also have higher enthalpies of desorption than hydrides with similar vapor pressures at a given temperature.

The formation of metal ammine complexes and the thermodynamics of ammonia desorption from these have been thoroughly described in the early chemical literature. From these literature data, it is possible to find general trends for the NH_3

(18) Van Vechten, J. A. Presented at the 2007 APS March Meeting, Denver, CO;; American Physical Society: College Park, MD, 2007; Abstract S39.00010.
(20) Fournier, G. G. M.; Cumming, I. W.; Hellgardt, K. *J. Power Sources* **2006**, *162*, 198–206.
(19) Steele, R. B. *Chemtech* **1999**, (August), 28.
(21) Raróg-Pilecka, W.; Szmigiel, D.; Kowalczyk, Z.; Jodzis, S.; Zielinski, J. *J. Catal.* **2003**, *218*, 465–469.
(22) Li, X.-K.; Ji, W.-J.; Zhao, J.; Wang, S.-J.; Au, C.-T. *J. Catal.* **2005**, *236*, 181–189.
(23) Boisen, A.; Dahl, S.; Nørskov, J. K.; Christensen, C. H. *J. Catal.* **2005**, *230*, 309–312.
(24) Schlögl, R. *Angew. Chem., Int. Ed.* **2003**, *42*, 2004–2008.
(25) Eggmann, T. *Kirk-Othmer Encyclopedia of Chemical Technology: Ammonia*; John Wiley & Sons, Inc.: New York, 2001.
(26) Appl, M. *Ullmann's Encyclopedia of Industrial Chemistry: Ammonia*; Wiley-VCH Verlag GmbH & Co. KGaA: Weinheim, 2007.
(27) Mosher, D.; Tang, X.; Arsenault, S. High Density Hydrogen Storage System Demonstration Using $NaAlH_4$ Based Complex Hydrides. FY 2006 Annual Progress Report, DOE Hydrogen Program; U.S. Department of Energy: Washington, DC, 2006; pp 281–284. (available online at http://www.hydrogen.energy.gov/pdfs/progress06/iv_a_1_mosher.pdf).
(28) Liu, X.; Zhu, Y.; Li, L. *Int. J. Hydrogen Energy* **2007**, *32*, 2455–2460.
(29) Nomura, K.; Fujiwara, S.; Hayakawa, H.; Akiba, E.; Ishido, Y.; Ono, S. *Journal of the Less-Common Metals* **1991**, *169*, 9–17.
(30) Suissa, E.; Jacob, I.; Hadari, Z. *J. Less-Common Metals* **1984**, *104*, 287–295.
(31) El-Osairy, M. A.; el-Osery, I. A.; Metwally, A. M.; Hassan, M. A. *Int. J. Hydrogen Energy* **1993**, *18*, 517–524.
(32) Laidler, K. J.; Meiser, J. H. *Physical Chemistry*, 3rd ed.; Houghton Mifflin Co.: New York, 1999.
(33) Elmøe, T. D.; Sørensen, R. Z.; Quaade, U.; Christensen, C. H.; Nørskov, J. K.; Johannessen, T. *Chem. Eng. Sci.* **2006**, *61*, 2618–2625.
(34) Biltz, W.; Messerknecht, C. *Z. Anorg. Allg. Chem.* **1923**, *129*, 161–175.

desorption properties of metal ammine halides.[35–37] The most general trend in these original data is that the desorption enthalpy of ammonia increases from chloride through bromide to iodide. The data available for fluorides indicate that fluoride does indeed follow the same trend, but, in fact, only a few metal ammine fluorides have been investigated in detail.[35,37–39] The effect of the metal cation is not as clear, but some trends can be seen. For the alkali and alkaline earth metals, the enthalpy of desorption decreases down through the groups,[37,38] and for the transition metals, the enthalpy of desorption increases slightly when moving from left to right in the Periodic Table, i.e., from manganese to nickel in oxidation state 2+.[37]

For a metal ammine complex to be considered useful as an indirect hydrogen storage material, it needs to desorb ammonia in a relatively narrow temperature range around or above ambient temperature. For the storage to be safe, the ammonia vapor pressure should preferably be below 1 bar at ambient temperature. Possibly, somewhat higher pressures could be handled appropriately in practical systems. However, with such materials, leaks would represent a significant hazard. At the same time, 1 bar of ammonia pressure should preferably be reached below 650 K for all desorption steps to avoid desorption of ammonia becoming too energy intensive. This is so because the ammonia decomposition reaction is best conducted above 650 K, where a sufficiently high rate can be achieved and simultaneously a sufficiently low equilibrium ammonia concentration is reached. Moreover, the gravimetric and volumetric hydrogen density of the chosen metal ammine salt(s) should clearly be as high as possible. This criterion obviously favors light cations and anions such as alkali metals and fluorides. These are, however, impractical because the alkali metals do not bind ammonia sufficiently well at ambient temperature according to the above criteria, and the fluorides are usually toxic and can form hydrofluoric acid when they are heated to desorb the ammonia.[39]

So far, the only metal ammine complex which has been investigated in any detail as an indirect hydrogen storage material is $Mg(NH_3)_6Cl_2$.[40] $Mg(NH_3)_6Cl_2$ was chosen initially because it has a vapor pressure of only 2.2 mbar at 300 K, and additionally $MgCl_2$ is both widely available and nontoxic. However, other salts can similarly bind ammonia to form interesting indirect hydrogen storage materials. For one, $CaCl_2$ binds eight ammonia molecules to form $Ca(NH_3)_8Cl_2$ at 300 K and 1 bar of NH_3. This gives an even higher indirect hydrogen storage density than that achieved in $Mg(NH_3)_6Cl_2$ on both a mass and volume basis, but it also results in an equilibrium ammonia pressure of 0.77 bar at 300 K. In $Ca(NH_3)_8Cl_2$, only six of the NH_3 molecules are coordinated directly to calcium. The last two are more freely bound in the crystalline structure.[41] $MnCl_2$ and $NiCl_2$ coordinate ammonia to form $Mn(NH_3)_6Cl_2$ and $Ni(NH_3)_6Cl_2$, respectively. Both of these have higher molar masses than $Mg(NH_3)_6Cl_2$, but as their crystal densities are also higher,[42] the volumetric hydrogen contents are essentially the same as in $Mg(NH)_6Cl_2$. The temperatures at which the equilibrium vapor pressure is 1 bar for the first desorption step in the four different complexes are 305 ($Ca(NH_3)_8Cl_2$), 358 ($Mn(NH_3)_6Cl_2$), 413 ($Mg(NH_3)_6Cl_2$), and 449 K ($Ni(NH_3)_6Cl_2$).[43] The theoretical storage capacities of the metal ammine complexes are given in Table 2, and desorption enthalpies for the individual desorption steps are reported separately in Table 3.

Table 2. Indirect Hydrogen Storage Capacity of Four Metal Ammine Salts

	ρ,[a] g/cm^3	gravimetric H, wt % H	volumetric H, kg H/L
$Mg(NH_3)_6Cl_2$	1.25	9.19	0.115
$Ca(NH_3)_8Cl_2$	1.19	9.78	0.116
$Mn(NH_3)_6Cl_2$	1.41	7.96	0.112
$Ni(NH_3)_6Cl_2$	1.53	7.83	0.119

[a] Crystal densities.[42]

Table 3. Ammonia Desorption Enthalpies for Each Desorption Step for Four Different Metal Ammine Complexes[43]

$Mg(NH_3)_nCl_2$		$Ca(NH_3)_nCl_2$		$Mn(NH_3)_nCl_2$		$Ni(NH_3)_nCl_2$	
n	ΔH_{des}, kJ/mol	n	ΔH_{des}, kJ/mol	n	ΔH_{des}, kJ/mol	n	ΔH_{des}, kJ/mol
6→2	55.7	8→4	41.0	6→2	47.4	6→2	59.2
2→1	74.9	4→2	42.3	2→1	71.0	2→1	79.5
1→0	87.0	2→1	63.2	1→0	84.2	1→0	89.8
		1→0	69.1				

In utilizing the present approach for indirect hydrogen storage above the gram scale, it is important that the complexes can be compacted into tablets or other shaped bodies with as little void space as possible. This was previously reported to be possible for $Mg(NH_3)_6Cl_2$, and it was found that, during desorption of ammonia from tablets of this salt, a sponge-like structure maintaining the shape of the original tablet was formed featuring a nanopore system, which facilitates desorption of ammonia from the interior of the compact material.[44,45]

The compactability, the ability to form of nanopores, and the kinetics of ammonia desorption are investigated in this study for $Ca(NH_3)_8Cl_2$, $Mn(NH_3)_6Cl_2$, and $Ni(NH_3)_6Cl_2$, and the results are reported in the following sections.

Experimental Methods

Commercial anhydrous salts ($CaCl_2$, Alfa Aesar, 97%; $NiCl_2$, Aldrich, 98%; $MnCl_2$, Aldrich, 98%) were transferred to the reaction vessel in a glovebox containing dry air (6−8 ppm H_2O) and dried at 400−500 °C in a stream of N_2 before use. The vessel was purged with NH_3 gas (Hede Nielsen, N45) and left overnight under a pressure of NH_3 slightly above 4 bar. NH_3 uptakes were determined gravimetrically. Each metal ammine halide was pressed into tablets to determine the maximal bulk density of the storage material. Tablets of the material were also subjected to measurements of pore size distributions. These were performed using nitrogen absorption and desorption measurements on a Micrometrics ASAP 2020N, with pretreatment of the samples at temperatures and pressures chosen to give the desired levels of NH_3 desorption.

(35) Ephraim, F. *Chem. Ber.* **1912**, *45*, 1322–1331.
(36) Biltz, W.; Hüttig, G. F. *Z. Anorg. Allg. Chem.* **1919**, *109*, 88–110.
(37) Biltz, W. *Z. Anorg. Allg. Chem.* **1923**, *130*, 93–139.
(38) Biltz, W.; Hansen, W. *Z. Anorg. Allg. Chem.* **1923**, *127*, 1–33.
(39) Patil, K. C.; Secco, E. A. *Can. J. Chem.* **1972**, *50*, 567–573.
(40) Christensen, C. H.; Sørensen, R. Z.; Johannessen, T.; Quaade, U.; Honkala, K.; Elmøe, T. D.; Køhler, R.; Nørskov, J. K. *J. Mater. Chem.* **2005**, *15*, 4106–4108.
(41) Westman, S.; Werner, P.-E.; Schuler, T.; Raldow, W. *Acta Chem. Scand.* **1981**, *35*, 467–472.
(42) Gmelin Data: 2000−2006, Gesellschaft Deutscher Chemiker licensed to MDL Information Systems GmbH; 1988−1999, Gmelin Institut für Anorganische Chemie und Grenzgebiete der Max-Planck-Gesellschaft zur Foerderung der Wissenschaften.
(43) Lepinasse, E.; Spinner, B. *Rev. Int. Froid.* **1994**, *17*, 309–321.
(44) Hummelshøj, J. S.; Sørensen, R. Z.; Kustova, M. Y.; Johannesen, T.; Nørskov, J. K.; Christensen, C. H. *J. Am. Chem. Soc.* **2006**, *128*, 16–17.
(45) Jacobsen, H. S.; Hansen, H. A.; Andreasen, J. W.; Shi, Q.; Andreasen, A.; Feidenhans'l, R.; Nielsen, M. M.; Ståhl, K.; Vegge, T. *Chem. Phys. Lett.* **2007**, *441*, 255–260.

Table 4. Tablet Densities

	ρ_{tablet}, g/cm^3	$\rho_{crystal}$, %	volumetric H, kg H/L
$Mg(NH_3)_6Cl_2$[33]	1.19	95	0.11
$Ca(NH_3)_8Cl_2$	1.18	99	0.12
$Mn(NH_3)_6Cl_2$	1.34	95	0.11
$Ni(NH_3)_6Cl_2$	1.41	95	0.11

Desorption characteristics were determined by temperature-programmed desorption (TPD). Samples of 0.5 g were transferred to a closed test tube under an NH_3 atmosphere and heated following a desired temperature ramp. NH_3 was released into a carrier stream of Ar through a T-joint with a thin connection tube to maintain the NH_3 atmosphere over the sample. This procedure gave an NH_3 pressure slightly above atmospheric pressure over the ammine sample. For TPDs of $Mg(NH_3)_6Cl_2$, a sample obtained from Amminex A/S was used as received. The ammonia content in the carrier stream was determined using a Fischer-Rosemount NGA 2000 equipped with an MLT analyzer calibrated to NH_3 concentrations from 0.03 to 30%. Desorption rates were calculated from the ammonia content in the carrier stream and the flow of Ar, which was kept constant at 213 mL of N/min using a calibrated Brooks 5850 TR mass flow controller. For all four metal ammine salts, TPDs were obtained with heating rates of both 1 and 5 K/min.

Results and Discussion

The behavior of the four different metal ammine chlorides during TPD is shown in Figure 3. In accordance with literature data, the trend in temperature for the first desorption peak is Ca < Mn < Mg < Ni. During TPD, $Ca(NH_3)_nCl_2$ has stable compositions with n = 8, 4, 2, and 1, and essentially all ammonia desorbs in the temperature range of 300−550 K. $Mn(NH_3)_nCl_2$ has stable compositions with n = 6, 2, and 1 and two compositions with n < 1. Stable structures with less than one ammonia molecule per metal atom are well known for a range of transition metal ammine salts and are therefore not unlikely, even though they have not been previously reported for $MnCl_2$. For this compound, essentially all ammonia desorbs in the temperature range of 350−675 K. TPDs of $Mg(NH_3)_nCl_2$ were reported previously, and there are stable compositions with n = 6, 2, and 1. Here, essentially all ammonia desorbs in the temperature range of 410−700 K. During TPD, $Ni(NH_3)_nCl_2$ shows stable compositions with n = 6, 2, and 1, and all ammonia desorbs in the temperature range of 440−700 K. Independently of the temperature ramp, all the TPD peaks start within a few degrees of the temperature for 1 bar equilibrium pressure calculated from literature data.[43] This and the nearly exponential rise in desorption rate with temperature indicate that desorption is equilibrium-limited, even at high desorption rates. During fast desorption, the endothermic reaction causes the sample to cool, which is evident as a small deviation from the predefined temperature ramp when the desorption peaks (data not shown). This cooling will, in effect, decrease the equilibrium vapor pressure and thereby alter the desorption rate. Hence, for large samples, heat transport to the reaction zone seems to be the main limitation on the desorption rate for all four metal ammine salts studied. This is also supported experimentally, as the shape of TPD peaks depends on the sample size (data not shown). When the sample is large, the peak is broadened and the slopes (both increasing and decreasing) are less steep. This corresponds to a larger temperature distribution inside the sample. In an earlier work, computational modeling showed heat transport to be the main limiting factor for desorption from $Mg(NH_3)_6Cl_2$.[33] The present results indicate that it is a general feature for metal ammine salts that desorption is not limited by diffusion kinetics or large activation energies, but only by thermodynamic equilibrium, and hence by heat transport to the reaction zone.

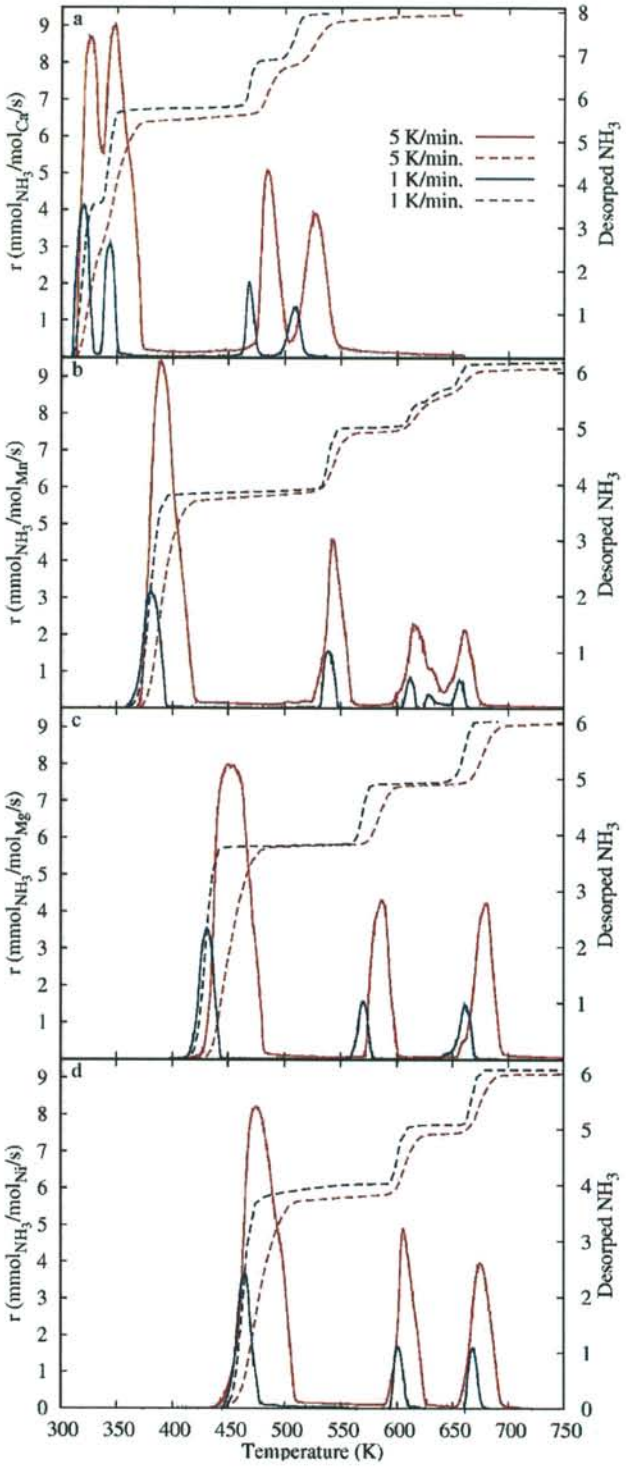

Figure 3. TPDs of (a) $Ca(NH_3)_8Cl_2$, (b) $Mn(NH_3)_6Cl_2$, (c) $Mg(NH_3)_6Cl_2$, and (d) $Ni(NH_3)_6Cl_2$, with a temperature ramp of 5 K/min (red) and 1 K/min (blue). The solid lines show the desorption rate, and the dashed lines show the total amount of desorbed ammonia.

The desorption of ammonia from $Ni(NH_3)_6Cl_2$ was also examined by thermogravimetric analysis coupled with a mass spectrometer. This confirmed that the sample was maintained

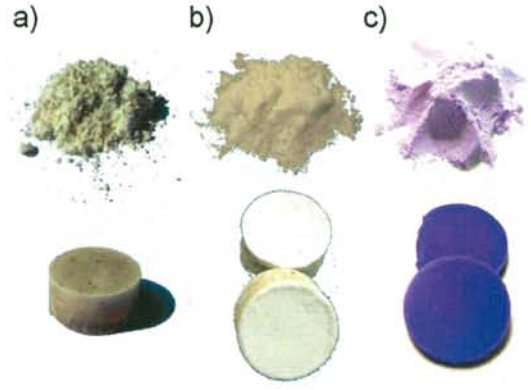

Figure 4. Photos of (a) $Mn(NH_3)_6Cl_2$, (b) $Ca(NH_3)_8Cl_2$, and (c) $Ni(NH_3)_6Cl_2$ as powder and tablets.

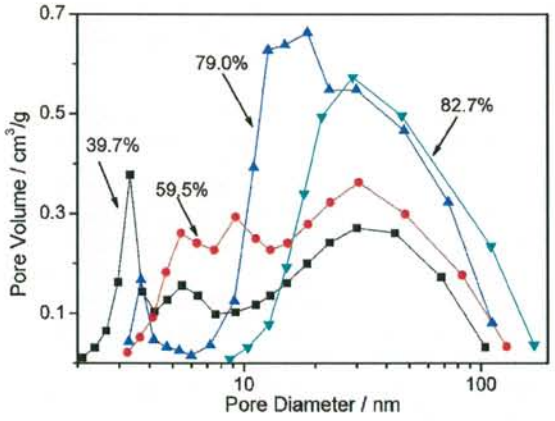

Figure 5. Pore structures developed after different levels of ammonia desorption from a $Mn(NH_3)_6Cl_2$ tablet.

at complete ammonia saturation during handling and that the only gas which desorbed from the sample was ammonia.

The densities of the metal ammine chloride tablets are reported and compared to the crystal densities in Table 4. In all cases, the metal ammine halides exhibit tablet densities of at least 95% of their crystal densities. Photos of powders and tablets are given in Figure 4.

For desorption of ammonia to be facile from dense bodies of metal ammine complexes such as the present tablets, it is important that a pore structure develops through which ammonia can leave the tablet without a long diffusion path in the solid state. The development of nanopores during ammonia desorption has previously been demonstrated experimentally for $Mg(NH_3)_6Cl_2$.[44,45] Here, pore size distributions for both $Mn(NH_3)_6Cl_2$ and $Ni(NH_3)_6Cl_2$ were measured after desorption of part of the ammonia from dense tablets of these materials. Before the measurements, the samples must be evacuated at ambient temperature or higher. Therefore, some NH_3 necessarily desorbs before the first measurement. For $Ni(NH_3)_6Cl_2$, this loss is negligible since the vapor pressure at room temperature is very low. Hence, the porosity in the initial tablet could be characterized carefully. For $Mn(NH_3)_6Cl_2$, the initial porosity can be calculated from the tablet density in Table 4 and the crystal density in Table 2 to be 0.07 cm^3/g. In Figure 5, it is seen that, in the first part of desorption of NH_3 from $Mn(NH_3)_6Cl_2$, pores of 2−3 nm are formed along with some pores around 30−50 nm. As more and more NH_3 is desorbed, the smaller pores disappear while the number of larger pores increases. From 79.0% desorbed to 82.7% desorbed, something

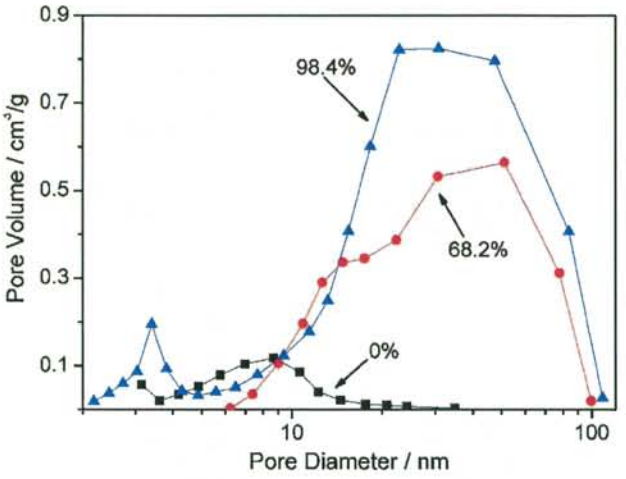

Figure 6. Pore structures developed after different levels of ammonia desorption from a $Ni(NH_3)_6Cl_2$ tablet.

Table 5. Pore Characteristics for $Mn(NH_3)_6Cl_2$

NH_3 desorbed, %	BET area, m^2/g	average pore size, nm	total pore volume, cm^3/g
0.0			0.07
39.7	89.6	10.9	0.308
59.5	84.0	15.6	0.421
79	91.7	20.3	0.560
82.7	43.3	35.7	0.507

Table 6. Pore Characteristics for $Ni(NH_3)_6Cl_2$

NH_3 desorbed, %	BET area, m^2/g	average pore size, nm	total pore volume, cm^3/g
0.0	12.0	6.8	0.051
68.2	53.9	25.5	0.432
98.4	120.5	21.1	0.687

different happens. The pores of 20−30 nm diameter disappear without the number of pores in the size range 30−50 nm increasing. For $Ni(NH_3)_6Cl_2$, the data are not as detailed, but it is evident from Figure 6 that, from a relatively small pore volume with pore sizes distributed from 3 to 20 nm in the initial tablet, a larger volume of pores in the size range 10−100 nm develops as NH_3 desorbs. As a consequence of this development in pore structure, the average pore sizes and total pore volumes in both salts generally increase during the desorption. Table 5 lists the Brunauer−Emmett−Teller (BET) areas measured at various stages during the desorption of NH_3 from $Mn(NH_3)_6Cl_2$. They are almost constant until the last measurement, where a decrease is seen. For $Ni(NH_3)_6Cl_2$, however, the BET area continues to increase during the desorption process (see Table 6). As the increase in surface area makes more surface available for desorption of ammonia, this facilitates desorption of ammonia from the interior of dense bodies of the material.

Modeling of Ammonia Desorption. A series of periodic density functional theory (DFT) calculations, using the Dacapo planewave pseudopotential implementation,[46–48] were performed to determine this method's ability to accurately calculate ammonia desorption enthalpies for metal ammine salts, specifically $Mg(NH_3)_6Cl_2$, $Ca(NH_3)_8Cl_2$, $Mn(NH_3)_6Cl_2$, and $Ni(NH_3)_6Cl_2$. The calculations were also used to provide additional understanding of

(46) Kresse, J. *Comput. Mater. Sci.* **1996**, *6*, 15–50.
(47) Vanderbilt, D. *Phys. Rev. B* **1990**, *41*, 7892–7895.
(48) Hammer, B.; Hansen, L. B.; Norskov, J. K. *Phys. Rev. B* **1999**, *59*, 7413–7421.

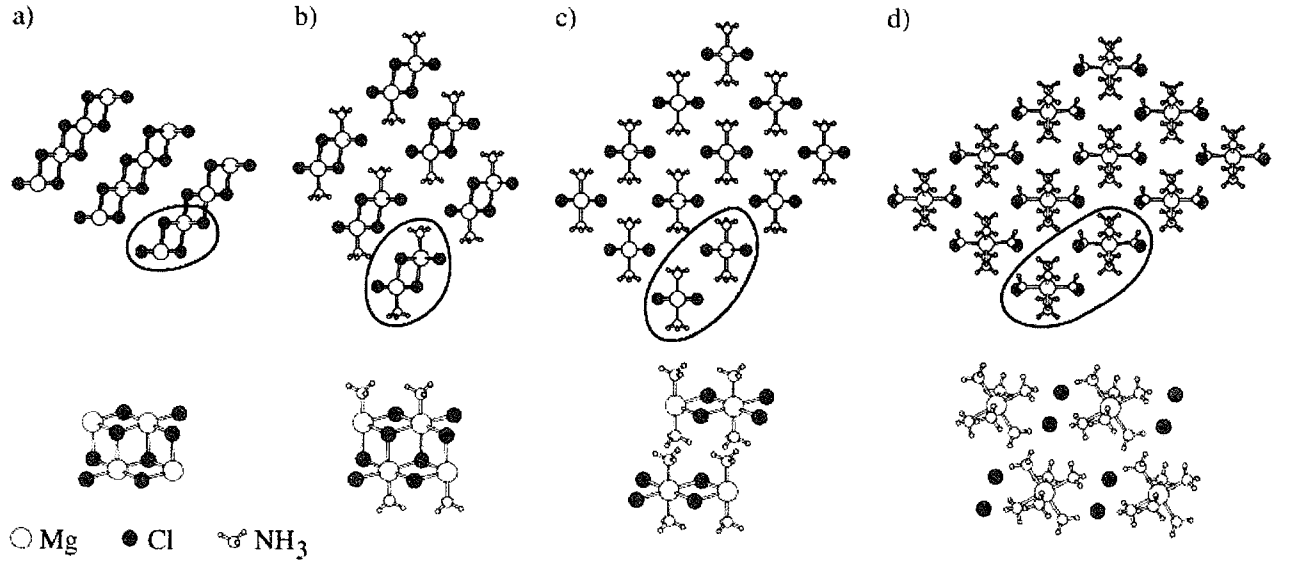

Figure 7. Optimized structures found using DFT for (a) $MgCl_2$, (b) $Mg(NH_3)Cl_2$, (c) $Mg(NH_3)_2Cl_2$, and (d) $Mg(NH_3)_6Cl_2$, viewed along the chains that continue infinitely in and out of the picture. Four formula units are shown from the side, corresponding to the highlighted fragments in the end view.

the mechanistic details underlying the fast ab/desorption processes observed for these materials as described above, and finally also to predict potential electronic trends, which can be utilized in the design of novel metal ammines with optimized properties in hydrogen/ammonia storage.

Calculation of Desorption Enthalpies. We determine the desorption enthalpy of going from one phase to another as the difference in total energy between the most stable structures found for the two phases plus the gas-phase energy of the released ammonia molecules. The energy of an ammonia molecule in the gas phase is calculated by placing one molecule in a vacuum cube of side length 10 Å; zero-point energies are not included.

Structures of $Mg(NH_3)_nCl_2$. To determine the most stable structures for the different ammine phases, a rigorous search was first performed on the $Mg(NH_3)_nCl_2$ ($n = 6, 2, 1, 0$) systems based on the experimentally reported structures.[49–52] In all the structures, a central magnesium atom is coordinated octahedrally to six ligands, i.e., either chlorine atoms for $n = 0$, ammonia molecules for $n = 6$, or a combination of the two for $n = 2$ or 1, as shown in Figure 7.

For $n = 6$, the structure is of the K_2PtCl_6 type[49] and is traditionally described as octahedral $Mg(NH_3)_6$ complexes contained in a cubic lattice of chlorine atoms, with Mg body-centered and NH_3 face-centered in every second cube of chlorine atoms, but the structure can also be described as chains of $Mg(NH_3)_6Cl_2$, as seen in Figure 7d, running along the face diagonals of the cubes. In the optimized DFT structure, the experimentally observed K_2PtCl_6 structure is slightly distorted.

For $n = 2$, each chlorine atom is shared by two neighboring magnesium atoms in edge-sharing octahedral chains. The space group is *Cmmm*, with cell parameters $a = 8.73$ Å, $b = 8.82$ Å, and $c = 4.17$ Å somewhat larger than the experimental ones of $a = 8.18$ Å, $b = 8.21$ Å, and $c = 3.76$ Å.[50]

For $n = 1$, a chlorine atom is shared by three magnesium atoms in edge-sharing double octahedral chains. In the experimental structure found for $Ni(NH_3)Cl_2$,[51] which is believed to be isostructural with the $Mg(NH_3)Cl_2$ equivalent, the double octahedral chains have two orientations in the *I2/m* space group. This structure was reproduced in our calculations; however, a structure very similar to this one with respect to coordination of the H atoms, but with only one orientation of the chains, was found to have the same energy. For practical computational reasons, the simple structure as shown in Figure 7b was chosen for further calculations.

For $n = 0$, the octahedra of chlorine atoms with central magnesium atoms share half of their edges, resulting in layers of $MgCl_2$ of the $CdCl_2$ type. The space group is $R\bar{3}m$, with $a = 3.78$ Å and $c = 18.52$ Å, compared to $a = 3.64$ Å and $c = 17.67$ Å in the experiment.[52] As found in experiments,[52] the octahedra that are occupied by Mg are flattened, and the empty octahedra between the layers are elongated. The ratio of the short and the long edges of the occupied octahedra are $r = 0.92$, close to the value of $r = 0.934$ from the experiment.[52] In general, the lattice is a little expanded in the calculations due to the RPBE[48] functional used. The RPBE functional is known to overestimate lattice constants slightly. For a weakly bonded system like the one treated here, we expect to see this problem even more clearly—this is a general feature of GGA-type exchange correlation functionals. We will show in the following that this does not affect the ability of the RPBE functional to describe trends in stability of the ammines.

The interaction between individual $Mg(NH_3)_nCl_2$ chains in the respective structures can be examined quantitatively by comparing the total energy of a $Mg(NH_3)_nCl_2$ structure with the total energy of a $Mg(NH_3)_nCl_2$ chain in vacuum. This shows that the energy per Mg atom needed to move a chain of $Mg(NH_3)_nCl_2$ from the bulk to vacuum is 26, 48, and 76 kJ/mol for $n = 1$, 2, and 6, respectively. For $n = 0$, the corresponding value is 15 kJ/mol, calculated as the binding between fragments (highlighted in Figure 7a) of the $MgCl_2$ layers. The layers of $MgCl_2$ are actually slightly repulsive in this description.

To understand the nature of the interaction between the chains and layers of $Mg(NH_3)_nCl_2$, we use density difference plots, where the ground-state electron density of a given structure is subtracted from that of the individual atomic species comprising

(49) Olovsson, I. *Acta Crystallogr.* **1965**, *18*, 889–893.
(50) Leineweber, A.; Friedriszik, M. W.; Jacobs, H. *J. Solid State Chem.* **1999**, *147*, 229–234.
(51) Leineweber, A.; Jacobs, H.; Ehrenberg, H. *Z. Anorg. Allg. Chem.* **2000**, *626*, 2146–2152.
(52) Partin, M. *J. Solid State Chem.* **1991**, *95*, 176–183.

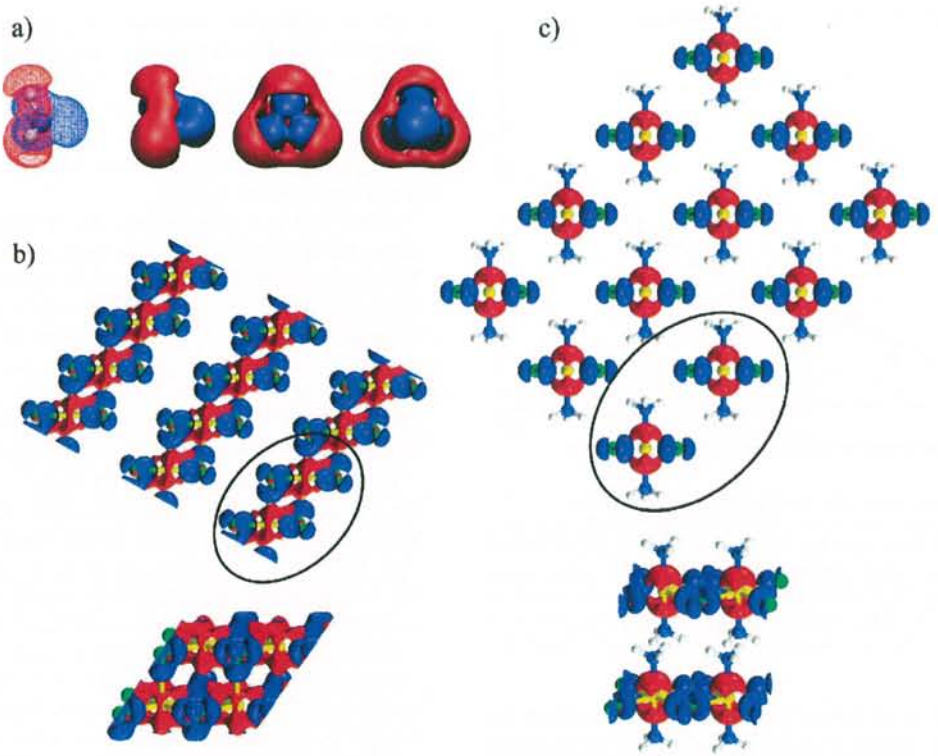

Figure 8. Density difference plots of (a) a NH_3 molecule, (b) $MgCl_2$, and (c) Mg and Cl in $Mg(NH_3)_2Cl_2$ (yellow, Mg; green, Cl; blue, N; and white, H). Blue areas correspond to an excess of electrons or negative charge, and red indicates depletion of electrons or positive charge. In (b) and (c), four formula units are shown from the side, corresponding to the highlighted fragments in the end view.

the structure treated alone and in the same positions. This effectively shows how the electron density is redistributed, and by plotting isosurfaces of density increments and decrements, negatively and positively charged areas become visible.

Some density difference plots are shown in Figure 8, where one can see (i) the lone pair of ammonia and the positively charged hydrogen atoms (Figure 8a); (ii) how the electrons concentrate around the chlorine atoms in a $MgCl_2$ layer (Figure 8b), with the negatively charged areas protruding the layer, rendering them slightly repulsive; and (iii) the charge redistribution caused by Mg and Cl alone in the $Mg(NH_3)_2Cl_2$ structure (Figure 8c), showing how the ammonia molecules fit nicely. In general, the lone pair of ammonia connects to the positively charged areas surrounding the magnesium atoms, and the positively charged hydrogen atoms connect to the negatively charged areas near the chlorine atoms.

Thus, the chains for $n = 6$, 2, and 1 are interconnected by the electrostatic attraction between the positively charged H atoms of an ammonia molecule and the negatively charged Cl atoms (Figure 8a,c). For $n = 0$, the layers are slightly repulsive, and the real structure is therefore mainly held together by van der Waals forces, which are not accurately described in these DFT calculations.

Structures of the Ca, Mn, and Ni Salts. The structures found for the Mg salt were also used for the three other salts (Ca, Mn, Ni) by simply exchanging the metal atoms and letting the structures relax while scaling the unit cell size linearly until a minimum in total energy was reached.

For $Mn(NH_3)_nCl_2$ and $Ni(NH_3)_nCl_2$, this approximation is expected to be rather precise, since these salts are known to be isostructural with the magnesium analogue for $n = 6$ and 0 and for nickel with $n = 2$ as well.[49,53,54] The $Ca(NH_3)_nCl_2$ structures, on the other hand, are different and, moreover, go through $n = 8$, 4, 2, 1, and 0. However, since the experimental enthalpies for the 8→4 and 4→2 transitions are very close in energy (41 and 42 kJ/mol, respectively; see Table 3), we rely on the 6→2 reaction enthalpy of the model to provide a reasonable approximation for both of these; here, an enthalpy of 41 kJ/mol was chosen for comparison with the 6→2 reaction enthalpy of the model.

Results I: Desorption Enthalpies from a Stable Structure Comparison. The calculated desorption enthalpies are compared with experimental values (see Figure 9), and it is seen that the DFT model is able to quite accurately describe the trends in desorption enthalpies of the metal ammine salts studied here.

A straight line is obtained in Figure 9, but the slope is less than 1; i.e., the calculated enthalpies of desorption are too low by a certain factor. The inclusion of zero-point energies or the use of other exchange-correlation functionals only amounts to a shift of the line and cannot account for the slope being less than 1. Although the absolute numbers are not accurate, the trend is very clear, and the precision of Figure 9 is usually considered more than acceptable in a DFT study like this.[48]

Fast Ab/Desorption Processes. To understand the fast ab/desorption of ammonia in the metal ammine salts, we considered the structures again, but this time from the perspective of how ammonia can get in and out of these materials. We restrict the discussion to involve only the isostructural Mg, Mn, and Ni salts and focus on the magnesium salt as a representative.

As mentioned previously, clean $MgCl_2$ has a layered structure, while the structures of $Mg(NH_3)_nCl_2$ for $n = 1$, 2, and 6 consist

(53) Ferrari, A.; Bigliard, G.; Braibant, A. *Acta Crystallogr.* **1963**, *16*, 846–847.
(54) Leineweber, H. *J. Solid State Chem.* **2000**, *152*, 381–387.

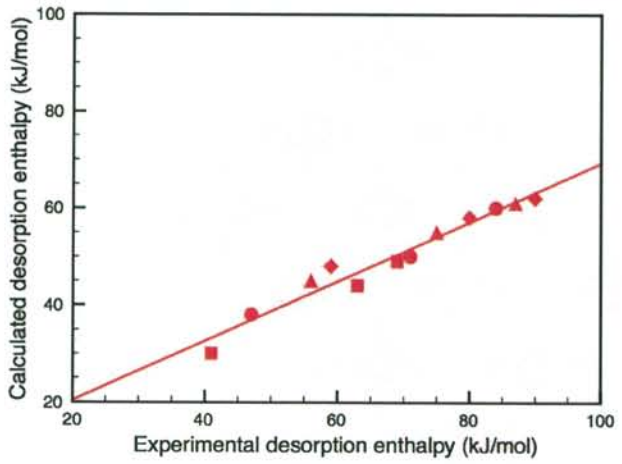

Figure 9. Calculated versus experimental desorption enthalpies for the different desorption steps, 6→2, 2→1, and 1→0, of $Mg(NH_3)_6Cl_2$ (triangles), $Ca(NH_3)_8Cl_2$ (squares), $Mn(NH_3)_6Cl_2$ (circles), and $Ni(NH_3)_6Cl_2$ (diamonds) and in a comparison of stable structures. The calcium salt is approximated by model hexaammine salt $Ca(NH_3)_6Cl_2$, which follows the same desorption route as the three other salts. In this approximation, the first desorption step is representative of the first two desorption steps of the real octaammine salt, $Ca(NH_3)_8Cl_2$.

of chains (see Figure 7). Going from one phase to another, the chains/layers of the initial structure are either cleaved to absorb ammonia or recombined to desorb ammonia. For the 6→2/2→6 reactions, the chains are merely stretched/compressed (see Figure 7). In all cases, the resulting chains or layers are rearranged to produce the final structure.

The details of this cleavage and recombination and the detailed mechanism for transport of ammonia into and out of the materials are unknown, but both desorption and absorption are known from experiments to be facile.[40] We shall first consider the situation where bulk diffusion of ammonia is the dominant transport process.

Bulk Diffusion in Metal Ammines. The transport of ammonia out of the systems during desorption could be dominated by bulk diffusion of ammonia. Indeed, from Figure 7, it seems likely that, if ammonia desorbs by diffusing along the chains of $Mg(NH_3)_nCl_2$, the system can transform from one bulk phase directly to another in a continuous way. However, the barriers for diffusion need to be sufficiently small that no competing mechanisms become dominant.

The barriers for diffusion along the chains of $Mg(NH_3)_nCl_2$ have been calculated to be 58, 135, and 121 kJ/mol for $n = 6$, 2, and 1, respectively; this is clearly too high for $n = 2$ and 1 when compared with the experimental desorption enthalpy. If bulk diffusion of ammonia were indeed rate-limiting, one would expect the last two peaks in a TPD experiment to be broader than the first peak, which is not the case, as seen in Figure 3.

Although the bulk diffusion picture cannot be ruled out, at least for the $n = 6$ case, an alternative mechanism would be desirable. In the following, such a mechanism, which explains the fast kinetics for both the absorption and desorption processes, is proposed.

Restructuring at the Surface. We now consider the rather weak binding between the individual chains in $Mg(NH_3)_nCl_2$ (15, 26, 48, and 76 kJ/mol for $n = 0$, 1, 2, and 6, respectively), which allows for an alternative desorption process in which the individual chains are released from the surface to facilitate desorption or absorption of ammonia from or to the chains (see Figure 10), as investigated in the following.

Three principles underlie the proposed mechanism for understanding the dynamics of ammonia absorption and desorption: (a) it is energetically preferred for Mg to retain a six-fold coordination to the ligands (either Cl or NH_3), (b) chains are released from the surface to facilitate desorption or absorption, and (c) reactions involving a minimal number of chains are expected to be faster.

When a chain is released from the hexammine (Figure 10a), it releases four of its six NH_3 molecules per Mg and transforms into a diammine chain, thus maintaining the energetically preferred six-fold coordination of the Mg atoms (four Cl's substitute the released NH_3). If the hexammine chain were to release more than four NH_3 molecules directly, it would require the expectedly slower combination of two or more chains to keep the Mg atoms fully coordinated. The formed diammine chains will subsequently arrange into the bulk structure of $Mg(NH_3)_2Cl_2$.

As the temperature is further increased, chains break off from the diammine structure (Figure 10b). For this desorption reaction, a minimum of two chains must combine to release (half their) NH_3 molecules, in order to maintain the six-fold Mg coordination. The resulting monoammine chains later rearrange into the bulk structure of $Mg(NH_3)Cl_2$.

Similarly, for the monoammine structure (Figure 10c), chains combine in pairs to give $Mg(NH_3)_{0.5}Cl_2$ chains. This combination of chains to release NH_3 and form chains of lower ammonia content can, in principle, continue until all the ammonia is desorbed and the layered structure of $MgCl_2$ is formed. The intermediate $n < 1$ chains are, in general, not expected not to be stable, and therefore not detected in the experiments, except for $Mn(NH_3)_nCl_2$, which finds a stable arrangement of the $Mn(NH_3)_{0.5}Cl_2$ chains (see Figure 3b).

For absorption the picture is reversed, and the chains/layers are cleaved instead of combined (Figure 10d−f).

Results II: A New Scheme for Calculating Desorption Enthalpies. We have presented a model for the detailed mechanism behind desorption and absorption processes in metal amine salts, and we now return to the modeling of desorption enthalpies. In the alternative mechanism, the system does not transform directly from one stable structure to the next during desorption. Instead, it goes through an intermediate state where chains of the final phase are free and uncoordinated. These free chains could combine sufficiently fast into the final structure to make it reasonable to compare the energies of the stable structures, as done in Figure 8. However, it is also interesting to model the desorption enthalpies under the assumption that the free chains are sufficiently long-lived to be detected experimentally. In that case, the relevant energy to calculate is the difference between the initial ammine in its stable bulk form and the final ammine as a chain in vacuum. For the 1→0 transition, the relevant free chains are the $Mg(NH_3)_{0.5}Cl_2$ chains, as shown in Figure 10c.

This can easily be done in the DFT calculations, and the results of this scheme applied to all four salts are again compared with apparent experimental desorption enthalpies and shown in Figure 11.

Although the straight line in Figure 11 has a slope of 1, it does not confirm the mechanism presented in Figure 10, nor does it prove that desorption in the TPD experiments is not equilibrated. The slope of less than 1 in Figure 9 could very well be due to limitations in the calculations. However, it does provide a valid way to predict desorption enthalpies using DFT, which appears to be more precise than comparing the energies of the stable structures. More importantly, the mechanism which, as mentioned, is also compatible with the equilibrium situation

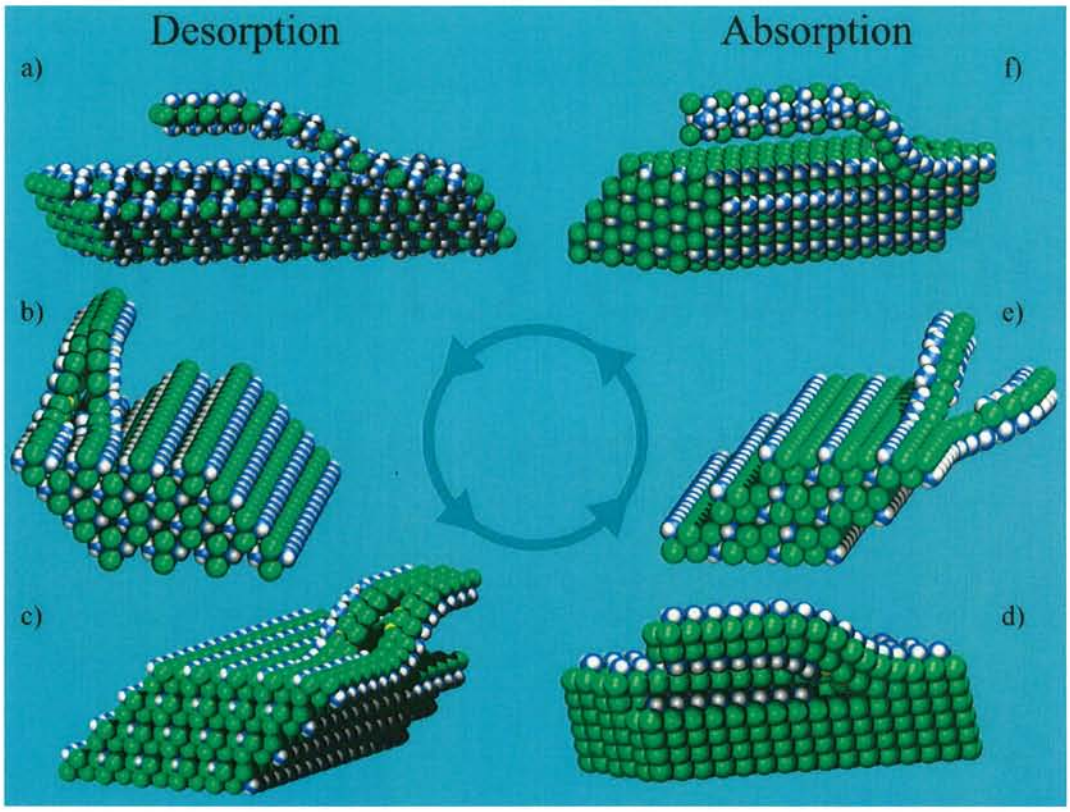

Figure 10. Proposed mechanism for desorption and absorption of ammonia in $Mg(NH_3)_nCl_2$, $Mn(NH_3)_nCl_2$, and $Ni(NH_3)_nCl_2$.

Ⓦ Animations illustrating front and side views of the desorption of ammonia from modeling studies are available.

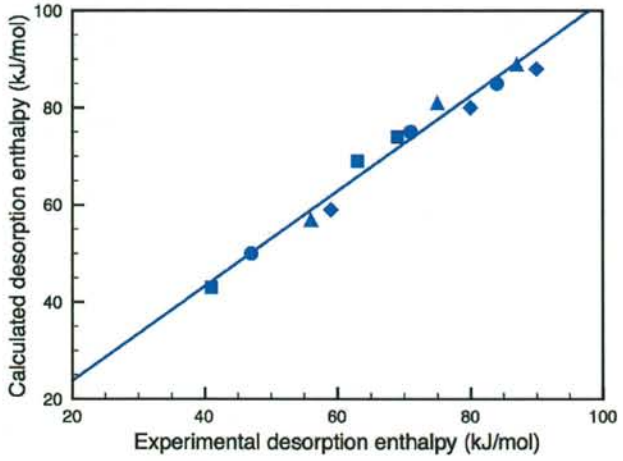

Figure 11. Calculated versus apparent experimental desorption enthalpies for the different desorption steps of $Mg(NH_3)_6Cl_2$ (triangles), $Ca(NH_3)_8Cl_2$ (squares), $Mn(NH_3)_6Cl_2$ (circles), and $Ni(NH_3)_6Cl_2$ (diamonds) for the proposed mechanism in Figure 10.

explains why desorption and absorption can happen fast in all the steps of the ab/desorption processes.

Conclusion

It is demonstrated that metal ammine complexes can be utilized as reversible, indirect hydrogen storage materials. The desorption of ammonia from $Ca(NH_3)_8Cl_2$, $Mn(NH_3)_6Cl_2$, and $Ni(NH_3)_6Cl_2$ is shown to be controlled mainly by thermodynamic equilibrium and heat transfer, as previously shown for $Mg(NH_3)_6Cl_2$. It is shown that the metal ammine complexes can be compacted to tablets with densities very close to the crystal densities and still maintain the same desorption properties. This is due to the development of nanopores in the tablets during desorption of ammonia. The nanopores facilitate diffusion of ammonia through the dense tablets.

DFT calculations are shown to reproduce accurately the trends in desorption enthalpies for all the systems studied. On the basis of extensive DFT calculations, we propose a mechanism for absorption and desorption of ammonia from metal ammine salts in which chains of the ammines are released from the surface of the crystal to explain the fast ab/desorption processes observed experimentally.

Acknowledgment. The authors thank Marina Y. Kustova and Mo Hongling Sønnichsen for experimental assistance and Amminex A/S for providing $Mg(NH_3)_6Cl_2$. The Danish National Research Foundation sponsors the Center for Sustainable and Green Chemistry. Lundbeck Foundation sponsors the Center for Atomic-scale Materials Design. The project is also supported by The Danish Council for Strategic Research (project no. 2104-05-0016) and the European Commission DG Research (contracts SES6-2006-51827/NESSHy and MRTN-CT-2006-032474/HYDROGEN).

Supporting Information Available: Table of thermodynamic properties of 90 metal ammine complexes. This information is available free of charge via the Internet at http://pubs.acs.org.

JA076762C

Journal of Materials Chemistry

www.rsc.org/materials

Volume 18 | Number 20 | 28 May 2008 | Pages 2285–2392

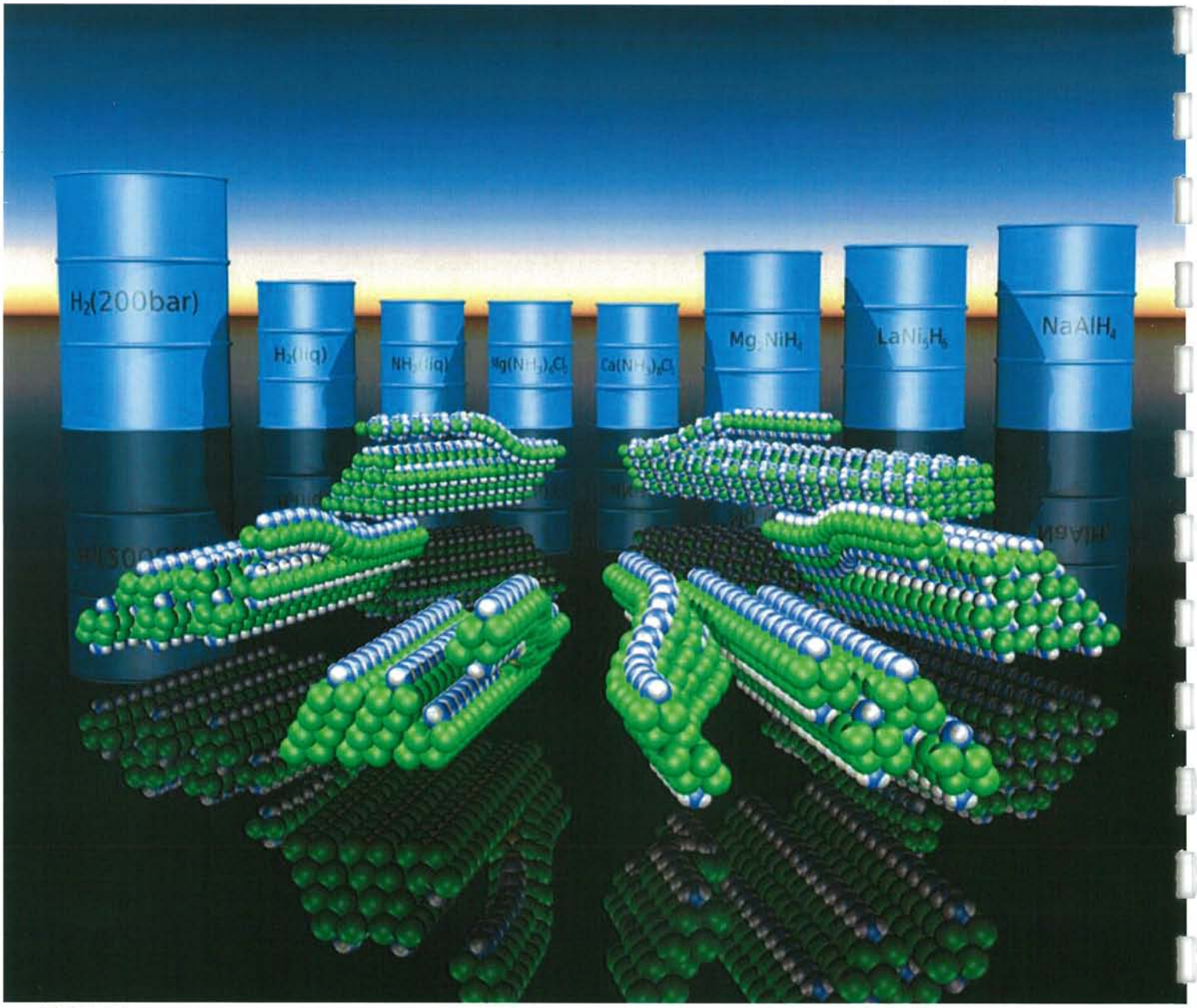

ISSN 0959-9428

Theme issue: Hydrogen Storage and Generation

FEATURE ARTICLE
Tejs Vegge *et al.*
Ammonia for hydrogen storage: challenges and opportunities

FEATURE ARTICLE
Roel van der Krol *et al.*
Solar hydrogen production with nanostructured metal oxides

RSC Publishing

0959-9428(2008)18:20;1-#

Ammonia for hydrogen storage: challenges and opportunities†

Asbjørn Klerke,[a] Claus Hviid Christensen,[a] Jens K. Nørskov[b] and Tejs Vegge*[c]

Received 2nd January 2008, Accepted 13th March 2008
First published as an Advance Article on the web 3rd April 2008
DOI: 10.1039/b720020j

The possibility of using ammonia as a hydrogen carrier is discussed. Compared to other hydrogen storage materials, ammonia has the advantages of a high hydrogen density, a well-developed technology for synthesis and distribution, and easy catalytic decomposition. Compared to hydrocarbons and alcohols, it has the advantage that there is no CO_2 emission at the end user. The drawbacks are mainly the toxicity of liquid ammonia and the problems related to trace amounts of ammonia in the hydrogen after decomposition. Storage of ammonia in metal ammine salts is discussed, and it is shown that this maintains the high volumetric hydrogen density while alleviating the problems of handling the ammonia. Some of the remaining challenges for research in ammonia as a hydrogen carrier are outlined.

Introduction

There are significant challenges related to the production, distribution and storage of hydrogen as a significant energy carrier of the future.[1] The requirements of the transportation sector have received particular attention, as outlined in the FreedomCAR 2015 system targets:[2] high reversible storage capacity (3 kWh kg^{-1} or 9 wt.% hydrogen and 2.7 kWh L^{-1} or 0.081 (kg H_2) L^{-1} system), fast kinetics (0.02 (g H_2) s^{-1} kW^{-1}), good reversibility (1500 cycles), ambient operating temperature (−40 to 60 °C), low cost ($2 kWh^{-1} or $67 (kg H_2)$^{-1}$), high hydrogen purity (<1 ppm CO) and safety (applicable standards).

Among these required properties, research efforts have primarily been focused on finding materials that feature the highest potential hydrogen storage capacity. Meeting this target alone is a significant challenge, which is accentuated by the fact that up to half the storage capacity by weight is often lost in the system integration.[3] The search for ultra-high capacity materials has led to the synthesis and characterization of more and more exotic and reactive compounds: complex metal hydrides like $NaAlH_4$,[4,5] $LiAlH_4$[6,7] and AlH_3,[8] metal organic frameworks (MOFs),[9] borohydrides like $LiBH_4$[10,11] and $Mg(BH_4)_2$,[12] destabilized borohydrides,[13] ammonia borane[14] and amide/imide systems.[15] All display high potential storage capacities, but fall short on a number of the other targets. Currently, complex metal hydrides do not reach the target for reversible hydrogen storage capacity, MOFs require operational temperatures around liquid nitrogen (−196 °C), systems based on borohydrides are practically irreversible and suffer from relatively slow kinetics,[16] production and regeneration of ammonia borane is very costly,[17] and the amide/imide systems have low reversible capacity.

Among hydrogen's main competitors as an energy carrier, methane/natural gas and methanol offer clear advantages in terms of energy capacity and distribution infrastructure, but suffer from their intrinsic carbon content causing end-user CO_2 emissions, since onboard capture is not feasible. Furthermore, the IEA (International Energy Agency) recently projected that a gap between production and demand of natural gas may occur

[a]*Center for Sustainable and Green Chemistry, Department of Chemistry, Building 206, Technical University of Denmark, DK-2800 Kgs. Lyngby, Denmark*
[b]*Center for Atomic-scale Materials Design, Department of Physics, Building 310, Technical University of Denmark, DK-2800 Kgs. Lyngby, Denmark*
[c]*Materials Research Department, Risø National Laboratory for Sustainable Energy, Building 228, Technical University of Denmark, DK-4000 Roskilde, Denmark. E-mail: tejs.vegge@risoe.dk*
† This paper is part of a *Journal of Materials Chemistry* theme issue on hydrogen storage and generation. Guest editor: John Irvine.

Asbjørn Klerke

Asbjørn Klerke earned his M.Sc. from the Technical University of Denmark in 2006. He is currently pursuing a PhD degree at the Center for Sustainable and Green Chemistry, under the supervision of Prof. C. H. Christensen. The focus of the PhD project is hydrogen from ammonia stored in metal ammine complexes, with special focus on the catalytic ammonia decomposition over transition metal surfaces.

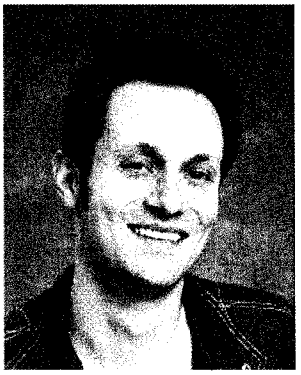

Tejs Vegge

Tejs Vegge is a senior scientist and leader of the Energy Storage and Conversion group at Risø National Laboratory for Sustainable Energy, Technical University of Denmark. His group focuses on characterization and design of novel materials and catalysts for hydrogen and ammonia storage, using integrated density functional theory calculations and advanced neutron and X-ray scattering techniques.

 This journal is © The Royal Society of Chemistry 2008

as soon as 2010–2012;[18] effectively rendering this solution short term and environmentally non-sustainable.

Aside from hydrogen, ammonia provides the only carbon-free chemical energy carrier solution for the transportation sector. Ammonia is not a greenhouse gas (GHG), and in light of the enormous global climate challenges with respect to GHG outlined, *e.g.*, in the Kyoto protocol, combined with a high hydrogen density, NH_3 could be an interesting alternative to hydrogen.

Ammonia is primarily produced from natural gas, but a large number of coal-based ammonia plants are currently being put into production;[19] an aspect which is particularly important for countries like China, with a rapidly expanding need for transportation, limited oil and gas resources, but enormous coal reserves.[20] A highly developed ammonia infrastructure is already in existence, and with a centralized, coal-based production of ammonia with simultaneous sequestration of the produced CO_2, ammonia could offer not only a short term solution to needs of the transportation sector, but a long-term, zero-carbon-emission solution with a projected lifespan of 200 years.[21] Still, ammonia is often disregarded as a potential fuel in the transportation sector, primarily because of its too high toxicity,[22] but recent research on reversible NH_3 storage in metal ammines (see Fig. 1), *e.g.* $Mg(NH_3)_6Cl_2$[23] and $Ca(NH_3)_8Cl_2$,[24] illustrates how a toxicity lower than that of gasoline can be obtained, while maintaining a practical, reversible storage capacity of up to 10 wt.% hydrogen.[23,24]

For use in polymer electrolyte membrane fuel cells (PEMFC), ammonia must first be decomposed into nitrogen and hydrogen, but NH_3 can be decomposed catalytically at temperatures above 300 °C (Fig. 1) with present-day catalysts. This is, however, an area of active research and the development of superior decomposition catalysts remains a worthwhile challenge for an ammonia-powered transportation sector.

In the following, we review the status, challenges, and perspectives of ammonia stored in metal ammines as a carrier material in the transportation sector, and place the results in the context of state-of-the-art in hydrogen storage materials and existing transport fuels.

Ammonia synthesis

The use of ammonia as an energy carrier has several advantages.[25] One of these is that most of the technologies for production and transportation are well developed and already in widespread use on an industrial scale.[26] The synthesis of ammonia in the Haber–Bosch process is among the largest and best studied chemical processes in the world.[27] The annual production of ammonia (mainly for agricultural use) exceeds 120 million tons.[28] The synthesis reaction is performed under 200–350 bar pressure over a multi-promoted iron catalyst operated at temperatures from 300 to 550 °C in a reactor with two to four catalyst beds giving around 15% conversion to ammonia. The unconverted synthesis gas is recycled. The hydrogen for the synthesis process is primarily produced from methane by steam reforming and water gas shift reactions.[29] Although ammonia synthesis is an exothermic reaction (Fig. 1), the practical production of ammonia from hydrogen and nitrogen incurs a small energy loss of 1.5 GJ t^{-1} compared to the 28.4 GJ t^{-1} energy stored in the ammonia. In comparison, the production of hydrogen has an energy cost of 8.0 GJ t^{-1}.[30] Hydrogen production is necessary for all proposed hydrogen-based energy carriers, but in the case of ammonia, this can also come from other sources than methane. The current price of ammonia is in the range of \$250–300 t^{-1}, the equivalent of \$1.4–1.7 $(kg\ H_2)^{-1}$.[31] This price is mainly governed by the price of methane that constitutes above 75% of the running cost of ammonia production.

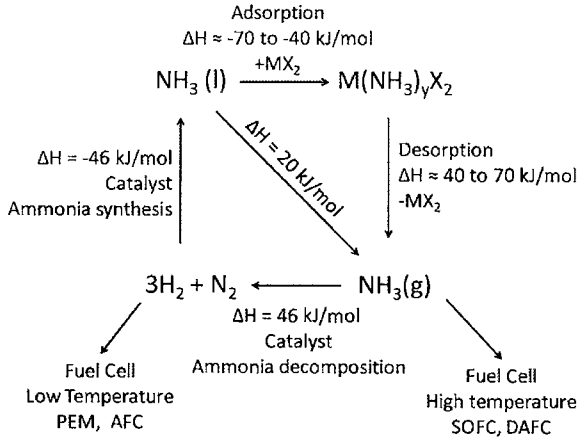

Fig. 1 The life-cycle of hydrogen stored as ammonia in metal ammines, $M(NH_3)_yX_2$.

Ammonia production is a prime candidate for CO_2 sequestration, because CO_2 is being removed from the synthesis gas by scrubbing to avoid deactivation of the ammonia synthesis catalyst. Furthermore, ammonia plants are typically located close to natural gas reservoirs, where the captured CO_2 might be pumped back.[30]

The hydrogen for ammonia synthesis can also be produced from coal by gasification. Coal is interesting for hydrogen production for several reasons; first of all, coal is cheap compared to other hydrocarbon energy sources,[20] secondly, the coal reserves are large enough to last for at least 200 years,[20] and finally, coal can be efficiently converted into hydrogen by gasification with a high efficiency.[32–34] Thus, even though an intense search for alternatives to coal is continuously on-going, the end result could be that we will need to exhaust all the available coal reserves.

Ammonia safety

The risk of explosion is an essential safety concern in the transportation sector, which can block the potential use of any energy carrier. High capacity carriers are generally very reactive, but significant differences can be observed in the flammability and explosion limits (see Table 1).

From Table 1, it is clear that hydrogen is very flammable, as are natural gas/methane, methanol, and gasoline vapors, whereas ammonia is not flammable in air. With respect to explosion limits, both hydrogen and ammonia require significantly higher concentrations than gasoline vapor and natural gas.

The toxicity of ammonia is clearly also an important safety aspect. Comparing the toxicity of liquid ammonia to that of gasoline and methanol, liquid ammonia is approximately three orders of magnitude higher in "apparent toxicity", *i.e.* the vapor pressure relative to the toxicity, at room temperature.[37] The apparent toxicities takes both the IDLH (Immediately Dangerous to Life or Health) concentration and the vapor

Table 1 Vapor pressures of different energy carriers, their relative toxicities, flammability and explosion limits in air[29,34–36]

	Vapor pressure, p_i, at 293 K/bar	IDLH[a] (ppm)	Apparent toxicity $p_{i,293K}$/IDLH	Flammability limits (in air)	Explosion limits (in air)
Gasoline	0.047	750	63	1.4–7.6%	1.1–3.3%
Methanol	0.13	6000	21.6	6–36%	5.5–44%
Hydrogen	—	—	—	4–74%	18.3–59%
Natural gas	—	—	—	5.3–15%	5.7–14%
Liquid ammonia	8	300	$\sim 2.7 \times 10^4$	—	16–25%
$Mg(NH_3)_6Cl_2$	1.4×10^{-3}	300	4.65	—	—

[a] NIOSH: Immediately Dangerous to Life or Health (IDLH) concentration.

pressure into account, since substances with a low vapor pressure can have a low IDLH concentration and still rate safer than a substance with higher IDLH concentration but higher vapor pressure.

For ammonia stored in metal ammines, *e.g.* $Mg(NH_3)_6Cl_2$, the apparent toxicity falls below those of both gasoline and methanol; in comparison, the promising and intensely studied borohydrides[12] are known to display partial release of highly flammable and toxic diborane during hydrogen desorption.[38,39] Safety issues remain a main challenge for using ammonia in the transportation sector, but the considerations outlined above are in line with a recent EU-funded report, which concluded that "the use of ammonia as a transport fuel wouldn't cause more risks than currently used fuels".[40]

Storage and transportation of ammonia

The infrastructure for handling and transporting bulk ammonia is already well established. Liquid ammonia is being transported around the world in ships, pipelines, trains and trucks.[25,41,42] The transportation of liquid ammonia in closed systems to decentralized sites for production and regeneration of metal ammine salts can minimize the overall cost and be scaled up while maintaining safety, but some additional steps need to be taken to minimize the risks involved.[40] For automotive applications, the end user should therefore not come in contact with liquid ammonia, only the metal ammines produced and regenerated at a nearby location.

As outlined above, the toxicity and vapor pressure of liquid ammonia make it undesirable for direct use in mobile applications, mainly because of the potential risk of accidents where ammonia is released and because of the technical challenges of securing the end user against contact with liquid ammonia during refilling and while performing periodical maintenance.[25,42]

The storage of ammonia is currently done in two different ways: for large quantities up to 50 000 t, ammonia is stored at 1 bar and −33 °C in insulated tanks. The temperature is kept down by slow vaporization, and the ammonia vapor is continually compressed back to a liquid. For small tanks, below 1500 t, ammonia is stored under pressure in stainless steel spheres.[29]

Ammonia and fuel cells

The direct use of ammonia in high temperature solid oxide fuel cells (SOFC) has been shown to work with a performance similar to pure hydrogen[43,44]—in fact, even surpassing it at temperatures above 200 °C.[45] The SOFC can also run on other fuels like methanol or methane, but these fuels need to be reformed and this gives a possibility of carbon poisoning of the anode.[46,47] The carbon oxide-free ammonia can be fed directly into a high temperature SOFC and the endothermic ammonia decomposition reaction will help cool the SOFC, which combined with an entropy gain means that ammonia as a direct fuel increases the fuel cell performance at high temperatures.[45]

In low temperature fuel cell systems, such as polymer electrolyte membrane (PEMFC) and alkaline fuel cells (AFC), ammonia needs to be decomposed to hydrogen and nitrogen before it is fed to the fuel cell. In some applications, it might be desirable to remove the inert nitrogen to supply a concentrated hydrogen stream. This can be done, *e.g.*, by use of a hydrogen-selective membrane system.[48,49] The ammonia decomposition is done catalytically over a suitable catalyst at temperatures from *ca.* 300 to 520 °C (see below). The ammonia decomposition reaction is equilibrium-limited, so unconverted ammonia must be taken properly into account when the fuel cell system is designed. If the system operates with an AFC, ammonia is tolerated and can be recycled to the decomposition unit.[50] For proton-conducting fuel cells such as PEMFC and PAFC (phosphoric acid fuel cell), ammonia is problematic since the acidic electrolyte reacts with ammonia and thereby deactivates. This means that for continuous operation, the ammonia concentration must be below 1 ppm.[51]

Ammonia decomposition

The ammonia decomposition reaction has traditionally been studied to gain more information about the ammonia synthesis catalyst.[52] This is slowly changing as ammonia is gradually becoming more widely accepted as one of the more promising hydrogen carriers.[53] At present, the commercially used catalyst for ammonia decomposition is nickel on alumina,[54] which is mechanically strong and heat resistant, but further development and optimization are needed.

During the last ten years, different research groups have developed and optimized catalysts specifically for use in ammonia decomposition for production of CO_x-free hydrogen.[55–57] There now exists a general consensus that caesium-promoted ruthenium supported on graphite is the best known catalyst.[58,59] Several studies have shown that barium is also a useful promoter for ammonia decomposition on ruthenium surfaces.[60]

The currently best promoted ruthenium catalysts are sufficiently active at temperatures from about 300 °C. In Fig. 2, two different studies of the decomposition rate of ammonia are shown. The first is a study by Raróg-Pilecka *et al.*,[58] which shows

 This journal is © The Royal Society of Chemistry 2008

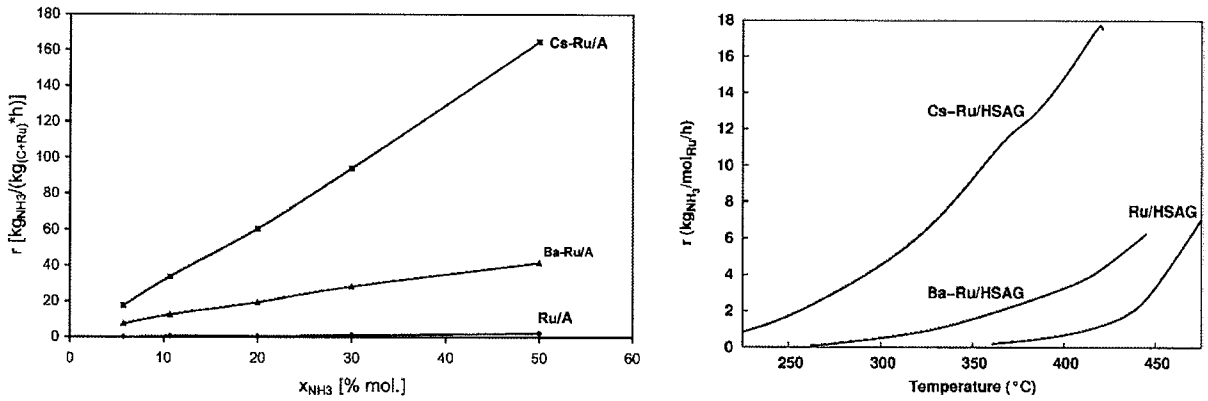

Fig. 2 Dependence of the ammonia decomposition rate on x_{NH3} over the Ru/C catalyst at 400 °C (left).[58] The temperature dependence of the ammonia decomposition rate for Ru/HSAG in micro-fabricated reactors[61] (right).

the decomposition rate in a conventional reactor at various ammonia concentrations and at a fixed temperature of 400 °C. The second study shows the rate of ammonia decomposition as a function of temperature, at a constant inlet gas concentration of 20% ammonia in argon and for a constant flow rate. These experiments were performed in micro-fabricated reactors, which feature excellent heat transport to the endothermic reaction.[61]

The challenge with low temperature ammonia decomposition is that the equilibrium conversion is dependent on the temperature and the reaction is endothermic, *i.e.* the concentration of ammonia at equilibrium increases with decreasing temperature. At 425 °C and 1 bar pressure, the equilibrium conversion of ammonia is 98–99%, which makes unconverted ammonia a significant challenge for the overall system efficiency if the temperature is lowered with a conventional reactor design. Furthermore, the decomposition rate decreases significantly when equilibrium is approached according to the general formula $r = r^{+}(1 - \beta)$, where β describes the approach to equilibrium as a factor between 0 and 1.[62] To avoid the equilibrium limitation, removal of the hydrogen through a membrane is an option,[63] which would provide a pure hydrogen feed, free of ammonia and nitrogen, and it will help to increase the conversion by shifting the equilibrium further towards complete conversion.

Solid storage of ammonia

The idea of using ammonia as a hydrogen carrier has been promoted by the further development of safe storage of ammonia in solid form by binding it in metal ammine complexes.[23] A large number of metal salts are known to form stable metal ammines, and these are generally well described in the classical chemistry literature.[64–66]

The solid storage of ammonia solves the safety issues of driving with ammonia in liquid form under pressure. At the same time, the volumetric hydrogen density is high for the metal ammines compared to that of liquid ammonia and metal hydrides as shown in Fig. 3. Fig. 3 also compares the mass of the different hydrogen storage materials, and among the solid materials, the metal ammines stand out by being lighter than the metal hydrides, but heavier than the liquids and gases, when the weight of the storage tank is not taken into consideration. The current developments in high pressure hydrogen storage move towards lighter cylinders of composite materials but still with a high weight compared to the stored amount of gas, and the safety issues of driving and refueling to pressures between 35–70 MPa need to be carefully considered. Liquid hydrogen is difficult to handle on a small scale, mainly because of the very low temperature of −252 °C and the evaporation loss of 2–3% per day. The amount of insulation also adds to the mass and volume of the overall storage system.[67] Liquid ammonia needs to be transported in pressurized tanks, and for the safety issues mentioned above, it appears unlikely to obtain the required public acceptance. This leaves the solid storage of hydrogen and ammonia as the best alternatives for mobile use.

From the literature values, suitable metal ammine salts can be selected for a given application. So far, the best studied material is $Mg(NH_3)_6Cl_2$, which was selected due to the low vapor pressure of 2 mbar at room temperature (see Table 1) and the

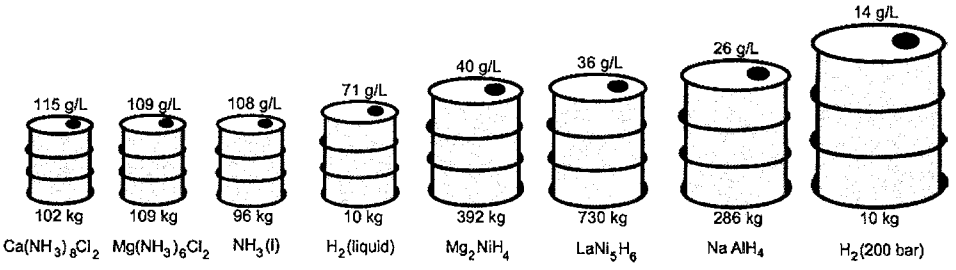

Fig. 3 Mass and volume of 10 kg hydrogen stored reversibly by 8 different methods, based on the best obtained reversible densities reported in the literature without considering the space or weight of the container.[29,68–73]

high gravimetric (9.19 wt.%) and volumetric (109 (g H_2) L^{-1}) hydrogen density available from a compacted tablet.[23] Recently, research on $Ca(NH_3)_8Cl_8$ has also shown promise for mobile applications, since the hydrogen density is as high as 9.78 wt.% and the release of ammonia is achieved at lower temperatures than that of $Mg(NH_3)_6Cl_2$, thereby reducing the energy needed to desorb the ammonia, but also the stability at 60 °C.[2]

The lower desorption temperature of $Ca(NH_3)_8Cl_8$ results in a higher ammonia vapor pressure at room temperature (0.7 bar), but this is still an order of magnitude lower than that of liquid ammonia.[24] The number of metal ammines investigated for use as hydrogen storage materials is still quite small, but due to their similar chemical nature, the general findings can be used as a guideline for the behavior of other metal ammines. This has been tested by detailed modeling using density functional theory (DFT) calculations, which showed good agreement between theoretical calculations and experimental data.[74] DFT calculations are able to reproduce the experimentally observed trend in desorption enthalpies for various ammines at all decomposition steps,[24] making such calculations a valuable tool in the design and prediction of novel metal ammine compounds with specific stabilities, *e.g.* by varying the metal or halide components in the ammine salt.

Release of ammonia from metal ammines has been investigated in several papers[53,75,76] in the efforts to map out their chemical and physical properties. Generally, metal ammines reversibly absorb and desorb ammonia as shown in Fig. 1, where the desired absorption and desorption enthalpies are also indicated. When the enthalpy of desorption of the first ammonia is below 40 kJ mol^{-1}, the vapor pressure at room temperature is close to 1 bar, making absorption of ammonia in the salt difficult. If the desorption enthalpy of the last ammonia is above 70 kJ mol^{-1}, the temperature needed for desorption is too high for practical applications—with the possible exception of the SOFC, where sufficient heat will typically be easily available.

The desorption kinetics of metal ammines has mainly been studied by temperature programmed desorption (see Fig. 4). These experiments show that generally, the metal ammines have very similar properties and can be formed into compact tablets essentially without any voids that would lead to a loss of volumetric storage capacity. Even in this compact form (>95% of bulk density), they maintain their excellent properties with respect to fast ammonia desorption kinetics.[74] Generally, the desorption characteristics can be estimated directly from the desorption enthalpies and the fact that the metal ammines have very similar entropies.[77] A main limitation of ammonia desorption is heat transfer, since the activation energy for ammonia desorption is relatively low and because the metal ammines are poor heat conductors; hence the required heat is mainly transported by the ammonia gas.[78] Another reason for the fast desorption is the intrinsic formation of a nanoporous, sponge-like skeletal structure from the compact metal ammines during ammonia desorption, which has recently been documented in a detailed *in situ* small-angle X-ray scattering (SAXS) study.[76] This is an important aspect, since compact tablets of metal ammines maintain their physical shape even after desorption of all the ammonia, corresponding to a loss of approximately half the mass and three quarters of the occupied volume. The formation of nanopores has also been investigated by DFT

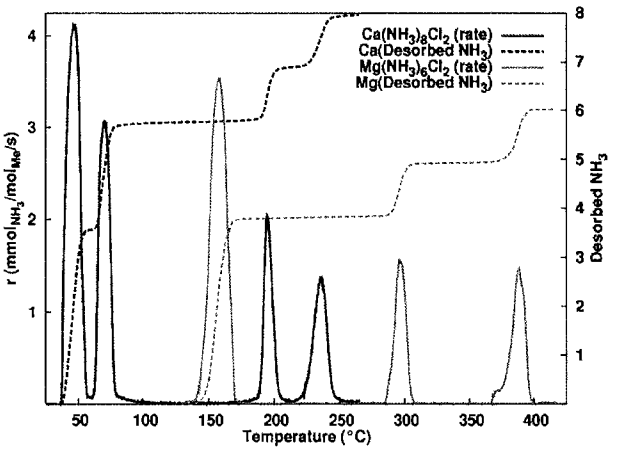

Fig. 4 Temperature programmed desorption of ammonia from $Ca(NH_3)_8Cl_2$ and $Mg(NH_3)_6Cl_2$ measured with a heating of 1 °C min^{-1} (adapted from ref. 24).

calculations, which show that metal ammine crystals can release ammonia by a change of the lattice constant and a slight internal rearrangement; this can be interpreted as the individual crystallites gradually shrinking to form pores.[75]

Solid state storage of ammonia has the additional advantage that the storage density can be considered constant at temperatures around 0 °C. This is not the case for liquid ammonia as shown in Fig. 5, where the vapor pressure and volumetric hydrogen density is plotted as function of the temperature in a normal operating interval.

System integration

For practical use of ammonia and metal ammines as hydrogen carries on a larger scale, efficient system integration must be achieved to minimize the energy loss. This means that the waste heat from the fuel cell and the catalyzed ammonia decomposition process must be used efficiently to release ammonia from the metal ammine and to heat the ammonia feed gas.[79] The safety

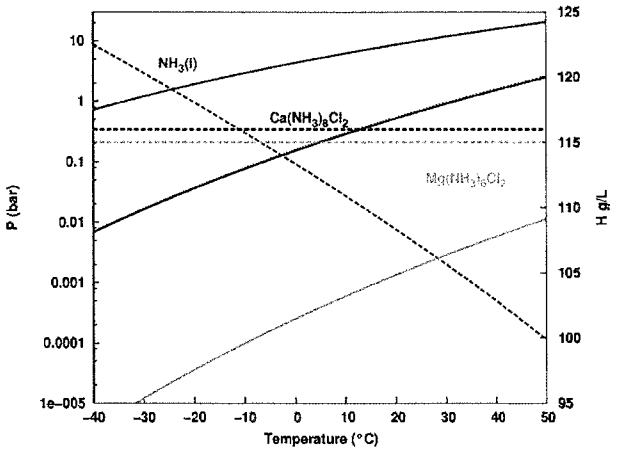

Fig. 5 The temperature dependence of the vapor pressure (solid lines) and volumetric hydrogen densities (dashed lines) for NH_3 (l), $Ca(NH_3)_8Cl_2$ and $Mg(NH_3)_6Cl_2$.

This journal is © The Royal Society of Chemistry 2008

issues concerning liquid ammonia also make it important to design a system where the end user does not come into contact with liquid ammonia during refueling. This can be done by handling the regeneration of the metal ammine salts at decentralized locations, where the heat of formation can also be reused.

If the metal ammine system is integrated with a high temperature SOFC, the waste heat from the fuel cell is more than sufficient to supply the heat required for ammonia release and ammonia decomposition at the anode. As previously mentioned, ammonia has the advantage over reformed methane or methanol in a SOFC that it is carbon-free and that no reformer is needed.[80] The residual ammonia and unused hydrogen can be sent directly to a (catalytic) burner as is common practice with most operating SOFCs, and the ammonia will contribute to lowering NO_x emissions.[81]

Systems using ammonia together with low temperature fuel cells using proton conducting membranes are more complicated for various reasons. The heat from the fuel cell is available at low to intermediate temperatures, which is sufficient for complete desorption of ammonia from $Ca(NH_3)_8Cl_2$, but not for *e.g.* $Mg(NH_3)_6Cl_2$. However, any required additional heat can come from the ammonia decomposition reactor that will operate at temperatures from 300 °C, which is the minimum temperature if the ammonia residue should be below 2%. The challenge is that the decomposition is an endothermic process requiring 46 kJ $(mol\ NH_3)^{-1}$. The heat for ammonia decomposition needs to be supplied by electrical heating or by burning hydrogen or ammonia. The remaining ammonia from the decomposition needs to be removed to keep the ammonia concentrations <1 ppm to avoid poisoning of the fuel cell. This can be done efficiently by leading the gas through an acid media which can reduce the ammonia concentration down to ppb levels. More elegantly, the unconverted ammonia could also be removed by absorption into $MgCl_2$ or $CaCl_2$ or other even more reactive metal salts, to (re)form the metal ammine.

The possibilities are plentiful and very little research effort has so far gone into this technology compared to other related subjects, such as CO poisoning in PEMFC or DMFC.

Outlook and perspective

The utilization of ammonia as a potential hydrogen carrier is still receiving limited attention compared to *e.g.* the complex metal hydrides and other direct hydrogen storage methods, even though the ammonia technology seems to be significantly closer to market. The research devoted to the use of carbon-based hydrogen carriers as light hydrocarbons and methanol has also been substantial, although the challenges regarding CO_2 for the end user remaining unsolved. In this perspective, ammonia stored in metal ammines appears as an attractive alternative which can solve many of the main targets setup for a hydrogen storage material, *i.e.* fast kinetics, high hydrogen storage capability, high availability and low cost. The less attractive sides to ammonia as a hydrogen carrier include the current methane-based production of ammonia without carbon sequestration, and the toxicity of the liquid.

Recent research into solid state storage of ammonia in metal ammines has solved many of the problems regarding end user safety, since the main risk of exposure to liquid ammonia has been avoided. The metal ammines also have higher volumetric hydrogen densities than liquid ammonia and other proposed hydrogen storage materials. Desorption of ammonia from metal ammines can easily be controlled and the desorption temperature can be selected to fit a given application. The use of metal ammines is currently being commercialized for automotive applications in connection with SCR catalysts to reduce the amount of NO_x produced by diesel cars or trucks.[82]

There are several remaining challenges involved with an ammonia mediated hydrogen economy. A technology must be developed to remove CO_2 from the production system, but this is a general challenge for the idea of a carbon-free energy system. Alternatively, it would be very interesting if one could produce ammonia electrochemically in a process analogous to the one certain enzymes, the nitrogenases, use in nature.[83] This would allow decentralized, sustainable ammonia production on the basis of photo-voltaic cells or wind power. Optimization of the use of the energy stored in ammonia is also needed. This is possible, either from better ammonia decomposition catalysts or from better direct ammonia fuel cells. Other alternatives could be electrolysis of ammonia to hydrogen in an alkaline solution.[84] The benefit of electrolysis is clean hydrogen production at low temperature. Current fuel cell research is focusing on bridging the temperature gap between SOFCs and PEMFCs. That could give very efficient direct ammonia fuel cells with running temperatures from 400–600 °C.[85] In terms of storing ammonia in metal ammines, there appear to be many unexplored opportunities for designing suitable salts that feature a desired desorption temperature, as well as in mixtures with other hydrogen storage materials.[86] Finally, the establishment of fully integrated systems is required to achieve the necessary operating experience with all aspects of these systems.

Acknowledgements

The Center for Sustainable and Green Chemistry is sponsored by the Danish National Research Foundation and the Center for Atomic-scale Materials Design is supported by the Lundbeck Foundation. The authors acknowledge the European Commission DG Research (contracts SES6-2006-51827/NESSHy and MRTN-CT-2006-032474/HYDROGEN) and the Danish Council for Strategic Research (# 2104-05-0016).

References

1 G. Crabtree, M. Dresselhaus and M. Buchanan, *Phys. Today*, 2004, **57**(12), 39.
2 http://www1.eere.energy.gov/hydrogenandfuelcells/pdfs/freedomcar_targets_explanations.pdf.
3 D. Mosher, X. Tang and S. Arsenault, *High Density Hydrogen Storage System Demonstration Using $NaAlH_4$ Based Complex Hydrides*, FY 2006 Annual Progress Report, DoE Hydrogen Program, 2006, pp. 281–284.
4 D. Sun, S. S. Srinivasan, G. Chen and C. M. Jensen, Rehydrogenation, *J. Alloys Compd.*, 2004, **373**(1–2), 265–269.
5 T. Vegge, *Phys. Chem. Chem. Phys.*, 2006, **8**, 4853–4861.
6 G. Sandrock, J. Reilly, J. Greatz, W.-M. Zhou, J. Johnson and J. Wegrzyn, *J. Alloys Compd.*, 2006, **421**, 185–189.
7 A. Andreasen, T. Vegge and A. S. Pedersen, *J. Solid State Chem.*, 2005, **178**, 3672–3678.
8 Sandrock, J. Reilly, J. Greatz, W.-M. Zhou, J. Johnson and J. Wegrzyn, *Appl. Phys. A*, 2005, **A80**, 687–690.
9 H. Furukawa, M. A. Miller and O. M. Yaghi, *J. Mater. Chem.*, 2007, **17**, 3197.
10 A. Züttel, P. Wenger, S. Rentsch, P. Sudan, P. Mauron and C. Ernmenegger, *J. Power Sources*, 2003, **118**, 1.

11 Z. Łodziana and T. Vegge, *Phys. Rev. Lett.*, 2004, **93**, 145501.
12 K. Chłopek, C. Frommen, A. Leon, O. Zabara and M. Fichtner, *J. Mater. Chem.*, 2007, **17**, 3496.
13 J. J. Vajo, S. L. Skeith and F. Mertens, *J. Phys. Chem. B*, 2005, **109**, 3719.
14 A. Feaver, S. Sepehri, P. Shamberger, A. Stowe, T. Autrey and G. Cao, *J. Phys. Chem. B*, 2007, **111**, 7469–7472.
15 W. Lohstroh and M. Fichtner, *J. Alloys Compd.*, 2007, **332**, 446–447.
16 S. Orimo, Y. Nakamori, G. Kitahara, K. Miwa, N. Ohba, S. Towata and A. Zuttel, *J. Alloys Compd.*, 2005, **447**, 404–406.
17 P. V. Ramachandran and P. D. Gagare, *Inorg. Chem.*, 2007, **46**, 7810–7817.
18 http://www.iea.org.
19 J. F. Clausen and C. A. Zee, TRW-Systems and Energy, EPA contract 68-02-2635.
20 International Energy Agency (IEA), Key World Energy Statistics, 2007.
21 BP Statistical Review of World Energy, June 2007.
22 http://www.cdc.gov/niosh/.
23 C. H. Christensen, R. Z. Sørensen, T. Johannessen, U. Quaade, K. Honkala, T. D. Elmøe, R. Køhler and J. K. Nørskov, *J. Mater. Chem.*, 2005, **15**, 4106–4108.
24 R. Z. Sørensen, J. S. Hummelshøj, A. Klerke, J. B. Reeves, T. Vegge, J. K. Nørskov and C. H. Christensen, Indirect, reversible high-density hydrogen storage in compact metal ammine salts, *J. Am. Chem. Soc.*, submitted.
25 P. J. Feibelman, *Phys. Today*, 2005, **58**, 13–14.
26 L. Green, *Int. J. Hydrogen Energy*, 1982, **7**, 355–359.
27 R. Schlögl, *Angew. Chem., Int. Ed.*, 2003, **42**, 2004–2008.
28 International Fertilizer Industry Association, World Ammonia (NH3) Statistics by Region, 2006, http://www.fertilizer.org/ifa/statistics.asp.
29 M. Appl, *Ullmann's Encyclopedia of Industrial Chemistry: Ammonia*, Wiley-VCH Verlag GmbH & Co. KGaA, Weinheim, 2007.
30 I. Dybkjaer, in *Ammonia, Catalysis and Manufacture*, ed. A. Nielsen, Springer, Heidelberg, 1995, pp. 199–308.
31 ICIS pricing Chemical Pricing Reports, Ammonia, http://www.icispricing.com.
32 J. Wu, Y. Fang, H. Peng and Y. Wang, *Fuel Process. Technol.*, 2004, **86**, 261–266.
33 W. de Jong, Ö. Ünal, J. Andries, K. R. G. Hein and H. Spliethoff, *Biomass Bioenerg.*, 2003, **25**, 59–83.
34 P. Häussinger, R. Löhmuller and A. M. Watson, *Ullmann's Encyclopedia of Industrial Chemistry: Hydrogen*, Wiley-VCH Verlag GmbH & Co. KGaA, Weinheim, 2000.
35 A. English, J. Rovner, J. Brown and S. Davies, *Kirk–Othmer Encyclopedia of Chemical Technology: Methanol*, John Wiley & Sons, Inc., New York, 2005.
36 E. Fiedler, G. Grossmann, D. B. Kersebohm, G. Weiss and C. Witte, *Ullmann's Encyclopedia of Industrial Chemistry: Methanol*, Wiley-VCH Verlag GmbH & Co. KGaA, Weinheim, 2000.
37 http://www.cdc.gov/niosh/idlh/intridl4.html.
38 J. Kostka, W. Lohstroh, M. Fichtner and H. Hahn, *J. Phys. Chem. C*, 2007, **111**, 14026.
39 E. Jeon and Y. W. Cho, *J. Alloys Compd.*, 2006, **422**, 273.
40 N. J. Duijm, F. Markert and J. L. Paulsen, *Safety assessment of ammonia as a transport fuel*, Risø-R-1504(EN), 2005, http://www.risoe.dk/rispubl/SYS/syspdf/ris-r-1504.pdf.
41 T. Eggmann, *Kirk-Othmer Encyclopedia of Chemical Technology: Ammonia*, John Wiley & Sons, Inc., New York, 2001.
42 G. Thomas and G. Parks, *Potential Roles of Ammonia in a Hydrogen Economy*, U.S. Department of Energy, 2006.
43 G. G. M. Fournier, I. W. Cumming and K. Hellgardt, *J. Power Sources*, 2006, **162**, 198–206.
44 G. Meng, C. Jiang, J. Ma, Q. Ma and X. Liu, *J. Power Sources*, 2007, **173**, 189.
45 C. H. Christensen, presented at *International Symposium on Materials Issues in a Hydrogen Economy*, Richmond, Virginia, 2007.
46 C. M. Finnerty, N. J. Coe, R. H. Cunningham and R. M. Ormerod, *Catal. Today*, 1998, **46**, 137–145.
47 M. Itome and A. E. Nelson, *Catal. Lett.*, 2006, **106**, 21–27.
48 R. Metkemeijer and P. Achard, *Int. J. Hydrogen Energy*, 1994, **19**, 535–542.
49 R. Metkemeijer and P. Achard, *J. Power Sources*, 1994, **49**, 271–282.
50 K. Kordesch, V. Hacker, J. Gsellmann, M. Cifrain, G. Faleschini, P. Enzinger, R. Fankhauser, M. Ortner, M. Muhr and R. R. Aronson, *J. Power Sources*, 2000, **86**, 162–165.
51 R. Halseid, P. J. S. Vie and R. Tunold, *J. Power Sources*, 2006, **154**, 343–350.
52 J. B. Hansen, in *Ammonia, Catalysis and Manufacture*, ed. A. Nielsen, Springer, Heidelberg, 1995, pp. 149–198.
53 C. H. Christensen, T. Johannessen, R. Z. Sørensen and J. K. Nørskov, *Catal. Today*, 2006, **111**, 140–144.
54 http://www.nikki-chem.co.jp/eng/products/pro3_2.html.
55 A. S. Chellappa, C. M. Fisher and W. J. Thomson, *Appl. Catal., A*, 2002, **227**, 231–240.
56 T. V. Choudhary, C. Sivadinarayana and D. W. Goodman, *Catal. Lett.*, 2001, **72**, 197–201.
57 J. C. Ganley, E. G. Seebauer and R. I. Masel, *J. Power Sources*, 2004, **137**, 53–61.
58 W. Raróg-Pilecka, D. Szmigeel, Z. Kowalczyk, S. Jodis and J. Zielinski, *J. Catal.*, 2003, **218**, 465–469.
59 S.-F. Yin, B. Q. Xu, X. P. Zhou and C. T. Au, *Appl. Catal., A*, 2004, **277**, 1–9.
60 R. Z. Sørensen, L. J. E. Nielsen, S. Jensen, O. Hansen, T. Johannesen, U. Quaade and C. H. Christensen, *Catal. Commun.*, 2005, **6**, 229–232.
61 R. Z. Sørensen, A. Klerke, U. Quaade, S. Jensen, O. Hansen and C. H. Christensen, *Catal. Lett.*, 2006, **112**, 77–81.
62 A. Boisen, S. Dahl, J. K. Nørskov and C. H. Christensen, *J. Catal.*, 2005, **230**, 309–312.
63 http://www.powerandenergy.com/hy_separator.shtml.
64 F. Ephraim, *Ber. Dtsch. Chem. Ges.*, 1912, **45**, 1322–1331.
65 F. Ephraim, *Z. Phys. Chem.*, 1913, **81**, 513–542.
66 W. Biltz, *Z. Anorg. Allg. Chem.*, 1923, **130**, 93–139.
67 A. Zûttel, *Mater. Today*, 2003, **6**(September), 24–33.
68 D. Mosher, X. Tang and S. Arsenault, High Density Hydrogen Storage System Demonstration Using NaAlH4 Based Complex Hydrides, FY 2006 Annual Progress Report, DoE Hydrogen Program, 2006, pp. 281–284.
69 X. Liu, Y. Zhu and L. Li, *Int. J. Hydrogen Energy*, 2007, **32**, 2450–2454.
70 K. Nomura, S. Fujiwara, H. Hayakawa, E. Akiba, Y. Ishido and S. Ono, *J. Less-Common Met.*, 1991, **169**, 9–17.
71 E. Suissa, I. Jacob and Z. Hadari, *J. Less-Common Met.*, 1984, **104**, 287–295.
72 M. A. El-Osairy, I. A. El-Osery, A. M. Metwally and M. A. Hassan, *Int. J. Hydrogen Energy*, 1993, **18**(6), 517–524.
73 K. J. Laidler; and J. H. Meiser *Physical Chemistry*, 3rd edn, Houghton Mifflin Company, New York, 1999.
74 T. Vegge, R. Z. Sørensen, A. Klerke, J. S. Hummelshøj, T. Johannessen, J. K. Nørskov and C. H. Christensen, Indirect hydrogen storage in metal ammines, in *Solid State Hydrogen Storage: Materials and Chemistry*, ed. G. Walker, Woodhead Publishing, Cambridge, UK, 2008, in press.
75 J. S. Hummelshøj, R. Z. Sørensen, M. Y. Kustova, T. Johannesen, J. K. Nørskov and C. H. Christensen, *J. Am. Chem. Soc.*, 2006, **128**, 16–17.
76 H. S. Jacobsen, H. A. Hansen, J. W. Andreasen, Q. Shi, A. Andreasen, R. Feidenhans'l, M. M. Nielsen, K. Ståhl and T. Vegge, *Chem. Phys. Lett.*, 2007, **441**, 255–260.
77 E. Lepinasse and B. Spinner, *Rev. Int. Froid*, 1994, **17**, 309–321.
78 T. D. Elmøe, R. Z. Sørensen, U. Quaade, C. H. Christensen, J. K. Nørskov and T. Johannessen, *Chem. Eng. Sci.*, 2006, **61**, 2618–2625.
79 T. Johannessen and R. Z. Sørensen, *TCE*, 2005, **773**, 30–33.
80 N. Maffei, L. Pelletier, J. P. Charland and A. McFarlan, *Fuel Cells*, 2007, **4**, 323–328.
81 E. Fontell, M. Jussila, J. B. Hansen, J. Pålsson, T. Kivisaari and J. U. Nielsen, Wärtsilä – Haldor Topsoe SOFC Test System, presented at SOFC-IX, 2005, Quebec, Canada, May 15–20, http://www.topsoefuelcell.com/tofc/PDF/Wartsila%20-%20Haldor%20Topsoe%20SOFC%20Test%20System.pdf.
82 http://www.amminex.net/.
83 T. H. Rod, A. Logadottir and J. K. Nørskov, *J. Chem. Phys.*, 2000, **112**, 5343.
84 F. Vitse, M. Cooper and G. G. Botte, *J. Power Sources*, 2005, **142**, 18–26.
85 N. Maffei, L. Pelletier, J. P. Charland and A. McFarlan, *J. Power Sources*, 2005, **140**, 264–267.
86 P. A. Chater, W. I. F. David, S. R. Johnson, P. P. Edwards and P. A. Anderson, *Chem. Commun.*, 2006, 2439.

 This journal is © The Royal Society of Chemistry 2008

Catalysis Letters Vol. 112, Nos. 1–2, November 2006 (© 2006)
DOI: 10.1007/s10562-006-0167-y

Promoted Ru on high-surface area graphite for efficient miniaturized production of hydrogen from ammonia

Rasmus Zink Sørensen,[a] Asbjørn Klerke,[a] Ulrich Quaade,[b] Søren Jensen,[c] Ole Hansen,[c] and Claus Hviid Christensen[a,*]

[a]*Center for Sustainable and Green Chemistry (CSG), Department of Chemistry, Technical University of Denmark, 2800 Kgs Lyngby, Denmark*
[b]*Center for Individual Nanoparticle Functionality (CINF), Department of Physics, Technical University of Denmark, 2800 Kgs Lyngby, Denmark*
[c]*MIC - Department of Micro and Nanotechnology, Technical University of Denmark, 2800 Kgs Lyngby, Denmark*

Received 3 August 2006; accepted 10 August 2006

Promoted Ru/C catalysts for decomposition of ammonia are incorporated into micro-fabricated reactors for the first time. With the reported preparation technique, the performance is increased more than two orders of magnitude compared to previously known micro-fabricated reactors for ammonia decomposition. The catalytic activities for production of hydrogen from ammonia are determined for different promoters and promoter levels on graphite supported ruthenium catalysts. The reactivity trends of the Ru/C catalysts promoted with Cs and Ba are in excellent agreement with those known from earlier studies of both ammonia synthesis and decomposition, and it is shown how proper promotion can facilitate ammonia decomposition at temperatures below 500 K.

KEY WORDS: ammonia decomposition; hydrogen production; ruthenium catalyst; promotion; graphite support; micro-fabricated reactors.

1. Introduction

Ammonia has gained significant interest as a hydrogen source for fuel cells [1–4]. Stored safely, ammonia can become a favorable energy carrier [5, 6], but for use in low temperature fuel cells it must be catalytically decomposed to the elements before it can be utilized in the fuel cell.

One perceived area where fuel cells could make great impact is for miniaturized systems such as as "lab-on-a-chip". Often, power supplies or batteries for small systems are very bulky compared to the system it supports. Thin fuel cells would be optimal for solving this problem, if the fuel could be delivered from an equally compact system.

Promoted Ru catalysts on porous graphitized carbon are generally recognized as the most active for decomposition of ammonia [7–10]. Due to the immense importance of industrial ammonia production for fertilizers, catalysts for the synthesis have been studied intensively over the last century [11, 12]. Decomposition of ammonia has mainly been studied to obtain detailed insight into the synthesis reaction, but in later years decomposition of ammonia has attracted attention as a possible route to hydrogen production. Of the elements, Ru is the most active catalyst for both processes at a wide range of conditions [13–17]. Interestingly, Ru is more optimal under ammonia decomposition conditions than under industrially relevant ammonia synthesis conditions [18]. The highest activities are measured using graphite as the support [7–10], but unfortunately, graphite is not stable under ammonia synthesis conditions, as the high hydrogen pressure causes methanation of the graphite support [19, 20]. Graphite is far more stable under optimal decomposition conditions, which are at low pressures. This makes graphite supported Ru highly interesting for efficient decomposition of ammonia, and indeed several studies show such catalysts to exhibit superior activities [7–10].

So far, it has not been possible to integrate significant amounts of porous graphitized carbon supports in micro-fabricated reactors, and thus the best miniaturized systems used supports which are less optimal for ammonia decomposition [3, 21].

The most common approach to achieve a high surface area in micro-fabricated reactors is to manufacture the reactor itself to have a high surface area, e.g. by anodisation or by introduction of various structural components into the reactor chamber (walls, pillars etc.) [22]. Some groups have deposited support layers by filling the reaction chamber with a thin slurry followed by drying and sintering to produce a porous ceramic support [23, 24], while others used more advanced deposition methods such as chemical vapor deposition [25] or flame spray deposition [26]. Recently, a sol–gel method for filling up the entire reactor chamber with porous support was presented [27, 28], but unfortunately

*To whom correspondence should be addressed.
E-mail: chc@kemi.dtu.dk

1011-372X/06/1100–0077/0 © 2006 Springer Science+Business Media, Inc.

this is not a feasible route for introducing graphite support into micro-fabricated reactors.

Here, a method for incorporation of a porous graphite support into micro-fabricated reactors is presented, and higher volumetric activities for ammonia decomposition than previously reported for similar micro-fabricated reactors are demonstrated. Furthermore, the micro-fabricated reactors are well suited for catalyst studies, since they can be kept isothermal under most reaction conditions and the gas flow stays laminar (plug flow behavior) over a large range of space velocities. This is used to investigate promotion of the Ru/C system with Cs and Ba, which are effective and carefully studied promoters for ammonia decomposition over Ru/C. The effects of driving the decomposition reaction close to equilibrium at relatively low temperatures are studied as well.

2. Experimental

The graphite support is prepared using an aqueous solution of commercial food grade sucrose (140 g/L) to fix finely ground Timrex HSAG300 high-surface area graphite in micro-fabricated silicon reactors of 3–4μL reactor volume. The reactors are produced using Deep Reactive Ion Etching as previously described [29, 30]. Reactors are produced with reaction chambers of 8 mm × 1.5 mm × 0.3 mm. To facilitate assembly of the setup, manifold connections are made through the silicon slab itself, the reactor slab being fixed against high temperature stable rubber o-rings on the gas handling system. The limited lateral heat conduction of the silicon slabs makes it possible to heat the catalyst-loaded reaction chamber while maintaining a low enough temperature of the o-rings to keep them from melting.

HSAG300 graphite is deposited in a number of steps: First, the micro-fabricated reaction chamber is filled with sucrose solution, which is then dried on a hot plate at 80 °C. Before the next step, sucrose deposited outside the reaction chamber is removed by polishing. The reaction chamber is then completely covered with finely ground HSAG300 and the open reactor is pyrolyzed at 250 °C for 1 h. This creates a highly porous carbon support, which binds sufficiently to the silicon to enable removal of excess carbon powder, and cleaning the surface of the silicon slab.

The ruthenium catalyst is deposited on the support by incipient wetness impregnation using a well defined total volume of Ru-nitrosylnitrate (8.1 wt% Ru) dosed from a 10 μL syringe. All samples are impregnated to contain 10 wt% Ru on the graphite support and dried at 80 °C.

Promotion is accomplished in the same way as the Ru impregnation. The precursors for Cs and Ba promotion are $CsNO_3$ and $Ba(CH_3COO)_2$, respectively. Both precursors are deposited as 0.5 M aqueous solutions, and the reactors are dried at 80 °C before the final cleaning of the silicon surface.

The micro-fabricated reactor is closed with a pyrex lid and sealed by anodic bonding. Bonding takes place at 320 °C with a voltage of 1 kV, and gives a completely gas-tight reactor. At the same time, the elevated temperature causes calcination of the catalyst. Thorough cleaning is very important for the success of the anodic bonding as individual atoms from one surface must migrate into the other during bonding. For this reason, anodic bonding is normally performed in clean-rooms only, but by taking care in the cleaning process bonding is possible in an ordinary lab even when the micro-fabricated reactor is loaded with the supported catalyst.

Surface area measurements of supports prepared by the described method show significant reduction in the surface area of the graphite support in the reactors compared to the starting material. BET areas are 322 m^2/g before treatment with sucrose and 167 m^2/g after the graphite is glued onto silicon with pyrolyzed sucrose. Most of this loss of surface area can be ascribed to mass increase due to the sucrose, which constitutes approximately 30–50% of the total mass. Still, the resulting surface area is comparable to what was reported for other supports in micro-fabricated reactors [26, 27].

All catalysts are tested in a specially build setup where the reactor is held in place and connected to the gas handling system by a clamp in one end, while the reaction chamber is heated by a silicon heating element placed over the chamber. The gas mixture is dosed to the reactor from a mass-flow controller, and the composition of the exit gas is measured by a microGC. Gasses are separated in two different columns: a plot U column designed for short hydrocarbons and volatile primary amines, and a molecular sieve column designed for noble gasses and gasses such as nitrogen, oxygen and hydrogen. The plot U column is used for detection of ammonia and is operated at 60 °C, while the molecular sieve column is used primarily for detection of hydrogen and nitrogen and is operated at 50 °C. Both columns are fitted with thermal conductivity detectors (TCD). The inlet gas consists of 20 mole% NH_3 and 5 mole% He in a carrier stream of Ar, where He acts as an internal standard in the microGC. Dilution of the NH_3 was chosen in order to avoid large changes in linear space velocity through the reactor at high conversions since this would influence the residence time in the reactor and thereby change the measured conversions.

3. Results and discussion

The use of micro-fabricated silicon reactors is limited by the number of porous support materials that it is possible to deposit into the reaction chamber. These supports are currently limited to Al_2O_3, $MgAl_2O_4$, and SiO_2 deposited using sol–gel synthesis and TiO_2 using flame spray deposition [23, 26–28]. So far, there have

been no reports on a method for deposition of porous carbon or graphite in micro-fabricated reactors. The only reported example of a carbon-based support material in a micro-fabricated reactor is by Schimpf *et al.* [31], who produced a carbon film in a micro-fabricated reactor by carbonization of a polymer solution. This gave a 0.27–6.22 μm thick layer of carbonized polymer on the reactor walls. No surface area was reported. Graphite-structured carbon materials are so far known to be the best supports for ammonia decomposition on ruthenium [7–10]. In ammonia synthesis, methanation of the carbon support is a challenge [20, 32]. However, the rate of methanation depends strongly on the hydrogen pressure which will always be much lower in a technical ammonia decomposition reactor than in a synthesis reactor. Rossetti *et al.* [33] found that the methanation rate is lowered significantly by graphitization of the carbon. Thus, HSAG is favorable as a support for Ru in ammonia decomposition.

Figure 1 shows a magnified view of a sealed micro-fabricated reactor prepared with graphite support using sucrose glue. The support is seen as a fairly evenly distributed porous black layer filling up about half the volume of the reaction chamber.

Compared to previous results using the same reactor type but with alumina support, graphite is clearly favorable. Figure 2 compares the previously reported data for Ba promoted Ru on Al_2O_3 with a similar catalyst on graphite support. The increase in activity is obvious, and corresponds well to what would be expected according to literature findings [34]. It is also seen that even without promotion, an otherwise similar

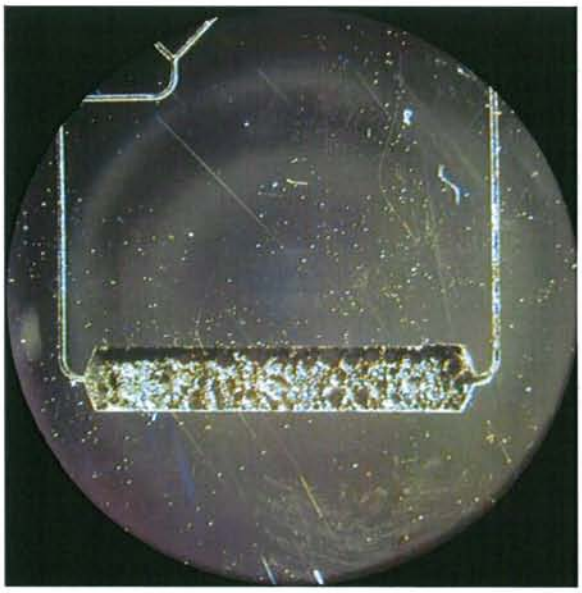

Figure 1. Micro-fabricated reactor prepared with graphite and sealed with a pyrex lid. The reactor chamber dimensions are 8 mm × 1.5 mm × 0.3 mm.

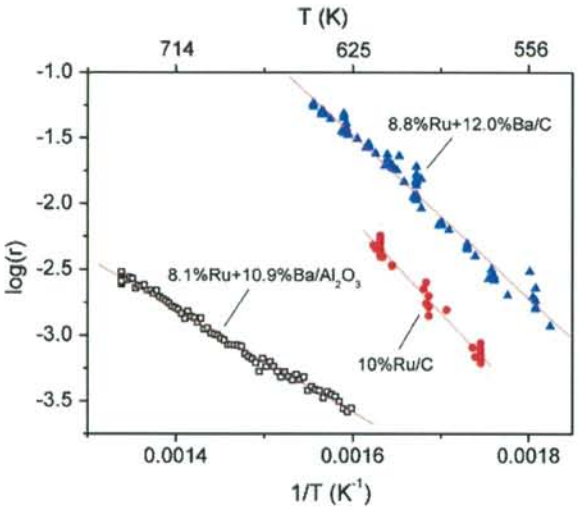

Figure 2. Activities of unpromoted and Ba promoted Ru/C catalysts compared to the Ru + Ba/Al_2O_3 catalyst reported in [21]. r is in $mol_{NH_3}/mol_{Ru}/s$.

Ru catalyst on graphite is far more active than the promoted Ru on Al_2O_3.

From literature [35–38], it would be expected, that promotion by Cs would give even higher activities than those obtained by Ba promoted Ru on graphite. Ba is thought to promote decomposition of ammonia by being present on the surface of Ru particles, where it acts as a structural promoter making more of the most active sites available for the rate-limiting N_2 dissociation [8], or as an electronic promoter [34, 39]. Additionally, TEM studies have shown Ba to be present as an oxide on the surface of small Ru crystals under low pressure ammonia synthesis conditions [40]. Furthermore, Ba stabilizes the active Ru particles and prevents agglomeration and sintering at temperatures above 500 °C [19]. Because the Ba species are present on the surface of the active ruthenium, the optimal amount of Ba promoter is relatively small, since it will cover active sites when the coverage increases. This is has been observed experimentally [35, 37]. Similarly there have been speculations about the mechanism for promotion by Cs [38, 41, 42] and it has in some cases been found to give increased activity compared with Ba promoted catalysts.

Thus, Ru/C catalysts were prepared both with Cs added in approximately the same amount as that used for Ba promotion, and also with about three times as much Cs.

These catalysts showed significant differences in activity. As seen in figure 3, the low Cs promotion gives significantly lower activity than the corresponding Ba promotion. This correspond well to what could be expected from the ammonia synthesis literature [38, 43], whereas the high Cs loading gives a dramatically higher activity than that achieved with the low Ba and Cs promoter loadings. Furthermore, the catalyst with high

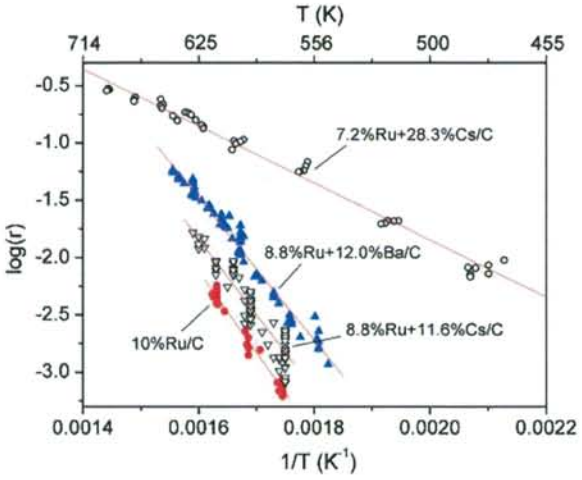

Figure 3. Activities of differently promoted Ru/C catalysts. The composition of each catalyst is given in the graph. r is in $mol_{NH_3}/mol_{Ru}/s$.

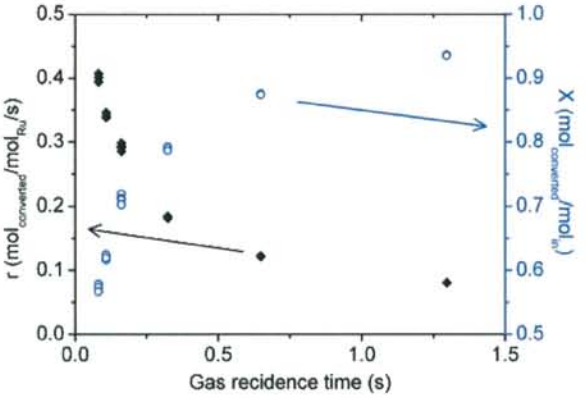

Figure 4. Comparison of rate and conversion as function of residence time at 694 K over a Ru + Cs/C catalyst with 7.2 wt% Ru and 28.3 wt% Cs.

Cs loading gave lower apparent activation energy than the other catalysts. This change means, that the lower the temperature, the higher is the relative effect of promotion, and even at 473 K the activity is as high as that of the Ba promoted catalyst at 590 K. This is particularly interesting for miniaturization, as lower operating temperature reduces heat losses and thereby enables a lower overall fuel consumption. Unfortunately, the equilibrium is shifted towards NH_3 for low temperatures giving to low equilibrium conversions at temperatures below 500 K. However, with the reported Cs promoted catalyst a large fraction of the ammonia can be decomposed at relatively low temperature while most of the remaining ammonia can then be decomposed in an even smaller hot zone reactor. In this way the reactor volume kept at high temperature can be reduced, saving considerable amounts of energy, and thus the volume needed for fuel storage will be smaller.

The primary concern when designing a micro–fabricated reactor for hydrogen production by ammonia decomposition is to achieve high conversion with the smallest possible amount of catalyst. The data in figure 4 shows that the overall rate of decomposition decreases when the system is pushed towards higher conversions. This can be attributed to a negative reaction order in H_2 and to a closer approach to equilibrium. For ammonia decomposition, these effects are not easily separable, and most likely they are both responsible for the observed apparent activation energies in figures 2 and 3 as these are measured at a constant gas flow that makes rate and conversion correlate.

For development of a small portable power supply the decreasing rate close to equilibrium is an adverse effect as the ultimate goal is full equilibrium conversion using the minimal amount of catalyst. One way of getting closer to this goal is to remove hydrogen continually e.g. through a Pd membrane. This has been done in larger systems but it demands a high pressure differential to get a useful flux through the membrane [44]. In micro-fabricated reactors, Ye *et al.* [45] have managed to integrate a 340 nm thin Pd film on a support of porous SiO_2. This Pd membrane allows diffusion of hydrogen with a flux of 0.112 mol m^{-2} h^{-1} and high selectivity (H_2/N_2 ratio of 44). Removing hydrogen through such a membrane would make it possible to maintain a high rate up to higher conversions and also enhance the fuel cell activity by providing pure hydrogen for the fuel cell.

4. Conclusions

Graphite supported catalysts for decomposition of ammonia is incorporated in a micro-fabricated reactor for the first time. Since graphite carrier gives the most active ruthenium catalysts for this reaction, its incorporation in the micro-fabricated reactors enable a significant increase in the activity per reactor volume. This is important for miniaturizing ammonia decomposition systems for hydrogen production. At the same time, high Cs promoter loading is shown to facilitate high ammonia decomposition rates at temperatures below 500 K.

Acknowledgments

The Danish National Research Foundation is sponsoring the Center for Sustainable and Green Chemistry and the Center for Individual Nanoparticle Functionality, the project is also supported by The Danish Council for Strategic Research (Project no. 2104-05-0016)

References

[1] T.V. Choudhary, C. Sivadinarayana and D.W. Goodman, Catal. Lett. 72 (2001) 197.
[2] T.V. Choudhary, C. Sivadinarayana and D.W. Goodman, Chem. Eng. J. 93 (2003) 69.

[3] J.C. Ganley, E.G. Seebauer and R.I. Masel, J. Power Sources 137 (2004) 53.
[4] J.C. Ganley, F.S. Thomas, E.G. Seebauer and R.I. Masel, Catal. Lett. 96 (2004) 117.
[5] R. Metkemeijer and P. Achard, Int. J. Hydrogen Energy 19 (1994) 535.
[6] C.H. Christensen, R.Z. Sørensen, T. Johannesen, U.J. Quaade, K. Honkala, T.D. Elmøe, R. Køhler and J.K. Nørskov, J. Mater. Chem. 15 (2005) 4106.
[7] W. Raróg, Z. Kowalczyk, J. Sentek, D. Skadanowski, D. Szmigiel and J. Zieliñski, Appl. Catal. A 208 (2001) 213.
[8] W. Raróg-Pilecka, E. Miśkiewicz, D. Szmigiel and Z. Kowalczyk, J. Catal. 231 (2005) 11.
[9] S.-F. Yin, B.Q. Xu, W.X. Zhu, C.F. Ng, X.P. Zhou and C.T. Au, Catal. Today 27 (2004) 93–95.
[10] S.-F. Yin, B.Q. Xu, X.P. Zhou and C.T. Au, Appl. Catal. A 277 (2004) 1.
[11] P.H. Emmett and J.T. Kummer, Ind. Eng. Chem. 35 (1943) 677.
[12] M. Bowker, Catal. Today 12 (1992) 153.
[13] Z. Kowalczyk, S. Jodzis and J. Sentek, Appl. Catal. A 138 (1996) 83.
[14] O. Hinrichsen, F. Rosowski, A. Hornung, M. Muhler and G. Ertl, J. Catal. 165 (1997) 33.
[15] M.C.J. Bradford, P.E. Fanning and M.A. Vannice, J. Catal. 172 (1997) 479.
[16] S.-F. Yin, B.Q. Xu, S.J. Wang, C.F. Ng and C.T. Au, Catal. Lett. 96 (2004) 113.
[17] S.-F. Yin, B.-Q. Xu, C.-F. Ng and C.-T. Au, Appl. Catal. B 48 (2004) 237.
[18] A. Boisen, S. Dahl, J.K. Nørskov and C.H. Christensen, J. Catal. 230 (2005) 309.
[19] Z. Kowalczyk, S. Jodzis, W. Raróg, J. Zielinñski and J. Pielaszek, Appl. Catal. A 173 (1998) 153.
[20] L. Forni, D. Molinari, I. Rossetti and N. Pernicone, Appl. Catal. A 185 (1999) 269.
[21] R.Z. Sørensen, L.J.E. Nielsen, S. Jensen, O. Hansen, T. Johannesen, U. Quaade and C.H. Christensen, Catal. Commun. 6 (2005) 229.
[22] G. Kolb and V. Hessel, Chem. Eng. J. 98 (2004) 1.
[23] K. Haas-Santo, M. Fichtner and K. Schubert, Appl. Catal. A 220 (2001) 79.
[24] L. Kiwi-Minsker and A. Renken, Catal. Today 110 (2005) 2.
[25] H.Y. Chen, L. Chen, Y. Lu, Q. Hong, H.C. Chua, S.B. Tang and J. Lin, Catal. Today 96 (2004) 161.
[26] U. Thybo, S. Jensen, S. Johansen, J. Johannessen, T. Hansen and O. Quaade, Catal J. 223 (2004) 271.
[27] O. Younes-Metzler, J. Svagin, S. Jensen, C.H. Christensen O. Hansen and U. Quaade, Appl. Catal. A. 284 (2005) 5.
[28] H.A. Hansen, J.L. Olsen, S. Jensen, O. Hansen and U. Quaade, Catal. Commun. 7 (2006) 272.
[29] U. Quaade, S. Jensen and O. Hansen, Rev. Sci. Instrum. 75 (2004) 3345.
[30] U. Quaade, S. Jensen and O. Hansen, J. Appl. Phys. 97 (2005) 044906.
[31] S. Schimpf, M. Bron and P. Claus, Chem. Eng. J. 101 (2004) 11.
[32] I. Rossetti, N. Pernicone and L. Forni, Appl. Catal. A 208 (2001) 271.
[33] I. Rossetti, N. Pernicone and L. Forni, Catal. Today 219 (2005) 102–103.
[34] T.W. Hansen, P.L. Hansen, S. Dahl and C.J.H. Jacobsen, Catal. Lett. 84 (2002) 7.
[35] S.E. Siporin, R.J. Davis, W. Raróg-Pilecka, D. Szmigiel and Z. Kowalczyk, Catal. Lett. 93 (2004) 61.
[36] W. Raróg-Pilecka, D. Szmigeel, Z. Kowalczyk, S. Jodis J. Zielinski, J. Catal. 218 (2003) 465.
[37] D. Szmigiel, W. Raróg-Pilecka, E. Miśkiewicz, Z. Kaszkur and Z. Kowalczyk, Appl. Catal. A 264 (2004) 59.
[38] Z. Kowalczyk, M. Krukowski, W. Raróg-Pilecka, D. Szmigiel and J. Zielinski, Appl. Catal. A 248 (2003) 67.
[39] Z. Kowalczyk, S. Jodzis, W. Raróg, J. Zieliński, J. Pielaszek and A. Presz, Appl. Catal. A 184 (1999) 95.
[40] T.W. Hansen, J.B. Wagner, P.L. Hansen, S. Dahl, H. Topsøe and C.J.H. Jacobsen, Science 294 (2001) 1508.
[41] W. Raróg, Z. Kowalczyk, J. Sentek, D. Skadanowski J. Zieliński, Catal. Lett. 68 (2000) 163.
[42] W. Raróg-Pilecka, E. Miśkięwicz, M. Matyszek, Z. Kaszkur L. Kepiński and Z. Kowalczyk, J. Catal. 237 (2006) 207.
[43] C. Liang, Z. Wei, Q. Xin and C. Li, Appl. Catal. A 208 (2001) 193.
[44] J.D. Holladay, Y. Wang and E. Jones, Chem. Rev. 104 (2004) 4767.
[45] S.-Y. Ye, S. Tanaka, M. Esashi, S. Hamakawa, T. Hanaoka and F. Mizukami, J. Micromech. Microeng. 15 (2005) 2011.

Chapter 18: Indirect hydrogen storage in metal ammines

Tejs Vegge*, Rasmus Zink Sørensen, Asbjørn Klerke, Jens Strabo Hummelshøj, Tue Johannessen, Jens K. Nørskov and Claus Hviid Christensen

*) Materials Research Department, Risoe National Laboratory

NanoDTU, Technical University of Denmark

Frederiksborgvej 399, DK-4000 Roskilde, Denmark

Email: tejs.vegge@risoe.dk

18.1 Introduction

This chapter is focused on the potential of indirect hydrogen storage by use of ammonia stored in metal ammines. The first section describes ammonia as a potential hydrogen storage medium, ammonia production and infrastructure, safety concerns and the energy costs involved in indirect storage.

Section 18.3 discusses the storage of ammonia in solid form using $MgCl_2$ as the model carrier material. The improved safety of ammonia stored in metal ammines, methods for preparation and powder compaction, low materials cost and easy scale-up are covered. This section is followed by a description of thermodynamic properties of different metal ammines, e.g. van't Hoff plots, desorption properties, reversibility and reloading, and selection of specific ammines by weighting parameters like safety and desorption temperature.

Section 18.5 deals with the design of novel metal ammine systems and focuses on the design of superior metal ammines by closely integrating experimental and calculational work. From a detailed

understanding of structure and stability, porosity and particle size, desorption and diffusion, and alloy formation, it is possible to engineer these materials on the nano, micro, and macro scale.

The last section (18.6) is focused on the commercial potential and perspectives of using metal ammines in connection with e.g. PEM and Solid Oxide Fuel Cells as well as Selective Catalytic Reduction (SCR) -DeNOx in the transport sector, and it includes comments on the global availability and low cost of the carrier salts. This section also provides the authors' perspectives on future trends and challenges in metal ammine research, along with links to the interested reader for further information on key articles, companies and web sites.

18.2 Indirect hydrogen storage in ammonia

The indirect storage of hydrogen in ammonia is a promising concept for storage and transportation of hydrogen. The use of liquid ammonia as an indirect hydrogen carrier is interesting because liquid ammonia meets the DOE 2015 system targets for hydrogen storage[1] with a gravimetric hydrogen density of 17.8 wt.% and a volumetric hydrogen density of 0.122 kg H/l at -33 °C and 0.105 kg H/l at 25 °C (Eggmann, 2001). Furthermore, the technological needs for production, storage and transportation of ammonia are well known and ammonia decomposition is viable, although not optimized for hydrogen production (Appl, 2007). In the following section, ammonia synthesis, transportation and decomposition will be described and safety issues of liquid ammonia will be discussed.

Synthesis of ammonia in the Haber-Bosch process is one of the best studied catalytic processes. The process was developed by Fritz Haber and Carl Bosch and patented in 1910 (Haber 1910); Haber was awarded the Nobel Prize in chemistry in 1918 for this work. Today, almost all ammonia production is

[1] http://www1.eere.energy.gov/hydrogenandfuelcells/mission.html#storage

based on the Haber-Bosch process, and it is one of the largest chemical processes in the world with a yearly production of approximately 120 million tons.[2] The main use of ammonia is as fertilizer for agriculture, which constitutes 80 % of the world production.

Ammonia synthesis is an exothermic process following the reaction scheme;

$$N_2(g) + 3H_2(g) \rightarrow 2NH_3(g) \qquad \Delta_r H_{298K} = -45.6 \text{ kJ/mol } NH_3 \quad (18.1)$$

While the reaction is exothermic, it is limited by reaction kinetics and will therefore not proceed without a catalyst. The catalyst is normally an iron catalyst; alternatively a supported ruthenium catalyst can be used, but the higher price of ruthenium compared to iron limits the use of the supported ruthenium catalyst (Maxwell, 2005).

The reaction conditions for the synthesis using the iron catalyst are typically at a pressure of 200 bars and an inlet temperature of 300 °C which, due to the exothermic reaction, increases to an outlet temperature of 450 °C (Appl, 2007).

The high reaction pressure is a direct result of the 'Principle of Le Chatelier', which states that 'A system at equilibrium, when subjected to a disturbance, responds in a way that tends to minimize the effect of the disturbance.' A compression is a disturbance of the equilibrium and a way to minimize the pressure increase is to reduce the total number of molecules in the gas phase (Atkins and Paula, 2002). The reaction temperature is thus a compromise between keeping a sufficient temperature for the iron catalyst to be active and keeping the equilibrium towards the products in the exothermic reaction. After the reaction, the gas has an ammonia content of 15 %, which is isolated from the reactants by condensation using the higher condensation temperature of ammonia (Appl, 2007). The unreacted hydrogen and nitrogen is then recycled. The energy cost of ammonia production with an iron catalyst is

[2] IFA – International fertilizer Industry Association, World Ammonia Statistics (2005)

about 28 GJ/t, corresponding to 75 % efficiency (theoretic limit: 20.9 GJ/t). The manufacturing cost of ammonia is mainly the price of natural gas which constitutes almost 70 % of the total cost (Eggmann, 2001). An alternative to the natural gas route is electrolysis of water at an expected energy cost of 35-40 GJ/t (Grundt and Christiansen, 1982).

For the ammonia synthesis to be sustainable, the hydrogen must be supplied from renewable resources. The problem of supplying sustainable hydrogen is a general challenge for the potential transition into a hydrogen economy. Initially, ammonia could be produced from natural gas where the CO_2 is segregated and sequestered on site.

Storing and transporting ammonia is mainly done in one of two ways. The first method is storing it in pressurised vessels at 16-25 bars, obtained by applying an over-pressure of inert gas. At ambient temperature, these vessels can contain up to 1500 t of ammonia (spherical diameter of 20-22 m). The second method involves storage in isolated tanks at the boiling point of ammonia (-33 °C) and ambient pressure; these tanks contain up to 50 000 t of ammonia (Appl, 2007). The pressure vessels are normally used for localized storage of ammonia, especially if the ammonia is transported to the storage facility under pressure by rail or truck. Pressurised storage would also be used for liquid ammonia as a transportation fuel. The insulated storage tanks are used for ammonia production sites, where the ammonia is condensed into a liquid and the tanks are cooled by the evaporating ammonia; the evaporated ammonia is condensed and pumped back. The insulated tanks would be the backbone of ammonia transportation and storage due to their lower cost and greater capacity.

For transportation of large amounts of ammonia over land, pipelines are the cheapest alternative in terms of price (see Figure 18.1). The high construction price of pipelines makes transportation by rail an alternative if smaller amounts of ammonia need to be transported (Appl, 2007).

The idea of using liquid ammonia as energy carrier originated in 1933, when Norwegian Hydro had an experimental car using anhydrous ammonia as the fuel for an internal combustion engine (Norsk Hydro, 1997).

In the 50's and 60's, different fuel cell systems were developed to run on aqueous solutions of ammonia. Part of the argument for choosing ammonia as an alternative energy carrier was the ability to transport and store ammonia (Young, 1963), which is otherwise one of the biggest challenges facing hydrogen storage materials.

For use in some types of fuel cells, the indirect storage of hydrogen in ammonia requires an efficient decomposition of ammonia with high conversion and low energy cost. The industrial catalyst for ammonia decomposition is nickel supported on alumina. The reaction is carried out at a temperature of 400-500 °C; the high temperature is necessary to ensure a high equilibrium conversion and thereby reduce the loss of unconverted ammonia. To remove the ammonia residue in the hydrogen, an ammonia absorber is needed, because ammonia poisons PEM fuel cells (Rajalashmi, *et al.*, 2003; Halsied, *et al.*, 2006).

During the last few years, efforts to optimize ammonia decomposition have led to the development of alternative catalysts, the most promising being caesium and barium promoted ruthenium catalyst supported on graphite (see Section 18.6.3) (Raróg-Pilecka, *et al.*, 2003; Yin, *et al.*, 2004; Boisen, *et al.*, 2005).

A limitation to the use of ammonia is the acute toxicity at large concentrations (>5000 ppm), which limits the use of liquid ammonia to stationary power supply. For ammonia to play a future role as an energy carrier for mobile applications, a safe, inexpensive and reliable storage system is needed (Thomas and Parks, 2006). The main safety problem in the transport sector is that, in case of an

accident, there should be no immediate risk of poisoning due to an ammonia spill. Acute poisoning is a great concern when using liquid ammonia, because a ruptured pressurized tank could lead to rapid ammonia release and suffocation. Furthermore, a pressurised tank leaking ammonia would make rescue efforts difficult and hazardous. A possible solution to these problems is solid storage of ammonia in metal ammines (Christensen, *et al.*, 2005).

18.3 Compact storage in solid metal ammine materials

Recent research has shown that solid storage of ammonia can be done efficiently in metal ammines. This is exemplified in this section by use of $Mg(NH_3)_6Cl_2$ as the primary reversible indirect hydrogen storage material. The section will discuss the preparation of $Mg(NH_3)_6Cl_2$ from $MgCl_2$ and gaseous NH_3, and the possibility of releasing ammonia from $Mg(NH_3)_6Cl_2$ is demonstrated using temperature programmed desorption (TPD), to illustrate that a main limitation to the release of ammonia is heat transfer in the salt. Methods to compact $Mg(NH_3)_6Cl_2$ for safe handling and easy use in mobile applications are also covered. Finally, the increased safety of ammonia stored in metal ammines is discussed.

The lifecycle of a metal ammine is illustrated in Figure 18.2. Here, the ammonia gas, which is produced from hydrogen and nitrogen, reacts with the dry salt to form the metal ammine. The formation of a metal ammine is an exothermic process and the reaction heat varies with the material and degree of saturation. After saturation, the ammonia can be released by heating the metal ammine; the energy required for desorption is the same as released during absorption. The desorbed ammonia can then be used in a fuel cell capable of using ammonia directly, e.g. SOFC, or be decomposed over a catalyst to hydrogen and nitrogen. The produced hydrogen can then be supplied to PEMFC or other types of fuel cells (see Section 18.6.2).

The absorption of ammonia into $MgCl_2$ proceeds in three steps as shown in reactions 18.2-4, each with a different enthalpy of formation. The formation of $Mg(NH_3)_6Cl_2$ from $MgCl_2$ and NH_3 releases 64 kJ/mol NH_3. This means that efficient heat removal during the ammine formation reaction is important to get fast ammonia absorption.

For magnesium chloride, the absorption of ammonia proceeds in three steps (Lepinasse and Spinner, 1994):

$$MgCl_2 + NH_3 \rightarrow Mg(NH_3)Cl_2 \qquad \Delta_f H = -87.0 \text{ kJ/mol } NH_3 \qquad (18.2)$$

$$Mg(NH_3)Cl_2 + NH_3 \rightarrow Mg(NH_3)_2Cl_2 \qquad \Delta_f H = -74.9 \text{ kJ/mol } NH_3 \qquad (18.3)$$

$$Mg(NH_3)_2Cl_2 + 4NH_3 \rightarrow Mg(NH_3)_6Cl_2 \qquad \Delta_f H = -55.7 \text{ kJ/mol } NH_3 \qquad (18.4)$$

The preparation of $Mg(NH_3)_6Cl_2$ on a laboratory scale is done in a stainless steel reactor designed to withstand the pressure of ammonia. The reactor is supplied with dry ammonia gas at pressures from 1 to 5 bars. The elevated pressure increases the rate of absorption, due to an increase in the pressure difference between equilibrium and applied pressure.

The absorption of ammonia into $MgCl_2$ gradually expands the crystal structure, resulting in a lowering of the density from 2.32 g/cm^3 for $MgCl_2$ to 1.25 g/cm^3 for $Mg(NH_3)_6Cl_2$; this comes from ammonia coordinating to the magnesium ion and thereby expanding the lattice constant of the crystal. This can also be seen as an increase in volume for one mole of $MgCl_2$ from 41 cm^3 to 158 cm^3 as it is saturated with ammonia (Pietsch, 1939), which can occur without decrepitation. The increase in volume is

important to take into account during reactor design, especially for a batch reactor, as the expanding salt could cause the reactor to rupture.

The ammonia storage capacity of saturated $Mg(NH_3)_6Cl_2$ is 51.8 wt.%, corresponding to a gravimetric hydrogen density of 9.19 wt.% and a volume density of hydrogen calculated from the crystal density of 115 g/L. The volumetric density is close to that of liquid ammonia at -33 °C. The hydrogen storage capacity of the material is also above the DOE 2015 system targets for hydrogen storage on both gravimetric and volumetric scale.

The production of anhydrous $MgCl_2$ on an industrial scale is well known as an intermediate product in the production of magnesium metal from electrolysis of molten $MgCl_2$. The pure $MgCl_2$ is produced by either chlorination of MgO or $MgCO_3$ in the presence of carbon or CO, or by dehydrogenation of brines with high magnesium chloride content. The brine can be treated in several ways depending on the specific chemical composition (Amundsen et al., 2003). An interesting process is the Queensland Metal Corp. process developed in Australia, where Magnesite ($MgCO_3$) is dissolved in hydrochloric acid and mixed with glycol and vacuum distilled. The resulting product is treated with anhydrous ammonia to form $Mg(NH_3)_6Cl_2$. The $Mg(NH_3)_6Cl_2$ is then washed with methanol saturated with ammonia and dried at a maximum of 120 °C to give dry $Mg(NH_3)_6Cl_2$ (Amundsen et al., 2003).

The obvious safety advantage of storing ammonia in $Mg(NH_3)_6Cl_2$ is that the vapour pressure is only 2 mbar at room temperature, compared to the ~8 bars for liquid ammonia, making $Mg(NH_3)_6Cl_2$ safe to use in mobile applications. This means that $Mg(NH_3)_6Cl_2$ can be handled with minimal safety precautions at ambient temperature, and only a weak odour of ammonia can be detected. The characteristic odour of ammonia is easily detected in concentrations below 20 ppm. At the same time,

$Mg(NH_3)_6Cl_2$ is not flammable or explosive in air, which is otherwise a general problem for energy storage materials.

Furthermore, the handling of a solid is more robust and safer than handling a toxic liquid under pressure. The added safety comes with a price of higher weight, although this is not a problem for small tanks, because the weight is compensated for by the reduced weight of the storage tank compared to liquid ammonia. A secondary cost is that of desorbing ammonia by heating $Mg(NH_3)_6Cl_2$. The temperature needed for desorption can be investigated with temperature programmed desorption (TPD), and repeated TPD measurements can be used to demonstrate the reversibility of the absorption/desorption process.

Two TPD measurements of $Mg(NH_3)_6Cl_2$ can be seen in Figure 18.3; the two runs are performed on the same sample to demonstrate that the process is reversible. The figure also shows a dense tablet before and after desorption with corresponding masses to show that the material retains its macroscopic shape after desorbing half of the total mass.

When desorption of ammonia starts, the rate of desorption increases exponentially with temperature (see Figure 18.3). The exponential increase stops one third of the way towards the peak maximum, due to the development of a heat gradient in the sample. The gradient develops because of the endothermic desorption, and makes heat transfer a main limitation to desorption. The heat transfer limitation is mainly because $Mg(NH_3)_6Cl_2$ is a poor heat conductor. This means that the gas has to do much of the heat transfer and since the heat conductivity of a gas is low, heat transfer is limiting, especially if fast desorption is needed (Sørensen et al., 2007).

For use in an ammonia mediated hydrogen economy, $Mg(NH_3)_6Cl_2$ needs to be compacted. This is to minimize the space required to store the salt and to make handling easy. At the same time, the compaction should not interfere with the desorption kinetics of ammonia. To investigate the desorption from dense $Mg(NH_3)_6Cl_2$, a sample of 1g was pressed to a tablet at 4 tons (see Figure 18.3). The tablet was then used for measurements of the desorption rate by TPD. The measurements show that the tablet has essentially the same desorption kinetics as the powder. This means that even after the compaction into a tablet, the ammonia release is controllable and fast (Christensen et al., 2005). To determine how much $Mg(NH_3)_6Cl_2$ can be compacted, the volume and weight of the tablet is measured and the results show that the tablet has a density of 95 % of the crystal density; hence close to the theoretical storage limit.

Due to the development of an internal pore structure during ammonia desorption (see Section 18.5), ammonia is easily released from even large blocks with this level of compaction. This makes indirect hydrogen storage in $Mg(NH_3)_6Cl_2$ favourable based on weight and volume compared to other hydrogen storage technologies. Figure 18.4 shows a comparison of six modes of hydrogen storage based on available literature data for realisable reversible hydrogen capacities. Only data for the storage materials are used, while weight and volume of the necessary containers are not taken into account. After desorption of ammonia, the remaining $MgCl_2$ is hygroscopic and should therefore be kept dry. If the sample absorbs water it will gradually form the stable $Mg(H_2O)_6Cl_2$ which can be converted to dry $MgCl_2$, but the water interaction is so strong that residual water (~1 %) can not be forced out by heating. Furthermore, since $Mg(NH_3)_6Cl_2$ requires a rather high temperature for desorption of the last ammonia molecule, it is interesting to investigate other metal ammines to analyze if they have better physical and chemical properties for specific applications.

18.4 Selecting metal ammine storage materials

18.4.1 Coordination complexes: a well known class of materials

Metal ammines for indirect storage of hydrogen are selected from the large group of complexes ammonia forms with different metal salts. The formation and stabilities of these complexes have been studied in detail in the early chemical literature, in order to understand the nature of bonds between ligands and central metal atoms, and information therefore exists on the ability of a large number of inorganic salts to form ammine complexes (Lepinasse and Spinner, 1994; Biltz, 1923). In the complex, ammonia coordinates to the central metal cation by donating both electrons from its lone-pair to form the ligand bond (Cotton et al., 1995); an example of such an ammine complex is given in Figure 18.5. Complex formation exists both in solution and in the solid state, but for use as indirect hydrogen storage media, only the solid metal ammines are of interest. When the materials are heated, ammonia is released in a solid-gas reaction without formation of a liquid phase. These transitions have previously been examined for use in refrigeration (Lepinasse and Spinner, 1994), where the difference in equilibrium vapour pressure of ammonia from one metal ammine complex to one with a different composition (see Table 18.1) is used to cool the reactor from which ammonia is desorbing; by having one salt which desorbs ammonia at low temperature while another salt absorbs ammonia at the same pressure but at a higher temperature. By heating the absorber unit, the vapour pressure over this metal ammine will rise, making the process run in the reverse direction. To make such a system technically interesting, the complex formation and decomposition must be fully reversible, and thus the

reversibility of these solid-gas reactions has been studied for this purpose (Lepinasse and Spinner, 1994; Goetz et al., 1997).

The stable vapour pressure of ammonia over different metal salts at a given temperature varies by several orders of magnitude (see Table 18.1). It is therefore important to select metal ammines for hydrogen storage intelligently. The requirements for such a storage system are quite specific, so the same metal ammine may not be optimal for all applications.

18.4.2 Safe storage

From the viewpoint of safety during storage, the optimal metal ammine must have a vapour pressure of ammonia below 1 bar at ambient temperatures, so that rupture of a storage vessel will lead to a minimal release of ammonia to the surroundings. This ensures that ammonia will not flow due to pressure differences when the container is opened (by accident or intent), but only be released by diffusion, which is a comparatively slow process. For increased safety and ease of handling, metal ammines can be chosen with vapour pressures low enough to allow handling outside of closed containers without compromising worker safety, see Table 18.1. As one example, $Mg(NH_3)_6Cl_2$ has roughly the same ammonia vapour pressure at room temperature as a solution of ammonia in water sold as cleaning agent in many supermarkets, i.e. 2 mbar.

18.4.3 Thermal release of ammonia

To release ammonia from metal ammine complexes, thermal energy must be supplied analogous to the release of hydrogen from metal hydrides. For optimal storage of energy in hydrogen storage materials,

an important aspect is that hydrogen, or in the indirect case ammonia, should be released with the input of the minimal amount of energy. In an energy supplying unit, the energy for thermal release must in some way come from the unit itself. This makes the optimal metal ammine one which releases ammonia at the desired pressure at a low temperature, or with the consumption of as little energy input as possible. Preferably, the energy is supplied by waste heat from a fuel cell, and the required temperature should therefore be lower than the operating temperature of the fuel cell. Temperature, ammonia pressure and safety are closely related, as the energy input required to release the ammonia also determines the vapour pressure at a given temperature.

Most metal ammines desorb ammonia in a number of steps with different thermodynamic properties, where equatorial ligands tend to desorb before the apical (see Figure 18.5). This means that the temperature necessary to achieve the desired ammonia pressure over the initial metal ammine is not sufficient to maintain this pressure when an ammine with a lower coordination number remains after partial desorption of the coordinated ammonia. In the ideal case, all ammonia is released in a one-step process at a single temperature as is the case for $Ba(NH_3)_8Cl_2$ (Biltz, 1923); alternatively, the smallest possible difference in enthalpy, ΔH, from the first desorption to the last is favourable. In this respect, $Mn(NH_3)_6Cl_2$ is unfavourable, as $Mn(NH_3)_6Cl_2$ has 1 bar ammonia pressure at 80 °C, while the last stable structure $Mn(NH_3)Cl_2$ reaches 1 bar ammonia pressure at 354 °C (Biltz, 1923). $Sr(NH_3)_8Cl_2$ is closer to the goal, as $Sr(NH_3)_8Cl_2$ has 1 bar ammonia pressure at 35.3 °C while the last stable structure $Sr(NH_3)Cl_2$ reaches 1 bar ammonia pressure at only 85.2 °C (Biltz, 1923).

18.4.4 Trends in metal ammine stabilities

Possible configurations of base salts for metal ammines are numerous. All metal ions can form complexes with ammonia as ligand, and these complex ions can form salts with a large number of possible anions. In principle, nearly all metal salts can form ammines giving hundreds of possible combinations. For indirect hydrogen storage applications, not all salts are equally practical and the challenge is to find a salt or salts, which gives the Pareto optimal compromise (Pareto, 1971) between the different parameters presented in this section. Van't Hoff plots are a powerful tool to compare the ammonia ab-/desorption properties of metal ammines. However, the number of possible candidates is so large, that a graph showing them all has limited value in printed form. It is possible to identify the lines with the desired equilibrium for the application at hand and Figure 18.6 shows the equilibrium lines for the stable ammines of 30 base salts. In the figure, the lines for $Mg(NH_3)_xCl_2$ which were discussed in Section 18.3 are highlighted. To make the comparison of stabilities more clear, values for ΔH for the stable complexes for coordination of ammonia to the 30 inorganic salts presented in Figure 18.6 are listed in Table 18.1.

The entropy change, ΔS, for the release of ammonia from a metal ammine is in the range of 220-240 J/mol K (Lepinasse et al., 1994). For a number of the salts, ΔS is not known, and in these cases 230 J/mol K has been used for the calculation of vapour pressures. ΔS for the desorption of hydrogen from direct hydrogen storage materials is in the range 80-160 J/mol K (Bonnetot et al., 1980, Kapischke et al., 1998, Srivastava et al., 1999). This has the consequence that if we consider a metal ammine and a hydride with the same enthalpy of formation, the vapour pressure over the ammine will be much higher (the van't Hoff plot is shifted to higher pressures). In other words, if an ammine and a hydride have the same vapour pressure at a given temperature, the ammine has the higher enthalpy of formation and

hence the vapour pressure over the ammine varies much more with temperature than that over the hydride. High variation of pressure with temperature is favourable, since it minimizes the necessary temperature change to go from safe storage pressure to delivery pressure. On the other hand, more energy must be supplied when the enthalpy is high, but in this respect it should be noted that each mole of ammonia releases 1.5 moles of hydrogen when decomposed, and thus the enthalpy of formation of an ammine can be 1.5 times that of a corresponding hydride to give the same desorption energy per mole hydrogen.

While the entropy for release of ammonia from a metal ammine is virtually independent of the choice of base salt, the enthalpies vary significantly. It is generally observed that for each metal, ammines of iodide are more stable than ammines of bromide, which are again more stable than ammines of chloride (Biltz, 1923). No ammines of fluoride are shown, as they are not very well examined, but existing data indicates that they fit this trend and are less stable than the ammines of chlorides (Patil and Secco, 1972). Ammines of fluoride also have the significant drawback as indirect hydrogen storage materials that the relevant salts do not take up ammonia directly from either the gas or liquid phase. This effect is caused by the crystal bonds in the pure metal fluorides being so strong that combined ammonia coordination and crystal expansion is not a favourable reaction (Biltz and Rahlfs, 1927). Ammines of a number of fluorides have been synthesized by more complex routes (Patil and Secco, 1972), but these will probably not be viable for energy storage as the coordination is not directly reversible. A number of sulphates of transition metals have also been found to form metal ammines, while the alkali and alkaline earth metal sulphates do not coordinate ammonia at sufficiently high temperatures (Ephraim, 1926). The thermodynamics of decomposition of metal ammine sulphates is not well described in the literature and has thus been left out of the comparisons. The trend for metal ions is less clear than for the anions, but it is evident that for the halides of the alkaline earth metals, Ba complexes are less stable

than Sr and Ca complexes which are nearly equally stable, while Mg complexes are significantly more stable (Biltz, 1923), indicating a correlation with the size of the cation. For ammines of halides of divalent transition metals there is a trend for Mn through Ni, where ammines of Ni(II) halides are most stable, and ammines of Co(II), Fe(II) and Mn(II) halides are progressively less stable (Biltz, 1923).

18.4.5 Weight, volume and price

Another important aspect concerning the selection of the optimal metal ammine material is the hydrogen density, both gravimetrically and volumetrically. The gravimetric hydrogen density is of course determined by the number of ammonia molecules coordinated to each metal atom relative to the combined masses of the central metal ion, the anion(s) and the ligands (viz. NH_3). High coordination numbers favour the heavier alkaline earth metals which form stable ammines with up to 8 ammonia molecules per central metal atom ($Ca(NH_3)_8Cl_2$ holds 9.78 wt% hydrogen), while the lightest metal salts would be light alkali metal fluorides and chlorides where e.g. $Li(NH_3)_3Cl$ has a gravimetric hydrogen content of 9.70 wt%.

For the metal ammine also to have a high volumetric hydrogen density, it must have both a high gravimetric hydrogen density, a high crystal density and be compactable to a density close to the crystal density without loosing its ability to release ammonia sufficiently fast. The factors governing this will be discussed in detail in the next section.

The final and, in many cases probably, decisive parameters in determining which metal ammine is optimal for an application will be the price and availability of the metal salt, i.e. NaCl, $MgCl_2$ or $CaCl_2$ are cheap and abundant, while BeI_2 or $CoBr_2$ would be much harder to come by Sigma-Aldrich[3].

18.5 From nano to macro scale design of metal ammines

The important properties of the metal ammines when used as materials for indirect hydrogen storage can be understood and explained at the atomic scale. In this section, an atomic scale model of the sample system $Mg(NH_3)_6Cl_2$ based on Density Functional Theory (DFT) calculations shows how atomic structures, energies and dynamics can be connected to macro scale properties such as shape, uptake and decomposition rates, porosity and reaction enthalpies. The model is based on experimentally observed structures (Hummelshøj et al. 2006, Leineweber, Friedriszik and Jacobs 1999, Leineweber, Jacobs and Ehrenberg 2000, Olovsson 1965, Partin and O'Keeffe 1991) and it is expected to be applicable to other metal ammines. A detailed understanding of the systems at the atomic scale is a prerequisite for the design of new and better materials.

18.5.1 Atomic structures and ab-/desorption pathways

From the atomic structures we can understand why the ab- and desorption processes are fast, why they are easily reversible and how an observed self porosity may arise. DFT calculations, using the DACAPO planewave basis set implementation (Hammer, Hansen and Nørskov, 1999), confirm the stability of the experimentally proposed structures, as seen in Figure 18.7. To confirm that a structure is

[3] http://www.sigmaaldrich.com

in fact stable, one compares the energy with the energies of the other phases, e.g., the monoamine phase is stable since $E_{Mg(NH_3)Cl_2} < ½ (E_{Mg(NH_3)_2Cl_2} + E_{MgCl_2})$.

In Figure 18.7, it is seen that the uptake of ammonia in $MgCl_2$ can happen continuously if the $MgCl_2$ layers (a) are cleaved into chains when the first ammonia molecules are introduced to form $Mg(NH_3)Cl_2$ (b). These double octahedral chains are then cleaved once more to form octahedral chains of the $Mg(NH_3)_2Cl_2$ salt (c). When the last four ammonia molecules are introduced, the chains are stretched and rearranged to produce the K_2PtCl_6 structure of $Mg(NH_3)_6Cl_2$ (Olovsson, 1965) (d); see also Figure 18.5. For the desorption process the direction can simply be reversed.

The material is known to retain its macroscopic shape during the ab-/desorption of ammonia (Figure 18.3), which implies an ab-/desorption mechanism where ammonia diffuses into the bulk and takes the system stepwise through (a)→(b)→(c)→(d) in Figure 18.7 and vice versa. For this to occur readily, diffusion of ammonia in all the structures would need to be fast enough not to become rate limiting.

18.5.2 Diffusion and porosity

Recent DFT calculations yield activation energies for NH_3 diffusion in $Mg(NH_3)_2Cl_2$ and $Mg(NH_3)Cl_2$ phases, which are significantly higher than the desorption enthalpies (Voss et al., 2007). These findings could support an alternative mechanism, in which chains of the ammine salt are ripped of the surface to facilitate the ab-/desorption of ammonia as shown in Figure 18.8. A possible explanation is that the energy cost per Mg for releasing a chain from the bulk structure is lower than the barrier for ammonia diffusion in all but the $Mg(NH_3)_6Cl_2$ structure. However, the free chains involved in this mechanism

are expected to rearrange readily into the final structures and thus both absorption and desorption should be very fast and reversible.

An analysis of the calculated unit cell dimensions during desorption shows the lattice contracts as ammonia is removed. Given the macroscopic shape is retained; this is only possible if voids or a porosity develops simultaneously. In a macroscopic system, the salt is polycrystalline and the desorption process can be followed using, e.g. small-angle X-ray scattering (SAXS), which reveals the gradual formation of a skeletal structure (Figure 18.9(b)) and the ultimate creation of an intrinsic nano-scale porosity in the $MgCl_2$ crystallites (c) (Jacobsen et al., 2007). The observed dimensions of the nano-pores agree with BET/BJH results in Hummelshøj et al. (2006), and the nano-pores can be removed upon reammoniating the samples.

Another factor in the uptake rate is the open layered structure of $MgCl_2$. The ammonia molecules can cleave the layers into chains as shown in Figure 18.8 (Sørensen et al., 2007). Experimental support is found in the slow uptake of ammonia in $CaCl_2$, where the structure is not layered, while transition metal chlorides, which all have layered structures, absorb ammonia fast.

18.5.3 Stabilities and binding energies

DFT calculations also provide the total energies of the structures, and combined with calculations of gas phase ammonia, it is possible to compare stabilities and reaction enthalpies of the different steps of

the decomposition; which clearly shows that the binding energy per ammonia molecule is lowered as more ammonia is absorbed in the crystal.

The reaction enthalpy of a decomposition step is determined from the calculations as the difference in total energy between the two phases involved plus the gas phase energy of the released ammonia molecules. This is calculated for the decomposition steps of $Mg(NH_3)_6Cl_2$, $Ca(NH_3)_8Cl_2$, $Mn(NH_3)_6Cl_2$ and $Ni(NH_3)_6Cl_2$ and compared with experimental observations (Lepinasse and Spinner, 1994) in Figure 18.10 for two calculational schemes: a) where the energies of the stables structures of the two phases are compared directly, and b) where the energy of the stable structure of the initial phase is compared to the energy of a free chain of the final phase (inspired by the proposed mechanism in Figure 18.8). The structures found for the Mg salt were also used for the three other salts (Ca, Mn, Ni) by simply exchanging the metal atoms and letting the structures relax, while scaling the unit cell linearly, until a minimum in total energy was reached. Both comparison schemes show excellent agreement with experimental observations (Lepinasse and Spinner, 1994; Sørensen et al., 2007) when it comes to trends, and the latter model also agrees quantitatively (Sørensen et al., 2007).

18.5.4 Designing superior materials

The insight provided by the atomic model and the model itself is very helpful, when one wants to improve the metal ammine salts for indirect hydrogen storage and design new and better materials. If, for instance, one would optimize the binding energies of ammonia to obtain a higher safety versus economy ratio of the system, it is possible to partially exchange the metal or halide atoms for atoms with stronger bonds to ammonia and calculate all the binding energies. An improved structure would then need to be tested to check if the system has retained its favourable properties like, e.g. fast

diffusion and uptake kinetics. All this can be done in the calculations, and the candidate materials predicted by DFT calculations should then be synthesized in the laboratory and tested for their real life properties, before the design of a superior material is successfully completed.

18.6 Commercial applications and future trends

18.6.1 From research project to real systems and applications

As discussed above, research in metal ammine chemistry involves thermodynamic properties, intrinsic absorption/desorption kinetics and molecular material behaviour on the atomic scale. The task of advancing basic research in material science into real systems and applications requires a change in focus from fundamental material properties to system design and integration. The chemical engineering challenges related to mass and heat transfer in solid ammonia storage units present some of the main difficulties in systems that are beyond the scale of milligrams or grams in the research laboratory. Fundamental studies of storage materials - metal hydrides as well as metal ammine complexes and other technologies - are often done by characterizing the storage capacity and kinetics in terms of TPD studies. Practical systems, on the other hand, should be designed to give a well-defined ammonia (or hydrogen) output that is independent of any given 'position' in the TPD profile.

As described, solid metal ammine complexes can be prepared as very dense materials without any significant internal pore volume, because the porosity needed for ammonia transport is generated as the ammonia release progresses. This allows for ammonia release over large material length scales. Still, the mass transport facilitated by the *in situ* generated pore structure has to be combined with an

understanding of heat transfer resistance, since the ammonia desorption from a metal ammine complex is endothermic.

The release of ammonia can be facilitated by providing desorption heat in several ways:

- as waste heat from an integrated process
- by sacrificing a given amount of the storage capacity as a chemical heat source by way of ammonia (or hydrogen) combustion or
- as direct electrical input through a heating element that compensates for the endothermic ammonia release from the material.

These different approaches are illustrated in the following three system examples:

Plug-and-play ammonia delivery system

In many applications requiring safe, simple and mobile generation of ammonia, system efficiency may not be the most critical specification. Thus, ammonia release can be facilitated simply by applying electrical energy (see Figure 18.11) or process waste heat to release ammonia for a given ammonia-demanding process. Besides use in an ammonia cracker or a fuel cell system, one interesting example of a near-term mass market application is on-board Ammonia Storage and Delivery Systems (ASDS) for NOx removal on passenger cars.[4]

Stand-alone hydrogen generator

Hydrogen is made available by combining a storage cartridge with a catalytic ammonia cracker in which part of the released ammonia is used as an energy source for both the endothermic cracking of ammonia and the release of additional ammonia from the storage material (see Figure 18.12).

[4] NOx removal (DeNOx) from diesel or lean-burn gasoline engines can by done by selective catalytic reduction (SCR) by controlled dosing of ammonia to the exhaust line. As in many other applications, pressure vessels of liquid ammonia are too hazardous for cars and safe storage in solid form enables on-board transportation. Ammonia may also be stored on-board indirectly as an aqueous solution of urea (AdBlue™), but the storage density is three times lower and the chemical conversion of urea must take place before ammonia is available in the exhaust line (Elmøe et al., 2006).

Integrated fuel cell system

Ammonia can be released continuously by use of the waste heat of a fuel cell. As a result, the system efficiency is only limited by the fuel cell itself and the efficiency of the ammonia cracking reactor. The operating temperature of the fuel cell determines the choice of the base salt in the metal ammine (see Table 18.1).

18.6.2 System integration: Applications for all fuel cell types

PEM Fuel Cells

For systems based on low-temperature PEMFCs, the optimal metal ammine would be a material that has a suitable ammonia release profile below 80 °C. This would take advantage of heat integration similar to the way in which waste heat is used to release hydrogen from a metal hydride canister. The metal ammine complex should release the ammonia without causing any additional system losses than that of the ammonia cracker (a theoretical efficiency of 86 % and typically above 70 % in real systems; Thomas & Parks, 2006).

The choice of metal ammine for PEMs could be $Sr(NH_3)_8Cl_2$ or $Ca(NH_3)_8Cl_2$. $Sr(NH_3)_8Cl_2$ releases seven out of the eight bound ammonia molecules at a suitable supply pressure level below 80 °C, and $Ca(NH_3)_8Cl_2$ releases six out of eight (Table 18.1). The remaining ammonia molecules are bound more strongly and do not present a safety problem during the recharging and handling of empty fuel cartridges. Using a high-temperature PEM would provide waste heat at a higher temperature and thus enable the utilization of an even larger fraction of the stored ammonia. For both types of PEMs, ammonia traces from the cracker outlet have to be reduced to a level below ten ppm, to avoid poisoning of the membrane (Faleschini et al., 2000; Rajalashmi et al., 2003; Halsied et al. 2006). This can be done efficiently by an absorber or by a membrane, and the purification is easier to handle than, e.g. CO

removal from a reformed methanol system, which requires low-temperature shift and preferential oxidation (PROX) or a membrane (Qi et al., 2007; Choudhary and Goodman, 2002).

Alkaline fuel cells (AFC)

The use of an alkaline fuel cell also involves an ammonia cracker, but since the electrolyte of the AFC is not sensitive to ammonia traces, the system is slightly simpler because of the elimination of the purification step. In addition, alkaline cells can run at slightly elevated temperatures (like the high-temperature PEM or higher), and they do not contain expensive platinum. AFCs could be operated with the same choice of metal ammine complex as the PEM.

Solid oxide fuel cell (SOFC)

Direct ammonia feed to a SOFC has been demonstrated several times (Wojcik et al., 2003; Fournier et al., 2006; Ma et al., 2006). Whether hydrogen atoms are fed as H_2 or as an equivalent amount of NH_3, there is little or no difference in the fuel cell output (Wojcik et al., 2003). The SOFC actually benefits from the slightly endothermic internal cracking of ammonia on the anode which helps to cool the fuel cell. Methane can also be fed directly to an SOFC. However, the feed has to be de-sulfurized and humidified when using methane, and there is a risk of undesired carbon deposition during the preheating of the methane from room temperature to the operating temperature of the SOFC. Ammonia storage in $Mg(NH_3)_6Cl_2$ is well suited for use with an SOFC since there are no system losses leading to a reduction in actual storage density. The cracking and release of ammonia are done completely through utilization of fuel cell waste heat. It has been demonstrated that a $MgCl_2$-based ammonia storage cartridge containing several kilograms of material can feed a 750 W SOFC with ammonia,[5] illustrating that the storage concept already meets the demands of practical fuel cell applications.

Bridging the temperature gap with proton-conducting ceramics: Direct ammonia fuel cells

[5] www.amminex.com

The huge temperature gap between the SOFC (above 600°C) and the PEM/AFC (below 200 °C) can be bridged by a fuel cell using proton-conducting ceramics (PCC) as the membrane material. Using proper impregnation of the anode with a platinum-free ammonia decomposition catalyst, the cell can operate as a Direct Ammonia Fuel Cell (DAFC) at 350-450°C (Ganley, 2006). Internal ammonia decomposition does not face the typical equilibrium limitation as hydrogen is transported through the membrane as protons. Combined with safe ammonia storage, the DAFC could have a great impact on the future scenario for automotive applications. It is based on an inexpensive base-fuel and storage material, low-cost catalyst for the fuel cell, suitable operating temperature (below 450 °C) and efficient heat integration. This is suitable for use with almost all interesting versions of the metal ammines, and the storage density is as high as that of liquid ammonia at close to 120 kg H_2/m^3 with a mass density above 9 wt.%.

Contrary to the SOFC, the fuel is not 'diluted' in the DAFC anode by water, because water is formed on the cathode. This simplifies water management and balance-of-plant, and the moderate operating temperature is better for fast start-up and shut-down while allowing for a wider compatibility of construction materials in general. At present, the DAFC fuel cell is much less mature than the PEM or the SOFC, and more research and development needs to be done in this field.

18.6.3 Ammonia decomposition

The use of metal ammines as indirect hydrogen storage materials is obviously entirely dependent on the process of efficiently converting ammonia to hydrogen. Ammonia synthesis from the elements is, as discussed previously, an exothermic reaction (see Equation 18.1) and consequently the decomposition of ammonia is endothermic ($\Delta H = 45.6$ kJ/mol NH_3).

Thus, decomposition of ammonia to hydrogen (and nitrogen) requires an energy input, and since the decomposition reaction is very slow even at relatively high temperatures, a catalyst is also needed. Since the reaction is an equilibrium reaction, it is not possible to completely decompose ammonia into hydrogen. Maximizing the efficiency of a complete fuel cell system utilizing metal ammines for hydrogen storage therefore requires both efficient heat integration to minimize losses and a properly designed catalyst system to achieve a sufficiently fast hydrogen production rate. For fuel cell systems that are not tolerant to ammonia, it is also necessary to include an ammonia scavenger. These units are already well-known in the chemical industry. Historically, ammonia decomposition has received most of its attention as a model reaction studied to gain fundamental insight into the technically important ammonia synthesis reaction (Hansen, 1995). However, a few industrial ammonia decomposition plants are currently in operation to produce deuterium-enriched ammonia by coupling consecutive synthesis-decomposition cycles combined with distillation. These plants operate at moderate pressures but at quite high temperatures (ca. 600 °C).

Even though the primary objective in most studies has not been an optimization of the decomposition catalyst or the ammonia decomposition reaction conditions, considerable empirical knowledge on the decomposition already exist. During the last decades, catalytic ammonia decomposition has continuously gained attention as a possible source of CO_x-free hydrogen (Choudhary et al., 2001). At the same time, the continuously improving fundamental understanding of the ammonia synthesis reaction (Honkala et al., 2005) has also led to significant advances in our understanding of the ammonia decomposition reaction.

It is clear that the multi-promoted iron catalyst optimized for industrial ammonia synthesis (Stoltze, 1995) cannot be used for ammonia decomposition. First of all, iron-based catalysts are unstable due to formation of bulk iron nitride under decomposition conditions. The reason is that ammonia synthesis for thermodynamic reasons (Principle of Le Chatelier) is conducted at high pressures (see Section 18.2), whereas ammonia decomposition is preferentially done at low pressures. Moreover, during ammonia synthesis, the equilibrium is approached from low ammonia concentrations, whereas it is approached from high ammonia concentrations during ammonia decomposition. At high ammonia pressures, iron rapidly transforms into iron nitride. The different reaction conditions also mean that a single catalyst is not optimal for both reactions, and this difference can now be expressed in quantitative terms (Boisen et al, 2005). Today, the most promising catalysts for ammonia decomposition are based on supported ruthenium promoted with cesium and/or barium. Interestingly, such catalysts supported on carbon were implemented as ammonia synthesis catalysts in a few industrial plants during the 1990s and were found to be particularly promising at high ammonia pressures (Tennison, 1991). For ammonia synthesis, one challenge with these catalysts was to stabilize the carbon support from methanation that occurs by hydrogenation and leads to catalyst degradation.

It would be useful to find alternative support materials that are completely resistant to hydrogenation. (Jacobsen, 2000; Hansen et al., 2001). However, this is not an issue for ammonia decomposition due to the much lower hydrogen pressures. Highly active ruthenium-based decomposition catalysts that are active at temperatures about 350-400 °C have been developed (Raróg et al., 2001) and have even been prepared for use in miniaturized catalytic systems (Sørensen et al., 2006). With this approach, the heat required for decomposition must be supplied from an external source such as an electrical heating

element. It is estimated that with such an approach, less than 25% of the hydrogen produced needs to be used for heating purposes, either by combusting the hydrogen in a heat exchange reactor or by converting it to electricity in the fuel cell, and using that to heat the decomposition reactor. In such an approach, the waste heat should also be used to desorb ammonia from the metal ammine storage material. Another approach that might prove worthwhile could be to develop a low-temperature auto-thermal ammonia decomposition process where air is fed to the decomposition reactor in exactly the amount required to supply the heat required for decomposition by combustion of some of the generated hydrogen.

18.6.4 Fuel supply: bulk production of storage materials

As mentioned in Section 18.2, a mature distribution network already exists for ammonia. Combined with the fact that there are many types of salts that can store ammonia, and it is easy to imagine sustaining a reliable fuel supply. $MgCl_2$ and $CaCl_2$ are good examples of low-cost materials suitable for high- and low-temperature fuel cell applications.

$MgCl_2$ can be extracted from sea salt. In fact, there are about four million tons of $MgCl_2$ in one cubic kilometre of sea water (Kipouros & Sadoway 2001). A mid-sized car operating on four kg H_2 and a DAFC would need approximately 22 kg of salt carrier. Consequently, almost 200 million ammonia storage cartridges could be made from the $MgCl_2$ present in one cubic kilometre of sea water. Ammonia could be produced from either reforming fossil fuels (with centralized CO_2 sequestration) or from ammonia synthesis utilizing hydrogen produced by renewable resources (Christensen et al., 2006).

The potential distribution path would be bulk transport of ammonia, (re)filling of cartridges and exchange of storage cartridges on a vehicle (Johannessen and Sørensen, 2005), see Figure 18.13. Choosing on-board refilling of the "ammonia-hydride" with ammonia gas would likely be prohibited by the need for removal of the absorption heat during a 4-10 minute refilling time. This is equivalent to the challenge of fast refuelling faced by metal hydride canisters which need an internal heat exchanger of 0.3-1 MW capacity during the refilling of H_2.

In some remote applications, e.g. for portable or small mobile devices, the cartridges can be emptied just once,[6] while most mainstream applications would require an infrastructure for refilling cartridges. The fuel could be provided as solid storage cartridges for the end-user applications. This would be supported by liquid ammonia for recharging where (re)filling stations with decent throughput form a base for safe handling of liquid ammonia by trained personnel. This ensures no end-user is ever in contact with liquid ammonia.

The use of ammonia as an efficient hydrogen carrier can be scaled up to bulk production facilities using inexpensive, widely available materials and well known production technology. These facilities could easily provide fuel for various types of fuel cell systems in both niche and mass markets.

The general use of metal ammine complexes can be further kick-started by the utilization of on-board ammonia storage and delivery systems for NOx aftertreatment on diesel or lean-burn vehicles. The implementation will create experience with vehicle integration, safety and distribution. In addition, bulk production of compact ammine cartridges for DeNOx (AdAmmine™) will drive down the

[6] Unlike rechargeable or one-time batteries, a used metal ammine cartridge can be thrown away in the field without causing damage to the environment; the remaining waste is a salt.

production cost for emerging niche applications while broad entry into mass markets slowly develops in the future.

18.6.5 Continued reading material

References to relevant scientific articles, websites and commercial products pertaining to specific research topics have been provided continuously throughout the chapter. For the interested reader, additional information on the more general properties of ammonia synthesis and catalysis can be found in the following textbooks: 'Catalytic Ammonia Synthesis: Fundamentals and Practice' (Ed.) Jennings, J. R., Plenum Press, New York (1991) and 'Ammonia: Catalysis and Manufacture' (Ed.) Nielsen, A., Springer-Verlag, Berlin (1995).

Further commercial insight into catalytic ammonia synthesis and production can be found at Haldor Topsoe A/S (www.topsoe.com); for the practical use of ammonia as a fertilizer, IFA, the International Fertilizer Industry Association can provide extra information (www.fertilizer.org), and for the commercial use of metal ammines as energy storage materials and materials for SCR-DeNOx, please refer to Amminex A/S (www.amminex.com).

References

Amundsen K, Aune T K, Bakke P, Eklund H R, Haagensen J Ö, Nicolas C, Rosenkilde C, Van den Bremt S, Wallevik O (2003), *Ullmann's ,Encyclopedia of Industrial Chemistry: Magnesium*, Weinheim, Wiley-VCH Verlag GmbH & Co. KGaA.

Appl M (2007), *Ullmann's Encyclopedia of Industrial Chemistry: Ammonia*, Weinheim, Wiley-VCH Verlag GmbH & Co. KGaA.

Atkins P, Paula J (2002*), Atkins' Physical Chemistry*, Oxford, Oxford University Press.

Biltz W (1923), 'Beiträge zur systematischen Verwandtschaftslehre. XXIV. Über das Vermögen kristallisierter Salze, Ammoniak zu binden' Z. anorg. allgem. Chem., 130, 93-139

Biltz W, Rahlfs E (1927), 'Beiträge zur systematischen Verwandtschaftslehre. XLV. Über Reaktionsermöglichung durch Gitterweitung und über Ammoniakate der Fluride.' Z. anorg. allgem. Chem., 166, 351-376

Boisen A, Dahl S, Nørskov J K, Christensen C H (2005), 'Why the optimal ammonia synthesis catalyst is not the optimal ammonia decomposition catalyst', *J. Catal.*, 230, 309-312.

Bonnetot B, Chahine G, Claudy P, Diot M, Letoffe J M (1980), 'Sodium tetrahydridoaluminate $NaAlH_4$ and hexahydridoaluminate Na_3AlH_6 molar heat capacity and thermodynamic properties from 10 to 300 K', J. Chem. Thermodyn., 12 (3), 249-254

Choudhary T V and Goodman D W (2002), 'CO-free fuel processing for fuel cell applications', *Catalysis Today* 77, 65–78.

Choudhary T V, Sivadinarayana C, Goodman D W, Catalytic ammonia decomposition: COx-free hydrogen production for fuel cell applications, Catal. Lett. (2001), 72(3-4), 197-201

Christensen C H, Johannessen T, Sørensen R Z and Nørskov J K (2006), 'An ammonia-based hydrogen economy', *Catal. Today* **111** (1/2): 140-144.

Christensen C H, Sørensen R Z, Johannessen T, Quaade U J, Honkala K, Elmøe D, Køhler R, Nørskov J K (2005), 'Metal ammine complexes for hydrogen storage', *J. Mater. Chem.*, 15, 4106-4108.

Cotton F A, Wilkinson G, Gaus P L (1995), *Basic inorganic chemistry*, New York, John Wiley & Sons

Eggmann T (2001), *Kirk-Othmer Encyclopedia of Chemical Technology: Ammonia*, John Wiley & Sons, Inc.

Elmøe T D, Sørensen R Z, Ulrich Quaade, Christensen C H, Nørskov J K and Johannessen T (2006), 'A high-density ammonia storage/delivery system based on $Mg(NH_3)_6Cl_2$ for SCR-DeNOX in vehicles', *Chem. Eng. Sci.*, **61** (8) 2618-2625.

El-Osairy M A, el-Osery I A, Metwally A M, Hassan M A (1993), 'Two-dimensional dynamic analysis of metal hydride hydrogen energy storage conduction bed models', *Int. J. Hydrogen Energy*, 18 (6), 517-524.

Ephraim F (1926), 'Über die Ammoniakate von Metallsulfaten', Ber., 59B 1219-1231

Faleschini G V, Hacker, Muhr M, Kordesch K and Aronsson R (2000), 'Ammonia for High Density Hydrogen Storage', *Fuel Cell Seminar Abstracts*, Portland, OR.

Fournier G G M, Cumming I W and Hellgardt K (2006), 'High performance direct ammonia solid oxide fuel cell', *Journal of Power Sources*, **162** (1): 198-206.

Ganley J (2006), 'Intermediate Temperature direct Ammonia Fuel Cell', presentation at *Ammonia Fuel III*, Denver, CO.

Goetz W, Spinner B, Lepinasse E (1997), 'A solid-gas thermochemical cooling system using $BaCl_2$ and $NiCl_2$', *Energy*, 22 (1), 49-58

Grundt T, Christiansen K (1982), 'Hydrogen by water electrolysis as basis for small scale ammonia production - A comparison with hydrocarbon based technologies', *Int. J. Hydrogen Energy*, 7 (3), 247-257.

Haber F (1910),'Improvements in the Manufacturing of Ammonia', *Patent No.* 14,023, U.K.

Halsied R, Vie P J S, Tunold R (2006), 'Effect of ammonia on the performance of polymer electrolyte membrane fuel cells', *J. Power Sources* 154, 343-350.

Hammer, B, Hansen, L, Nørskov, J K (1999), ' Improved adsorption energetics within density-functional theory using revised Perdew-Burke-Ernzerhof functionals', *Phys. Rev. B*, 59, 7413-7421.

Hansen, J B (1995), "Kinetics of Ammonia Synthesis and Decomposition" p. 149 in "*Ammonia: Catalysis and Manufacture*" (Ed.) Nielsen, A., Springer-Verlag.

Hansen T W, Wagner J B, Hansen P L, Dahl S, Topsøe H, Jacobsen C J H (2001), "Atomic-scale in-situ Transmission Electron Microscopy of a Promoter of a Heterogeneous Catalyst" *Science* 294, 1508

Häussinger P, Lohmüller R, Watson A M (2000), Ullmann's Encyclopedia of Industrial Chemistry, *Hydrogen*, Wiley-VCH Verlag GmbH & Co. KGaA.

Honkala K, Remediakis I, Logadottir A, Nørskov J K, Hellman A, Dahl S, Carlsson A, Christensen C H (2005), 'Ammonia Synthesis from First Principles Calculations', *Science* 307, 555.

Hummelshøj J S, Sørensen R Z, Kustova M Y, Johannessen T, Norskov J K and Christensen C H (2006), 'Generation of Nanopores during Desorption of NH_3 from $Mg(NH_3)_6Cl_2$', *J Am Chem Soc,* 128 (1), 16-17.

Jacobsen H S, Hansen H A, Andreasen J W, Shi Q, Andreasen A, Feidenhans'l R, Nielsen M M, Ståhl K and Vegge T (2007); 'Nanoscale structural characterization of $Mg(NH_3)_6Cl_2$ during NH_3 desorption: An *in situ* small angle X-ray scattering study', *Chem Phys Lett., 441, 255-260.*

Jacobsen J H (2000), "Novel Class of Ammonia Synthesis Catalysts" *Chem. Commun.* 2000, 1057.

Johannessen T (2005) and Sørensen R Z, 'Handheld hydrogen - a new concept for hydrogen storage', *TCE* (773): 30-32.

Kapischke J, Hapke J (1998), 'Measurement of the pressure-composition isotherms of high-temperature and low-temperature metal hydrides', *Exp. Therm Fluid Sci.*, 18, 70-81

Kipouros G J (2001) and Sadoway D R, 'A thermochemical analysis of the production of anhydrous $MgCl_2$', *Journal of light materials*, **1**, 111-117.

Laidler K J, Meiser J H (1999), *Physical Chemistry*, third edition, New York, Houghton Mifflin Company

Leineweber A, Friedriszik M W and Jacobs H (1999), 'Preparation and Crystal Structures of $Mg(NH_3)_2Cl_2$, $Mg(NH_3)_2Br_2$, and $Mg(NH_3)_2I_2$', *J Solid State Chem,* 147 (1), 229-234.

Leineweber A, Jacobs H and Ehrenberg H (2000), 'Crystal structure of $Ni(NH_3)Cl_2$ and $Ni(NH_3)Br_2$', *Z Anorg Allg Chem,* 626 (10), 2146-2152.

Lepinasse E and Spinner B (1994), 'Cold production through coupling of solid-gas reactors I: Performance analysis', *Int J Refrig,* 17 (5), 309-322.

Liu X, Zhu Y, Li L (2007), 'Hydriding characteristics of Mg_2Ni prepared by mechanical milling of the product of hydriding combustion synthesis', *Int. J. Hydrogen Energy*, article in press

Ma Q, Peng R, Tian L, Meng G (2006) 'Direct utilization of ammonia in intermediate-temperature solid oxide fuel cells', *Electrochemistry Communications,* 8,1791–1795.

Maxwell G R (2005), *Synthetic Nitrogen Products – A Practical Guide to the Products and Processes*, New York, Kluwer Acedemic.

Mosher D, Tang X, Arsenault S (2006), 'High Density Hydrogen Storage System Demonstration Using $NaAlH_4$ Based Complex Hydrides", FY 2006 Annual Progress Report, DoE Hydrogen Program, 281-284

Nomura K, Fujiwara S, Hayakawa H, Akiba E, Ishido Y, Ono S (1991), 'Magnesium-nickel alloy hydride compacts prepared by cylindrical explosion shock compression', *Journal of the Less-Common Metals*, 169, 9-17

Norsk Hydro (1997), *Worth a try Research and Development in Norsk Hydro through 90 years*, Oslo, Norsk Hydro.

Olovsson I (1965), 'Packing principles in the structures of metal ammine salts', *Acta Crystallogr,* 18, 889-893.

Pareto V (1971), *Manual of Political Economy*, New York, Augustus M Kelley Pubs

Partin D and O'Keeffe M (1991), 'The structures and crystal chemistry of magnesium chloride and cadmium chloride', *J Solid State Chem,* 95 (1), 176-183.

Patil K C, Secco E A (1972), 'Metal Halide Ammines. II. Thermal Analyses, Calorimetry and Infrared Spectra of Flouride Ammines and Hydrates of Bivalent Metals', *Can. J. Chem.*, 50, 567-573

Pietsch E (1939), *Gmelins Handbuch der anorganischen Chemie 8th edition: Magnesium teil B*, Berlin, Verlag Chemie G.M.B.H.

Qi A, Peppley B and Karan K (2007), 'Integrated fuel processors for fuel cell application: A review', *Fuel Processing Technology* **88**, 3–22.

Rajalashmi N, Jayanth T T, Dhathathreyan K S (2003), 'Effect of carbon dioxide and ammonia on polymer electrolyte membrane fuel cell stack performance', *Fuel Cells*, 3, 177-180.

Raróg W, Kowalczyk Z, Sentek, J, Składonowski D, Szmigiel D, Zieliñski J (2001), Decomposition of ammonia over potassium promoted ruthenium catalyst supported on carbon, *Appl. Catal. A*: Gen. 2001, 208, 213-216.

Raróg-Pilecka W, Szmigeel D, Kowalczyk Z, Jodis S Zielinski J (2003), 'Ammonia decomposition over the carbon-based ruthenium catalyst promoted with barium or cesium', *J. Catal.*, 218, 465-469.

Sørensen R Z, Hummelshøj J S, Klerke A, Reves J B, Vegge T, Nørskov J K, Christensen C H (2007), 'Indirect, reversible high-density hydrogen storage in compact metal ammine salts', to be submitted.

Sørensen, R. Z., Klerke, A., Jensen, S., Hansen, O., Quaade, U., Christensen, C. H. (2006), 'Promoted Ru on High-Surface Area Graphite for Efficient Miniaturized Production of Hydrogen from Ammonia', *Catal. Lett.* 112, 77.

Srivastava S, Srivastava O N (1999), 'Hydrogenation behaviour with regard to storage capacity, kinetics, stability and thermodynamic behaviour of hydrogen storage composite alloys, $LaNi_5/La_2Ni_7$, $LaNi_3$', *J. Alloys Compd.*, 290, 250-256

Stoltze P (1995), 'Structure and Surface Chemistry of Industrial Ammonia Synthesis Catalysts" p. 21, Kinetics of Ammonia Synthesis and Decomposition' in "*Ammonia: Catalysis and Manufacture*" (Ed.) Nielsen, A., Springer-Verlag

Suissa E, Jacob I, Hadari Z (1984), 'Experimental Measurements and general conclusions on the effective thermal conductivity of powdered metal hydrides', *Journal of the Less-Common Metals*, 104, 287-295

Tennison, S R (1991), "Alternative N on iron Catalysts" in "*Catalytic Ammonia Synthesis: Fundamentals and Practice*" p. 303, (Ed.) Jennings, J. R., Plenum Press

Thomas G, Parks G (2006), *Potential roles of ammonia in a hydrogen economy – A study of issues related to the use of ammonia on-board vehicular hydrogen storage*, Washington, U.S. Department of Energy.

Voss J, Hummelshøj, Gudmundsdottir H, J S, Nørskov J K, Vegge T (2007), "Thermally assisted tunneling of NH_3 in $Mg(NH_3)_6Cl_2$", to be submitted.

Wojcik A (2003), Middleton H, Damopoulos I and Van herle J, "Ammonia as a fuel in solid oxide fuel cells", *J. Power Sources,* **118**, 342.

Yin S F, Xu B Q, Zhou X P, Au C T (2004), 'A mini-review on ammonia decomposition catalysts for on-site generation of hydrogen for fuel cell applications', *Appl. Catal. A*, 277, 1-9.

Young G J (1963), *Fuel Cells vol. 2*, New York, Reinhold Publishing Corporation.

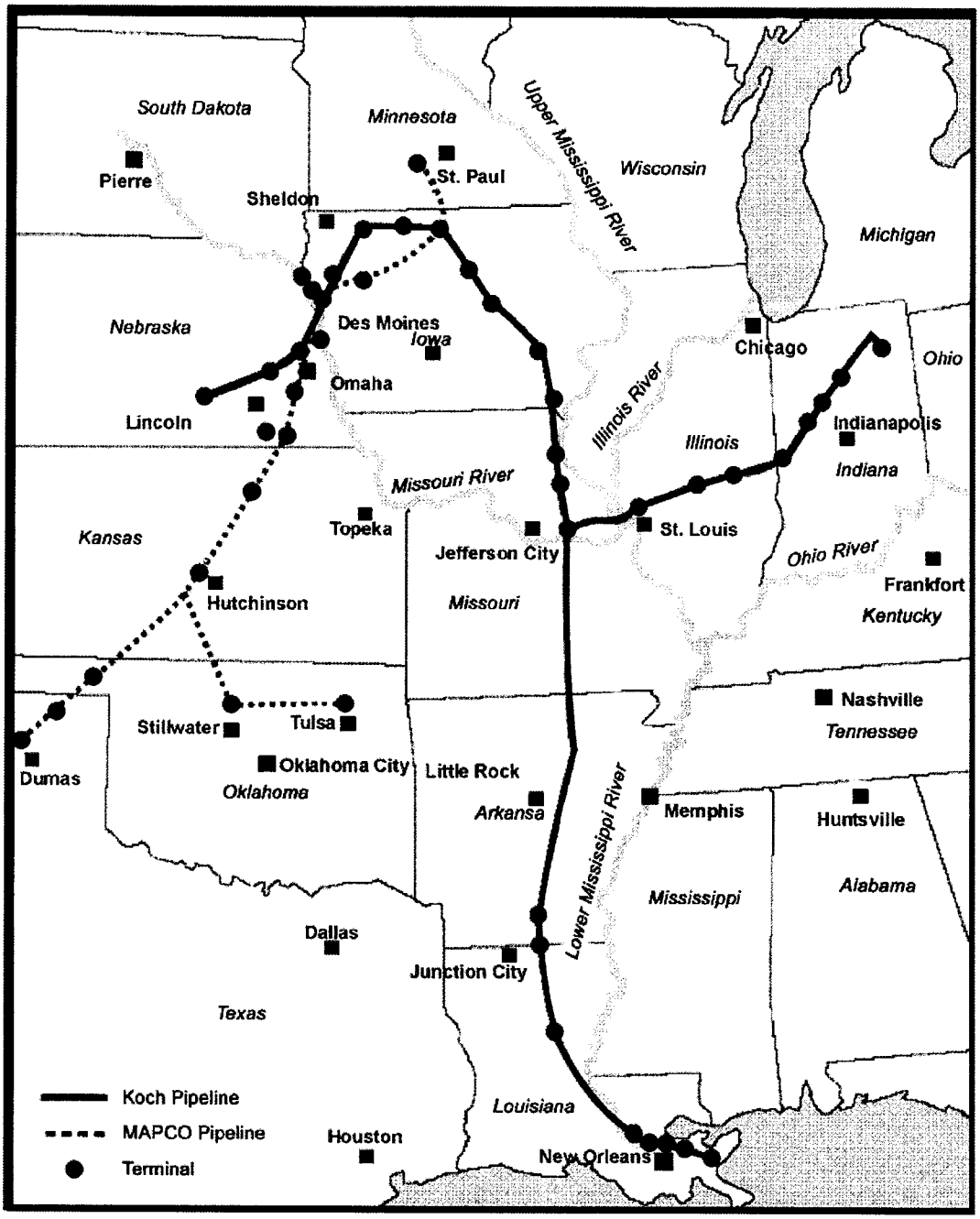

Figure 18.1: Ammonia Pipelines in the U.S. Midwest (adapted from Thomas and Parks, 2006).

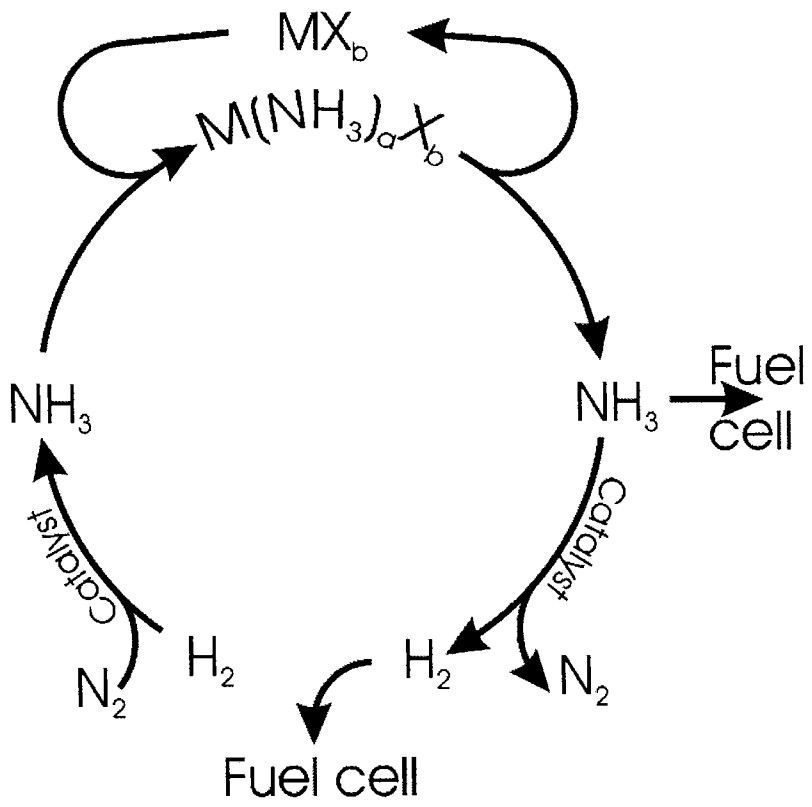

Figure 18.2: The Hydrogen cycle in an ammonia mediated hydrogen economy (adapted from Sørensen et al., 2007).

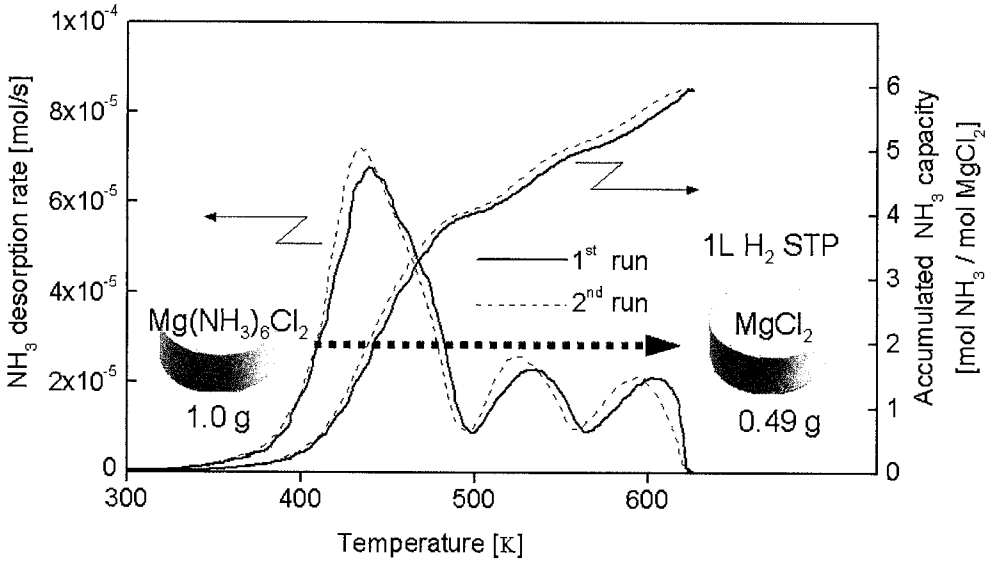

Figure 18.3: Two TPDs of $Mg(NH_3)_6Cl_2$ to demonstrate that ammonia can be ab- and desorbed reversibly. The pictures show a dense tablet before and after desorption with corresponding masses (adapted from Christensen et al., 2005).

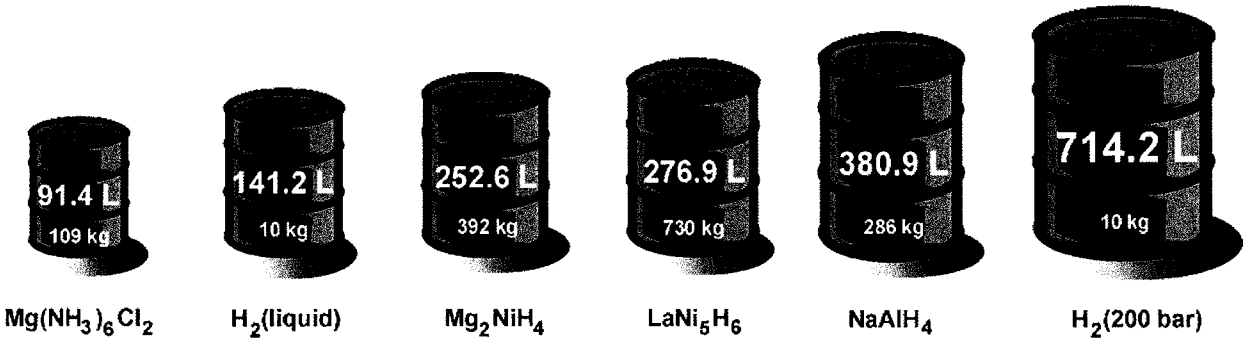

Figure 18.4: Drums with 10 kg hydrogen equivalent. Figures are based on the best available literature data for practical, reversible hydrogen storage including reported void fractions, but excluding weight and volume of the containers. Data is collected from (Mosher et al., 2006) for $NaAlH_4$, (Liu et al., 2006), (Nomura et al., 1991) and (Suissa et al., 1984) for Mg_2NiH_4, (El-Osairy et al., 1993) for $LaNi_5H_6$, (Häussinger et al., 2000) for H_2(l) and (Christensen et al., 2005) for $Mg(NH_3)_6Cl_2$. The density of H_2(g) at 200 bar is calculated from data in (Laidler and Meiser, 1999).

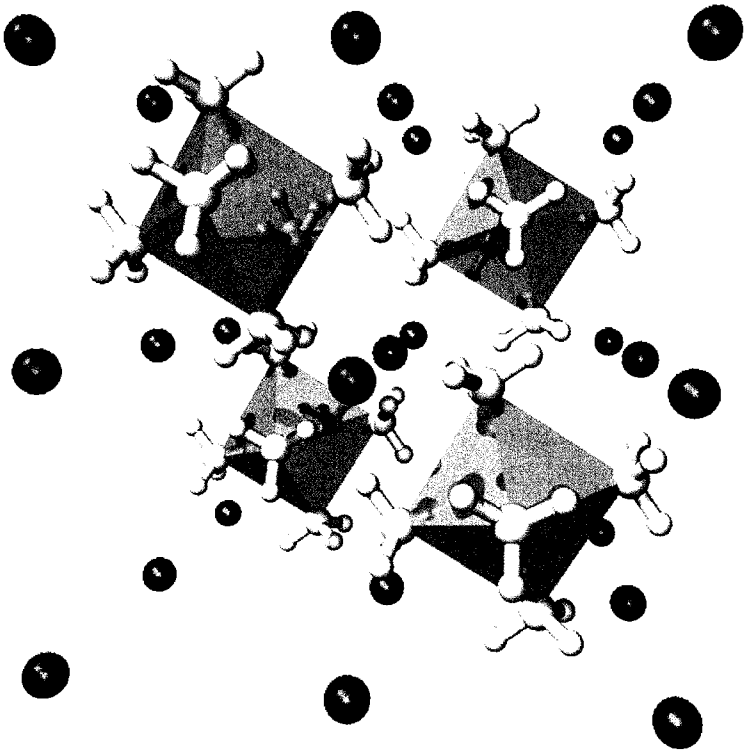

Figure 18.5: The K_2PtCl_6 structure of $Mg(NH_3)_6Cl_2$ where the octahedral $Mg(NH_3)_6$ complexes are contained in a cubic lattice of chlorine atoms with a side-length of 5.45Å. Ammonia molecules are white and chlorine atoms are black, while the magnesium atoms are not shown, but situated in the centre of each octahedron; the structure can be described as chains running along the body diagonal of the Cl cubes.

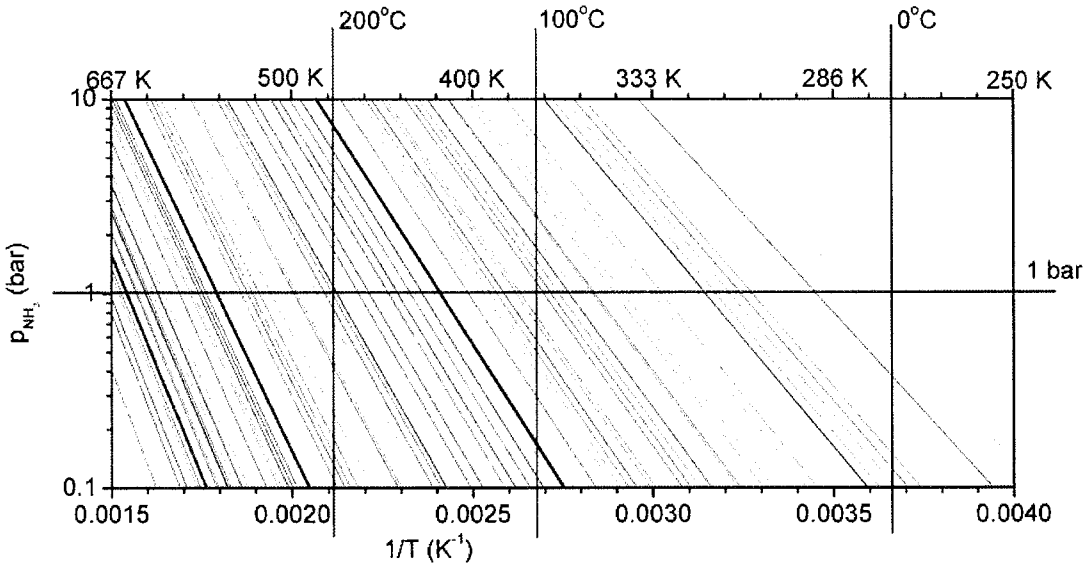

Figure 18.6: Van't Hoff plots of the equilibrium ammonia pressure versus temperature for the 90 metal ammines listed in Table 18.1. The bold lines represent the different stages of $Mg(NH_3)_6Cl_2$ decomposition.

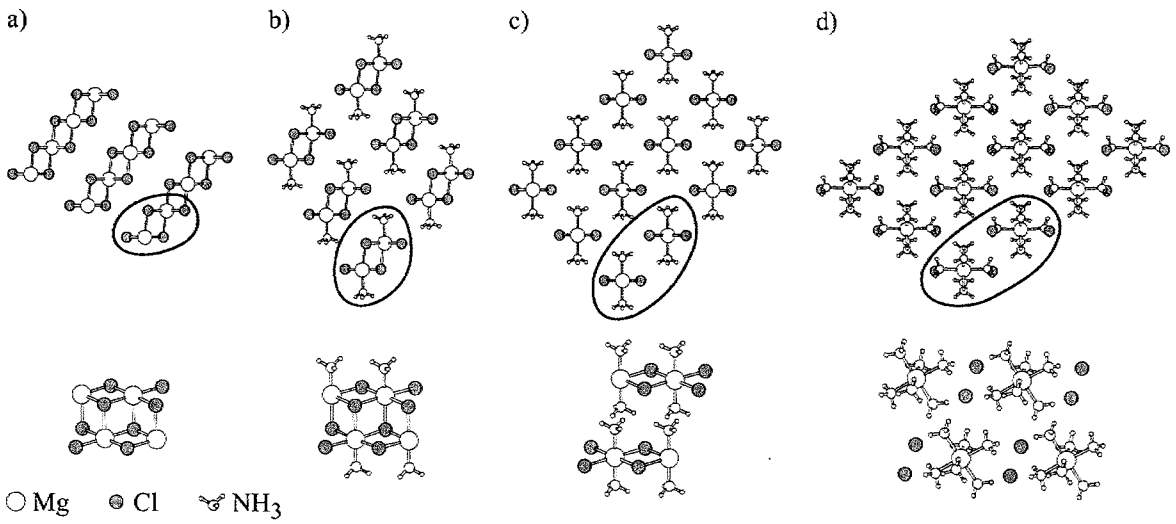

Figure 18.7: The full sorption cycle of $Mg(NH_3)_6Cl_2$. From a) $MgCl_2$ to the left through b) the mono: $Mg(NH_3)Cl_2$, c) di: $Mg(NH_3)_2Cl_2$ and d) hexammine structures (adapted from Sørensen et al., 2007). Upper part: a view along the "indefinite" chains; lower part: four formula units showed from the side, corresponding to the highlighted fragments (upper). The three layers of $MgCl_2$ (a) are cleaved into $Mg(NH_3)Cl_2$ chains (b), which are cleaved once more to produce the $Mg(NH_3)_2Cl_2$ chains (c), which are stretched to make space for four additional ammonia molecules in the $Mg(NH_3)_6Cl_2$ structure (d).

Table 18.1: Storage properties for the ammines of 30 metal halides. For each salt the tabulated values are: The hydrogen density of the stable ammine at 0 °C and 1 bar ammonia, the vapour pressure of this ammine at 100 °C, the temperature where the highest and lowest coordinated ammines reaches an equilibrium vapour pressure of 1 bar, and the enthalpies for release of ammonia from the stable coordination compounds. All data are calculated from Biltz (1923); Lepinasse and Spinner (1994).

Salt	Highest wt%H	P initial at	T for 1 bar (°C)		ΔH at coordination nr.:							
	< 1bar at 0°C	100°C (bar)	Initial	Final	9	8	6	5	4	3	2	1
$CaCl_2$	9.8	1.9E+01	32	242		41.0			42.3		63.2	69.1
LiCl	9.7	5.5E+00	61	114						44.8	48.1	51.9
$MgCl_2$	9.2	1.6E-01	142	375			55.7				74.9	87.0
$SrCl_2$	8.2	1.6E+01	35	85		41.4						48.1
$MnCl_2$	8.0	2.4E+00	80	354			47.4				71.0	84.2
$FeCl_2$	7.9	6.9E-01	109	374			51.3				76.2	86.9
$NiCl_2$	7.8	5.3E-02	168	396			59.2				79.5	89.8
$CoCl_2$	7.8	2.9E-01	129	384			54.0				78.1	88.3
LiBr	7.8	1.1E+01	45	151					42.7	46.4	49.0	56.9
$CaBr_2$	7.2	1.9E+01	32	306		41.0	49.0				71.5	77.8
$BaCl_2$	7.0	5.4E+01	8	8		37.7						
$MnBr_2$	6.4	3.8E-01	122	351			53.1				77.1	83.8
$MgBr_2$	6.3	1.3E-02	201	403			63.6				84.1	90.8
$SrBr_2$	6.3	4.2E+00	67	251		45.6					63.6	70.3
LiI	6.0	1.7E+00	88	225					48.5	51.0	57.7	66.9
$FeBr_2$	5.7	1.6E-01	143	374			55.8				83.1	86.9
$NiBr_2$	5.7	1.0E-02	205	374			64.2				85.4	86.9
$CoBr_2$	5.6	6.5E-02	163	381			58.6				84.4	87.9
$BaBr_2$	5.6	1.4E+01	38	95		41.8			42.7		44.4	49.4
SrI_2	5.1	3.7E+00	70	297		46.0	52.7				64.9	76.6
BaI_2	5.0	1.4E+01	61	145	41.8	44.8	46.4		47.3		56.1	
MgI_2	4.8	8.0E-04	265	431			72.2				94.5	
$SnCl_2$	4.7	3.7E+01	17	17					38.9			
CaI_2	4.6	6.4E-02	163	335			58.6				79.5	81.6
MnI_2	4.4	5.1E-02	169	341			59.3				82.5	
FeI_2	4.4	3.3E-02	179	364			60.7				85.6	
CoI_2	4.4	2.5E-02	185	198			61.5				63.3	
NiI_2	4.4	4.7E-03	224	340			66.7				82.3	
$SnBr_2$	4.2	1.9E+01	32	151				41.0		52.3	56.9	
SnI_2	3.3	1.1E+01	45	226				42.7		49.8	55.7	66.9

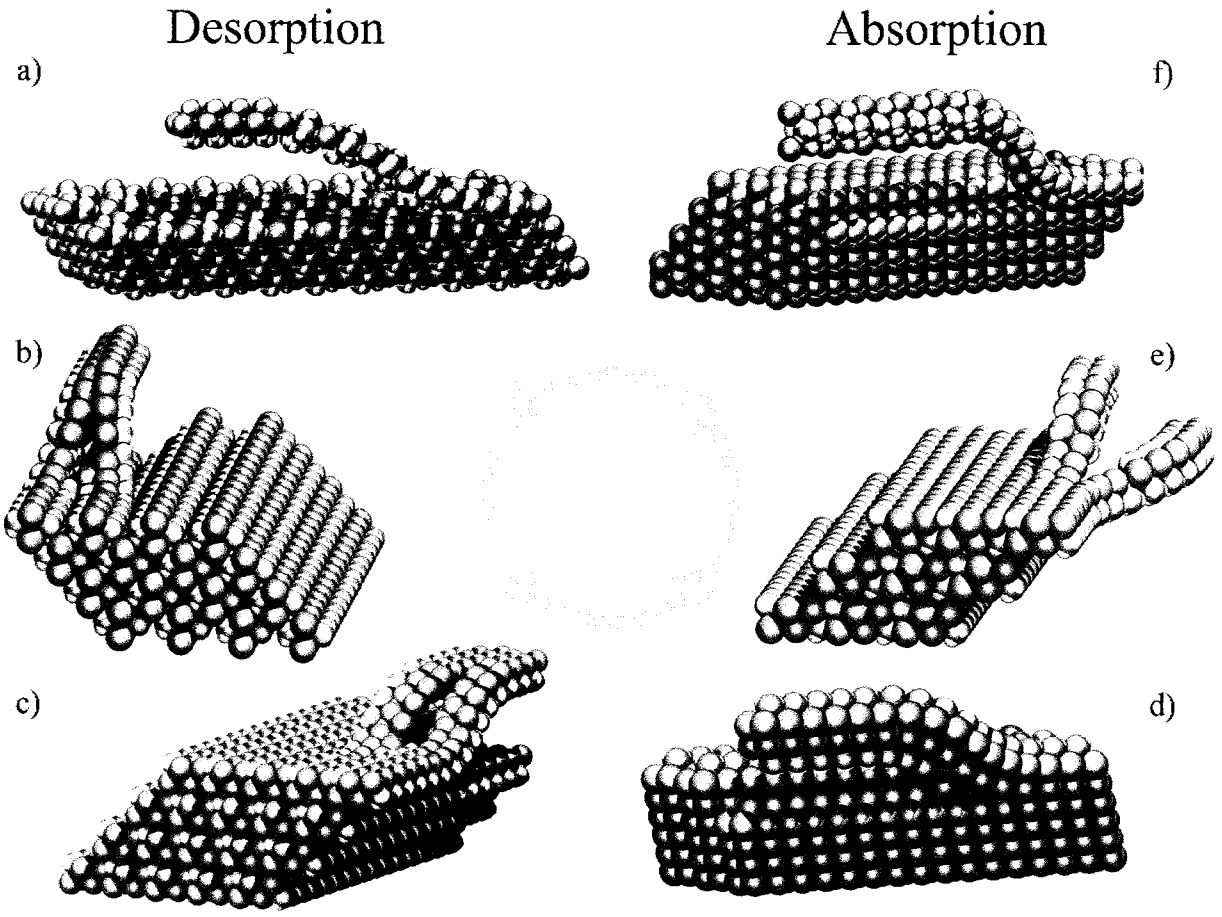

Figure 18.8: An alternate mechanism for desorption and absorption of ammonia in $Mg(NH_3)_xCl_2$, $Mn(NH_3)_xCl_2$ and $Ni(NH_3)_xCl_2$. The compression/combination of chains during desorption (a, b and c) or stretching/cleavage of chains/layers during absorption (d, e and f), can happen readily, when the chains are released from the surface. The number of under-coordinated magnesium atoms is kept to a minimum at all times.

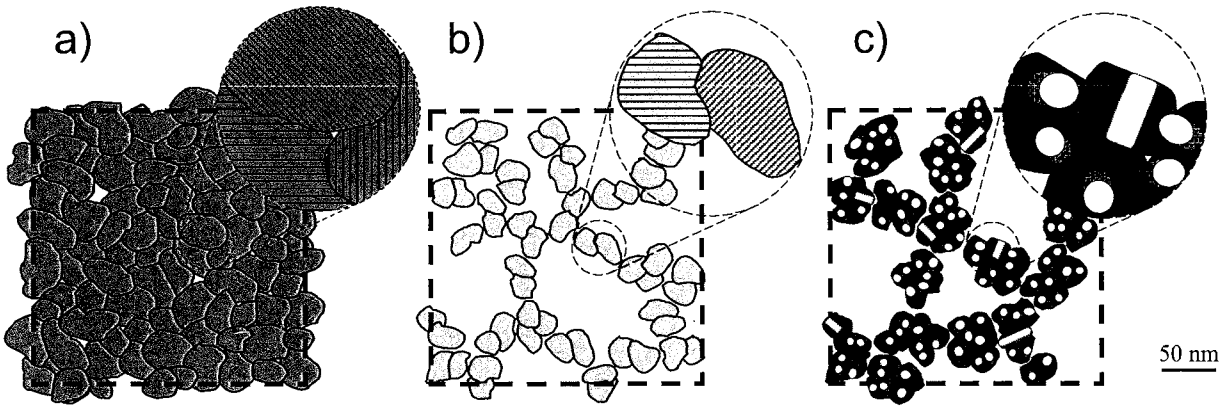

Figure 18.9: The porous system which arise from the lattice contraction in the polycrystalline $Mg(NH_3)_6Cl_2$ salt. Here the systems are a) $Mg(NH_3)_6Cl_2$, b) $Mg(NH_3)_2Cl_2$ and c) $MgCl_2$. The internal d=10-20 nm $MgCl_2$ porosity is crucial to the fast desorption and reloading of the storage system (adapted from Jacobsen et al., 2007).

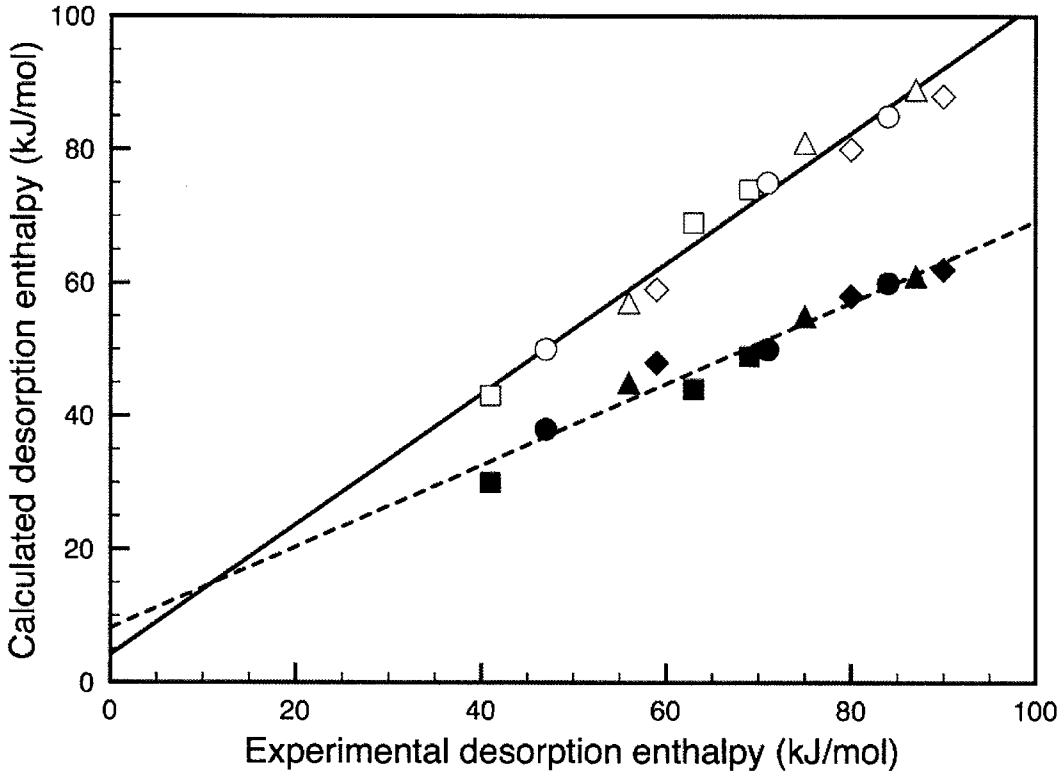

Figure 18.10: Calculated versus experimental desorption enthalpies for the different desorption steps, 6→2, 2→1, 1→0, of $Mg(NH_3)_6Cl_2$[triangle], $Ca(NH_3)_8Cl_2$[square], $Mn(NH_3)_6Cl_2$[circle] and $Ni(NH_3)_6Cl_2$[diamond] for two calculational schemes. Filled symbols represent the energy difference between the stable structures and the unfilled symbols the difference between the stable initial structure and the energy of the final structure as free chains. For both schemes the calcium salt is approximated by a model hexaammine salt, $Ca(NH_3)_6Cl_2$, which follows the same desorption route as the three other salts; here, the first desorption step is representative of the first two desorption steps of the real octaammine salt, $Ca(NH_3)_8Cl_2$.

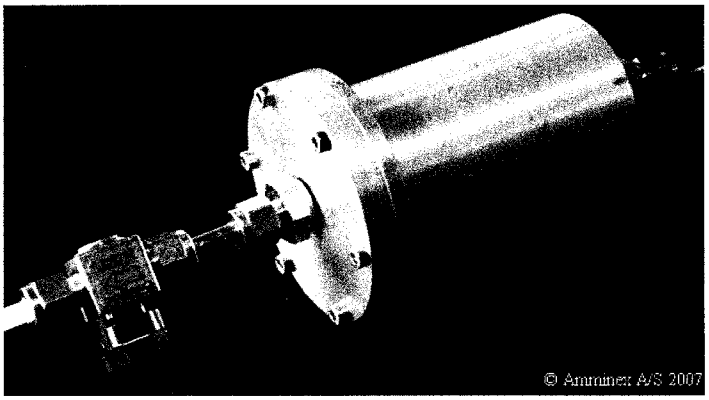

Figure 18.11 A photograph of a plug-and-play ammonia generator. The unit is plugged directly to 220 V or 110 V and generates 1-1.2 L of ammonia gas per minute. The power consumption is 40-45 W, which corresponds to the ammonia desorption enthalpy. The unit is operated below 80°C, orientation independent and is simple to operate.

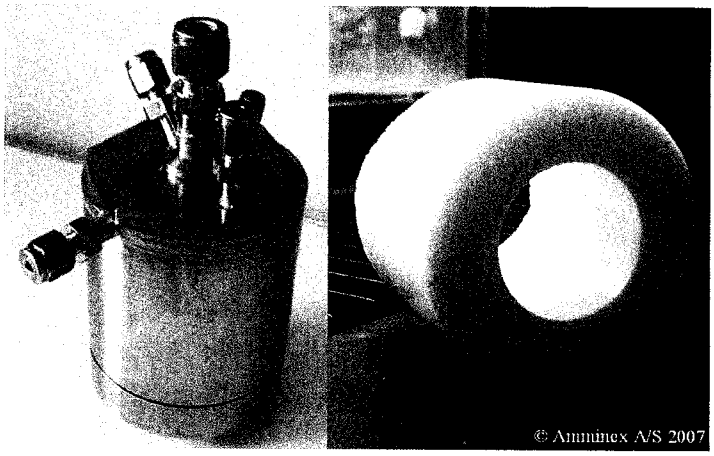

Figure 18.12 A photograph of an integrated hydrogen generator based on solid ammonia storage and ammonia decomposition. The storage material is shaped in the form of a ring, and the ammonia cracker is integrated inside the storage container surrounded by the material.

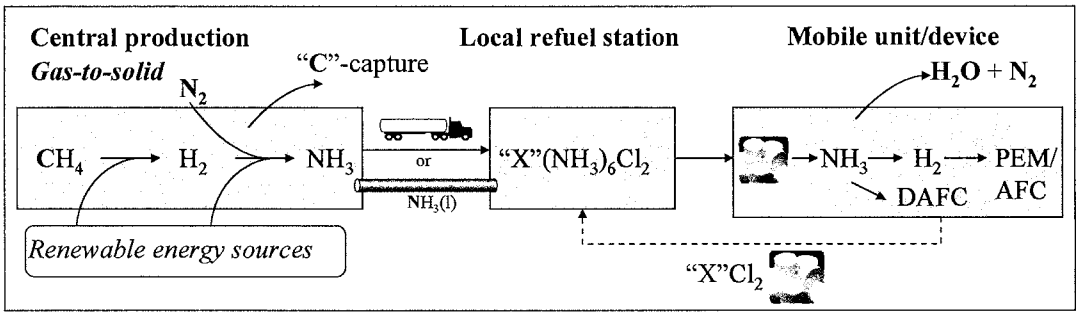

Figure 18.13 Potential distribution path of ammonia fuel (adapted from Johannessen and Sørensen, 2005).

Asbjørn Klerke, Jakob Engbæk, Rasmus Zink Sørensen, Rasmus Fehrmann.

Ammonia and Metal Ammines for high Density Hydrogen Storage

Introduction

The challenge of efficient storage and transportation of hydrogen for use in fuel cells still needs to be addressed. In the following it is described how ammonia has potential to become one of the important indirect hydrogen carriers. Aside from hydrogen, ammonia provides the only carbon-free chemical energy carrier solution, giving no CO_2 emission at the enduser. Ammonia is not a green house gas (GHG), and in light of the global climate challenges with respect to GHG outlined, *e.g.* in the Kyoto protocol, combined with a high hydrogen density, NH_3 could be an interesting alternative to direct hydrogen storage.

Ammonia is also interesting because the infrastructure for production, storage, and transportation, is well known technology from the fertilizer industry. The synthesis of ammonia in the Haber-Bosch process is one of the largest chemical processes with a yearly production of 120 million tons, but this is only enough to support a minor fraction of the hydrogen that will be needed in a future hydrogen economy. Ammonia is primarily produced from natural gas, but hydrogen for the synthesis could be supplied from wind or solar power via electrolysis or any other green source of hydrogen. The synthesis of ammonia is also a prime candidate for CO_2 sequestration to prevent emission of CO_2, because the synthesis gas is already cleaned for CO_2 by pressure swing absorption. Furthermore ammonia plants are typically located near natural gas sites where the CO_2 can be pumped back into the ground. Bulk ammonia is transported and stored as a liquid under pressure or cooled to -33°C.

Indirect Hydrogen Storage in Ammonia and Metal Ammines

Ammonia as energy storage medium, either for direct use in a combustion engine or indirectly by decomposition to hydrogen and nitrogen, is not new. Several comparative studies of ammonia and other fuels have been made [1,2]. The main conclusion in these studies is that ammonia is a useful alternative to hydrocarbons. Furthermore ammonia is competitive with hydrocarbons in price pr. unit of energy.

Ammonia is a good medium for hydrogen storage on both weight and volume as seen in figure 1. For use in portable devices ammonia can be stored as a high density solid in a range of metal ammine salts. The metal ammines lower the ammonia vapor pressure making them safe to handle and use. In figure 1, mass and volumetric hydrogen densities for storage of 10 kg

hydrogen reversibly by 8 different methods is shown[3]. It can be seen that the metal ammines have higher volumetric hydrogen densities than liquid ammonia at room temperature.

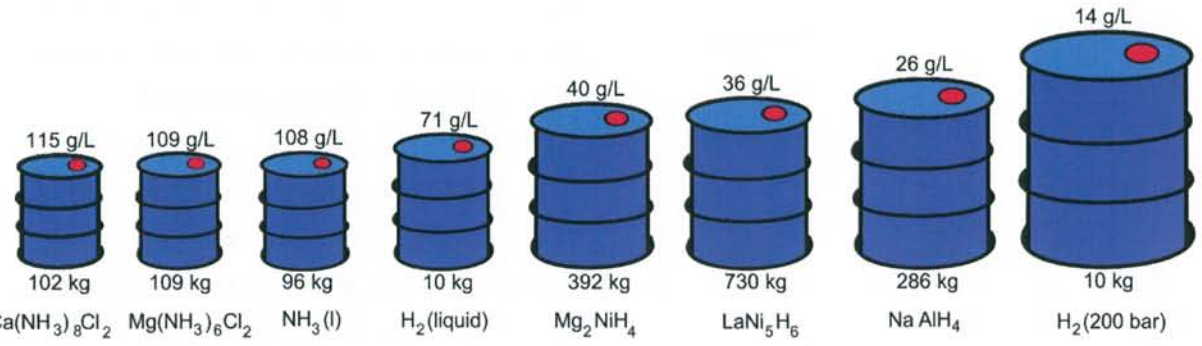

Figure 1: Mass and volume densities of 10 kg hydrogen stored reversibly by 8 different methods, based on the best obtained reversible hydrogen densities reported in the literature without considering the space or weight needed for the container[3].

Desorption of ammonia from metal ammines is easy and only limited by heat transportation[4]. This has been showed using temperature programmed desorption (TPD) measurements. Examples of TPDs can be seen in Figure 2. This also shows that the desorption characteristics are similar for the four investigated salts. The largest variation is the onset temperature of desorption which is determined by the enthalpy. Furthermore the metal ammines can be efficiently compressed and thereby obtain high volumetric hydrogen densities. This can be seen in table 1.

Table 1: Tablet densities and their volumetric and gravimetric hydrogen content[4].

	ρ_{tablet} g/cm^3	% of $\rho_{crystal}$	Volumetric H kgH/L	Gravimetric H wt%H
$Mg(NH_3)_6Cl_2$	1.19	95	0.11	9.19
$Ca(NH_3)_8Cl_2$	1.18	99	0.12	9.78
$Mn(NH_3)_6Cl_2$	1.34	95	0.11	7.96
$Ni(NH_3)_6Cl_2$	1.41	95	0.11	7.83

The densities of the metal ammine chloride tablets are reported and compared to the crystal densities. All the tested metal ammine halides have tablet densities of at least 95% of their crystal densities. The metal ammines can be compressed into a solid medium and still maintain a high desorption rate. This is due to the formation of nanopores during desorption of ammonia[5].

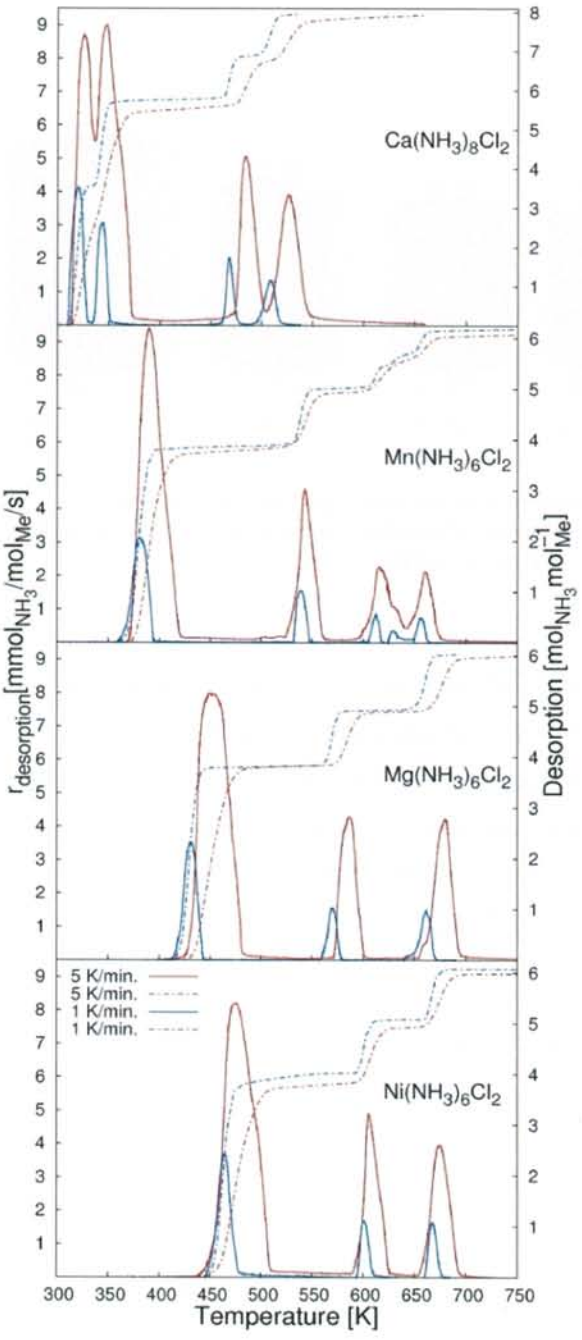

Figure 2: TPDs of $Ca(NH_3)_8Cl_2$, $Mn(NH_3)_6Cl_2$, $Mg(NH_3)_6Cl_2$, and Ni(NH3)6Cl2, with a temperature ramp of 5K/min (red) and 1K/min (blue). The solid lines show the desorption rate and the dashed lines show the amount of ammonia desorped pr metal [4].

Desorption characteristics for the four metal ammine chlorides during TPD are shown in figure 2. As expected from literature data, the trend in temperature for the first desorption peak is Ca<Mn<Mg<Ni. During TPD, $Ca(NH_3)_nCl_2$ has stable compositions with n = 8, 4, 2, 1 and essentially all ammonia desorbs in the temperature range 300-550 K. $Mn(NH_3)_nCl_2$ has stable compositions with n = 6, 2, 1 and two compositions with n<1. Stable structures with less than 1 ammonia molecule pr metal atom are well known for a range of transition metal complexes, and are thus not unlikely even though they have not been reported previously for $MnCl_2$. Essentially all ammonia desorbs in the temperature range 350-675 K. TPDs of $Mg(NH_3)_nCl_2$ were also reported previously and have stable compositions with n = 6, 2, 1. Essentially all ammonia desorbs in the temperature range 410-700 K. During TPD, $Ni(NH_3)_nCl_2$ has stable compositions with n = 6, 2, 1 and all ammonia desorbs in the temperature range 440-700 K. Independently of the temperature ramp, all the TPD peaks start within few degrees of the temperature for 1 bar equilibrium pressure calculated from literature data[6]. This and the near exponential rise in desorption rate with temperature indicates that desorption is equilibrium-limited even at high desorption rates.

The number of metal ammines investigated for use as hydrogen storage materials is still quite small, but due to their similar chemical

nature, the general findings can be used as a guideline for the behavior of other metal ammines. This has been tested by detailed modeling using density functional theory (DFT) calculations, which showed good agreement between theoretical calculations and experimental data[7]. DFT calculations are able to reproduce the experimentally observed trend in desorption enthalpies for various ammines at all decomposition steps[4], making such calculations is a valuable tool in the design and prediction of novel metal ammine compounds with specific properties, *e.g.* by varying the metal or halide components in the ammine salt.

Ammonia Decomposition

The ammonia released from metal ammines, can be used directly in a solid oxide fuel cell or a direct ammonia fuel cell. In both types of fuel cells the ammonia is reformed on the anode to form nitrogen and water by reaction with hydroxide in alkaline type fuel cells or by reaction with oxide ions in SOFC and other oxide conducting fuel cells.

The development of new fuel cells is fast but so far the commercialization of new designs is slow. Demo plants with SOFC are operating on different reformed fuel feeds, but no larger tests with ammonia have been published. Therefore the best alternative is to make a separate unit for decomposition of ammonia to hydrogen and nitrogen. This feed can then be used in low temperature fuel cells like PEMFC or PAFC.

The research on ammonia decomposition catalysts show that ruthenium nano-particles supported on high surface area graphite (HSAG) and promoted with cesium is the most active catalyst[8,9,10].

The ammonia decomposition unit is designed for a hydrogen production for a 500-1000W PEMFC. This power demand is chosen as a practical size for a prototype, large enough to have efficient insulation and heat management, and small enough to handle in the laboratory in standard equipment. The power can be used for a small vehicle or as a power back up. This power demand can be covered by decomposition of 4-9 L/min ammonia.

The decomposition of ammonia to hydrogen is endothermic and the reaction can be seen in scheme 1. The heat for the decomposition is supplied by catalytic combustion of ammonia over commercial platinum on alumina catalyst, the reaction is shown in scheme 2.

$2NH_3 \rightarrow N_2 + 3H_2$ $\Delta H=92$ kJ/mol (1)

$2NH_3 + 3/2O_2 \rightarrow N_2 + 3H_2O$ $\Delta H=-633$ kJ/mol (2)

From the enthalpies it can be calculated that catalytic combustion of one mole ammonia develops enough energy for decomposition of 6.8 mole ammonia. With this limit of the system a minimum of 0.73 L/min. ammonia need to be combusted to decompose 5 L/min ammonia. This ratio is not possible to achieve in practice due to heat loss and the need for high temperatures (800-900K) for the decomposition reaction to reach an equilibrium conversion of over 99.8%. This makes heat exchange very important and still energy will be lost as low temperature heat. Some of the heat in the exit gas can be used to desorp ammonia stored in a metal ammine salt and thereby increase the overall energy efficiency of the system. The basic schematic of the ammonia decomposition unit can be seen in Figure 3.

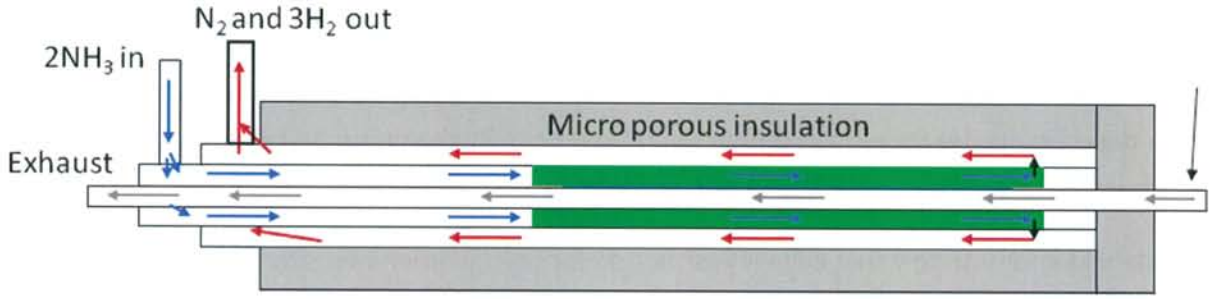

Figure 3: Schematic of ammonia decomposition unit, middle (gray arrows)catalyst bed is Pt on Al_2O_3 for catalytic combustion of ammonia, green bed is Ru on high surface area graphite (HSAG) promoted with Cs for catalytic ammonia decomposition

The design shown in Figure 3 is selected to minimize the energy loss. This is done by placing the ammonia combustion catalyst inside the double pipe, so as much heat as possible can be transferred to the decomposition unit. With this design it is possible to decompose 4.5-5 l/min ammonia by combusting 1L/min. This is an energy efficiency of 74%. If the decomposition unit is build together with a metal ammine storage system for ammonia the hot exhaust can be used to desorp ammonia.

The flow control to the combustion catalyst is important to avoid harmful emission of NO_X and N_2O. They are formed primarily if the ammonia air mixture is oxygen rich. To measure the oxygen amount in the combustion mixture a lambda sensor was used. Exhaust gas samples were taken out at different lambda values around one to verify that a lambda close to one or 450 mV is optimal also for the catalytic combustion of ammonia. The gas samples are investigated with FTIR to determine the amount of slip ammonia and harmful emissions. The results can be seen in Figure 4.

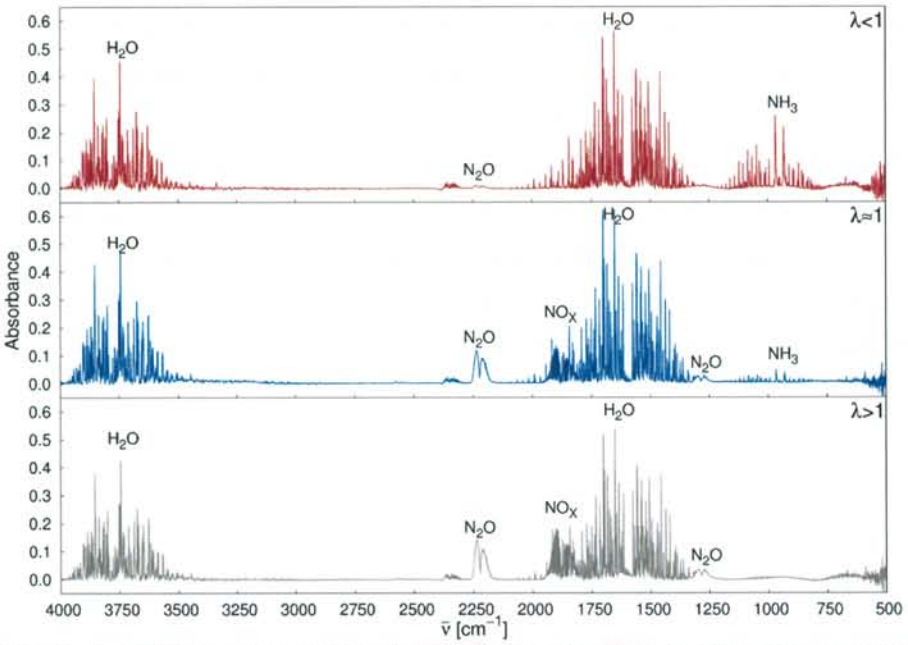

Figure 4: FTIR spectrums for ammonia combustion for lambda close to one.

From the FTIR spectrums in Figure 4, it can be seen that if the lambda value is below one, which mean low oxygen to ammonia ratio, that trace amounts of N_2O can be seen and no NO_X, but not all the ammonia is combusted. The data is as expected as long as there are a surplus ammonia, NO_X formation is depressed but there are still traces of N_2O, this can be seen in the top spectra and lambda below one. At lambda close to one, only trace amounts of ammonia is left and there is a large increase in N_2O and starting formation of NO_X. Finally when lambda is above one and the mixture is oxygen rich, all ammonia is combusted but both formation of N_2O and NO_X increase. The problem with formation of N_2O and NO_X could be avoided with another catalyst.

The tradeoff between not combusting all the ammonia and formation of harmful emissions of N_2O and NO_X, will probably favor not combusting all the ammonia. The main reason for this is that N_2O is a green house gas with a long life time in the atmosphere and NO_X causes smog in urban environments. Ammonia on the other hand is relatively harmless and reacts with the soil as fertilizer. Ammonia can also easily be captured in a solid acid filter, this could be sulphated carbon.

The catalyst for ammonia decomposition is ruthenium promoted with cesium and supported on high surface area graphite (HSAG). This is a very active catalyst and can push the conversion close to the theoretical equilibrium conversion, given by the thermodynamic Gibbs energy. As prototype the catalyst works as expected and gives high conversion, but there are two issues

that need to be dealt with mainly coming from the HSAG support. The first is pressure drop duet to, the fine structure of the graphite support and difficulties in making a suitable particle size gives a large pressure drop over the catalyst bed. The second problem is methanation of the graphite, this is due to the fact that ruthenium is a methanation catalyst and that the inside of the catalyst gets very hot (1000K). After the decomposition the reformed gas needs cleaning of slip ammonia. This is done in a sulphated carbon filter. Finally the reformed and clean gas can be fed to a fuel cell. In Figure 5 the reformed ammonia gas is investigated with FTIR to determine the efficiency of the reformer and filter.

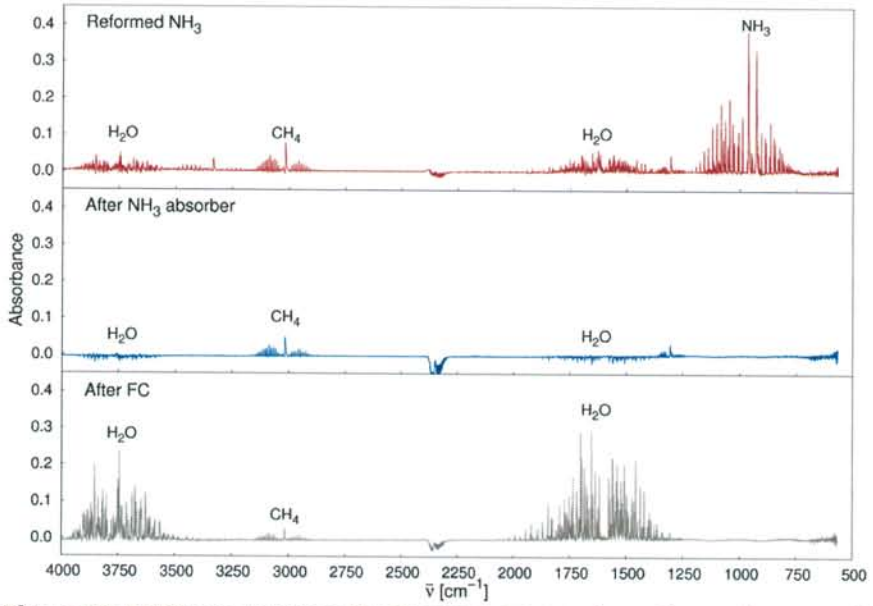

Figure 5: FTIR spectrums of reformed ammonia, reformed ammonia after ammonia slip filter, and finally after the fuel cell.

From the first two spectra in Figure 5 it can be seen that both ammonia and water is removed from the reformed ammonia when it is passed through the sulphated carbon filter. It can also be seen that almost identical amounts of methane is found. The methane is produced from the support material and therefore it is planned to change catalyst support to $MgAl_2O_4$-spinel. This support can handle high temperatures and at the same time it should be easier to lower the pressure drop over the catalyst bed. The last spectrum after the fuel cell is a small experiment, where a PEMFC is feed with the reformed and clean ammonia and as expected the only by product is water.

The data from the experiment of running a fuel cell on the feed of reformed ammonia cleaned in a sulphated carbon filter can be seen in Figure 6. Here a fuel cell is run first on hydrogen

and then the gas is changed to the reformed ammonia. All the experiments are at constant current and with the same cell. The change in voltage over time on different feeds is most likely the drying of the membrane, but this is pure speculation. The data is first try at making power directly from the cleaned ammonia reformat.

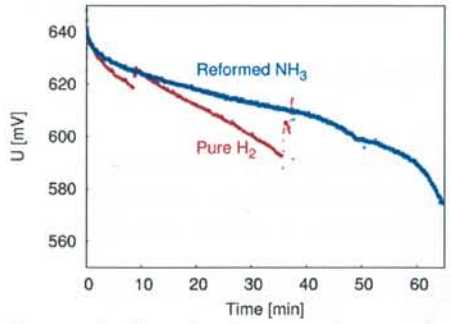

Figure 6: Constant current experiments, with a fuel cell fed with hydrogen and reformed ammonia.

The experiment is done to demonstrate that an ordinary fuel cell can run on the reformed ammonia out of the box. The drop in voltage over time is probably due to drying out of the membrane. The fuel cell was a test cell supplied by IRD fuel cells.

Conclusion

This overview has demonstrated the possibilities of using ammonia as an energy carrier in the hydrogen economy. It has been demonstrated that an efficient ammonia decomposer with high efficiency can be constructed. It has been shown that metal ammines can be used as a solid ammonia storage medium avoiding the hazards of handling and transporting liquid ammonia under pressure. Finally it has been shown that a fuel cell can run directly on the cleaned ammonia reformate. There are still some challenges involved with designing a complete system but the different components are being developed. This involves integration of an ammonia storage unit based on metal ammines, with the developed ammonia decomposition unit and finally connecting it to a full size fuel cell stack.

Acknowledgements

The project is supported by The Danish Council for Strategic Research (Project no. 2104-05-0016). The project is also supported by Signe Shim and IRD Fuel Cells, who supplied the fuel cell.

and then the gas is changed to the reformed ammonia. All the experiments are at constant current and with the same cell. The change in voltage over time on different feeds is most likely the drying of the membrane, but this is pure speculation. The data is first try at making power directly from the cleaned ammonia reformat.

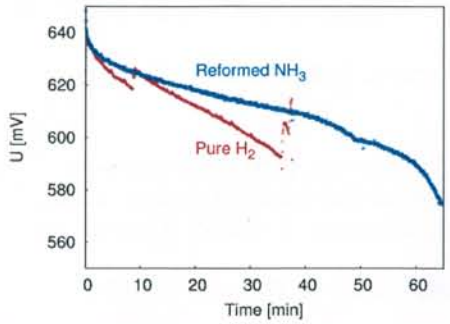

Figure 6: Constant current experiments, with a fuel cell fed with hydrogen and reformed ammonia.

The experiment is done to demonstrate that an ordinary fuel cell can run on the reformed ammonia out of the box. The drop in voltage over time is probably due to drying out of the membrane. The fuel cell was a test cell supplied by IRD fuel cells.

Conclusion

This overview has demonstrated the possibilities of using ammonia as an energy carrier in the hydrogen economy. It has been demonstrated that an efficient ammonia decomposer with high efficiency can be constructed. It has been shown that metal ammines can be used as a solid ammonia storage medium avoiding the hazards of handling and transporting liquid ammonia under pressure. Finally it has been shown that a fuel cell can run directly on the cleaned ammonia reformate. There are still some challenges involved with designing a complete system but the different components are being developed. This involves integration of an ammonia storage unit based on metal ammines, with the developed ammonia decomposition unit and finally connecting it to a full size fuel cell stack.

Acknowledgements

The project is supported by The Danish Council for Strategic Research (Project no. 2104-05-0016). The project is also supported by Signe Shim and IRD Fuel Cells, who supplied the fuel cell.

Compact Hydrogen Production from Ammonia Stored in Solid Metal Ammines

Asbjørn Klerke[1], Rasmus Z. Sørensen[1], Claus H. Christensen[1], Ulrich Quaade[2] and Jens K. Nørskov[3]

[1]*Center for Sustainable and Green Chemistry, Department of Chemistry, Building 206, Technical University of Denmark, DK-2800 Kgs. Lyngby, Denmark*

[2]*Center for Individual Nanoparticle Functionality, Department of Physics, Building 307, Technical University of Denmark, DK-2800 Kgs. Lyngby, Denmark*

[3]*Center for Atomic-Scale Materials Physics Design, Department of Physics, Building 307, Technical University of Denmark, DK-2800 Kgs. Lyngby, Denmark*

aklerke@kemi.dtu.dk, zink@kemi.dtu.dk, chc@kemi.dtu.dk, quaade@fysik.dtu.dk, norskov@fysik.dtu.dk.

Key Words: Metal ammines; ammonia decomposition; hydrogen storage; micro-fabriacated reactors.

Abstract

Metal ammine complexes constitute an alternative way of indirect hydrogen storage. So far, the best studied material is $Mg(NH_3)_6Cl_6$ that has a hydrogen density of 9.1 wt% and 115 g/L which is well above the DOE 2015 targets. The ammonia is easily desorbed at temperatures below 650K and the process can be reversed by applying an ammonia pressure of 1 bar. This facile release of ammonia is attributed to the development of nano-pores in the metal ammine salt during the desorbtion of ammonia. This is important for the ammonia desorption from dense tablets that is compacted to above 95% of the crystal densities of the metal ammine salts. The use of metal ammine salts makes it possible to optimize the storage and catalytic decomposition of ammonia as two separated systems and then combine them together for various applications[1].

The decomposition of ammonia can be done catalytically over a transition metal catalyst. We have shown that this can be done in micro-fabricated reactors with high surface area graphite as the support material and promoted ruthenium as the catalyst. High conversion is achieved at temperatures below 650K[2]. The temperature necessary for decomposition is important to minimize energy consumption in the system.

1: Introduction

The raising concern over dwindling resources and the environmental impact of burning fossil fuels has generated interest in using hydrogen as an alternative energy carrier. So far, the challenges to overcome for a hydrogen economy to be feasible remain significant and require a sustained focused effort in development of economic viable solutions for production, storage and use of hydrogen as an energy carrier[3,4,5,6,7,8].

Widespread use of hydrogen as a fuel is limited the by lack of a safe, efficient system for its storage[9]. The large deviation from ideality upon compression, the low condensing point and low density even in the liquid state, has limited the use of conventional storage systems and a plethora of strategies for direct storage of hydrogen have been proposed[10,11,12,13,14,15,16]. While elegant in terms of a low number of chemical conversions in the storage process, there are still a large number of challenges to be dealt with before large-scale direct hydrogen storage becomes economically and technically viable for implementation in every day applications. This has led to increased interest in indirect storage of hydrogen e.g., in the form of methanol, ethanol or ammonia[17,18].

The indirect storage of hydrogen in ammonia is a promising concept for storage and transportation of hydrogen. The use of liquid ammonia as an indirect hydrogen carrier is interesting because liquid ammonia can meet the DOE 2015 system targets for hydrogen storage with a gravimetric hydrogen density of 17.8 wt.% and a volumetric hydrogen density of 0.122 kg H/l at -33 °C and 0.105 kg H/l at 25 °C[19]. Furthermore, the technological needs for production, storage and transportation of

ammonia are well known and ammonia decomposition is viable, although not optimized for hydrogen production[20]. The transportation of ammonia can be done by rail, truck or in pipelines. In figure 1 the already existing liquid ammonia pipelines in the U.S. Midwest are shown.

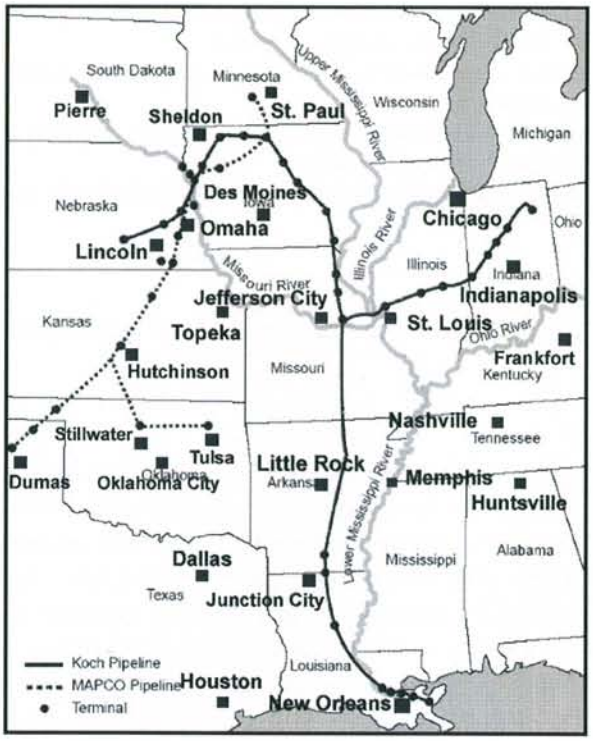

Figure 1. Liquid ammonia pipelines in the U.S. Midwest[18].

Synthesis of ammonia in the Haber-Bosch process is one of the best studied catalytic processes. Today, almost all industrial ammonia production is based on the Haber-Bosch process and it is one of the largest chemical processes in the world with a annual production of approximately 130 million tons. The main use of ammonia is as fertilizer for agriculture, which constitutes 80 % of the world production[21].
For many applications the safety of liquid ammonia is a concern so methods for solid storage of ammonia in metal ammines are very interesting.

Figure 2. Mass and volume of 10 kg H stored reversibly by 6 methods[22].

In Figure 2, the hydrogen storage density of a selection of the more promising direct hydrogen storage approaches is compared to the recently published method of hydrogen storage in the metal ammine salt $Mg(NH_3)_6Cl_2$. The figure is based on the best obtained reversible densities reported in the literature without considering the space occupied by the container[23,24,25,26,27,28], and from this it is evident that reversible storage of 10 kg H in a compact and convenient way is not at all trivial.
The lifecycle of a metal ammine during hydrogen storage and release is illustrated in Figure 3. Here, the ammonia gas, produced from hydrogen and nitrogen, reacts with the dry salt to form the metal ammine.

The formation of a metal ammine is an exothermic process and the reaction heat varies with the given metal salt and degree of saturation. After saturation, the ammonia can be released by heating the metal ammine; the energy required for desorption is obviously the same as that released during absorption. The desorbed ammonia can then be used in a fuel cell capable of using ammonia directly, e.g. SOFC, or be decomposed over a catalyst to hydrogen and nitrogen. The produced hydrogen can then be supplied to PEMFC or other types of fuel cells.

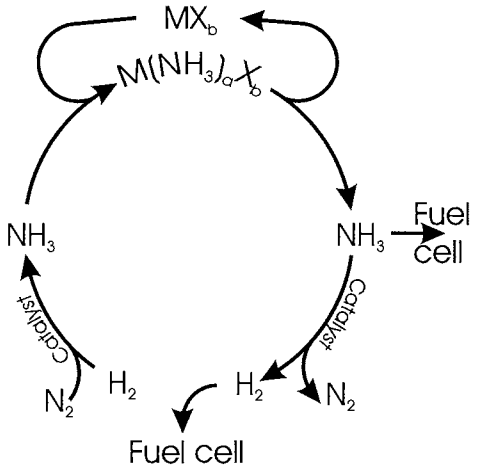

Figure 3. Principle of hydrogen storage in metal ammine complexes of the general formula $M(NH_3)_aX_b$[22].

The ammonia storage capacity of saturated $Mg(NH_3)_6Cl_2$ is 51.8 wt.%, corresponding to a gravimetric hydrogen density of 9.19 wt.% and a volume density of hydrogen calculated from the crystal density of 115 g/L. The volumetric density is close to that of liquid ammonia at -33 °C. The hydrogen storage capacity is also above the DOE 2015 targets for hydrogen storage on both gravimetric and volumetric scale.

The use of metal ammines as indirect hydrogen storage materials is obviously entirely dependent on the possibilities of efficiently converting ammonia to hydrogen. The decomposition of ammonia is endothermic ($\Delta H = 45.6$ kJ/mol NH_3).

Thus, decomposition of ammonia to hydrogen (and nitrogen) requires an energy input, and since the decomposition reaction is very slow even at relatively high temperatures, a catalyst is also needed. Since the reaction is an equilibrium reaction, it is not possible to completely decompose ammonia into hydrogen.

During the last decades, catalytic ammonia decomposition has continuously gained attention as a possible source of CO_x-free hydrogen[29]. At the same time, the continuously improving fundamental understanding of the ammonia synthesis reaction[30] has also led to significant advances in our understanding of the ammonia decomposition reaction.

It is clear that the multi-promoted iron catalyst optimized for industrial ammonia synthesis[31] cannot be used for ammonia decomposition. First of all, iron-based catalysts are unstable with respect to formation of bulk iron nitride at the decomposition conditions. The reason is that ammonia synthesis for thermodynamic reasons (Principle of Le Chatelier) is conducted at high pressures, whereas ammonia decomposition is preferentially done at low pressures. Moreover, during ammonia synthesis, the equilibrium is approached from low ammonia concentrations, whereas it is approached from high ammonia concentrations during ammonia decomposition. At high ammonia pressures, iron rapidly transforms into iron nitride. Furthermore, the different reaction conditions also mean that a single catalyst is not optimal for both reactions, and this difference can now be expressed in quantitative terms[32]. Today, the most promising catalysts for ammonia decomposition are based on supported ruthenium promoted with cesium and/or barium. Interestingly, such catalysts supported on carbon were implemented as ammonia synthesis catalysts in a few industrial plants during the 1990ies and they were found to be particularly promising at high ammonia pressures[33].

Today, highly active ruthenium-based decomposition catalysts that are active at temperatures about 350-400 °C have been developed[34,35,36,37].
Here, a method for incorporation of a porous graphite support into micro-fabricated reactors is presented. The micro-fabricated reactors are well suited for catalyst studies, since they can be kept isothermal under most reaction conditions and the gas flow stays laminar (plug flow behavior) over a large range of space velocities. This is used to investigate promotion of the Ru/C system with Cs and Ba, which are effective and carefully studied promoters for ammonia decomposition over Ru/C. The effects of driving the decomposition reaction close to equilibrium at relatively low temperatures are studied as well[2].

2: Experiments

$Mg(NH_3)_6Cl_2$ was pressed into tablets to determine the maximal bulk density of the storage material. A tablet of the material were also subjected to measurements of pore size distributions. This was performed using nitrogen absorption and desorption measurements on a Micrometrics ASAP 2020N, with pretreatment of the sample at temperatures and pressures chosen to give the desired levels of NH_3 desorbtion.
Desorbtion characteristics of $Mg(NH_3)_6Cl_2$ were determined by temperature programmed desorbtion (TPD). Samples of approximately 0.5g were transferred to a closed test tube under NH_3 atmosphere and heated following a desired temperature ramp. NH_3 was released into a carrier stream of Ar through a T-joint with a thin connection tube to maintain the NH_3 atmosphere over the sample. This procedure gave an NH3 pressure slightly above atmospheric pressure over the ammine sample. For TPDs of $Mg(NH_3)_6Cl_2$, a sample obtained from Amminex A/S was used as received. The ammonia content in the carrier stream was determined using a Fischer-Rosemount NGA 2000 equipped with an MLT analyzer calibrated to NH_3 concentrations from 0.03-30%. Desorption rates were calculated from the ammonia content in the carrier stream and the flow of Ar which was kept constant at 213 NmL/min using a calibrated Brooks 5850 TR mass flow controller. TPDs were obtained with heating rates of both 1 and 5 K/min.
The graphite support is prepared using an aqueous solution of commercial food grade sucrose (140 g/L) to fix finely ground Timrex HSAG300 high-surface area graphite in micro-fabricated silicon reactors of 3-4 μL reactor volume. The reactors are produced using Deep Reactive Ion Etching as previously described[38,39]. Reactors are produced with reaction chambers of 8mm × 1.5mm × 0.3mm. To facilitate assembly of the setup, manifold connections are made through the silicon slab itself, the reactor slab being fixed against high temperature stable rubber o-rings on the gas handling system[2].

3: Results and Discussion

The desorption characteristics for $Mg(NH_3)_6Cl_2$ during temperature programmed desorption (TPD) are shown in figure 4. TPDs of $Mg(NH_3)_xCl_2$ were also reported previously and this salt have stable compositions with x = 6, 2 and 1. Essentially all ammonia desorbs in the temperature range 410-700 K.

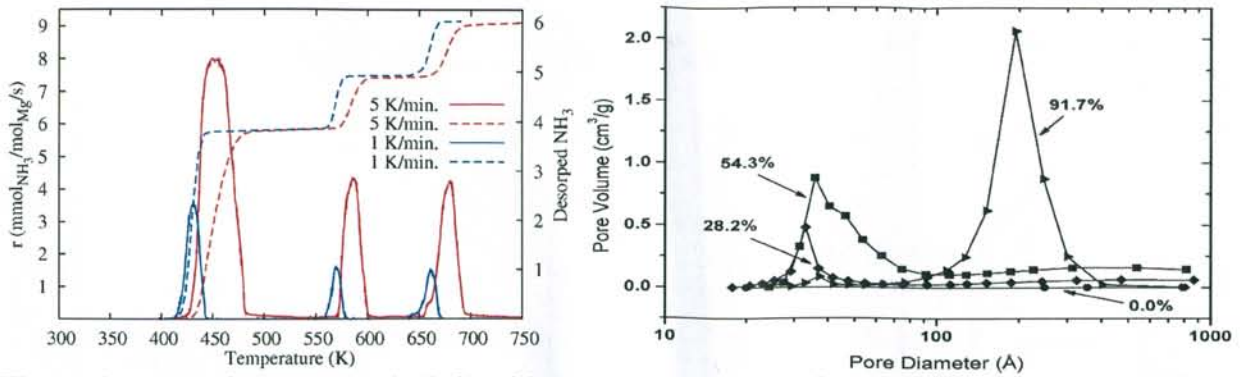

Figure 4: TPDs of $Mg(NH_3)_6Cl_2$ (left) with a temperature ramp of 5K/min (red) and 1K/min (blue). The solid lines show the desorption rate and the dashed lines show the total amount of desorbed ammonia. Pore size distribution for $Mg(NH_3)_xCl_2$ (right) at different degrees of desorption corresponding to x~6,2,1,0[1].

The TPD peaks start within few degrees of the theoretical temperature for 1 bar equilibrium pressure independently of the temperature ramp. This and the near exponential rise in desorption rate with temperature indicates that desorption is equilibrium-limited even at high desorption rates.
For desorption of ammonia to be facile from dense bodies of metal ammine complexes like e.g. tablets, it is important that a pore structure develops through which ammonia can leave the tablet without a long diffusion path in the solid state. The development of nano-pores has been shown for $Mg(NH_3)_6Cl_2$ during desorption in figure 4 (right)[40].
Figure 5 shows a magnified view of a sealed micro-fabricated reactor prepared with graphite support using sucrose glue. The support is seen as a fairly evenly distributed porous black layer filling up about half the volume of the reaction chamber.

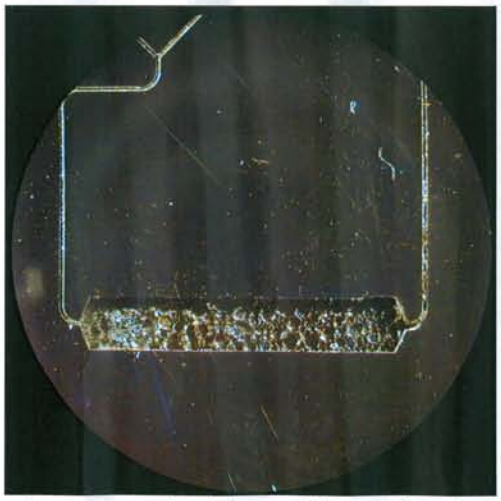

Figure 5 Micro-fabricated reactor prepared with graphite and sealed with a pyrex lid. The reactor chamber dimensions are 8mm × 1.5mm × 0.3mm[2].

Ru/C catalysts were prepared and tested without addition of promoters and with the addition of both Cs and Ba in approximately the same amount as promoters, and with a high Cs loading corresponding to a 3 fold increase of the molar ratio of Cs to Ru.
The best catalyst was also test with different flows to demonstrate that the flow conversion and rate is related and is limited when the equilibrium is approached.

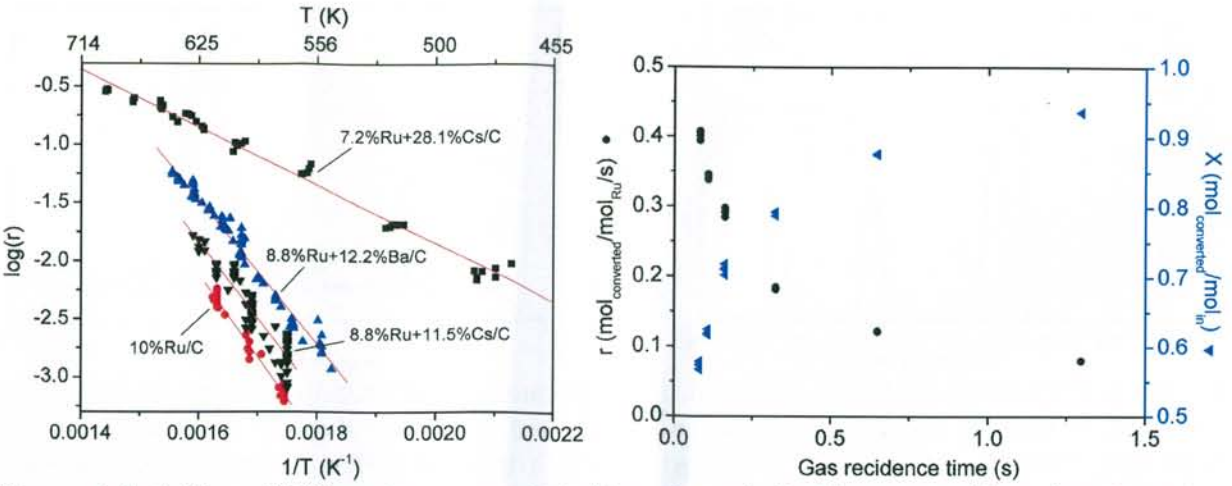

Figure 6 Activities of differently promoted Ru/C catalysts (left). The composition of each catalyst is given in the graph. r is in $mol_{NH3}/mol_{Ru}/s$. Comparison of rate and conversion (right) as function of residence time at 694K over a Ru+Cs/C catalyst with 7.2 wt% Ru and 28.3 wt% Cs[2].

As seen in figure 6 (left), the low Cs promotion gives significantly lower activity than the corresponding Ba promotion. This correspond well to what could be expected from the ammonia synthesis literature[41,42], whereas the high Cs loading gives a dramatically higher activity than that achieved with the low Ba and Cs promoter loadings. Furthermore, the catalyst with high Cs loading gave lower apparent activation energy than the other catalysts. This change means, that the lower the temperature, the higher is the relative effect of promotion, and even at 473K the activity is as high as that of the Ba promoted catalyst at 590K. This is particularly interesting for miniaturization, as lower operating temperature reduces heat losses and thereby enables a lower overall fuel consumption. Unfortunately, the equilibrium is shifted towards NH_3 for low temperatures giving to low equilibrium conversions at temperatures below 500K. However, with the reported Cs promoted catalyst a large fraction of the ammonia can be decomposed at relatively low temperature while most of the remaining ammonia can then be decomposed in an even smaller hot zone reactor. In this way the reactor volume kept at high temperature can be reduced, saving considerable amounts of energy, and thus the volume needed for fuel storage will be smaller.
The data in figure 6 (right) shows that the overall rate of decomposition decreases when the system is pushed towards higher conversions. This can be attributed to a negative reaction order in H_2 and to a closer approach to equilibrium. For ammonia decomposition, these effects are not easily separable, and most likely they are both responsible for the observed apparent activation energies in figure 6 (left) as these are measured at a constant gas flow that makes rate and conversion correlate.
For development of a small portable power supply the decreasing rate close to equilibrium is an adverse effect as the ultimate goal is full equilibrium conversion using the minimal amount of catalyst.

4: Conclusion

We have shown that metal ammine complexes, in combination with an ammonia decomposition catalyst, provide a new solid hydrogen storage medium, working below 620 K. The system has considerably higher measured reversible hydrogen content than any system considered until now. Furthermore we have integrated a graphite carrier into a micro-fabricated reactor. Graphite carriers are known for giving the most active ruthenium catalysts for ammonia decomposition. This enables a significant increase in the activity per reactor volume. That is important for miniaturizing ammonia decomposition systems for hydrogen production. At the same time, high Cs promoter loading is shown to facilitate high ammonia decomposition rates at temperatures below 500K.

[1] Christensen, C. H.; Sørensen, R. Z.; Johannessen, T.; Quaade, U.; Honkala, K.; Elmøe, T. D.; Køhler R.; Nørskov, J. K. *J. Mater. Chem.*, **2005**, *15*, 4106–4108.
[2] Sørensen, R. Z.; Klerke, A.; Quaade, U.; Jensen, S.; Hansen, O.; Christensen, C. H. *Catal. Lett,*. **2006**, *112*, 77-81.
[3] Dresselhaus, M.; Crabtree, G.; Buchanan, M. *Basic Research Needs for a Hydrogen Economy*, U.S. Department of Energy, **2003**.
[4] Crabtree, G.; Dresselhaus, M.; Buchanan, M. *Physics Today*, **2004**, *57, 12*, 39-44.
[5] Kennedy, D. *Science*, **2004**, *305*, 917.
[6] Turner, J. A. *Science*, **2004**, *305*, 972-974.
[7] Wu, W.; Kawamoto, K.; Kuramochi, H. *J. Mater. Cycles Waste Manag.*, **2006**, *8*, 70-77.
[8] Avci, A. K.; Önsan, Z. I.; Trimm, D. L. *Top. Catal.*, **2003**, *22*, 359-367.
[9] Takimoto, M.; Hou, Z. *Nature*, **2006**, *443*, 400-401.
[10] Zütel, A. *Naturwissenschaften*, **2004**, *91*, 157–172.
[11] Cheng, P.; Xiong, Z.; Lou, J.; Lin, J.; Tan, K. L. *Nature*, **2002**, *420*, 302-304.
[12] Bououdina, M.; Grant, D.; Walker, G. *Int. J. Hydrogen Energy*, **2006**, *31*, 177-182.
[13] Stephens, F. H.; Baker, R. T.; Matus, M. H.; Grant, D. J.; Dixon, D. A. *Angew. Chem. Int. Ed.*, **2006**, *45, 5*, 746-749.
[14] Bogdanović, B.; Felderhoff, M.; Pommerin, A.; Schüthe, F.; Spielkamp, N. *Adv. Mater.*, **2006**, *18*, 1198-1201.
[15] Latroche, M.; Surblé, S.; Serre, C.; Mellot-Draznieks, C.; Llewellyn, P. L.; Lee, J.-H.; Chang, J.-S.; Jhung, S. H.; Férey, G. *Angew. Chem. Int. Ed.*, **2006**, *45, 48*, 8227-8231..
[16] Welch, G. C.; Juan, R. R. S.; Masuda, J. D.; Stephan, D. W. *Science*, **2006**, *314*, 1124-1126.
[17] Metkemeijer, R.; Achard, P. *Int. J. Hydrogen Energy*, **1994**, *19*, 535-542.
[18] Thomas, G.; Parks, G. *Potential Roles of Ammonia in a Hydrogen Economy*, U.S. Department of Energy, **2006**.
[19] Eggmann, T. *Kirk-Othmer Encyclopedia of Chemical Technology: Ammonia*, John Wiley & Sons, Inc. **2001**.
[20] Appl, M. *Ullmann's Encyclopedia of Industrial Chemistry: Ammonia*, Weinheim, Wiley-VCH Verlag GmbH & Co. KGaA, **2007**.
[21] IFA, www.fertilizer.org/ifa/statistics.asp
[22] Vegge, T.; Sørensen, R. Z.; Klerke, A.; Hummelshøj, J. S.; Nørskov, J. K.; Christensen, C. H. *Solid-state hydrogen storage: materials and chemistry*, Woodhead Publishing Limited, **in print**.
[23] Mosher, D.; Tang, X.; Arsenault, S. *High Density Hydrogen Storage System Demonstration Using NaAlH4 Based Complex Hydrides*, FY 2006 Annual Progress Report, DoE Hydrogen Program, **2006**, 281-284.
[24] Liu, X.; Zhu, Y.; Li, L. *Int. J. Hydrogen Energy*, **2007**, article in press, DOI: 10.1016/j.ijhydene.2006.09.037.
[25] Nomura, K.; Fujiwara, S.; Hayakawa, H.; Akiba, E.; Ishido, Y.; Ono, S. *Journal of the Less-Common Metals*, **1991**, *169*, 9-17.
[26] Suissa, E.; Jacob, I.; Hadari, Z. *Journal of the Less-Common Metals*, **1984**, *104*, 287-295.
[27] El-Osairy, M. A.; el-Osery, I. A.; Metwally, A. M.; Hassan, M. A. *Int. J. Hydrogen Energy*, **1993**, *18* (6), 517-524.
[28] Laidler, K. J.; Meiser, J. H. *Physical Chemistry*, third edition, New York, Houghton Mifflin Company, **1999**.
[29] Choudhary, T. V.; Sivadinarayana, C.; Goodman, D. W. *Catal. Lett.*, **2001**, *72(3-4)*, 197-201.
[30] Honkala, K.; Remediakis, I.; Logadottir, A.; Nørskov, J. K.; Hellman, A.; Dahl, S.; Carlsson, A.; Christensen, C. H. *Science*, **2005**, *307*, 555.
[31] Stoltze, P. *Ammonia: Catalysis and Manufacture*, (Ed.) Nielsen, A., Springer-Verlag, **1995**.
[32] Boisen, A.; Dahl, S.; Nørskov, J. K.; Christensen, C. H. *J. Catal.*, **2005**, *230*, 309-312.
[33] Tennison, S. R. *Catalytic Ammonia Synthesis: Fundamentals and Practice*, (Ed.) Jennings, J. R., Plenum Press, **1991**.
[34] Raróg, W.; Kowalczyk, Z.; Sentek, J.; Składanowski, D.; Szmigiel, D.; Zieliński, J. *Appl. Catal. A*, **2001**, *208*, 213-216.
[35] Raróg-Pilecka, W.; Miśkiewicz, E.; Szmigiel, D.; Kowalczyk, Z. *J. Catal.* **2005**, *231*, 11-19.
[36] Yin, S.-F.; Xu, B. Q.; Zhu, W. X.; Ng, C. F.; Zhou, X. P.; Au, C. T. *Catal. Today*, **2004**, *93-95*, 27-38.
[37] , S.-F.; Xu, B. Q.; Zhou, X. P.; Au, C. T. *Appl. Catal. A*, **2004**, *277*, 1-9.
[38] Quaade, U.; Jensen, S.; Hansen, O. *Rev. Sci. Instrum.*, **2004**, *75*, 3345-3347.
[39] Quaade, U.; Jensen, S.; Hansen, O. *J. Appl. Phys.*, **2005**, *97*, 044906.
[40] Hummelshøj, J. S.; Sørensen, R. Z.; Kustova, M. Y.; Johannesen, T.; Nørskov, J. K.; Christensen, C. H. *J. Am. Chem. Soc.*, **2006**, *128*, 16-17.
[41] Kowalczyk, Z.; Krukowski, M.; Raróg-Pilecka, W.; Szmigiel, D.; Zielinski, J. *Appl. Catal. A*, **2003**, *248*, 67-73.
[42] Liang, C.; Wei, Z.; Xin, Q.; Li, C. *Appl. Catal. A*, **2001**, *208*, 193-201.